NEMATIC POLYMER AND ELASTOMER PARTICLES

Kirsty L Davey

PhD

University of York

Chemistry

June 2015

ABSTRACT

The creation of nematic polymer and elastomer particles in the micrometre size range with responsive properties by heterogeneous polymerisation techniques, specifically dispersion polymerisation and RAFT-assisted dispersion polymerisation, is reported. Control of size, size-distribution and confinement texture was achieved. A novel monomer design with a systematic approach was adopted in order to determine the effect of mesogen structure on the director configuration that would result within microscale nematic polymer particles, which revealed a change in the director configuration on the increase of just one CH_2 group on the side chains of the mesogen. This change in the director configuration revealed radial particles within polar solvents without the addition of a further surface analyte, and allowed for the controlled creation of nematic polymer particles with specific internal confinement textures, including the formation of an escaped twisted radial structure created through copolymerisation of two different nematic monomers. Careful investigations and modifications of dispersion polymerisation with the addition of a RAFT agent allowed for the synthesis of microscale nematic elastomer particles with confirmed network formation, a discovery that is previously unreported. These elastomeric particles were reversibly responsive to changes in their external environment, by showing confinement textures after swelling which correspond to the polarity of the solvent. The particles were also responsive to changes in temperature and survived multiple heat and cool cycles which is further indication of successful network formation. Electro-optical investigations of nematic polymer particles showed the reversible shape deformation of free nematic polymer particles as a result of the internal mesogenic units aligning with the field. This deformation is only observed with polymeric particles with a low glass transition temperature as the flexible polymer chains allow for mesogen reorientation, and is a different behaviour to what has been reported previously for low molecular weight droplets in an electric field.

TABLE OF CONTENTS

TABLE OF FIGURES

TABLE OF TABLES

TABLE OF SCHEMES

LIST OF ACCOMPANYING MATERIAL

Accompanying this thesis is a CD-ROM which can be found in an envelope on the inside back cover, and includes videos referenced in Chapter 6.

ACKNOWLEDGEMENTS

Firstly, I would like to thank the EPSRC and the Royal Society for funding my PhD research and allowing me this opportunity.

I would like to extend a special thank you to my supervisor Dr. Verena Görtz for offering me the chance to study for my doctorate at York and for pushing me to achieve my potential over the last four years. She has shown me much patience, encouragement and understanding.

I would also like to thank my second supervisor Dr. Isabel Saez who has been invaluable with her support of me throughout my PhD and has helped guide me through my last two years here at York.

I would also like to thank all the members of the liquid crystal research group at the University of York past and present who have provided help and advice beyond measure. I would like to give a special mention to Charlie, Dave, Katrina and Emily, who along with their advice have shared with me kindness, friendship and good humour.

My family and friends have been there for me through thick and thin, providing me with an ear, hugs, or a glass of wine (or three) whenever necessary.

I would not have gotten to where I am today without the endless love and support of my husband James. Even the daunting task of planning a wedding while we both were in the middle of our PhDs was possible with him at my side.

AUTHOR'S DECLARATION

I confirm that the work presented in this thesis, both written and experimental, is my own and has not been previously submitted for award at this or any other institution. It has not been previously published or presented elsewhere with the following exceptions:

- Talk entitled 'Liquid-crystalline polymer and elastomer particles' Kirsty Davey, V. Görtz, KMS prize winner's seminar, University of York, 8th October 2014

- Poster entitled 'Tuning the optical properties of nematic polymer particles' K. L. Davey, V. Görtz, Joliot – Curie Conference, Edinburgh, 16-17th September 2014

- Talk entitled 'Responsive microscale liquid-crystalline particles' Kirsty Davey, V. Görtz, 50 years of Chemistry celebration, University of York, 6th September 2014

- Poster entitled 'Tuning the optical properties of nematic polymer particles' K. L. Holdsworth, V. Görtz, International conference of liquid crystals (ILCC), Dublin, 29th June – 4th July 2014

- Poster entitled 'Tuning the optical properties of nematic polymer particles' K. L. Holdsworth, V. Görtz, Bruker poster competition, The University of York, 20th March 2014

- Talk entitled 'Nematic polymer particles with tuneable optical properties' K. L. Holdsworth, V. Görtz, European conference of liquid crystals (ECLC), Rhodes 22nd – 27th September 2013

- Talk entitled 'Controlling the director configuration in nematic polymer particles' K. L. Holdsworth, V. Görtz, British liquid crystal society (BLCS) AGM 2013, Cambridge University, 25-27 March 2013

- Poster entitled 'Liquid-crystalline elastomer particles of controllable size and shape' K. L. Holdsworth, V. Görtz, EPSRC visit, University of York, 31st January 2013

- Poster entitled ‘Liquid-crystalline elastomer particles of controllable size and shape’ K. L. Holdsworth, V. Görtz, New frontiers in anisotropic fluid particle composites conference, Royal Society Kavli House, Milton Keynes, 27th - 29th June 2012

- Poster entitled ‘Liquid-crystalline elastomer particles of controllable size and shape’ K. L. Holdsworth, V. Görtz, University of York, Cantor nanoscience day, 25th May 2012

- Poster entitled ‘Liquid-crystalline elastomer particles of controllable size and shape’ K. L. Holdsworth, V. Görtz, BLCS AGM 2012, Strathclyde University, 1-4th April 2012

CHAPTER 1:

INTRODUCTION

1 INTRODUCTION

1.1 THESIS OVERVIEW

Droplets of a nematic liquid crystal display unique textures that are not observed in the bulk because they are highly confined systems within non-planar topologies.[1] The textures that are observed result from a balance between bulk and surface interactions and are therefore dependent on parameters including droplet size[2] and surface anchoring.[3] Droplets of nematic materials such as 4-cyano-4'-pentylbiphenyl (5CB) have also been studied as colloidal systems, as emulsion droplets in hosts such as water, and have recently been exploited as sensors.[3-7] This thesis presents the preparation of liquid-crystalline polymer particles which exhibit similar responsive capabilities to nematic droplets whilst being more easily manipulated and with significantly longer lifetimes. The addition of a crosslinker to these systems allowed for the synthesis of nematic elastomer particles which have possible applications as micro-actuators[8-14] as well as being insoluble, swellable and deformable in response to stretching.[15, 16]

The focus of this thesis is in the previously unreported synthesis, characterisation and investigation of novel microscale nematic polymer and elastomer particles with defined confinement textures. A series of nematic monomers was synthesised and heterogeneous polymerisation methods were utilised. These particles were then analysed for properties such as director configuration, phase transitions, particle size and particle size variance. The particles were also subjected to the effect of changing temperatures, solvents and the application of an electric field to assess their response. The introduction chapter will cover fundamental aspects of liquid crystal properties including birefringence and elastic deformations with a focus on the nematic phase; confinement of liquid crystals within non planar topologies; polymeric liquid crystals; and polymerisation methods to prepare polymer particles and elastomeric systems. The synthesis of nematic monomers, polymers and elastomers is detailed in Chapter 2, with their characterisation featured in Chapter 3. Chapters 4 and 5 focus on optical investigations of nematic polymer and elastomer particles, respectively. These chapters include a previously unreported control of the director configuration by altering the mesogenic unit, as well as the reversible and responsive nature of microscale nematic elastomer particles with confirmed network formation. Chapter 6 details investigations into the effect of an electric field on different particle systems,

conclusions are drawn in Chapter 7 and the experimental methods and results are summarised in Chapter 8.

1.2 LIQUID CRYSTALS

The liquid crystal phases are states of matter present between the isotropic liquid and the crystalline solid, and thus have a degree of anisotropy whilst remaining fluid.[17, 18] The anisotropic properties of liquid crystals include birefringence,[19] and it is this interaction with light which gives liquid crystals the display applications for which they are most widely known. Shown in Figure 1.1 is a schematic representation depicting a typical crystalline solid with three-dimensional long-range order, an isotropic liquid with a completely random internal configuration and an idealised liquid-crystalline phase, which can display long range organisation in up to three dimensions. Liquid crystal phases are often referred to as mesophases and the molecules which comprise a liquid crystal phase as mesogens.[20] The liquid crystal phase illustrated in Figure 1.1 is the nematic phase, which is the least ordered and most fluid of the liquid crystal phases, and displays long-range orientational order in one dimension with no positional order. The liquid crystal units within a nematic phase are on average orientated parallel to one another in a preferred direction known as the director, given the symbol **n**. Other phases such as the smectic phases or blue phases have much higher degrees of order, but as the nematic phase is the only phase under investigation in this thesis, it will be the focus within this introduction. Although some of the concepts covered in the following discussion may apply to a variety of liquid-crystalline phases, they will be discussed with respect to the nematic phase.

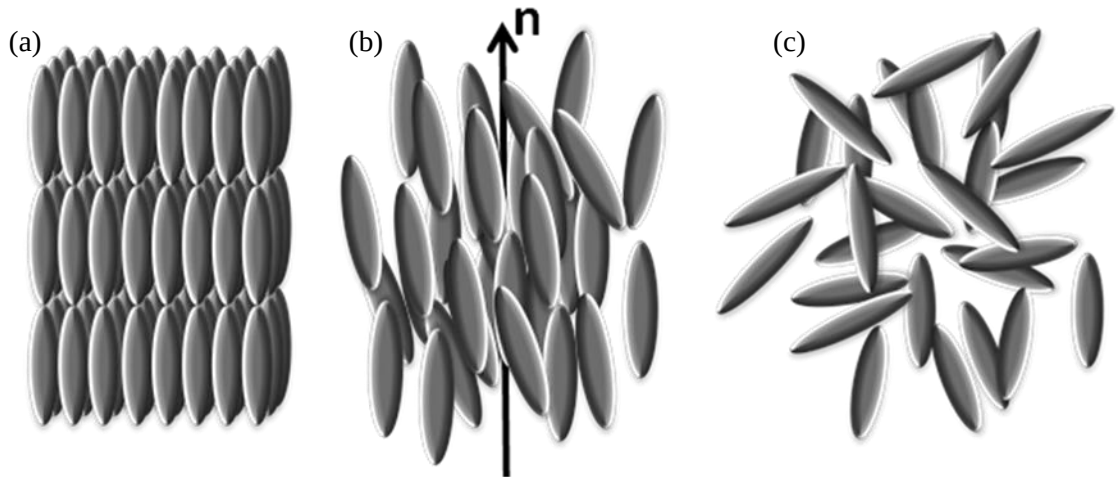

Figure 1.1: Schematic representation of (a) a crystalline solid, (b) a nematic liquid crystal and (c) an isotropic liquid.

A large variety of different materials can display liquid crystal phases. Lyotropic liquid crystal compounds, such as surfactants, display liquid crystal phases within a concentration range when dissolved in a solvent, often water.[21] Lyotropic liquid crystals have applications as detergents for cleaning products, as drug coatings which prevent premature release of the drug in the stomach[22] and are present in nature, for example DNA.[23] As these liquid crystal phases are displayed when the material is dissolved, the phase structure is highly dependent on concentration as well as on temperature.[24]

Compounds which exhibit liquid crystal phases within temperature ranges without being dissolved are referred to as thermotropic liquid crystals. The structure of the mesogens and the morphology of the liquid-crystal phases they form can vary greatly. Thermotropic liquid crystals, in particular the nematic phase, are best known for their application in displays.[17, 25] A thermotropic liquid crystal phase is not always observed upon heating as super-cooling of the liquid crystal can allow for a mesophase to be observed on cooling only, referred to as a monotropic phase transition. Transitions that occur on heating and cooling are known as enantiotropic phase transitions. Within this thesis the results are exclusively related to thermotropic liquid crystals, in particular thermotropic nematic materials, and so will be further discussed in the following.

1.2.1 *MESOGEN SHAPE*

The illustration in Figure 1.1(b) is representative of a nematic liquid crystal phase formed by rod-like molecules[20] in which the mesogenic units are rigid and approximately linear with one

significantly longer molecular axis. Although a typical rod-like mesogen has three different molecular axes, due to fast rotation (~10^{11} s^{-1}) about the longest axis[26] the mesogen is of degenerate symmetry about the long axis and its shape can therefore be approximated to that of a rod. The rotation about the shorter axes is much slower (~10^{6} s^{-1}) due to a lack of rotational freedom when the mesogens are in a liquid crystal phase. These rotation speeds are illustrated in Figure 1.2.

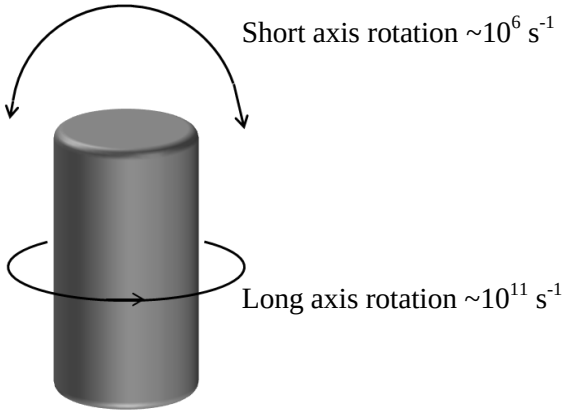

Figure 1.2: Rotations of a rod-like molecule in the nematic phase.

Liquid-crystalline phases can also be displayed by molecules that are disk-shaped[27] as well as by board-shaped mesogens,[28] and mesogens which contain a bent-core moiety.[29, 30] Schematic illustrations of a rod-like and a disk-like mesogen are shown in Figure 1.3.

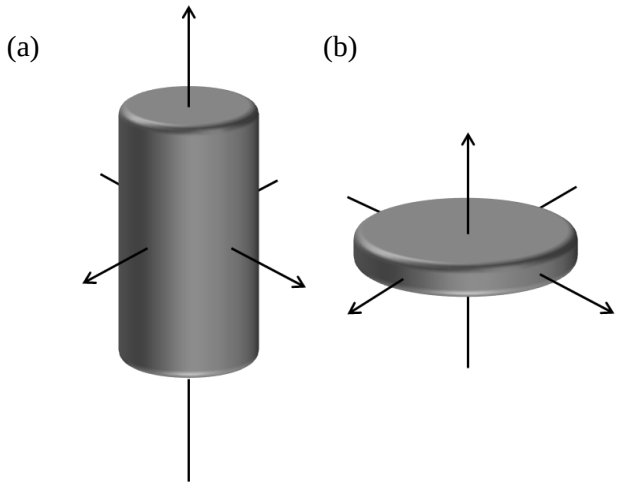

Figure 1.3: Illustration of a (a) rod like and (b) disk like mesogens.

Rod-like liquid crystals have widespread applications in displays.[26] As such, rod-like molecules have more widely understood phases and properties. The following discussions focus on the properties of the nematic phase of rod-like liquid crystals as they are the main focus of this thesis.

1.2.2 *STRUCTURE-PROPERTY RELATIONSHIPS IN THE NEMATIC PHASE*

A large number of nematic liquid-crystalline materials have been prepared,[17, 20] each with their own specific combination of structural moieties which determine the phase stability, phase transition temperatures, and physical properties of the material. A nematic rod-like liquid crystal will generally comprise of rings, linking groups and terminal substituents as indicated in Figure 1.4. As a certain degree of rigidity provides an anisotropic molecular structure, the core of a mesogen often comprises of linearly linked aromatic systems. A degree of flexibility is usually incorporated *via* terminal substituents in order to produce reasonably low melting points and stabilise the molecular alignment. Often a liquid crystal can comprise of two to four ring units within its core which will result in different length-to-breadth ratios.

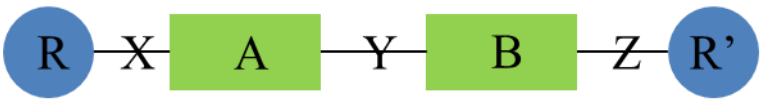

Figure 1.4: A general structural template for a liquid crystal, where A and B are core units, R and R' are terminal substituents and X, Y and Z are linker groups.

Generally, increasing the length-to-breadth ratio of a mesogen leads to the increased thermal stability of the mesophase. This trend is illustrated by the comparison of 4'-pentyl-4-cyanobiphenyl, and 4"-pentyl-4-cyanoterphenyl, shown in Figure 1.5.

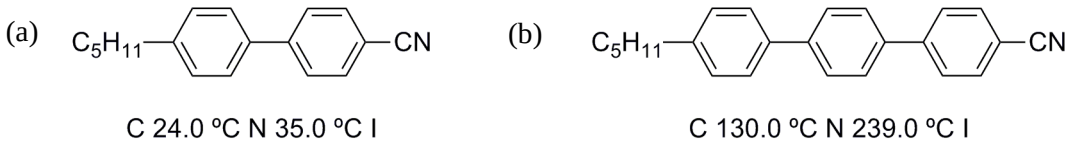

Figure 1.5: Structures and phase transitions of (a) 4'-pentyl-4-cyanobiphenyl, and (b) 4"-pentyl-4-cyanoterphenyl.

The thermal stability of a mesophase can also be increased by altering the terminal moieties of the mesogen in order to enhance the molecular conjugation. For example, replacing a terminal H with CH_3 group will typically improve the thermal stability, which can be increased further if a CN group is incorporated. Selecting appropriate terminal substituents is important as increasing the length of an alkyl or alkoxy terminal substituent extends the molecular length and increases interactions which result in the stabilisation of the nematic phase, whilst also increasing the flexibility of the system resulting in lower melting points and disrupting the molecular packing

required for nematic phase generation. An example of the effect a small change in terminal substituent can have on the resulting phase transitions of the material is illustrated in Figure 1.6 with the comparison of 4'-butyl-4-cyanobiphenyl and 4'-butyloxy-4-cyanobiphenyl.

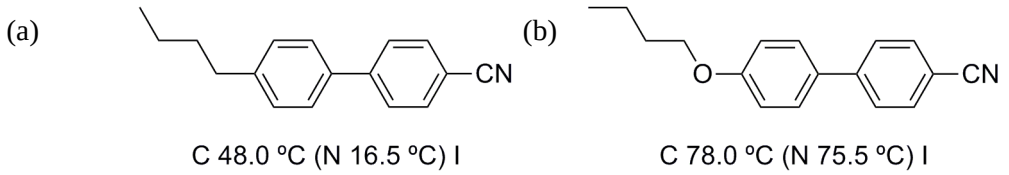

Figure 1.6: Structures and phase transitions of (a) 4'-butyl-4-cyanobiphenyl, and (b) 4'-butyloxy-4-cyanobiphenyl.

As can be seen in Figure 1.6 the addition of an ether linker results in a higher melting point, this is as a result of the ether extending the conjugation and therefore extending the rigid core. The length-to-breadth ratio is also affected by increasing the length of the terminal group and by the wider bond angle of an ether linker compared to a CH_2 linker, which reduces the breadth of the molecule by producing a more linear chain.

1.2.3 *ORDER PARAMETER*

The liquid crystal director, which is shown in Figure 1.1(b) labelled as **n**, is the direction in which the mesogenic units within a liquid crystal phase statistically point. The order parameter, *S*, denotes the average temporal and spatial distribution of the mesogenic units about the director. *S* is defined by equation 1, where θ is the angle at which each molecule is orientated with respect to the director.

$$S = 1/2 <3\cos^2\theta - 1> \quad (1)$$

In a completely random, isotropic orientation S=0, and when a material is perfectly aligned S=1. Within typical liquid crystal phases the order parameter can range from 0.3 to 0.9 and for a typical nematic phase has a value of approximately 0.4 to 0.7,[17] which indicates that the nematic phase is considerably disordered. The order parameter decreases as the temperature is raised towards the isotropic phase transition as a result of increasing disorder. A schematic representation of the correlation of order parameter of a typical nematic liquid crystal against temperature is shown in Figure 1.7. The order parameter decreases slightly within the nematic phase but abruptly becomes zero when the isotropic phase is reached.

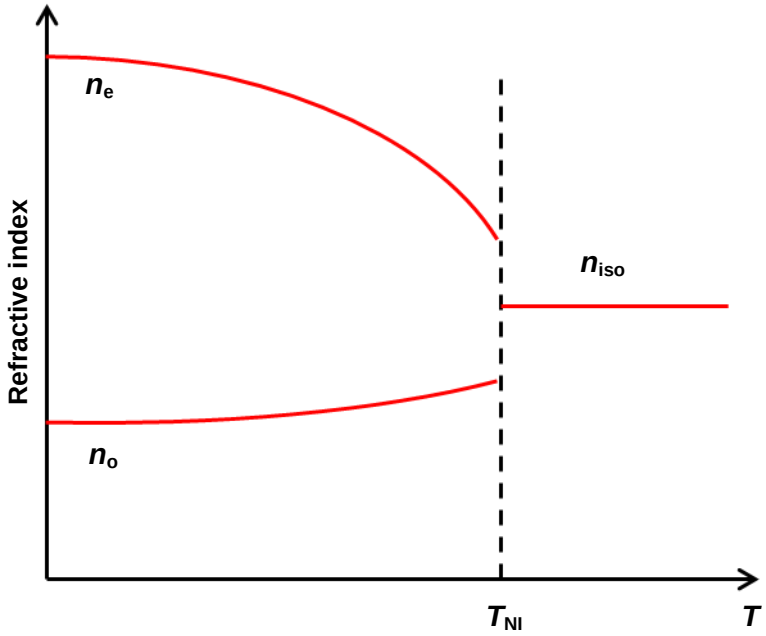

Figure 1.7: A representative plot of the ordinary (n_o) and extraordinary (n_e) refractive index against temperature (T) for a typical nematic liquid crystal with positive birefringence ($n_e > n_o$).

1.2.4 *ELASTIC DEFORMATIONS*

The lowest energy state of a liquid crystal would be a uniform director profile in which no defects are observed, though this is rarely observed naturally without an external influence such as an alignment layer or electric field. The Frank elastic constants K_1, K_2 and K_3 describe the energetic cost for the liquid crystal to undergo splay, twist and bend deformations from a uniform director profile, respectively.[18, 31] These elastic constants are different for each liquid crystal and vary in magnitude based on the order parameter of the phase, though are typically in the region of approximately 10^{-11} - 10^{-12} N.[32] The elastic constants relate to each other as stated in the Frank free energy density equation[31] as shown in equation 2. F is the contribution to the free energy density due to distortions in the phase, K_1, K_2 and K_3 are the elastic constants, and **n** is the normalised director.

$$F = 0.5\,[K_1\,(\nabla\cdot\mathbf{n})^2 + K_2(\mathbf{n}\cdot\nabla\times\mathbf{n})^2 + K_3(\mathbf{n}\times\nabla\times\mathbf{n})^2] \qquad (2)$$

Shown in Figure 1.8 are illustrations of these three bulk elastic distortions in a nematic liquid crystal: the splay, twist and bend deformations. The splay deformation results in a wedge shaped director profile, the twist deformation is as a result of the director turning about a perpendicular axis and the bend deformation is a turning of the director profile in the plane of the director. The relative magnitudes of the elastic constants of a specific liquid crystal determine the energy cost

of different deformations occurring. The deformation which is the most energetically favourable will be the most likely to be observed.

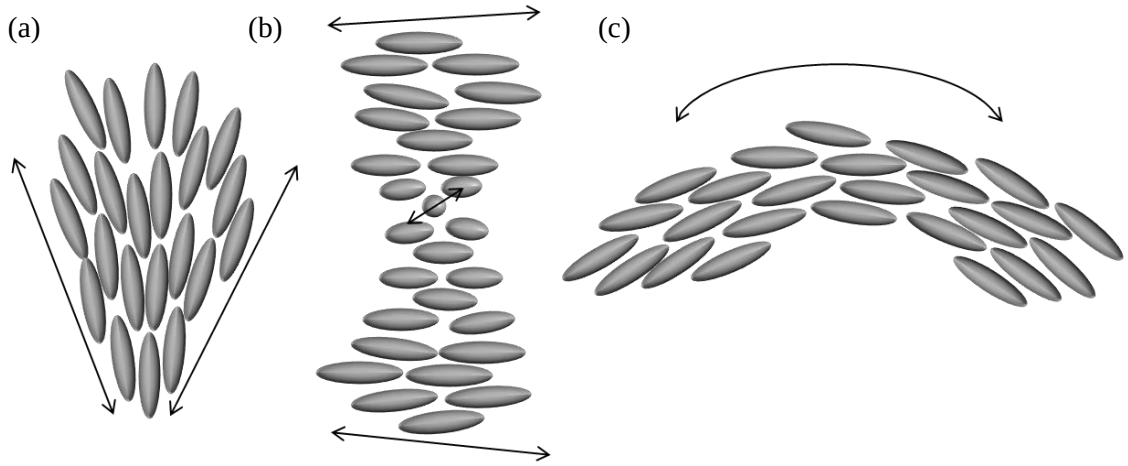

Figure 1.8: The splay (K_1), twist (K_2) and bend (K_3) deformations as they occur in the nematic phase, shown as (a), (b) and (c) respectively.

These deformations will occur naturally throughout the nematic liquid crystal without an external influence, but can also be imposed topologically by confining a liquid crystal. The director profile that is displayed is, as a result, a balance between the most favourable interactions of the liquid crystal with the surface and the most energetically favourable configuration of the liquid crystal within the confinement geometry, and may not be uniform throughout the entirety of the sample depending on the penetration depth of the interactions at the surface. Topological defects are therefore different from bulk defects, as bulk defects occur naturally whereas topological defects are imposed by the boundary conditions.

1.2.5 *DIELECTRIC ANISOTROPY*

A dielectric material is a material that can be polarized by an applied electric field.[33] Liquid crystals display anisotropy in their dielectric properties, such that they possess a dielectric permittivity parallel to the director $\varepsilon_{\text{para}}$, and a dielectric permittivity perpendicular to the director $\varepsilon_{\text{perp}}$. The dielectric anisotropy is the difference between these two permittivities as described in equation 3.

$$\Delta\varepsilon = \varepsilon_{\text{para}} - \varepsilon_{\text{perp}} \tag{3}$$

The dielectric anisotropy is related to the dipole moments within the molecules, as shown by an example in Figure 1.9. If the dielectric anisotropy of a liquid crystal is positive then director will

align parallel to an applied field of sufficient magnitude, whereas if the dielectric anisotropy of a liquid crystal is negative then the director will orientate perpendicular to the field.

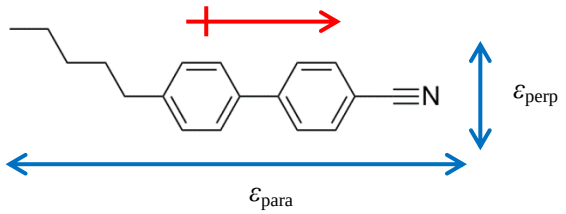

Figure 1.9: Diagram showing the dipole moment (red) and dielectric permittivities (blue) of a material with positive dielectric anisotropy, 5CB (4-cyano-4'-pentylbiphenyl).

1.2.6 *BIREFRINGENCE IN THE NEMATIC PHASE*

The anisotropy of liquid crystals allows for an interaction with light known as birefringence.[19] Optical birefringence is a phenomenon that results when the speed of light passing through an object is dependent on its direction of travel through that object. Thus, an incident light beam entering a birefringent material will be split into two rays, an ordinary ray and an extraordinary ray, which will be deflected at different angles and travel at different velocities. The speeds and velocities of these rays are dependent on the relative refractive indices. The extraordinary ray, which is often the light which is travelling in the direction of the optic axis, experiences a refractive index denoted as n_e. The ordinary ray, which is polarised perpendicular to the extraordinary ray, experiences a refractive index of n_o. The birefringence of a nematic liquid crystal can be defined as seen in equation 4.

$$\Delta n = n_e - n_o \tag{4}$$

A uniaxial liquid crystal is said to be positively birefringent when the extraordinary refractive index is greater than that of the ordinary component, such that Δn is greater than zero. In other words, the faster light direction is perpendicular to the director when the birefringence is positive.

Birefringence is observed for many different anisotropic crystals as well as liquid crystals. Within liquid crystals, the birefringence depends on the temperature of the system. When a liquid crystal is heated the birefringence steadily decreases as n_e and n_o approach each other, following the temperature dependence of the order parameter of the phase. When the isotropic phase is reached, only one refractive index is present and the material is no longer birefringent. This is illustrated in Figure 1.10.

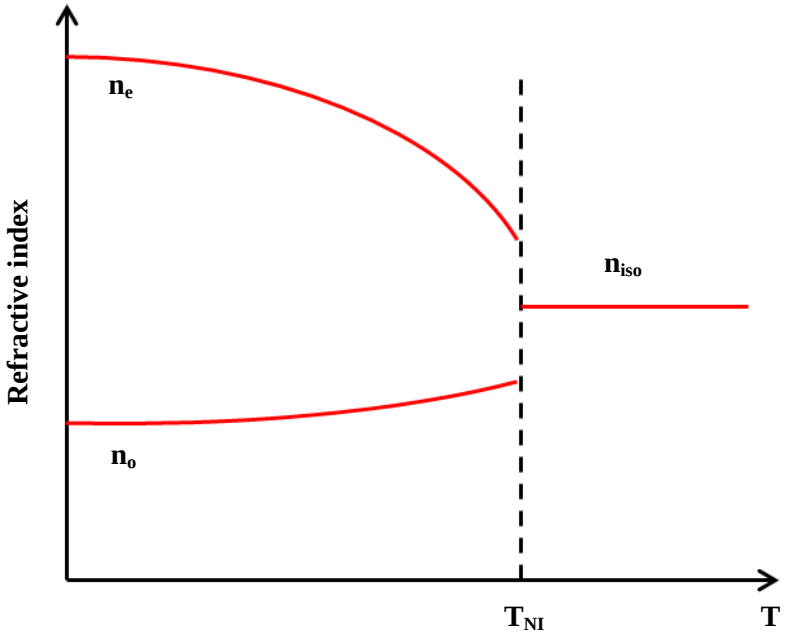

Figure 1.10: A representative plot of the ordinary and extraordinary ray against temperature T for a typical positively birefringent nematic liquid crystal.

1.2.7 *TEXTURES AND DEFECTS IN THE NEMATIC PHASE*

Linearly polarised light is light filtered to give vibration in a single plane, and is illustrated in Figure 1.11. Linear polarised light is utilised in polarised optical microscopy for the determination of liquid crystal phases.

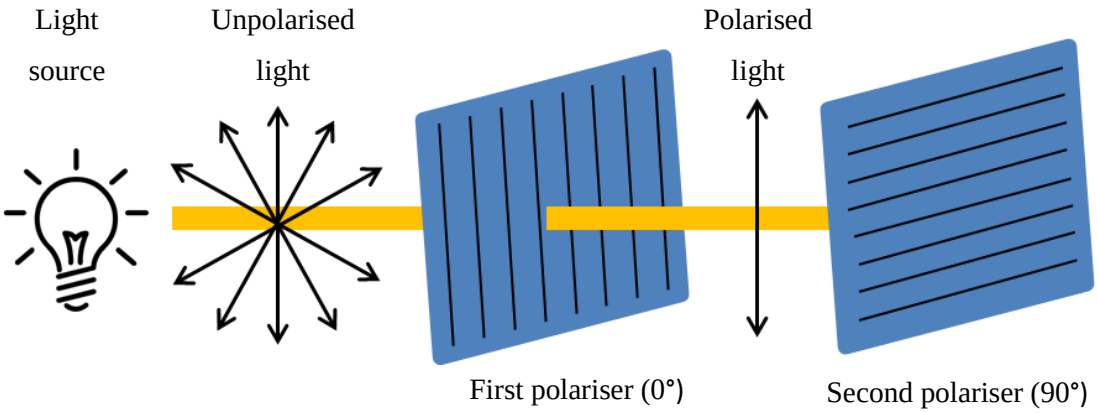

Figure 1.11: Schematic representation of the polarisation of light

Liquid crystal textures and defects can be studied using polarised optical microscopy and with experience allow for the assignment of the liquid crystal phase. Polarised optical microscopy

involves investigating a magnified view of a thin sample of a suspected liquid-crystalline material in between two polarisers, usually orientated at 90° to each other. The microscope slide on which the liquid crystal sample is contained is placed within a hot stage which can be accurately controlled to typically within ~0.1 °C.

Linear polarised light splits when it enters the anisotropic and birefringent nematic phase into ordinary and extraordinary rays with perpendicular polarisation with respect to each other. The rays travel through the birefringent liquid crystal at different speeds and a phase difference is developed which results in the formation of elliptically polarised light. The elliptically polarised light produces interference colours as it passes through the second polariser which gives a texture characteristic to a specific liquid crystal phase.

An example texture that is observed when a nematic phase is viewed using polarised optical microscopy is shown in Figure 1.12.

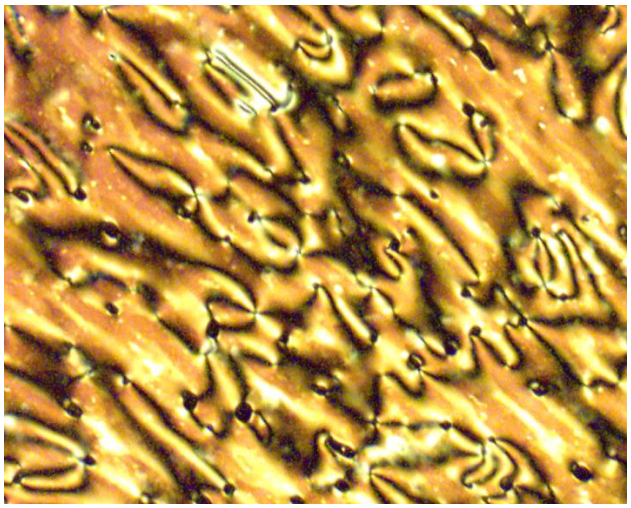

Figure 1.12: An example polarised optical micrograph depicting the *schlieren* texture of the nematic phase. Image taken at 55 °C on cooling at 5°C min^{-1} at 100 X magnification through crossed polarisers. Details can be found in Chapter 3.

The *schlieren* texture, as shown in Figure 1.12, is a texture characteristic of the nematic phase. Other textures which are observed and are typical of nematic phases are the thread-like texture and the marble texture.[34]

Defects are optically extinct singularities and can be seen within a nematic texture.[34] The black lines that emanate from these defects are referred to as *schlieren* brushes. Within the uniaxial nematic phase both 2- and 4- brush defects can exist. The director profile is defined within

schlieren brushes but not at the defect from which they emanate. These brushes appear black as they are regions where the nematic director field is orientated with either a polariser or the analyser, resulting in brushes being optically extinct. The possible mesogenic director configurations around defects which result in *schlieren* brushes in a nematic phase are shown in Figure 1.13.

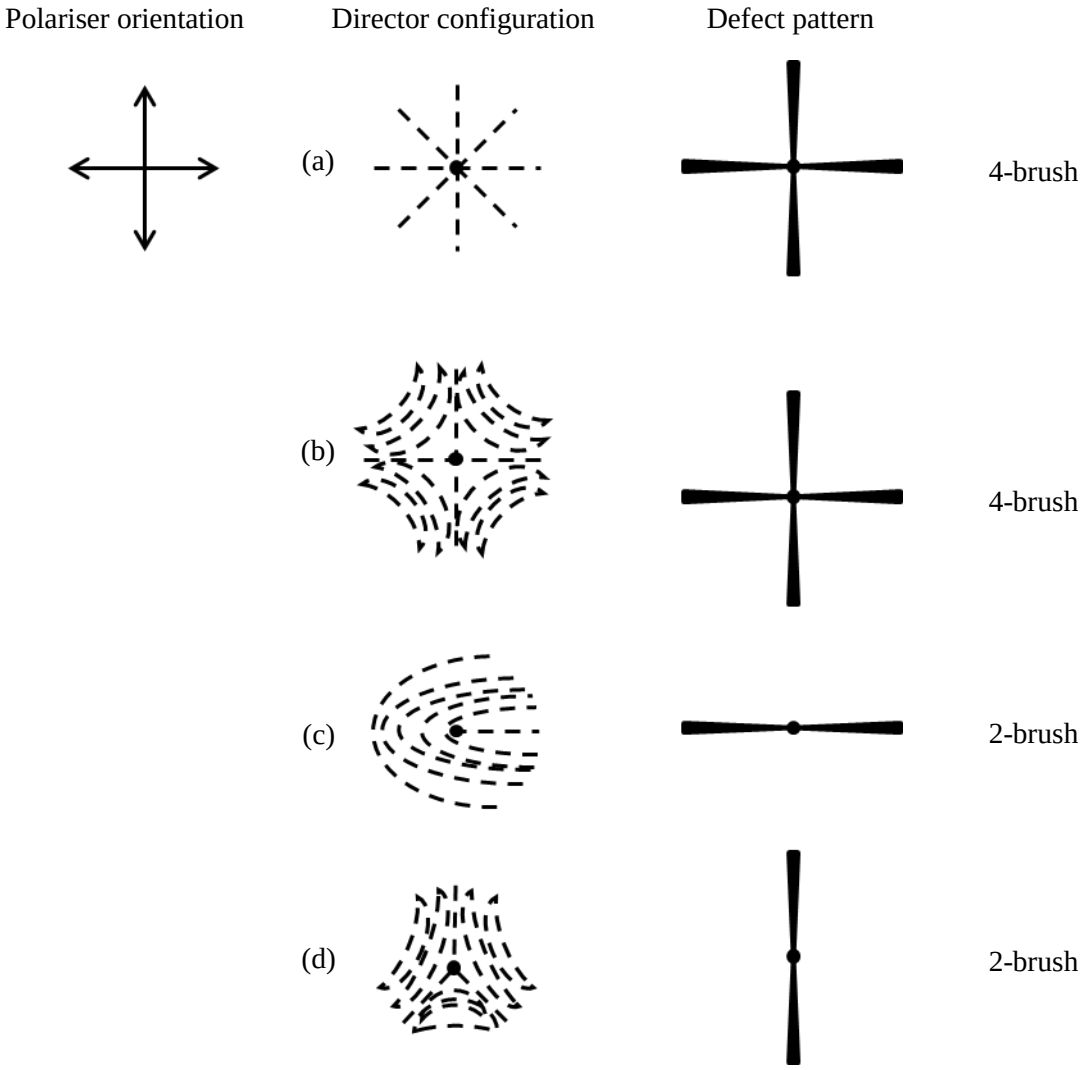

Figure 1.13: Schematic representation of 2- and 4-brush defects present in a nematic *Schlieren* texture.

The formation of *schlieren* brushes that can be seen in Figure 1.13, (a) and (b) result in the formation of 4-brush defects as a result of having four regions around the defect orientated with either the polariser or the analyser and therefore are optically extinct. In (c) and (d) there are only two regions where the mesogenic units are orientated with the polarisers, hence creating 2-brush defects.

1.2.7.1 Alignment layers

In order to promote a specific orientation of the mesogenic units within a thin film of nematic liquid crystal, the surface that the liquid crystal comes in contact with can be treated with an alignment layer. Alignment layers can promote a uniform, defect free organisation of the liquid crystal in a flat, thin film between two surfaces. Alignment layers can effectively orientate a liquid crystal sample, providing the strength of the interactions at the surface is sufficient to promote surface alignment throughout the whole sample.

Alignment layers can be chosen to promote either homogeneous or homeotropic alignment of the mesogens. Homogeneous and homeotropic alignment are illustrated in Figure 1.14.

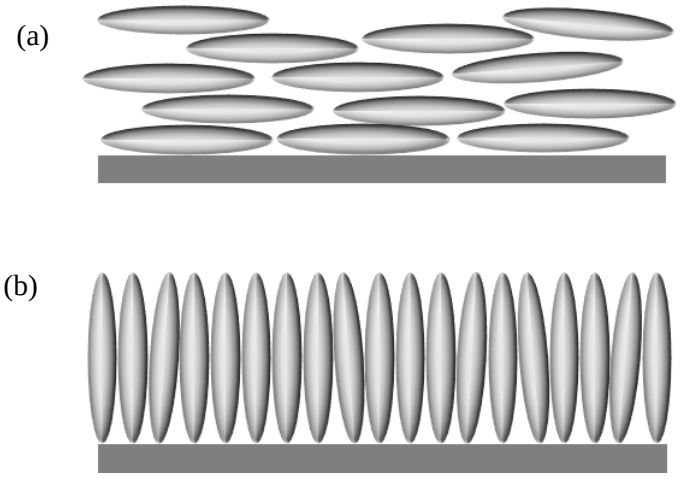

Figure 1.14: A schematic representation of (a) a homogeneous and (b) a homeotropic alignment of a liquid crystal.

As depicted in Figure 1.14, homogeneously aligned liquid crystals oriented parallel to the glass will have a defect-free birefringent appearance. Homeotropic alignment can be imparted by silanes such as octadecyltrichlorosilane (ODT) and lecithin. Homeotropically aligned liquid crystals are oriented perpendicular to the glass and appear dark when viewed using polarised optical microscopy as they are being viewed along the optic axis of the sample.

For display technologies, the main aim is the creation of a defect-free aligned thin film between parallel or perpendicular alignment layers. However, if one deviates from this scenario, defects can be created at will by choosing the correct confinement geometry. For the purpose of this thesis, spherical confinement including the dispersion of liquid crystals into microscale droplets,

is the most relevant and shall therefore be the subject of further discussion within this introduction.

1.3 NEMATIC LIQUID CRYSTALS IN SPHERICAL CONFINEMENT

Nematic liquid crystals can be confined within many different topologies, for example in mesoporous silica channels,[35-37] as droplets with handles,[38, 39] as dumbbells or as hollow droplets or shells,[1, 40-42] each with their own intrinsic director configurations. The confinement most relevant to the results discussed herein is within colloidal spherical droplets dispersed in an isotropic liquid as the host medium. The two most commonly observed director configurations for liquid crystals dispersed as spherical droplets are named bipolar[43] and radial[44] and are shown in Figure 1.15. These director configurations result from a preferred parallel and perpendicular organisation at the droplet surface, respectively.

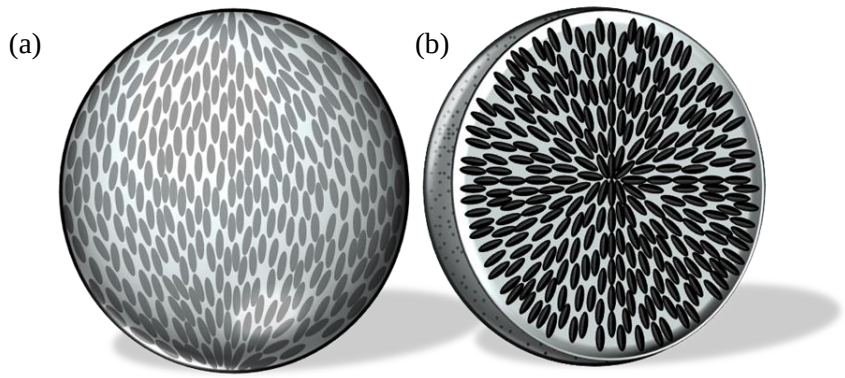

Figure 1.15: Illustrations depicting the internal mesogenic organisations of (a) bipolar and (b) radial liquid crystal droplets.

1.3.1 *BIPOLAR DROPLETS*

In bipolar droplets the nematic mesogens lie parallel to the surface, coalescing at two surface boojums at opposite sides of the droplet. These surface defects result in an extinction pattern in polarised optical microscopy that is dependent on the orientation of the droplet between the crossed polarisers, changing from a baseball extinction pattern to that of a Maltese cross as it rotates.[36] This characteristic changing texture is illustrated in Figure 1.16.

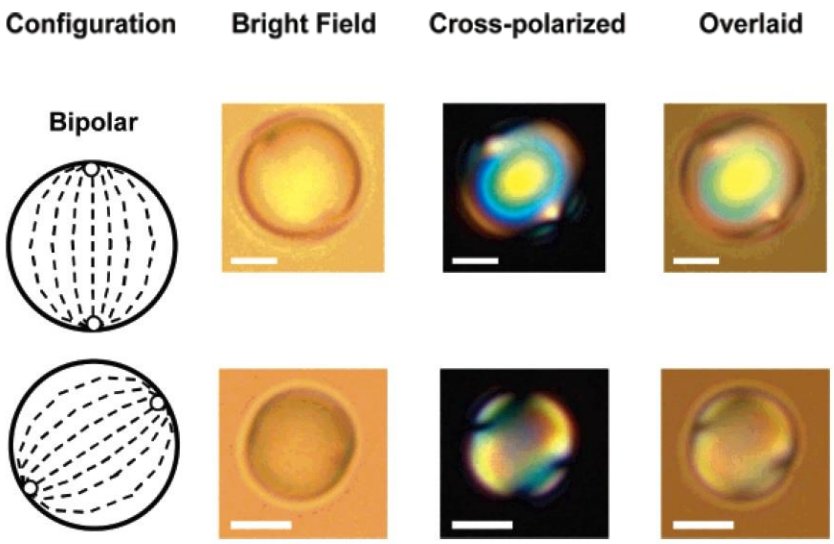

Figure 1.16: The bipolar extinction pattern changes on rotation. Reproduced from literature.[45]

The bipolar texture is the lowest energy director configuration with parallel surface anchoring as a result of the two surface defects being point defects at maximum distance from each other. A bipolar texture will be observed when the host medium or a surface analyte within the host medium imparts parallel surface anchoring so long as the favourability of this interaction exceeds the energetic cost of the bend deformation of the liquid crystal around the surface. The energy cost of the bend deformation will depend on liquid crystal itself as well as the relative droplet size as this influences the curvature that the liquid crystal is experiencing at the surface. Should the deformation energy increase, for example by an increase in surface curvature resulting in a much greater deformation, then once the energy cost exceeds that of the surface anchoring the liquid crystal is more likely to organise as dictated by the bulk and ignore surface influence. Generally, bipolar droplets are observed when liquid crystals are dispersed in polar solvents because polar solvents tend to impart a parallel surface anchoring at the liquid crystal droplet surface.[43, 46]

1.3.2 *RADIAL DROPLETS*

The radial director configuration results from a perpendicular surface anchoring of the mesogenic units, with the director profile coalescing into a central hedgehog defect. Radial droplets display a Maltese cross extinction pattern when observed by polarised optical microscopy independent of the particle's orientation between the crossed polarisers. This Maltese cross extinction pattern is shown in Figure 1.17. The elastic deformation of greatest importance with respect to the radial director configuration is the splay deformation, as the mesogens emanate from the central defect outwards towards the surface of the droplet. The perpendicular surface anchoring which results in

the liquid crystal organising into the radial director configuration is usually imparted by hydrophobic dispersing media or surface analytes such as sodium dodecyl sulfate (SDS).[3, 47]

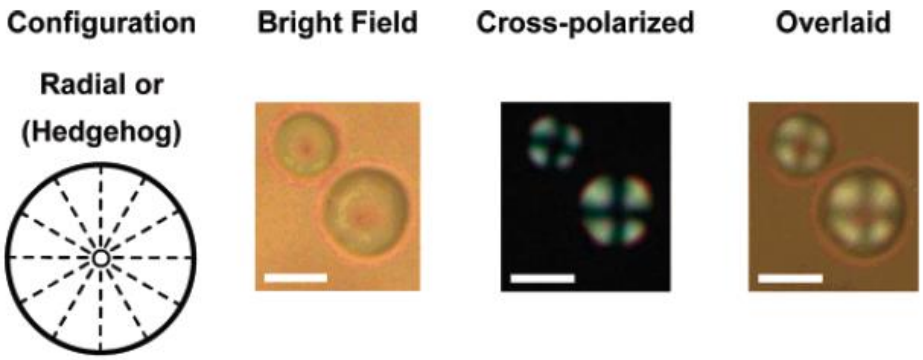

Figure 1.17: The radial extinction pattern shows a Maltese cross independent of orientation between the polarisers as a result of being symmetrical. Reproduced from literature.[45]

1.3.3 *OTHER DIRECTOR CONFIGURATIONS*

There a number of additional director configurations that can result when a nematic liquid crystal is dispersed on the microscale. Some of them are illustrated in Figure 1.18. These director configurations are often not the lowest energy configurations possible for a droplet in a particular solvent, and are escaped configurations that exist in the transition between two director configurations.[36]

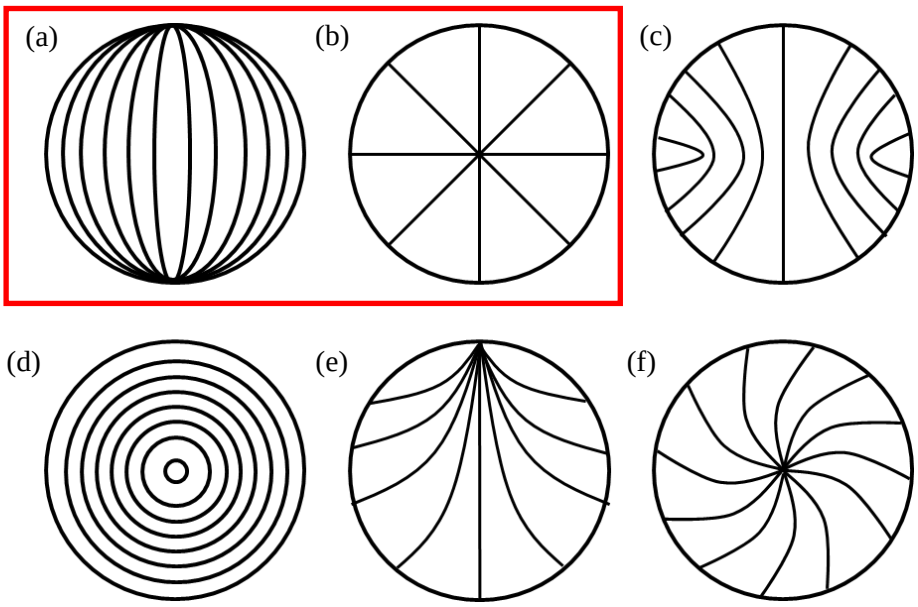

Figure 1.18: Director configurations found within liquid crystal droplets (a) bipolar (b) radial (c) axial (d) concentric (e) escaped radial and (f) twisted radial.

All of the director configurations discussed thus far relate to droplets of nematic liquid crystal, which bear the most relevance to the results discussed in this thesis. However, if a smectic liquid crystal is confined to a spherical droplet then the director configurations that can be observed may be different as a result of the smectic liquid crystal's layered structure. Most smectic director configurations for droplets contain a defect line as a result of the spherical shape not being conducive for the organisation of layers.[42, 48, 49]

1.3.4 *RESPONSIVE PROPERTIES*

As the director configuration that will be displayed by nematic droplets is as a result of a balance between the bulk and surface interactions of the liquid crystal, a change of director configuration can be observed on altering parameters such as droplet size (and therefore surface curvature), or surface anchoring parameters, *e.g.* by changing the dispersing solvent or the addition of a surface analyte.

Droplets of 5CB dispersed in water were evaluated by Abbott *et al.* for trends in director configuration with droplet size.[2, 3] 5CB droplets of approximately 10 μm in size display a bipolar configuration when dispersed in water as a result of a preferred parallel alignment at the droplet surface. The surface anchoring dictates the director configuration that is displayed as at this size, 5CB can accommodate the surface curvature. The bipolar configuration transforms on decreasing size into a radial configuration at sizes below approximately 1 μm *via* the escaped radial configuration as a result of the increasing curvature increasing the energy cost of the bend deformation. As the bend deformation becomes energetically unfavourable, the preferred surface anchoring is ignored in order to accommodate a less costly elastic deformation of the liquid crystal. This finding of a transformation to a radial configuration on decreasing the droplet size of 5CB in water is in direct contrast to computational investigations[50, 51] which predicted that at sizes below 1 μm the liquid crystal would ignore the surface and the confinement completely and display a uniform texture. These results are not necessarily transferrable to systems which involve other liquid crystal dispersions as the relative energies of the elastic deformations will be different. For 5CB, K_3 is greater than K_1 and so at high curvature the splay deformation is preferred. Different rod-like nematic liquid crystals will have elastic constants of different magnitudes and will therefore switch director configurations at different points.

The switch between the bipolar and radial director configuration on addition of analytes has also been observed for droplets of 5CB dispersed in water.[3, 52] In pure water, droplets of 5CB adopt a bipolar director configuration as a result of a preferred parallel surface alignment being imparted

by the solvent. On addition of sodium dodecyl sulfate (SDS) the director configuration changes to a radial configuration *via* an escaped radial intermediate. SDS is a surfactant that can be used to promote a perpendicular surface anchoring[45] in between flat surfaces, and is known to promote perpendicular surface anchoring in droplets of 5CB by creating a pseudo-hydrophobic environment around the droplet. As this transformation does not involve a change in the liquid crystal or the droplet size the switch must be purely controlled by changes in the surface anchoring. This responsive nature of liquid crystal droplets to changes in their external environment gives them applications as sensors on the microscale.

Nematic droplets have been used for the sensing of changes in pH,[22, 53] as well as sensing the presence of E-coli,[5] among others.[6, 47, 52, 54, 55] The response of droplets to magnetic and electric fields has also been investigated.[56, 57] Spherical liquid crystal droplets are good sensors because their large surface area to volume ratio means the internal mesogens experience a large influence from the surface, and are therefore more sensitive to changes in surface anchoring. Droplets as sensors have the added benefit of being able to pinpoint the location of the substance being detected within the sample as the director configuration of the droplets changes. Sensors in use today, for example dyes,[58] show a sample wide change on the addition of the substance to be detected and do not give information on the extent to which the substance has travelled through the sample. Dyes are also hard to remove from samples as they are dissolved within the sample. The droplets are immiscible and will therefore be less likely to affect the sample by interacting with the chemistry.

1.3.5 *CREATING NEMATIC DROPLETS*

The simplest method to create a dispersion of liquid crystal droplets is to shake a liquid crystal with an immiscible liquid. A more viscous immiscible liquid such as glycerol or silicone oil will increase the lifetime of the droplets by slowing down coalescence. This method produces droplets with a large degree of droplet size polydispersity, but this allows for deductions to be made about the effect of the droplet size on its response capabilities or director configuration. The size of the droplets created by this method can be reduced further by using a sonic bath in order to create the dispersion, which depending on the viscosity of the system can allow for the creation of droplets within the size range of a few micrometres. Steric stabilisers such as hydroxypropyl cellulose, poly(vinyl acetate) (PVA) or poly(vinylpyrrolidone) (PVP) can also be added into the dispersions which slow coagulation and hinder the approach of a second droplet by coating the droplet surface in extended polymer chains.[59]

Polymer dispersed liquid crystals (PDLCs) are another method by which liquid crystal droplets can be formed.[36, 60-62] PDLCs are typically produced by creating a homogeneous mixture of reactive monomer and liquid crystal which phase separates into droplets on polymerisation of the supporting polymer matrix, which can result in significant droplet size polydispersity.[63] PDLCs can also be synthesised in methods similar to these described for liquid-in-liquid dispersions, polymerising the matrix after the droplets of liquid crystal have been dispersed within it.[64] This method also creates a sample with a large degree of size polydispersity. The size of the droplets can be further reduced in this case by adding a co-solvent to the liquid crystal which is then evaporated before polymerisation. PDLCs can be used for switchable windows[65] as they can be switched from scattering (frosted) to transparent. In Figure 1.19(a) the PDLC has not been exposed to an electric field and the directors of the internal droplets are randomly orientated. Due to the random orientation of the liquid crystal droplets, any incident light is scattered resulting in an opaque appearance.[66] When a field is applied across the PDLC (Figure 1.19(b)), the directors within the droplets re-orient themselves along the direction of the applied field which allows light to travel through the system with minimal scattering as the droplet and polymer matrix are refractive index matched.

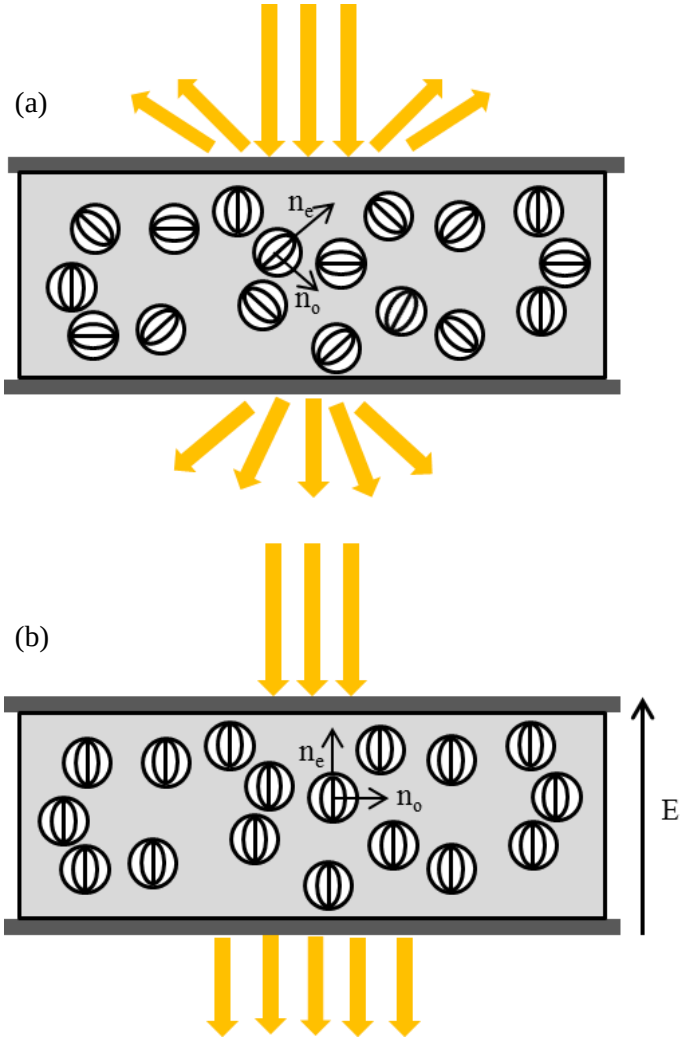

Figure 1.19: A polymer dispersed liquid crystal device for switchable windows (a) in the off state light is scattered (b) when an electric field is applied scattering in minimal.

Monodisperse liquid crystal droplets or droplets of a very specific size have been created by filling pre-synthesised polymer shells [67] made by polymerising a coating around premade silica particles and etching away the inside ready for filling.[2, 3] This method can be used to assess the correlation of droplet size to director configuration as it allows for fine control of the droplet size. This method may result in the droplets being less sensitive to changes in their external environment as a result of having a coating surrounding them. The liquid crystal will experience the surface anchoring induced by the polymer capsule, but the surface anchoring of the solvent may not penetrate sufficiently to orientate the director.

Monodisperse droplet dispersions and PDLCs have been created using microfluidics, a process by which a stream of liquid crystal is extruded into a co-flowing liquid.[68-71] The size of the droplets

that are obtained by microfluidics is limited by the size of the capillary from which the liquid crystal is extruded, as well as the viscosity of the extruded liquid crystal, resulting in droplets with a diameter no smaller than ~20 µm. Solvent can be added to the liquid crystal stream in order to reduce the size of the liquid crystals droplets, as it reduces the viscosity of the liquid crystal allowing for the extrusion of smaller droplets. The removal of the solvent by evaporation in order to reinstate the liquid crystal phase within the droplets will also result in a further size reduction. A schematic of a standard microfluidics set-up is shown in Figure 1.20.

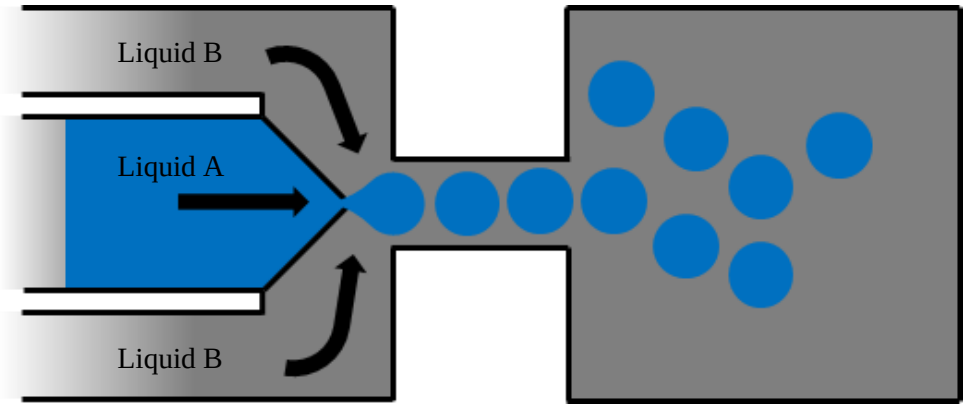

Figure 1.20: A schematic representation of a microfluidics device forming droplets of a liquid A within a co flowing liquid B. In the case of the creation of liquid crystal droplets, liquid A is a liquid crystal.

By using a polymerisable substance within the co-flowing liquid in microfluidics the dispersing liquid can be polymerised to form a monodisperse PDLC. Although microfluidics creates monodisperse samples it can only create relatively small samples of droplets and is therefore limited to small scale processes and would be unsuitable for industrial scale applications.

Application of colloidal liquid-crystalline droplets is somewhat limited by their lifetime and fragile nature. They cannot easily be transferred from one solution to another, cannot be excessively heated and will coagulate over time if suspended in free solution. Polymer dispersed droplets have much longer lifetimes but are not applicable as sensors as the droplet surface is surrounded by the polymer matrix and is therefore inaccessible to surface analytes. Additionally, liquid crystal droplets cannot be easily removed from a sample as they are fluid in nature – they therefore cannot be filtered. Centrifugation should allow the dispersing solution to be removed from the droplets but in this process the droplets are likely to be destroyed.

A major target of the research described in this thesis is to create nematic polymer particles and to investigate the potential for control of the director configuration in a similar way to what is observed for nematic droplets. Therefore, nematic polymers will now be introduced.

1.4 NEMATIC POLYMERS

Liquid crystal polymers are polymers within which a mesogenic moiety is incorporated. There are a number of different polymerisable units that can be incorporated onto a mesogen and this has an effect on the type of liquid crystal polymer that will result. The mesogens can be incorporated into the backbone of a polymer, as shown in Figure 1.21(a) to yield main-chain liquid crystal polymers, or the mesogens can be attached to the polymer backbone as a pendant group *via* a flexible spacer, as shown in Figure 1.21(b) and (c) to yield laterally attached side-chain liquid crystal polymers and terminally attached liquid crystal polymers respectively.

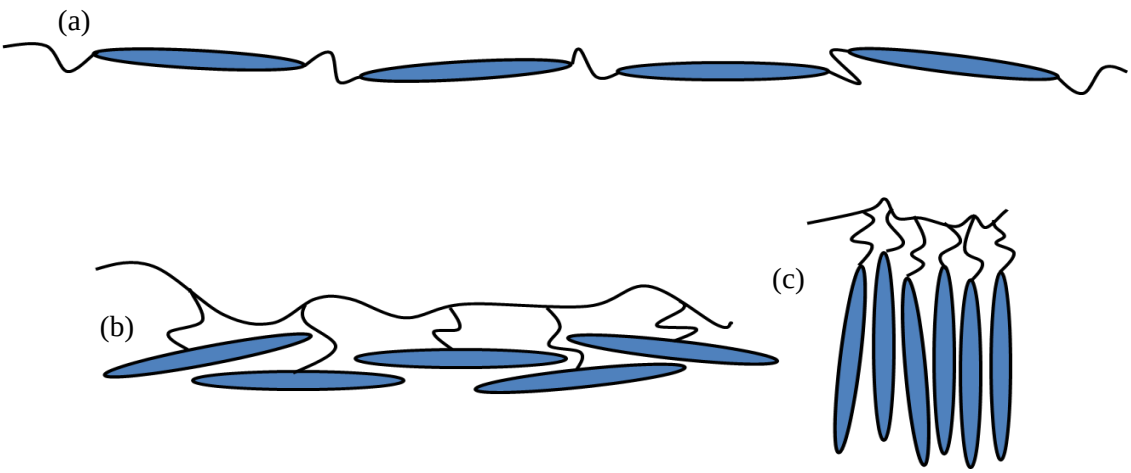

Figure 1.21: Schematic of (a) a main-chain liquid crystal polymer (b) a laterally attached side-chain liquid crystal polymer and (c) a terminally attached side-chain liquid crystal polymer.

Liquid crystal polymers often have an anisotropic polymer backbone conformation rather than an isotropic random coil conformation which is observed for non-mesogenic polymers. This anisotropy arises as a result of the coupling of the orientation of the ordered mesogenic units with the polymer backbone segments. The degree of anisotropy that the polymer chains display is dependent on the order parameter (S) of the liquid crystal, the degree of coupling to the mesogenic units and the temperature of the system.

1.4.1 *INFLUENCE OF THE POLYMER BACKBONE*

The polymerisable unit of the monomer, and therefore the polymer backbone, has a significant influence on the chemical and physical properties of the nematic polymer as a result of affecting the flexibility of the system. Some example polymer backbone structures are shown in Figure 1.22. Polymers featuring a methacrylate polymer backbone (indicated in Figure 1.22(a)) are quite rigid in nature. The flexibility increases when an acrylate polymer backbone is employed (indicated in Figure 1.22(b)) and increases further still for polysiloxanes (indicated in Figure 1.22(c)).

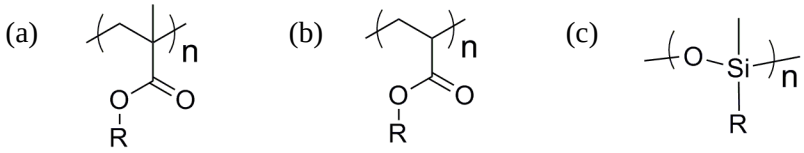

Figure 1.22: Examples of polymer backbone structures (a) a polymethacrylate, (b) a polyacrylate and (c) a polysiloxane.

The glass transition temperature decreases across the series due to the increasing flexibility of the backbone, and the nematic phase range of the polymer often increases as a result.

Flexible backbones reduce the coupling between the mesogen and the polymer backbone because the random-coil formation of a flexible chain is more easily distorted than that of a rigid one. With a flexible polymer backbone, the mesogenic organisation controls the conformation of the polymer backbone; conversely in rigid systems the polymer backbone conformation influences the mesogenic alignment and can affect the ability of the mesogenic units to organise. Therefore, polymers with more flexible backbones are more likely to show liquid-crystalline phase transitions as the mesogenic units have more freedom to organise anisotropically, as a result of being more decoupled.[20, 72]

Investigations were completed[73, 74] in order to quantitatively assess the effect of the polymer backbone on the phase transitions of liquid crystal polymers for which the mesogen and spacer groups were kept constant. A summary of the findings is shown in Figure 1.23.

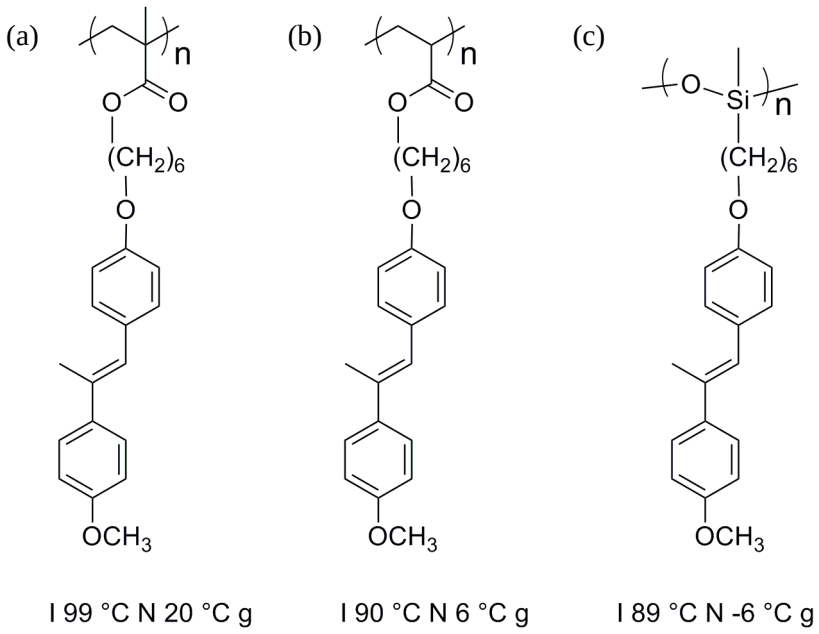

Figure 1.23: Liquid crystal polymers featuring a 6-[4-(4-methoxy-β-methylstyryl)phenoxy]hexyl side groups and (a) a methacrylate polymer backbone, (b) an acrylate polymer backbone and (c) a siloxane polymer backbone.

Increasing the flexibility of the polymer backbone across the series from polymethacrylate to polysiloxane reduces the glass transition temperature of the polymers and hence increases the phase range of the nematic phase, as can be seen in Figure 1.23.

The acrylate group polymerises to form a flexible polymer backbone which allows for the formation of liquid-crystalline phases whilst remaining compatible with heterogeneous polymerisation methods, and so shall be the polymerisable unit used within this thesis.

1.4.2 *Main chain liquid crystal polymers (MCLCP)*

As the mesogenic unit is incorporated directly into the polymer backbone within main chain liquid crystal polymers, they display a large degree of polymer chain anisotropy. If the linker group between the mesogenic units within the polymer backbone of a main-chain liquid crystal polymer is very short, the polymer remains quite rigid and cannot facilitate a layered structure, hindering the formation of smectic phases within the polymer.[17, 72] Main chain polymers with longer flexible units however, can more easily arrange in a layered configuration and smectic phases can be displayed.

An example of a main-chain liquid crystal polymer is shown in Figure 1.24, and is comprised of alternating rigid and flexible sections which provide a low enough glass transition temperature for liquid crystal phases to be exhibited.

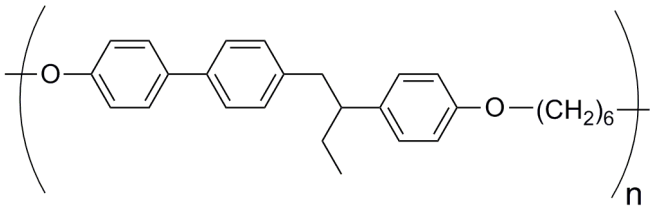

g 65 ºC N 135 ºC I

Figure 1.24: An example of a main chain liquid crystal polymer which can exhibit a nematic phase.

Main-chain liquid crystal polymers are not a focus within this research as the polymerisation methods typically used to create them cannot be easily adapted for creation of particles with heterogeneous polymerisation methods in polar solvents.

1.4.3 *SIDE CHAIN LIQUID CRYSTAL POLYMERS (SCLCP)*

In side-chain liquid crystal polymers, a flexible spacer is required in order to allow for the formation of the liquid crystal phase, as without a spacer present the random coil formation of the polymer backbone can dominate and supress the anisotropic organisation of the side groups and therefore the liquid crystal phase.[17, 73, 74] By increasing the length of the flexible spacer moiety the motions of the mesogenic units can be decoupled from those of the polymer backbone.[75] If there is sufficient coupling between the mesogenic units and the polymer backbone then the backbone will also display a degree of anisotropy imposed on it by the mesogenic organisation.

The pendant groups of a side-chain liquid crystal polymer can be attached *via* a terminal linker, and as such will be positioned perpendicular to the polymer backbone. These polymers are referred to as terminally attached side chain liquid crystal polymers.[76] The mesogenic units can also be attached laterally to the polymer backbone *via* a flexible spacer attached to the middle of the mesogenic unit, resulting in the mesogenic unit being positioned generally parallel to the polymer backbone. These systems are often referred to as laterally attached side chain liquid crystal polymers.[77]

Some example monomers which polymerise to form terminally attached side-chain liquid crystal polymers are shown in Figure 1.25.

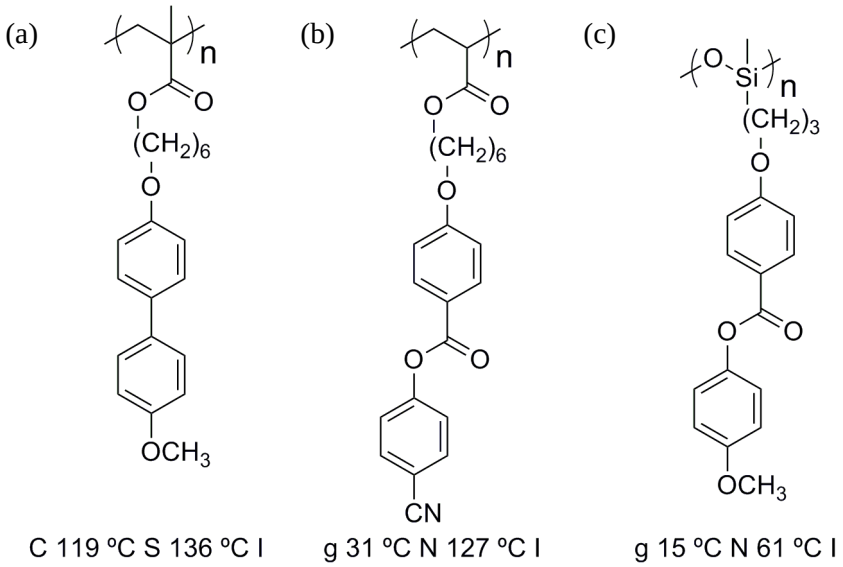

Figure 1.25: Examples of terminally attached side chain liquid crystal polymers (a) with a methacrylate polymer backbone (b) with an acrylate polymer backbone and (c) with a siloxane polymer backbone.

The polymer which is shown in Figure 1.25(b) exhibits a low glass transition temperature and wide nematic phase. This monomer has been used in previous investigations into the synthesis of liquid-crystalline polymer particles[78, 79] and so was an appropriate choice for investigation within this thesis as a proof-of-principle polymer.

Typically, in side-chain liquid crystal polymers with end-on attached mesogens, the backbone is oblate in conformation as the mesogenic units sit generally perpendicular to the polymer backbone. The angle of the mesogenic unit relative to the polymer backbone, and therefore the degree to which the polymer is either oblate or prolate, can be altered by changing the parity of the flexible spacer. An example of this odd – even effect with respect to terminally attached side-chain liquid crystal polymers is illustrated in Figure 1.26.

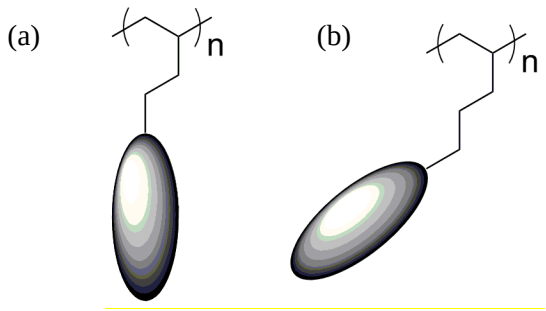

Figure 1.26: Odd-even effect of terminally attached side chain liquid crystal polymers (a) odd numbered spacer group, and (b) even numbered spacer group.

Laterally attached side chain liquid crystal polymers typically have a prolate backbone formation and do not often display smectic phases as the organisation of the mesogenic units does not facilitate a layered structure.[17] Mostly, laterally attached side-chain liquid crystal polymers will exhibit the nematic phase. Laterally attached side-chain liquid crystal polymers typically have a greater degree of coupling between the mesogenic unit and the polymer backbone which can result in the degree of anisotropy within the polymer backbone closely reflecting that of the mesogenic units.

Some example monomers which polymerise to form laterally attached side-chain liquid crystal polymers are shown in Figure 1.25.

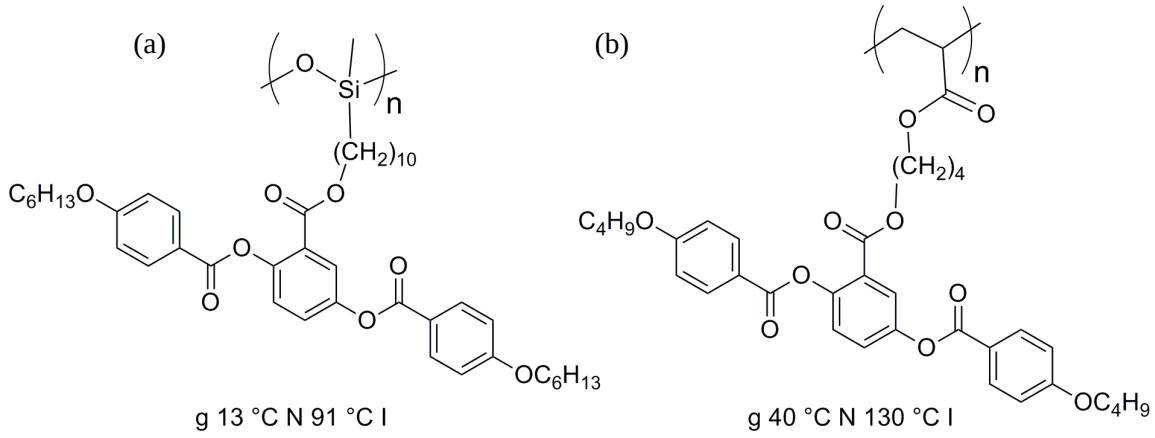

Figure 1.27: Examples of laterally attached side chain liquid crystal polymers (a) with a siloxane polymer backbone and (b) with an acrylate polymer backbone.

The polymer which is shown in Figure 1.27(b) exhibits a low glass transition temperature and generally wide nematic phase in. This nematic polymer has been previously studied[80, 81] and is known to exhibit an anisotropic polymer backbone with good responsive properties and so was an

appropriate choice for investigation within this thesis. It is also a polymer that has been widely studied for its actuation properties in liquid-crystalline elastomers.[11, 12, 15, 75, 77, 82] The formation of nematic elastomer particles is a significant aim within this thesis, and so nematic elastomers shall be the next topic introduced.

1.5 NEMATIC ELASTOMERS

Elastomeric liquid crystals are polymeric liquid crystals with a significant enough degree of crosslinking to result in full networking of the polymer chains. A fully networked liquid crystal elastomeric system is insoluble, swellable and if aligned may have the ability to actuate (described later).[15, 80, 83-86] Shown in Figure 1.28 is an illustration of an elastic network compared to a polymeric sample.

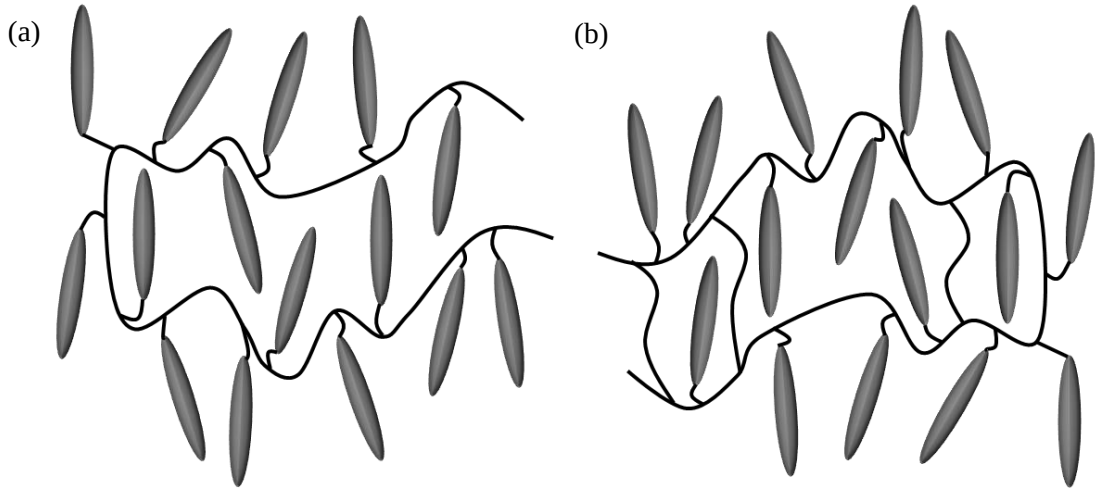

Figure 1.28: (a) a polymeric liquid crystal and (b) an elastomeric liquid crystal.

Elastomeric liquid crystals show similar liquid crystal textures to their low molecular weight and polymeric liquid crystal counterparts, though they do not display the same phase transitions because they do not flow. The crosslinking present in a liquid crystal elastomer can disrupt the liquid-crystalline order, often resulting in polydomain samples and smaller liquid crystal phase ranges than their polymeric counter parts. Crosslinking also results in increased rigidity which results in a higher glass transition temperature.

An elastomer film can be prepared by a variety of different methods, the simplest of which is to create a homogenous mixture of reagents, including a nematic monomer, crosslinker and initiator, and polymerise the mixture either when spread as a thin film or after filling a well of specific morphology.[11] The free radical polymerisation can be initiated either thermally or by UV

initiation, depending on the polymerisation initiator that is employed. Should it be required to impart nematic order on the film, then the polymerisation has to be performed within the nematic phase of the resulting elastomer.

Liquid crystal elastomers undergo a nematic to isotropic network phase transition at a temperature specific to their composition in a way analogous to low molecular weight and polymeric liquid crystals. The network formation within a liquid crystal elastomer can result in a macroscopic shape-change occurring as this transition occurs, as a result of crosslinked polymer chains adopting a random coil formation as the mesogenic units organise isotropically. This shape change is reversible and, depending on the type of liquid crystal polymer present within the elastomer, has been shown to show shape-changes of up to 400%.[11] Main-chain liquid crystal elastomers tend to change shape more dramatically than side-chain liquid crystal elastomers because the polymer backbone is more strongly coupled to the mesogens and is organised anisotropically, though shape changes are still observed when the mesogenic moiety is attached as a pendant if the mesogenic units and the polymer backbone display sufficient coupling. The degree to which an elastomer sample will change shape on its nematic to isotropic transition is also dependent on the alignment of the sample. Polydomain samples may not actuate because oppositely aligned domains can effectively cancel each other out. Figure 1.29 illustrates how a liquid crystal elastomer undergoes a shape change at its nematic to isotropic transition. An example of this shape change occurring in a main-chain liquid crystal elastomer is shown in Figure 1.30.

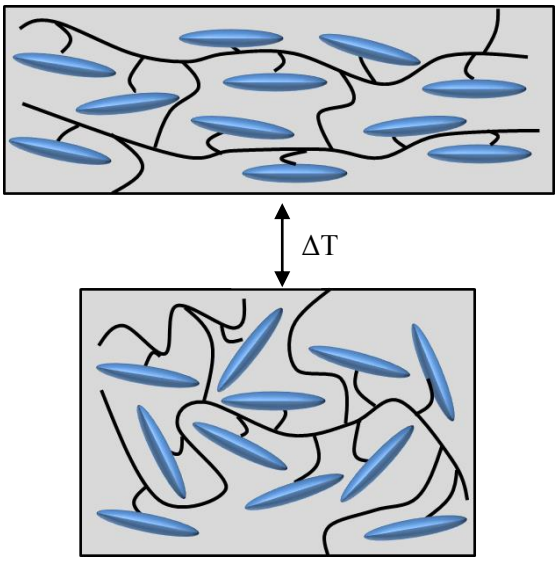

Figure 1.29: Schematic illustration showing the effect of a nematic to isotropic transition within a side-on liquid crystal elastomer.

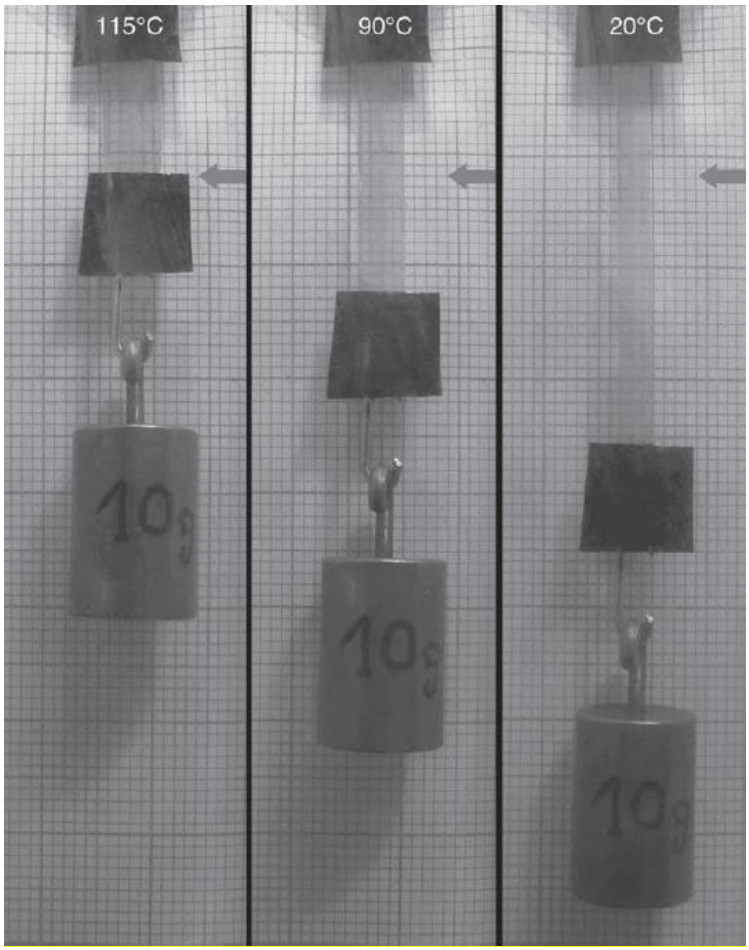

Figure 1.30: Image depicting a liquid-crystalline elastomer changing shape as it is heated. Reproduced from literature.[87]

This shape change with temperature can be utilised in the formation of actuators for the use in switches, valves, motors and stirrers.[11] Palffy-Muhoray *et al* used liquid crystal elastomers in order to create millimetre scale machines which can swim and fly.[88]

When a fully networked liquid crystal elastomer is exposed to a solvent in which the corresponding polymer would dissolve, the elastomer swells.[89] Swelling increases the size of an elastomer sample, as well as reducing the hardness, stiffness and tensile strength of the elastomer. Swelling in a solvent also results in the elastomer undergoing a reversible liquid crystal to isotropic phase transition as the solvent molecules completely disrupt the liquid-crystalline order of the mesogens. A schematic representation of this effect is illustrated in Figure 1.31. When the elastomer is dried the liquid-crystalline order will return.

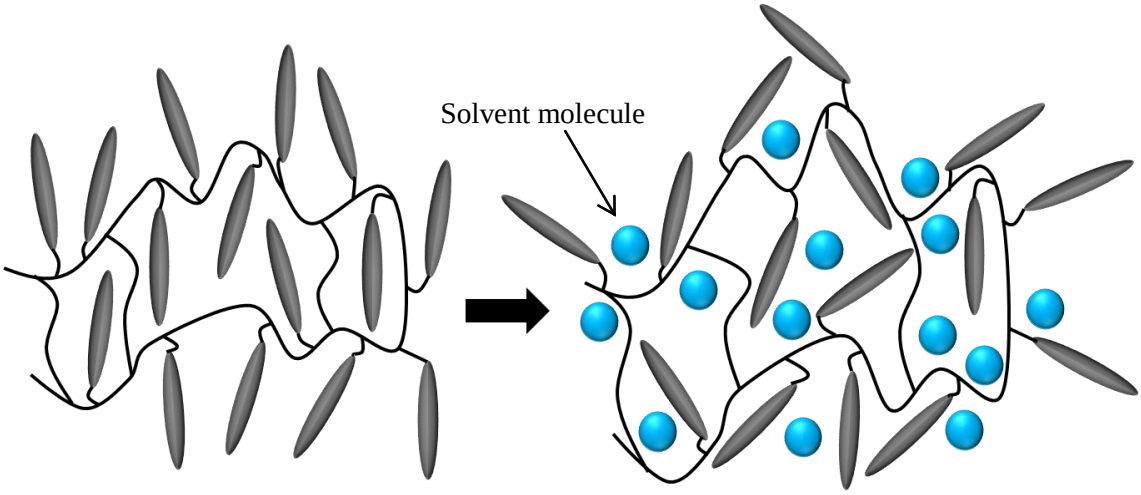

Figure 1.31: A schematic representation showing the disruption of the nematic phase as the elastomer swells with solvent.

If the degree of crosslinking within an elastomer is too substantial then the system will become too rigid and will no longer respond to the addition of solvents or increasing temperature. These extremely rigid and hard crosslinked systems are extremely temperature resistant and will display a high tensile strength but will not display liquid-crystalline or responsive behaviour and are therefore not nematic elastomers.

1.5.1 *Applications of elastomeric liquid crystals*

Liquid-crystalline elastomers have many varied possible applications because of their ability to change shape across a temperature range, swell reversibly with a response in their birefringence, and their ability to respond to external stimuli such as an electric field whilst remaining flexible and hard wearing.

The ability of a liquid crystal elastomer to undergo a shape change on increasing temperature gives them potential applications as artificial muscles as their contraction will allow them to impart a pulling force on an object. Careful engineering of the director profile within a liquid crystal elastomer film can cause bending or curling when the material undergoes its nematic to isotropic transition, allowing the elastomer to 'walk' across a surface,[90] swim,[91] or act as a valve or stirrer in micro-machinery.[92] Nematic elastomeric contact lenses have been created which allows for the focal point of the lens to be changed for reading or distance, whichever is needed.[93] By choosing a mesogenic unit which contains a UV active group which results in a *trans-cis* isomerisation of the mesogen, the shape change properties from which a number of elastomer

applications originate can be controlled by light as well as by temperature. This has been used in the creation of light driven motors.[94, 95]

Liquid crystal elastomers have the ability to link a mechanical effect, such as swelling or stretching, to an optical response provided by the mesogenic units. This results in a mechanical deformation of an elastomer film causing in a change in the birefringence of the film which could be used as an indicator for stress.[80]

1.6 NEMATIC POLYMER, ELASTOMER AND HARD PARTICLES

Liquid crystal polymers can be synthesised from mesogenic monomers in the presence or absence of a solvent. When polymerising a mesogenic monomer the polymerisation can be completed within the liquid crystal phase range of the resulting polymer, resulting in a greater degree of polymer chain anisotropy as the polymerisation takes place under the influence of the mesogenic organisation. Polymerising within the nematic phase of a nematic polymer can result in samples without defects if the liquid crystal is polymerised with an additional aligning influence, for example a rubbed surface or an electric field. A liquid crystal polymer can be cooled below its glass transition temperature into a nematic glass, retaining its internal mesogenic order as the liquid crystal organisation will be frozen within the glass.

The primary focus of this thesis is in the synthesis, characterisation and investigation of nematic polymer and elastomer particles with the aim of creating particles that display director configurations that are comparable to those discussed for nematic droplets in section 1.3 of this introduction.

Heterogeneous polymerisation methods are well established in the creation of polymeric particles, and more recently have also been employed to create liquid crystal polymer particles. Heterogeneous polymerisations are in most cases performed as free radical polymerisations, and it is only recently that other polymerisation methods (e.g. RAFT)[96] have been adopted for the creation of particles. The different types of heterogeneous polymerisation methods which have been employed for the preparation of liquid-crystalline particles are shown in Figure 1.32.[97-99] In most cases these have been carried out by free radical polymerisation which somewhat limits the choice of polymerisable units to those compatible with free radical polymerisation. The creation of liquid-crystalline polymer particles using main-chain liquid crystal polymers is therefore difficult.

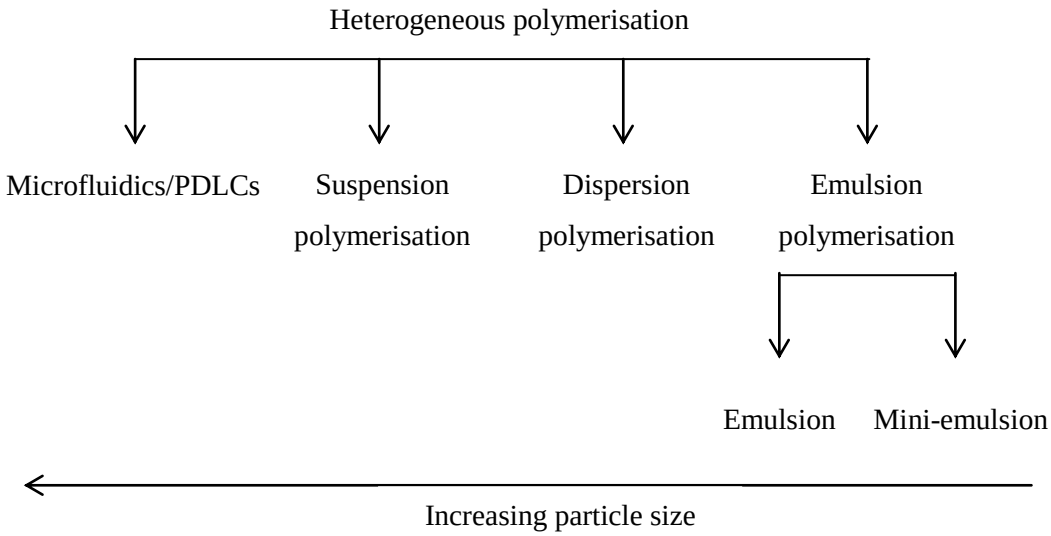

Figure 1.32: Heterogeneous polymerisation methods that have been employed in the creation of liquid-crystalline polymer and elastomer particles.

Dispersion polymerisation was selected because it allows for the creation of nematic polymer particles with a size range of approximately 1 – 5 μm with a low degree of polydispersity.[100, 101] Extrapolating findings of Abbott *et al.*[2, 3] on size dependent confinement in nematic droplets indicates that if nematic polymer particles exhibit similar behaviours to droplets then the chosen polymerisation method should create particles under approximately 10 μm in diameter, in order for those particles to display a completely surface controlled internal organisation. Liquid crystal droplets were shown to ignore the influence of the surface when below approximately 700 nm in diameter, as a result of unfavourable elastic deformations at high degrees of curvature. Particles below approximately 1 μm are also difficult to visualise and characterise using polarised optical microscopy because they are at the limit of optical resolution. Therefore, dispersion polymerisation should allow for the synthesis of nematic polymer particles observable by polarised optical microscopy, with controlled internal configurations, creating aligned nematic particles without the need for a further external aligning influence such as an electric field.[57]

Dispersion polymerisation requires the use of a solvent in which all the reagents are initially soluble but in which the polymer is insoluble. Once the polymerisation is initiated and the polymer chains begin to grow, their solubility in the reaction solvent reduces until they reach a critical chain length where they become insoluble. At this point a particle nucleates and swells with the uptake of monomer and growing polymer chains. As the polymer does not interact favourably with the solvent, the amount of solvent within the nucleated particles is minimal and

the polymerisation continues within the particles as it would in the absence of solvent. A summary of the dispersion polymerisation process is shown in Figure 1.33.

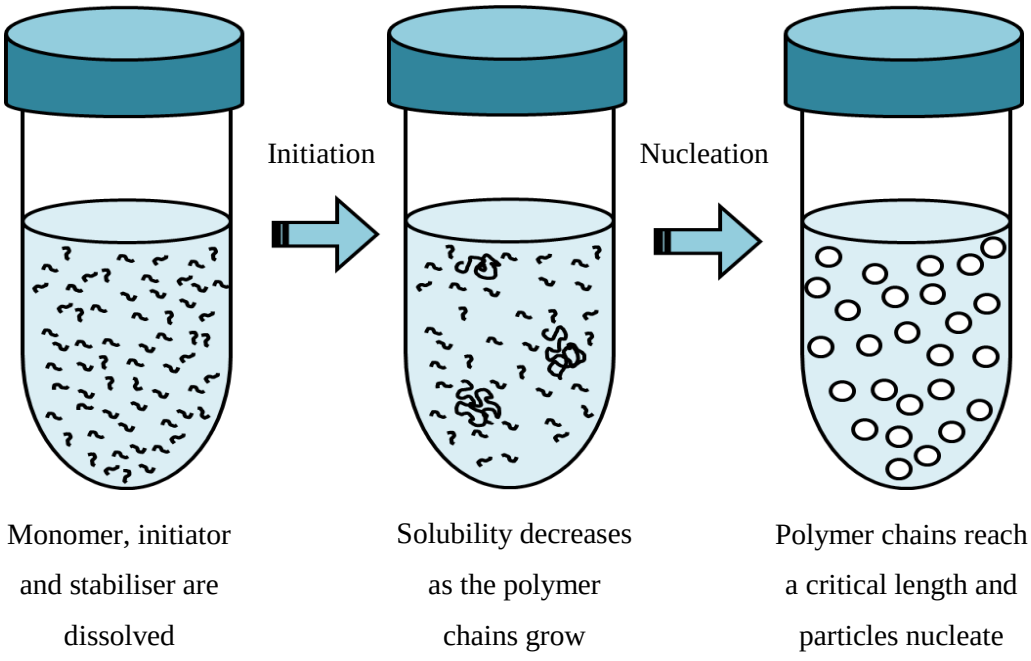

Figure 1.33: A schematic representation of particle formation within dispersion polymerisation.

Zentel *et al.*[78, 79, 102, 103] used dispersion polymerisation with a series of terminally attached nematic monomers in polar solvents and found it resulted in particles with bipolar director configurations as a result of a parallel mesogenic alignment to the particle surface. Comparatively, a perpendicular surface alignment and therefore a radial configuration, was achieved when particles were synthesised from non-polar reaction media.[78] These studies involved a variety of smectic and nematic monomers with terminal mesogen attachment, displaying a variety of structures and liquid crystal phase ranges. Mesogens with a lateral attachment to the polymer backbone were not investigated, though all of the different polymers investigated exhibited the same trend of director configuration with polymerisation media. These findings agree with previous results[6, 62, 104, 105] that indicate that nematic particles and droplets will adopt a bipolar configuration in polar solvents. Although Zentel has completed dispersion polymerisation with an array of solvent mixtures, the choice of nematic monomers investigated were limited and lacked a systematic approach, focusing on terminally attached liquid crystal mesogens which are known to show less polymer chain anisotropy than their laterally attached counterparts. The effect of monomer structure on the director configuration, or the responsive behaviour of the particles to changes in their external environment was not investigated.

Investigations into whether a bipolar director configuration will always result when the nematic particles are synthesised in polar media have also not previously been completed.

Nematic polymer particles in range of 100 - 500 nm can be synthesised by emulsion and mini-emulsion polymerisation.[106-108] The process involves two immiscible fluids being emulsified in the presence of a surfactant, one fluid contains the nematic monomer and polymerisation initiator. The emulsion of droplets is then polymerised either *via* UV or thermal initiation to create nematic polymeric particles. Theoretical results[51, 109, 110] indicate that although particles formed on the nanoscale regime are small enough to display monodomain internal structures, the surface curvature is of such unfavourable magnitude that the internal configuration is likely to disregard the surface influence to favour an orientation as a result of the bulk liquid-crystalline interactions.[2] These particles are beyond the resolution of polarised optical microscopy and their confinement textures can therefore not be determined experimentally. Particles synthesised from emulsion and mini-emulsion techniques can made larger by seeded growth polymerisation,[108, 111-113] and have also been used in the creation of hollow particles by removal of the seed particle after further polymerisation.[113]

Suspension polymerisation is a process where two immiscible layers are mixed and then polymerised. Suspension polymerisation creates droplets by stirring, resulting in the creation of large polymer particles in the range of 150 μm.[97] The liquid-crystalline polymer particles created by suspension polymerisation are too large for their internal director configurations to be fully controlled by the surface anchoring as the radius of the particle exceeds the penetration depth of the surface anchoring. This means these particles are too large for applications as sensors because they may not respond to changes at their surface.

Microfluidic techniques have also been used in the synthesis of nematic polymer particles in the size range of approximately 30 – 200 micrometres.[69] For example, a solution of nematic monomer and initiator in a microfluidic set up can be polymerised *in-situ* by UV initiated free radical polymerisation as the droplet travels along the capillaries of the microfluidic set-up.[13, 82, 114, 115] Polymerising the nematic monomer droplets while they travel along the capillaries allows for the flow-driven internal alignment of the mesogens to be polymerised into the particle,[43, 68] producing particles with parallel mesogenic organisation. Particles synthesised by microfluidics techniques are unlikely to have completely resolved surface controlled director configurations as a result of being larger than the penetration depth of surface anchoring. The monodispersity of systems created by microfluidics allows them to be assembled into monolayers[116-118] which can in theory be developed into photonic crystals.[119-124]

Polymer dispersed liquid crystal (PDLC) films can also be used in the synthesis of nematic polymer particles. A PDLC which comprises of droplets of nematic monomer within a soluble polymer matrix allows for the nematic monomer droplets to be polymerised by UV initiated free radical polymerisation, and the polymer matrix can then be dissolved to free the polymer particles. This synthetic method allows for the particles to be polymerised whilst the mesogenic organisation is impacted by the surface anchoring imparted by the polymer matrix.[57] Poly(vinyl acetate) is a polymer known to impart a parallel surface alignment on liquid crystal droplets dispersed within it, creating a matrix of bipolar droplets which can then be polymerised into particles.

Microscale elastomeric particles displaying the bipolar director configuration are of interest because the bipolar director configuration is anisotropic - in general all the mesogenic units within the bipolar configuration are orientated in the same direction. This internal alignment should allow the particles to display actuation in the same way as macroscopic fully aligned nematic elastomer films are capable. Displaying a shape change over a temperature range as the liquid crystal undergoes its nematic to isotropic transition[86, 125, 126] would allow for possible applications as microscale switches or valves,[9, 127] or as micro artificial muscles because actuators have the ability to impart force and can push or pull an object.[11, 94] Microscale elastomeric particles may also give an optical response to mechanical influences such as swelling or mechanical deformation. Mechanical deformation of the particles should result in a reversible change in the observed birefringence of the particles as a result of affecting the internal mesogenic alignment of the particles. Swelling of nematic elastomer particles should result in a completely reversible nematic to isotropic phase transition occurring as a result of the solvent disrupting the internal mesogenic order, which can then be evaporated to reinstate the nematic phase.

Microscale nematic elastic particles which have a resolved confinement texture have not yet been realised. The only examples of microscale elastomeric particles that exist in the literature are those created by microfluidics techniques in which the internal mesogenic configuration was imparted by the flow of the system through the capillary during the polymerisation process and not by the confinement of the system,[82, 128] or by stretching the precursor droplets before polymerisation to create prolate particles.[129] These prolate particles can be used as micro-stirrers in micro-machinery due to their shape anisotropy and possible response in an electric field.[130]

It is reasonable to assume, that similar to droplets and polymer particles of a nematic material, the particle size determines whether there is a need for an additional aligning influence to be present within the polymerisation for the elastomer particles to have significant internal alignment. The

surface anchoring strength will determine the size range that a droplet or particle can be and still exhibit full surface controlled internal alignment. With nematic elastomeric particles, the surface anchoring may need to be much stronger in order to display the same control over the internal structure when compared to droplets of the same size, because of the additional constraints the elastic network places on the mesogenic units. The elastic network further constrains the mesogenic units and makes the system more rigid and unable to flow, raising the energetic cost of the splay, twist and bend elastic deformations which may result in the liquid crystal ignoring the surface anchoring influence in order to reduce the deformation energy cost. The size range in which nematic elastomer particles displays full surface controlled internal alignment may therefore be much smaller than that observed for nematic droplets dispersed in equivalent solvents.

Nanoscale nematic elastomer particles have been synthesised by a mini-emulsion technique,[107, 131] producing nano-sized actuators. The shape change in this example was observed on heating above the nematic to isotropic transition temperature and was visualised by transmission electron microscopy (TEM) but in this case the shape change was irreversible and is therefore not true actuation. The director configuration within these particles was not established as the particles were below the minimum size resolvable for polarised optical microscopy, but a change in the overall shape of the particle on the nematic to isotropic transition indicates that the particles were overall anisotropic in nature. The irreversible nature of the shape change was rationalised as the cooling rate being too fast to allow for the nematic phase to reinstate before reaching the glass transition temperature of the elastomer - though if this was the case then gentle heating to temperatures above the glass transition but below the nematic-isotropic transition temperature should allow for the nematic phase to form fully and cause a reversal of the shape change. This reversal experiment was not conducted. The irreversible nature of the shape change raises questions about the success of the crosslinking, as the initial shape change could have resulted from significant polymer entanglement within the nanoscale nematic particles rather than significant network formation. The degree of crosslinking within the nano-sized actuators was not established quantitatively by experiment. Computational studies[51] indicate that below approximately 700 nm, the mesogens within a droplet will disregard the surface anchoring due to an unfavourable degree of surface curvature and display a uniform texture. This uniform texture would be conducive to shape change in elastomeric particles but the actual director configuration of the nanoscale actuators in this case cannot be established due to their size. There is also little evidence to support whether elastomeric particles behave in a fashion analogous to droplets of low molecular weight liquid crystal when confined due to the additional elastic constraints elastomeric mesogenic units experience.

The liquid-crystalline elastomer particles prepared by microfluidics have so far been above approximately 20 μm in diameter, which are too large for the internal configuration to be completely influenced by the surface anchoring. The lower size limit is imposed by the capillary widths within the instrument. If the particles are polymerised *in-situ* within the microfluidics device, they might display fully aligned internal structures as a result of the co-flowing solvent causing flow driven internal alignment of the mesogenic units as a result of the polymer chains being shear aligned while the particle is a precursor droplet. However, if the droplets are collected and there is a delay before polymerisation then the droplets will eventually lose the internal alignment caused by the flow. Liquid-crystalline elastomer particles in the range of a few hundred micrometres have been created using micro-fluidics[12, 13, 82, 132] where the solvent flow drove the internal alignment. This alignment was utilised to create a reversible shape change and was visualised using optical microscopy. In these examples the UV curing of the particles occurred within the microfluidic chamber. Particles can also be synthesised by trapping the liquid-crystalline monomer droplets extruded from a micro-fluidic device in a PVA polymer matrix and exposing this to UV light.[82] The PVA matrix in which the precursor droplets are trapped within before polymerisation imparts a parallel surface anchoring on the droplets which could result in a bipolar director configuration being observed,[57] though the droplet size is likely be too large to be conducive for full surface controlled internal alignment. An electric field can be applied across the polymer dispersed droplets in order to align the mesogenic units within the precursor droplets; this can then be exposed to UV light in order to form the liquid-crystalline elastomer particles whilst the mesogens are fully aligned with the field. Again, these aligned particles should then display actuation properties, but their alignment and shape change will not be as a result of confinement induced internal alignment.

A further aim of the research described in this thesis is the synthesis of nematic elastomer particles because they have the possibility of being reversibly and responsively swellable and insoluble.[126, 133] Dispersion polymerisation is an attractive prospect for creating liquid-crystalline elastomer particles because this method creates low micrometre-sized particles, meaning no external influence beyond the surface anchoring imparted on the particle by the solvent may be required to create aligned nematic particles. A method for creating microscale nematic elastomer particles by heterogeneous polymerisation methods has not yet been realised.

1.7 AIMS

The overriding aim of this PhD project was the creation and analysis of nematic polymer and elastomer particles by heterogeneous dispersion polymerisation. This involved the following specific targets:

- The synthesis of novel nematic monomers based on a structural variation of a known lateral side-chain nematic monomer; their structural characterisation by ^{1}H and ^{13}C NMR, MS, IR and EA, and the investigation of their phase properties by DSC and POM.
- The polymerisation of these monomers *via* a dispersion polymerisation process to create nematic polymer particles in the small micrometre size range.
- Investigation of these particles for factors affecting particle size, shape and variance; as well as phase properties and director configuration by methods including SEM, DSC and POM.
- The adaptation of heterogeneous dispersion polymerisation processes to create novel nematic elastomer particles in the small micrometre size range; their degree of network formation to be established by gel content analysis, heating and swelling studies.
- Investigation of the responsive nature of nematic polymer and elastomer particles to changes in surface anchoring, temperature and the presence of an electric field.

CHAPTER 2:

SYNTHETIC METHODS

2 SYNTHETIC METHODS

2.1 INTRODUCTION

This chapter outlines the synthesis of the monomers used throughout this thesis, as well as the different polymerisation methods used to synthesise polymers and microscale polymer particles.

2.1.1 *NOMENCLATURE*

Throughout this thesis the polymers will be primarily described according to the monomer they are made from and by which polymerisation method they were polymerised. As there is only one terminally attached monomer (**M1**), it shall be referred to as the 'terminal' monomer. The lateral monomers **M2- M9** will be referred to by their 'spacer' length as well as the length of the 'side chains.' This nomenclature is illustrated in Figure 2.1.

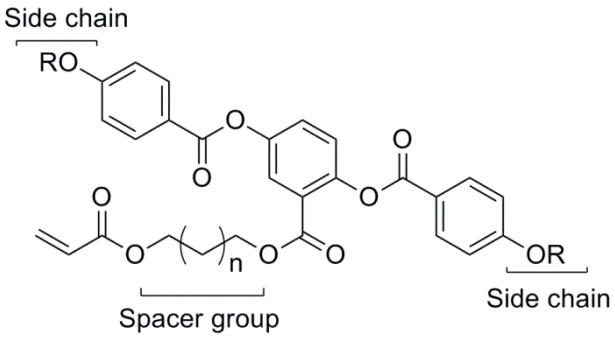

Figure 2.1: Monomer nomenclature.

2.2 MONOMERS

2.2.1 *INTRODUCTION*

An array of monomers were synthesised in order to investigate the effect of monomer structure on the resulting phase transitions, molecular weight, particle size and director configuration of nematic polymer and elastomer particles synthesised by various polymerisation techniques. The

monomers that were synthesised are depicted in Figure 2.2 and were synthesised following routes as shown in Scheme 2.1 and Scheme 2.2 in the next section.

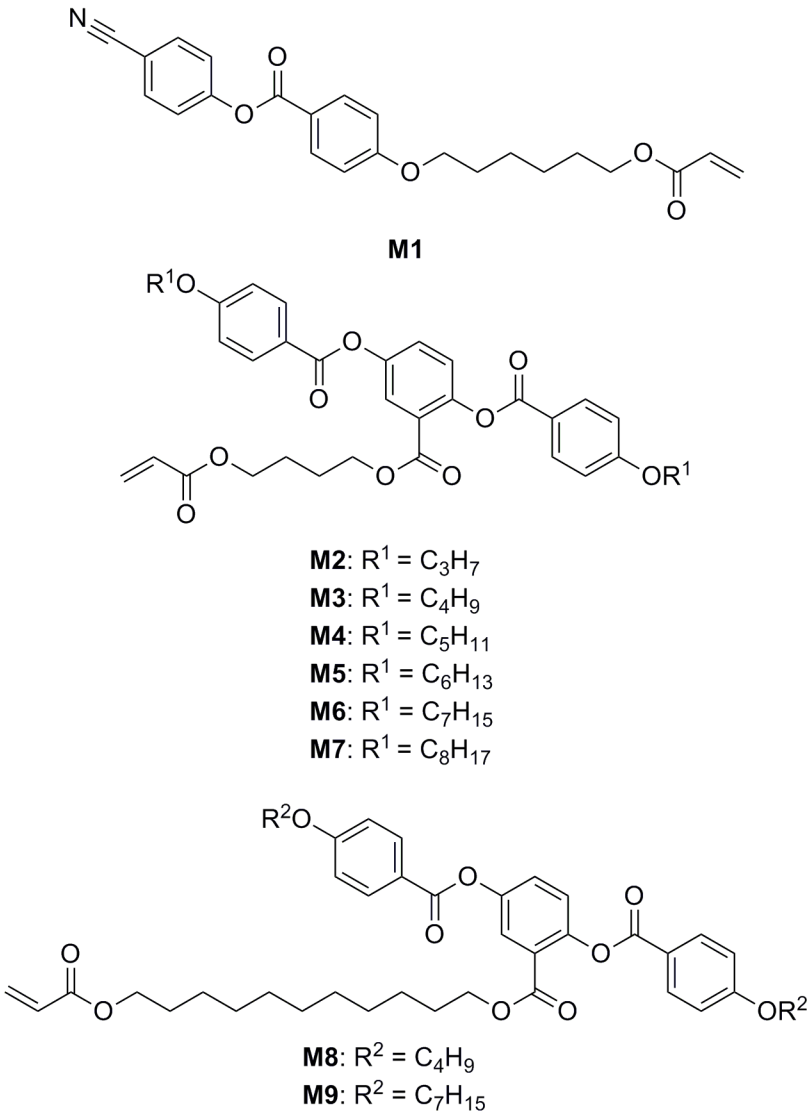

Figure 2.2: The monomers synthesised.

Monomer **M1** (4-[4-(6-acryloyloxyhexyloxy)benzyloxy]benzonitrile) is known in the literature and has been used in the synthesis of liquid crystal polymers,[134] including the synthesis of nematic polymer particles by dispersion polymerisation.[78, 79] As it has been previously used to create nematic polymer particles of known configuration, this monomer was chosen as a reference to ensure consistency in the employed dispersion polymerisations.

Monomers **M2**-**M9** have a polymerisable unit attached laterally to the mesogenic unit. Monomer **M3** ((4-acryloylbutyl)-2,5-di(4-butyloxybenzyloxy)benzoate) has been reported in the literature[80]

and is known to produce a wide range nematic phase in polymers and elastomers, a low glass transition temperature, and strong coupling between the mesogenic units and the polymer backbone resulting in significant polymer backbone anisotropy.[15, 75, 77] As discussed in the introduction, polymer backbone anisotropy increases the likelihood and magnitude of actuation in elastomers by coupling liquid crystal optical responsiveness to mechanical properties. Monomers **M2**-**M9** can be compared to the terminally attached monomer **M1,** which allows for the determination of the effect of type of mesogen and mesogen attachment to the polymer backbone on the phase transitions, liquid crystal polymer particle size and director configuration. Monomers **M2**-**M9** form a series in which the structure was changed to allow for systematic investigations into the effect of monomer structure on various particle properties, such as size and director configuration. The alkyl side chain groups were altered from propyl to octyl in **M2**-**M7**, and two spacer lengths to the polymerisable unit were also used - butyl in **M2-M7** and undecyl in **M8** and **M9**.

2.2.2 *SYNTHESIS*

M1 was synthesised *via* a pathway adapted from a literature procedure of a similar monomer[134] which is depicted in Scheme 2.1.

The first step in this reaction procedure was an etherification between the terminal alcohol group of ethyl 4-hydroxybenzoate and 6-chlorohexanol. The ethyl ester acts a protecting group for the carboxylic acid to prevent unwanted reactions at that site. Further reaction with strong base cleaved the ethyl protecting group on the carboxylic acid to yield the benzoic acid derivative **1**. The second step involved the coupling of the terminal alcohol on 4-(6-hydroxyhexyloxy)benzoic acid and acryloyl chloride to yield compound **2**; at this stage and onwards butylated hydroxytoluene (DBPC) was added as a polymerisation inhibitor to preserve the reactive acrylate group. The final step was the esterification of 4-(6-acryloyloxyhexyloxy)benzoic acid with 4-hydroxybenzonitrile, which afforded **M1** in good yield with no unwanted polymerisation of the acrylate species. Column chromatography and recrystallization proved an effective method of purification for all intermediates. Details of the synthesis and characterisation for all monomers can be found in the Experimental chapter.

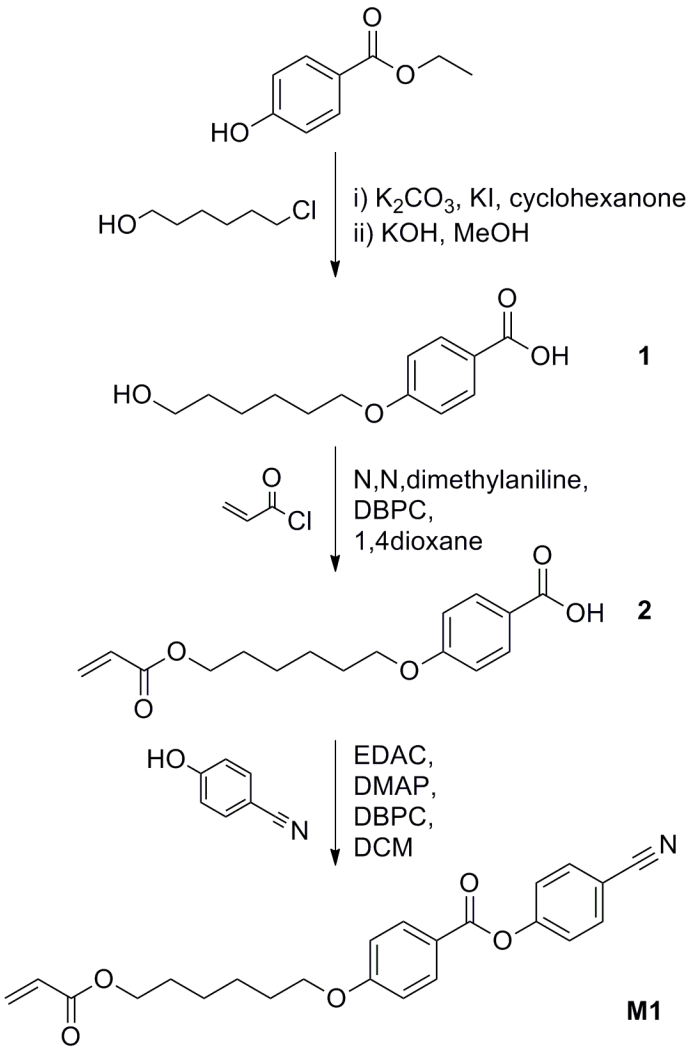

Scheme 2.1: Synthetic pathway for the synthesis of **M1.**

The synthetic pathway for the lateral monomers, **M2** – **M9**, is illustrated in Scheme 2.2. These monomers were synthesised *via* a procedure adapted from literature for the synthesis of **M3**.[80, 81, 133, 135]

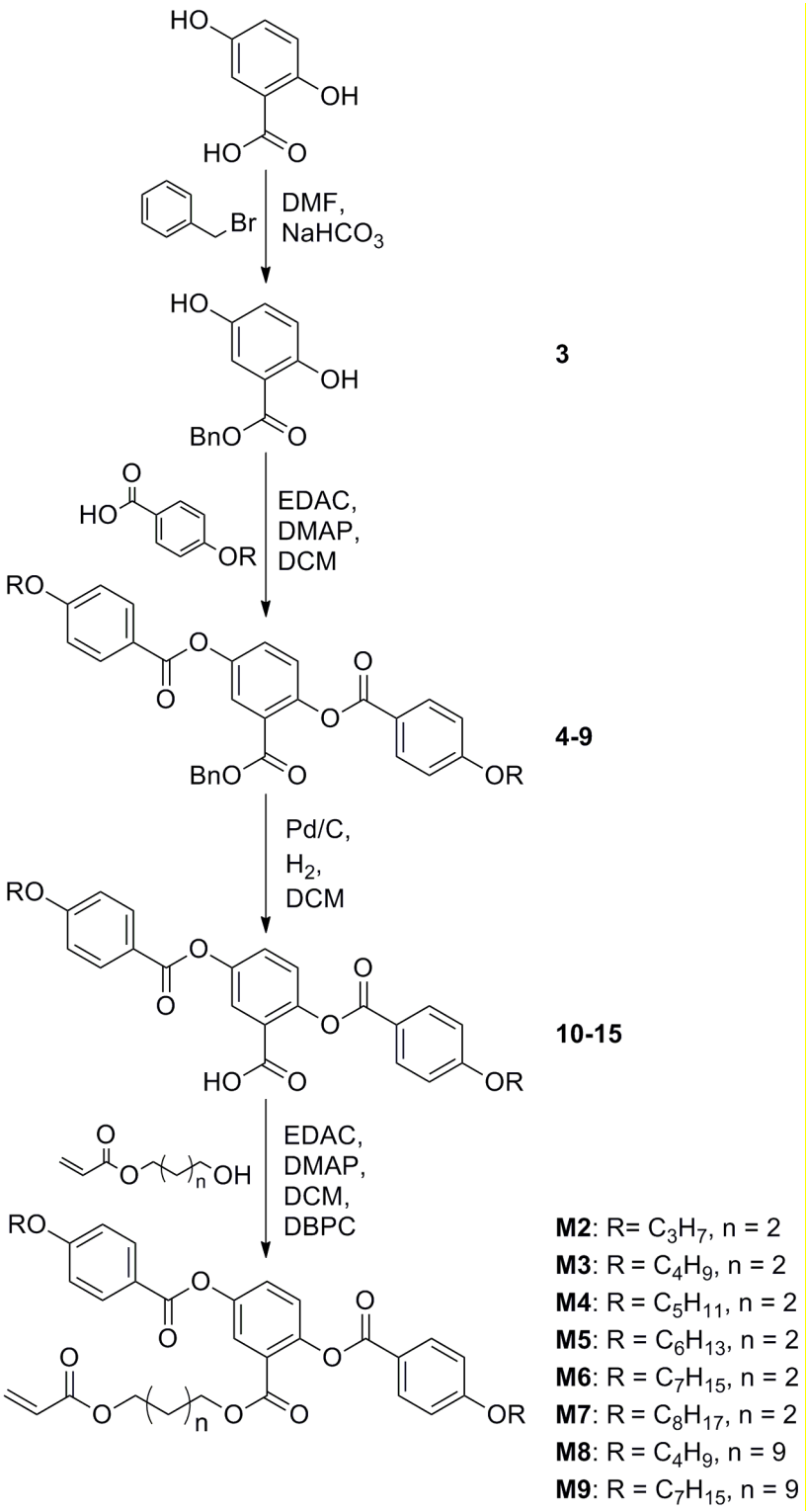

Scheme 2.2: Divergent synthetic pathway for the synthesis of **M2**-**M9.**

The carboxylic acid group on 2,5-dihydroxybenzoic acid was protected using benzyl bromide in DMF. $NaHCO_3$ was used as a weak base in this case to limit the deprotonation to the carboxylic acid group, yielding compound **3**. An esterification reaction using two equivalents of the

alkoxybenzoic acid (propyloxybenzoic acid to octyloxybenzoic acid) yielded the benzyl protected species **4-9** in high yield. The removal of the benzyl protecting group to yield compounds **10-15** was achieved using palladium catalysed hydrogenolysis in dichloromethane. The polymerisable unit was attached with its spacer group *via* a further esterification reaction to give final products **M2-M9** in high yield. Butylated hydroxytoluene (DBPC) was again added in this last step as a radical quencher to inhibit the polymerisation of the acrylate group. Again, column chromatography and recrystallisation proved effective methods for separation and purification of all steps and no unwanted polymerisation of the acrylate group occurred.

The synthetic pathway for the synthesis of 11-acryloylundecan-1-ol **16**, used in the creation of monomers **M2** – **M9** is described in Scheme 2.3.

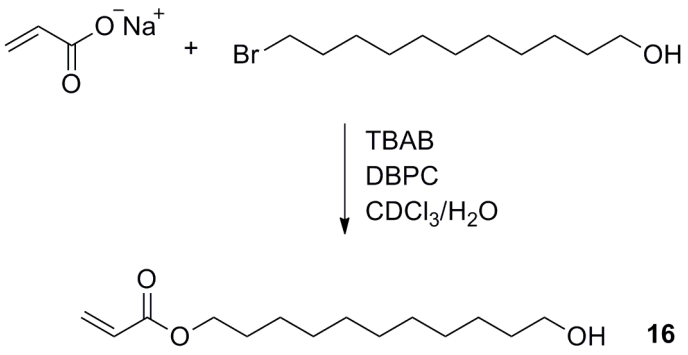

Scheme 2.3: Synthesis of 11-acryloylundecan-1-ol **16**.

This synthetic pathway was adapted from a literature procedure[136] detailing the synthesis of the methacrylate equivalent. The sodium acrylate, bromoundecanol and tetrabutylammonium bromide (TBAB) were refluxed with vigorous stirring in a mixture of chloroform and distilled water. This was a phase transfer process which allowed for 11-acryloylundecan-1-ol to be obtained in moderately high yield after three days. Butylated hydroxytoluene (DBPC) was added as a radical quencher to inhibit the polymerisation of the acrylate group. The 11-acryloylundecan-1-ol was extracted from the chloroform layer after it was washed with NaOH solution and then with distilled water. The solvent was removed *in vacuo* and the crude product was obtained as a clear off white oil and was used as received in further reactions.

2.3 SOLUTION POLYMERISATION

2.3.1 *METHOD*

Apart from the monomer used, the polymerisation method has a vast effect on the morphology, and properties of the resulting polymer, such as molecular weight, molecular weight distribution and phase transitions. For comparison, the monomers were therefore polymerised by a typical free radical solution polymerisation procedure.[137]

In order to polymerise the monomers by free radical solution polymerisation, they were dissolved in a solvent they were readily soluble in. The same solvent was chosen for all monomers to eliminate any solvent effects on the polymerisation. Dichloromethane was effective for all monomers. Rubber septum sealed glass vessels of the solutions of monomer (100 mg monomer in 2 mL DCM) and thermal radical initiator AIBN (2 wt% relative to monomer) were purged thoroughly with nitrogen for a period of 30 minutes before being heated to 65 °C with constant and vigorous stirring for 24 hours. After the polymerisation had been allowed to proceed for 24 hours, the mixture was allowed to cool to room temperature and then the polymer was precipitated into methanol. The sample was centrifuged (10 minutes at 2000 rpm), this sedimented the polymer and allowed the methanol to be decanted. The polymer was then re-dissolved in THF and re-precipitated into methanol in order to purify the polymer further, as any soluble impurities would remain within the THF. The polymer was again separated from the solvent by centrifugation and then dried thoroughly in a vacuum oven at approximately 80 °C before further analysis. For the exact reagents and conditions used in each case, please see the experimental chapter.

2.3.2 *METHOD DEVELOPMENT*

The solvent that is selected for solution polymerisation is slightly less crucial than for the dispersion polymerisation methods investigated within this thesis. As long as the monomer and polymer are sufficiently soluble the polymerisation will proceed to some degree. The degree of polymerisation within solution polymerisation can be limited by the solvent should it quench the propagating radicals.

Utilising dichloromethane (DCM) as the solvent for solution polymerisation allowed for high molecular weights to be achieved, but problems were encountered as the rubber seals on the

reaction vessels leaked dyes and impurities into the reaction as a result of the high vapour pressure of DCM within the vessel. The purification stage of solution polymerisation which involves the dissolution of crude polymer into a second solvent and re-precipitating was sufficient to remove these additional impurities. The properties of the solution polymerisation polymers will be discussed in comparison to polymers obtained *via* heterogeneous polymerisation methods in the general characterisation chapter.

2.4 HETEROGENEOUS POLYMERISATION

2.4.1 *INTRODUCTION*

Dispersion polymerisation was chosen above other methods by which particles can be created (emulsion, suspension polymerisation *etc.*) because, as discussed in the introduction, it is a method that produces polymer particles with a relatively low degree of particle size polydispersity in the desired size range of a few micrometres.

As discussed in the introduction, there are only very few examples in the literature in which nematic polymer particles have been synthesised by dispersion polymerisation. A terminal monomer used in a previous study[78] has been selected as a point of reference within the investigations described in this thesis.

2.4.2 *METHOD*

In order to polymerise the monomers by dispersion polymerisation, a monomer (100 mg) was dissolved in a carefully selected solvent (1 mL) in which the polymer is insoluble. Various solvents and solvent mixtures were used in order to optimise for particle size and particle size monodispersity for each monomer, as well as to assess the correlation between solvent and director configuration of the resulting particles. A steric stabiliser was utilised (polyvinylpyrrolidone with a molecular weight of ~55,000 g mol^{-1}) in order to prevent coagulation of the particles. The mixture was placed in a rubber septum sealed glass vessel and purged by bubbling nitrogen through the solvent for period of 30 minutes. During this period the vessel was kept in an ice bath to minimise solvent loss. After the vessel had been thoroughly purged it was placed in an oil bath at the reaction temperature (73 °C) with constant and vigorous stirring. A separate vessel containing the radical initiator AIBN (2 wt% relative to monomer) dissolved in the reaction solvent (0.6 mL) was also thoroughly purged for a period of 30 minutes

and then heated to 73 °C. The initiator was then injected by syringe into the reaction vessel through the septum to initiate the polymerisation process. The nucleation stage of the polymerisation can be observed as the reaction mixture becomes turbid. This is depicted in Figure 2.3. After the polymerisation had been allowed to progress for 24 hours, the vessel was removed from the heat and allowed to cool to room temperature before immediate purification. In order to clean the particles the solvent was removed and exchanged *via* a centrifugation process which removes the soluble impurities from the particle surfaces.

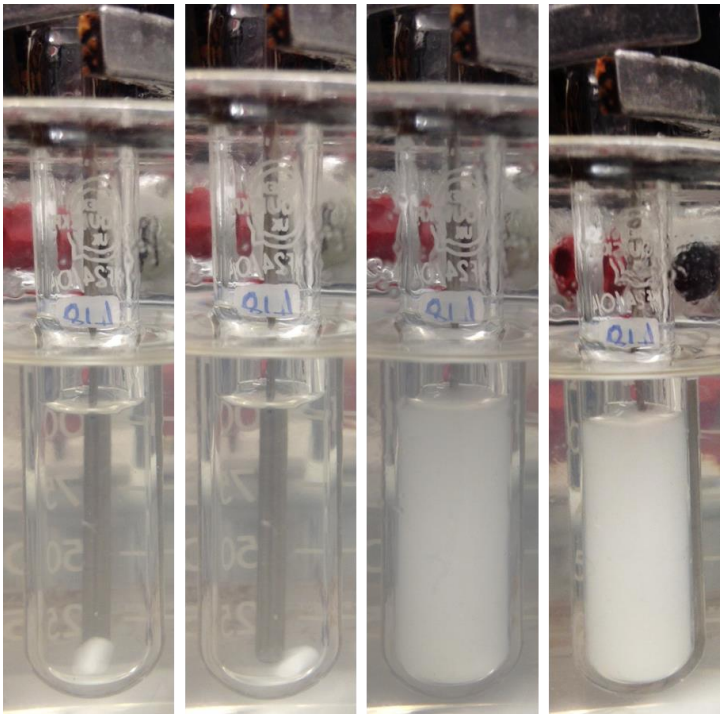

Figure 2.3: A series of images illustrating the nucleation stage of particle growth being observed as the reaction mixture becomes increasingly turbid.

2.4.3 *METHOD DEVELOPMENT*

The particle size and particle size polydispersity that can be achieved within dispersion polymerisation can be tuned by carefully adjusting the solvent and reaction conditions such as the temperature, stirring rate and amount of initiator or stabiliser present. Dispersion polymerisation is a very sensitive process and changing a small detail, for example a small change in polarity of the monomer, is enough to change the outcome as a result of affecting the solubility and nucleation point of the growing polymer chains in solution.

With systematic variation of the solvent composition the most effective solvent mixtures for promoting a fast singular nucleation stage with a good degree of polymerisation for each monomer were obtained. As the monomer polarity, reactivity and solubility changed with every monomer the solvents that were successful with some monomers were not necessarily that effective with others. General observations for some commonly investigated solvent mixtures are summarised in Table 2.1.

Table 2.1: Observations of the effect of different solvents within dispersion polymerisation

Solvent mixture	**Observations**
EtOH	Good monodispersity for polymers of **M2-M7**, creating samples with a good degree of polymerisation. Large and polydisperse particles obtained for polymers of **M8** and **M9** where degree of polymerisation was also much lower.
MeOH	Poor solubility of lateral monomers results in small particles and coagulates. Good degree of monodispersity for terminally attached monomer **M1**.
^{i}PrOH	High degree of particle size polydispersity and coagulates across all monomers.
1:1 EtOH: methoxyethanol	Monodisperse samples achieved from polymerisation of terminal monomer **M1**. Often creates large particles with significant particle size polydispersity for lateral monomers **M2-M9**. GPC analysis shows a lower degree of polymerisation.
5:1 EtOH: methoxyethanol	Particles synthesised from **M2-M9** still show a large degree of particle size polydispersity but overall particle size is reduced and degree of polymerisation is slightly improved.
10:1 EtOH: methoxyethanol	Particles of **M2-M9** comparable to those obtained from pure EtOH, although slightly larger and still with a smaller degree of polymerisation.

The solvent mixture can also affect the degree of polymerisation that is obtained, a contributing factor being that some of the solvents are more effective radical quenchers which can hinder the propagation of the polymer chains, for example methoxyethanol has an ether functionality which is a reasonably effective radical quencher.[138] The degree of polymerisation in turn seems to affect the particle size that is obtained, with larger particles being formed with low polymer molecular weights. This correlation between particle size and polymer chain length is likely caused by

shorter polymer chains being able to travel to the inside of the growing particles more easily and tangle less efficiently than longer polymer chains, this means the particle should potentially be more swellable.[139] Generally, particles synthesised from 1:1 EtOH: methoxyethanol are large, but gel permeation chromatography analysis shows that a lower average molecular weight was achieved than with EtOH alone.

The molecular weights obtained for polymer particles formed by dispersion polymerisation indicated that radical polymerisation is successful within the dispersion polymerisation process. Typically, the molecular weights are high as polymerisation occurs primarily as bulk polymerisation within the nucleated particles and is complete after 24 hours. It is worthwhile to note that for the monomers with undecyl alkyl spacer groups (**M8** and **M9**) the observed degree of polymerisation that was achieved is far lower than for the other monomers. A longer reaction time of 72 hours allowed for much higher molecular weights to be obtained, as shown in Table 2.2. However, prolonging the reaction time also lead to significant particle coagulation in the dispersion polymerisation process and therefore cannot be used.

Table 2.2: Molecular weights, degree of polymerisation and polydispersities of polymer particles made from **M8** and **M9** by a 24 or 72 hr dispersion polymerisation in EtOH. In each case 15 wt% PVP55 was used as the particle stabiliser and 2 wt% AIBN as the radical initiator. The degree of polymerisation was calculated by dividing the average polymer molecular weight by the molecular weight of the monomer in each case.

Material		Reaction time	M_n / g mol^{-1}	Degree of polymerisation	Molecular weight polydispersity [M_w / M_n]
M8	C4 chain, C11 spacer	24 h	19,000	26	2.97
		72 h	269,000	368	4.33
M9	C7 chain, C11 spacer	24 h	15,000	18	2.96
		72 h	368,000	451	3.90

2.4.3.1 Purification of nematic particles

The purification of the nematic particles was investigated to assess the degree to which impurities were removed, this involved effectiveness of the centrifugation process at removing PVP55 and unreacted monomer from the particle surfaces being investigated by ^{1}H NMR. Crude and clean

particles were analysed by ^{1}H NMR as well the washings. Example spectra are shown in Figure 2.4, along with the resonance assignments.

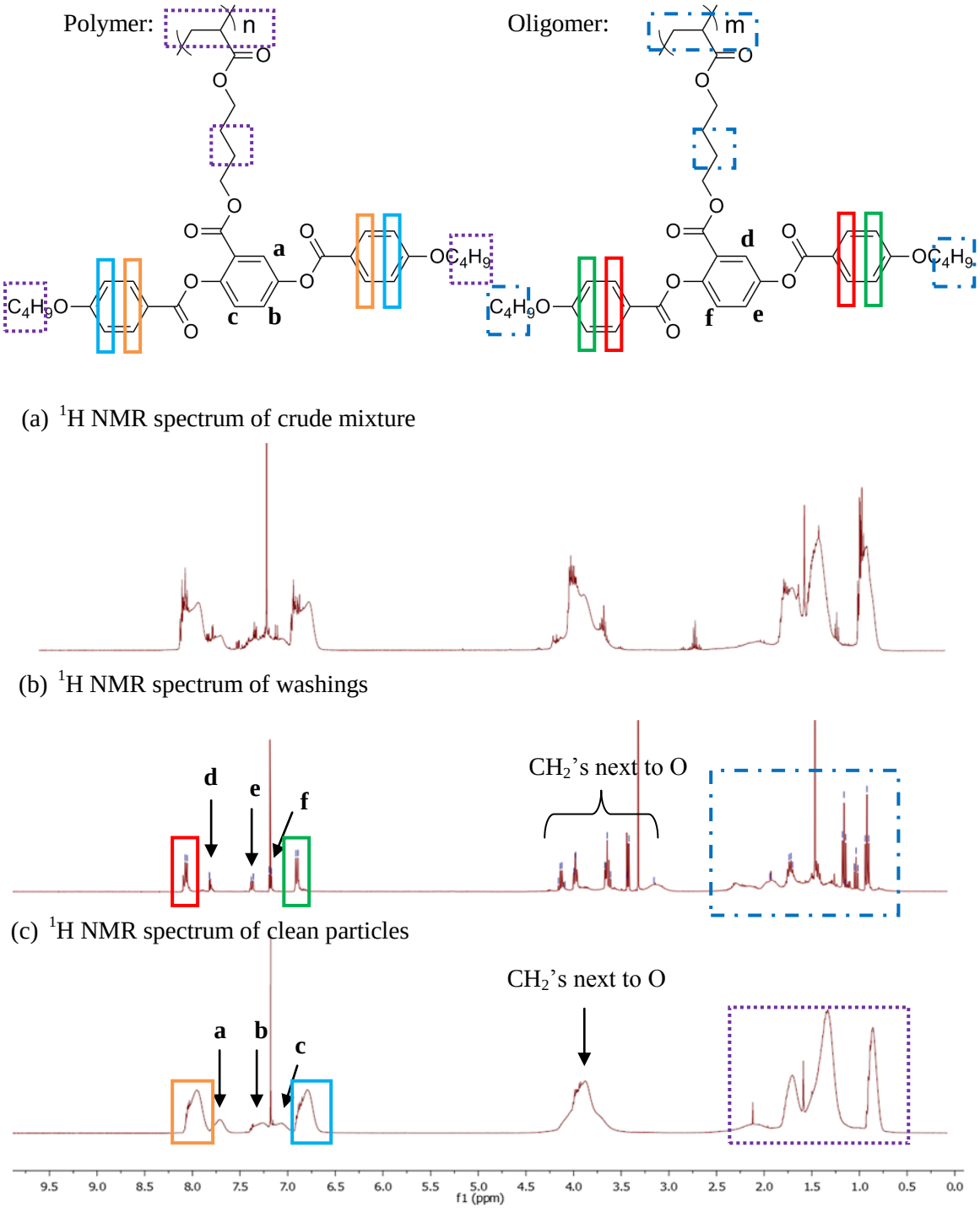

Figure 2.4: ^{1}H NMR spectra of the crude particles, washings and clean particles to show removal of PVP and low molecular weight contaminants by centrifugation. The sample shown is particles synthesised by dispersion polymerisation of **M3** in EtOH.

^{1}H NMR resonances of the polymer are broad and lose discrete couplings due to the slow rotation and chemical and magnetic inequivalence of the repeat units along the polymer chain, therefore any sharp peaks are evidence of low molecular weight impurities. As can be seen from the spectra above in Figure 2.4, the polymer particles are notably cleaner after the centrifugation process, with the absence of resonances which can be assigned to oligomeric chains, as is evidenced by the sharp resonances with observable couplings in the ^{1}H NMR spectrum of the washings and crude particles, which is then not present in the ^{1}H NMR spectrum of the clean particles. There is also evidence that the amount of polymer particles lost to the washing process is minimal. This investigation indicates that the centrifugation process is an effective method for cleaning the particles.

2.4.3.2 Achieving monodispersity

Obtaining a sample with a very narrow particle size distribution proved challenging as the conditions which result in a monodisperse sample from a particular monomer did not translate to other monomers in the series as the solvent affinities vary. An example of this effect is shown in Figure 2.5.

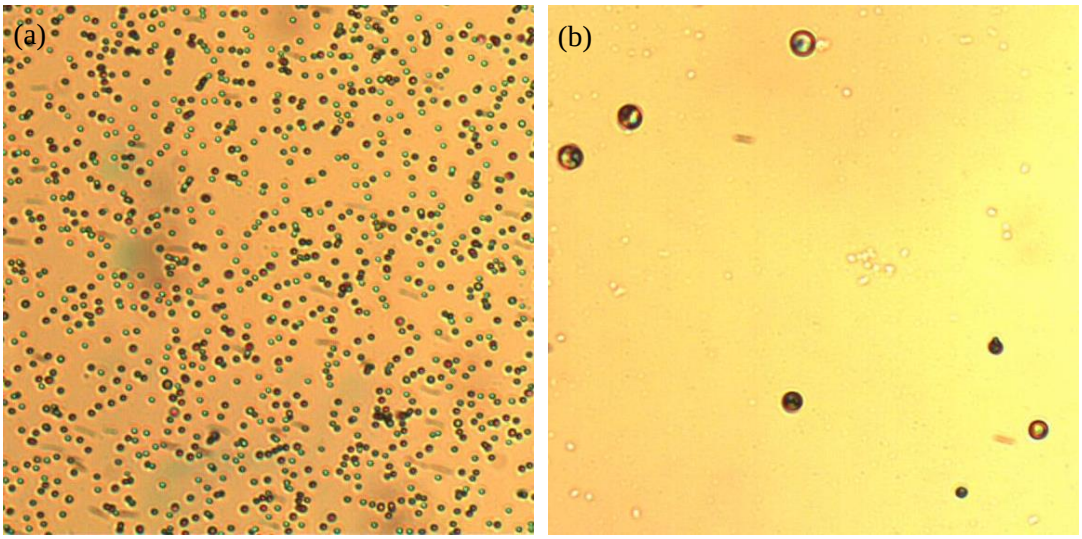

Figure 2.5: Polarised optical microscopy images illustrating the difference in particles size and variance obtained from dispersion polymerisation of (a) **M1** and (b) **M6** in 1: 1 EtOH: methoxyethanol. Images taken at room temperature through uncrossed polarisers with 200× magnification.

A sample of particles created using **M1** in 1:1 EtOH: methoxyethanol shows a good degree of monodispersity, with an average particle size of 1.28 μm and a particle size polydispersity of 5.4%. Comparatively, when this solvent mixture is used in a polymerisation of **M6** the result is

large polydisperse particles, with an average size of 5.1 μm and a particle size polydispersity of 25%. The particle size polydispersity of a sample is calculated as the coefficient of variance, C_v, which is calculated from the standard deviation and the mean as shown in equation 5, where σ is the standard deviation of sizes in the sample and μ is the mean size of the sample.

$$C_v = \sigma/\mu \quad (5)$$

However, a solvent change to EtOH results in a far more monodisperse sample for **M6**, as can be seen in the photomicrographs and SEM image in Figure 2.6.

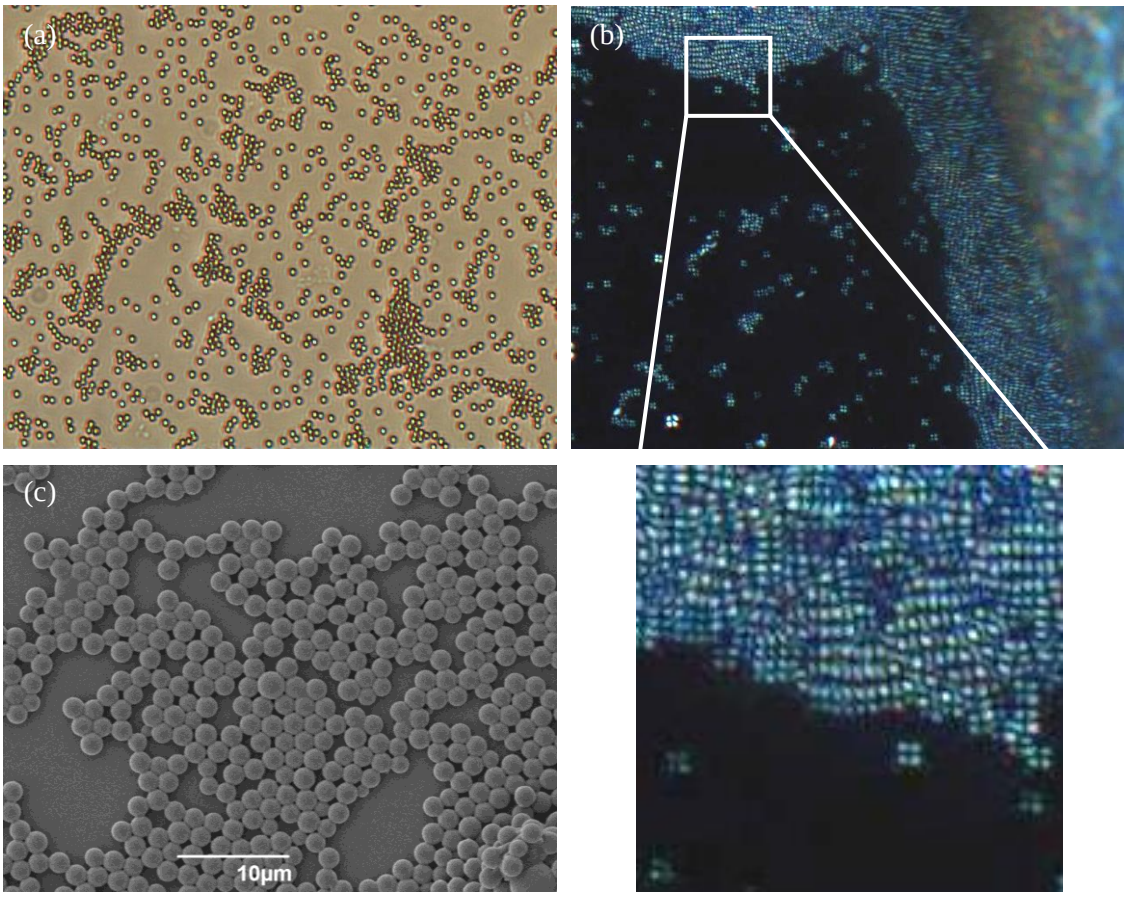

Figure 2.6: Polarised optical microscopy images showing particles synthesised from **M6** in EtOH. (a) Image taken through uncrossed polarisers, (b) image taken with crossed polarisers towards the edge of the coverslip. Polarised optical microscopy images taken at room temperature with 200× magnification and (c) SEM taken at 2500× magnification.

The packing which can be observed in Figure 2.6 (b) and in the magnified insert is the self-assembly to a monolayer by capillary flow forces which also further reduces the local particle size

polydispersity, as the capillary flow leads to size selection because particles of a similar size pack together and exclude the particles that do not fit.

2.4.3.3 The addition of a crosslinker

Another significant aim within this project was the synthesis of nematic elastomer particles with confirmed crosslinking using dispersion polymerisation. Adding a crosslinker at the start of the polymerisation process with the monomer feed results in the particles becoming misshapen or coagulating as the crosslinker affects the sensitive nucleation stage of particle growth within the polymerisation.[101] This is a well-known phenomenon within dispersion polymerisation. Adding a crosslinker does not guarantee that the polymer particles will be fully networked as was observed within this method development. It is therefore important to assess the degree of crosslinking obtained in each case by swelling, heating and gel analysis investigations as a fully networked sample should be swellable, insoluble, will not melt and will have significant gel content.[140]

Gel content analysis is a method by which the degree of crosslinking within a sample can be established. It is an experimental procedure which involves the extraction of any soluble polymer chains from an elastomeric system by centrifugation in order to determine the percentage of gel within the sample. Although gel content analysis provides an overview of the degree of gel content within the particles, it does not give any information about the distribution of crosslink points throughout the particle.

Gel content analysis may result in the gel content being reported as lower than it is in actuality if the centrifugation process was not completely effective in separating the soluble and insoluble fractions. For this reason, the reproducibility of gel content analysis as a method for assessing the degree of crosslinking was assessed by completing the analysis twice on the same sample. The results obtained from this experiment are shown in Table 2.3.

Table 2.3: Assessing the reproducibility of gel content analysis experiments using a sample of particles made from **M1** and **M2** respectively.

Sample Name	Gel / mg	Sol / mg	% gel by weight
M1 sample 1	5.83	2.76	**68%**
M1 sample 2	6.26	2.74	**70%**
M2 sample 1	5.71	1.48	**79%**
M2 sample 2	11.14	3.38	**77%**

As can be seen from the results depicted in Table 2.3, the results obtained for the gel content analysis are reproducible within 1-2%; therefore any significant variability seen across a series of the same monomer therefore lays within the samples themselves and not the method for establishing the gel content.

Winnik *et al.*[101, 141-143] describe a method in which the addition of a crosslinker is postponed until after the nucleation stage of polymer growth has completed, in order to prevent the crosslinker from affecting the nucleation stage and in turn lead to coagulation or affect the polymer shape and variance. As the crosslinker is added after the polymerisation begins it is feasible that the particles will have an uneven crosslink density throughout their composition which may result in hard regions and non-uniform swelling. The degree of crosslinking achieved in this case was established by gel content analysis.

Winnik and colleagues' delayed crosslinker addition method was adapted to accommodate nematic monomers with the hope of yielding nematic elastomer particles in the low micrometre size range. A series of experiments were performed varying parameters such as solvent mixture, crosslinker addition time and concentration allowed for fully networked particles to be achieved only for monomer **M1**. This method proved to be unsatisfactory for crosslinking with the lateral series of monomers **M2-M9**. This can be seen in the gel content analysis results shown in Table 2.4.

Table 2.4: Gel content analysis results for particles created by dispersion polymerisation with a delayed addition of crosslinker in various solvents.

Monomer		**Solvent**	**Gel fraction / mg**	**Soluble fraction / mg**	**% gel by weight**
M1	Terminal	MeOH	23.49	4.66	83.4%
M3	C4 chain, C4 spacer	MeOH	4.31	45.5	8.7%
M3	C4 chain, C4 spacer	EtOH	2.59	11.38	18.5%
M6	C7 chain, C4 spacer	MeOH	1.86	13.95	11.8%
M8	C4 chain, C11 spacer	MeOH	0.45	37.42	1.2%
M9	C7 chain, C11 spacer	MeOH	13.13	40.4	24.5%

With a delayed addition of crosslinker, crosslinking has only successfully occurred for particles made from the terminal monomer **M1** as the observed high percentage of gel in the particles indicates a near sample-wide network. However, for all lateral monomers tested the gel content of the samples is minimal, indicating that only negligible crosslinking had occurred during the polymerisation. A possible reason for this could be the increased viscosity of lateral systems

causing a slower reaction rate. Also, if the crosslinker does not have sufficient affinity to the monomer and growing polymer chains it may not be incorporated within the nucleated particles. Further investigation and different polymerisation methods were required in order to achieve a crosslinked sample for each monomer. Increasing the reaction time to 72 h did not greatly improve the degree of crosslinking that was achieved and also significantly reduced the particle yield due to coagulation.

2.4.3.4 Effect of reaction concentration

Within dispersion polymerisation with a delayed addition of crosslinker, a correlation between the reactant concentration and resulting particle size and topology was found with terminal monomer **M1**, the only monomer for which crosslinking was successful. This correlation allowed for the realisation of spherical and monodisperse 1.3 µm liquid-crystalline elastomer particles within a small concentration range, as well as smaller spherical particles at low concentration and non-spherical particles when the concentration was high. The particle size and particle polydispersity of all samples at different reaction concentrations can be found in Table 2.5.

Table 2.5: Size and polydispersities of particles created from **M1** in MeOH using different reaction concentrations and a crosslinker addition time of four minutes.

Concentration	**Description of Particles**	**Average particle Size**	**Coefficient of variance (C_v)**
0.35 mol dm^{-3}	Non-spherical and polydisperse	Average length: 1.01 µm Average width: 0.82 µm	66.9% 86.6%
0.27 mol dm^{-3}	Non-spherical and polydisperse	Average length: 0.6 µm Average width: 0.53 µm	46.4% 73.9%
0.15 mol dm^{-3}	Spherical and monodisperse	1.3 µm	6.3%
0.14 mol dm^{-3}	Spherical and bimodal	Smaller Fraction: 0.66 µm Larger Fraction: 0.99 µm	18.1% 83.5%
0.13 mol dm^{-3}	Spherical and bimodal	Smaller Fraction: 0.68 µm Larger Fraction: 1.24 µm	18.9% 54.4%

From Table 2.5 it can be deduced that the delayed addition of crosslinker is only successful within a very narrow concentration range. A relatively monodisperse sample is produced from a reaction concentration of 0.15 mol dm^{-3}, shown in Figure 2.7.

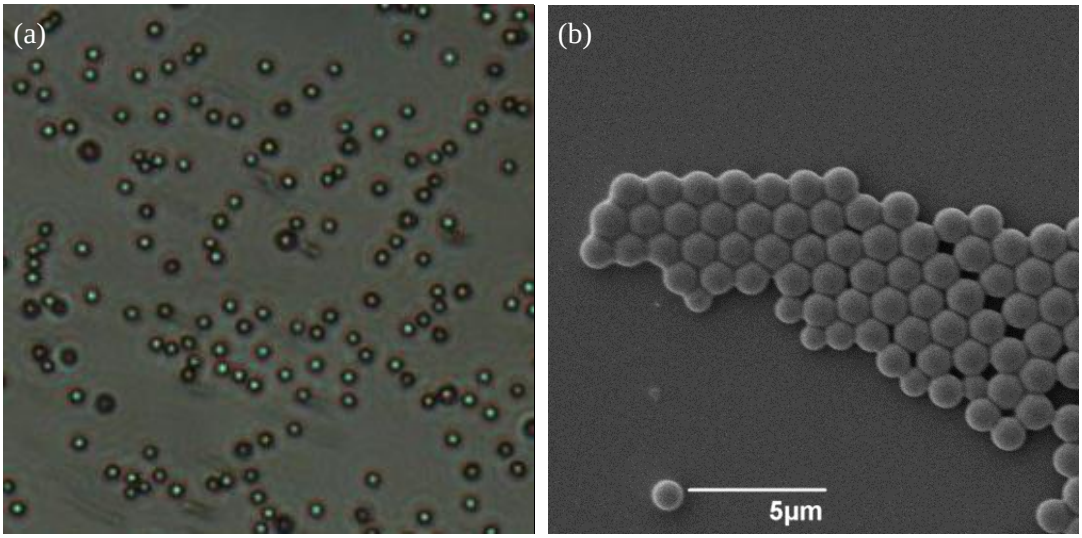

Figure 2.7: (a) Polarised optical microscopy (200× magnification, rt, slightly crossed polarisers) and (b) scanning electron microscopy photomicrographs (5000x magnification) of the particles produced at a reactant concentration of 0.15 mol dm^{-3}

The non-spherical nature of the particles at high concentration may be as a result of a fusing of nucleating particles due to the high concentration present in the dispersing solvent. The 'waistband' on the particles in the sample completed at 0.27 mol dm^{-3} is evidence of the fusing of particles, and can be seen in Figure 2.8.

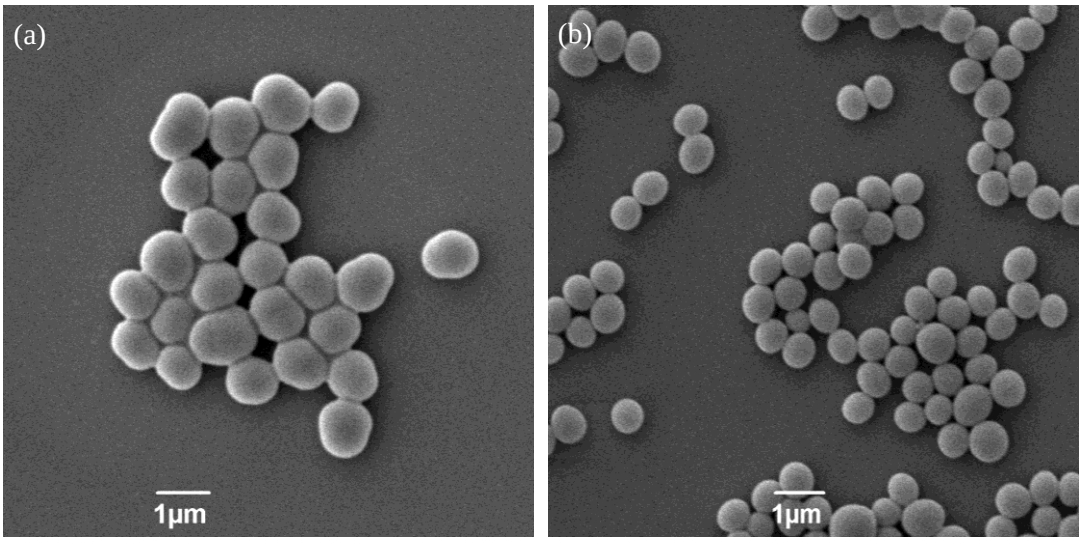

Figure 2.8: Scanning electron microscopy photomicrographs of the particles produced at a reactant concentration of (a) 0.27 mol dm^{-3} and (b) 0.35 mol dm^{-3} taken at room temperature at 10000× magnification.

In the sample created at 0.35 mol dm^{-3} the particles are smooth and spheroid with no waist banding, which may indicate coagulation of the nuclei is occurring much earlier, before

nucleation has completed. The formation of misshapen particles has been known to occur within dispersion polymerisation.[144, 145]

The high particle size polydispersity observed at low concentrations is as a result of bimodality. The samples display two size ranges of particles, with the smaller particles having a much lower degree of particle size variance than the larger. The bimodality is evidence of the occurrence of a second nucleation event occurring during the polymerisation, possibly as a result of the solubility being affected by changing the solvent to monomer ratio resulting in an extended nucleation period.

Overall, dispersion polymerisation proved not to be an effective method to produce nematic elastomer particles on the low microscale as it was only effective when the terminally attached monomer (**M1**) was employed and therefore an alternative method was investigated.

2.5 RAFT ASSISTED DISPERSION POLYMERISATION

2.5.1 *INTRODUCTION*

The addition of a RAFT (reversible addition-fragmentation chain transfer) agent[96, 142, 146] to dispersion polymerisation is another method by which crosslinking can be introduced into nematic particles and has been the focus of a recent Master's thesis.[147] RAFT-assisted dispersion polymerisation has been used to create monodisperse and crosslinked particles from various monomers.[96, 143, 148] RAFT agents have also been utilised in the synthesis of living particles[143, 148-151] whereby the particles can be grown further with the addition of more monomer. This allows for particles to be synthesised with a different surface composition to that of its core by changing the monomer feed and continuing the polymerisation.[150-153] RAFT agents follow a general structure which is illustrated in Figure 2.9 along with an example RAFT agent, DDMAT (2-(dodecylthiocarbonothioylthio)-2-methylpropionic acid).

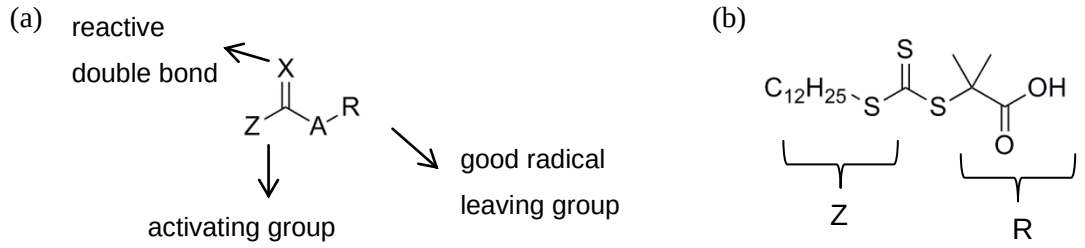

Figure 2.9: (a) general structure of a RAFT agent (b) the structure of DDMAT with the activating group labelled as 'Z' and the good radical leaving group labelled as 'R' as per the general structure.

The RAFT agent facilitates living chain transfer and allows for a greater monodispersity in polymer chain length to be achieved. RAFT-assisted dispersion polymerisation creates a large proportion of shorter polymer chains with a low degree of polydispersity. This is useful when applied to dispersion polymerisation as it allows for more polymer chains to grow in solution before the nucleation of particles begins. The longer pre- nucleation time this creates results in larger and more monodisperse particles compared to those created in its absence. The general mechanism for the chain transfer process is described in Figure 2.10.

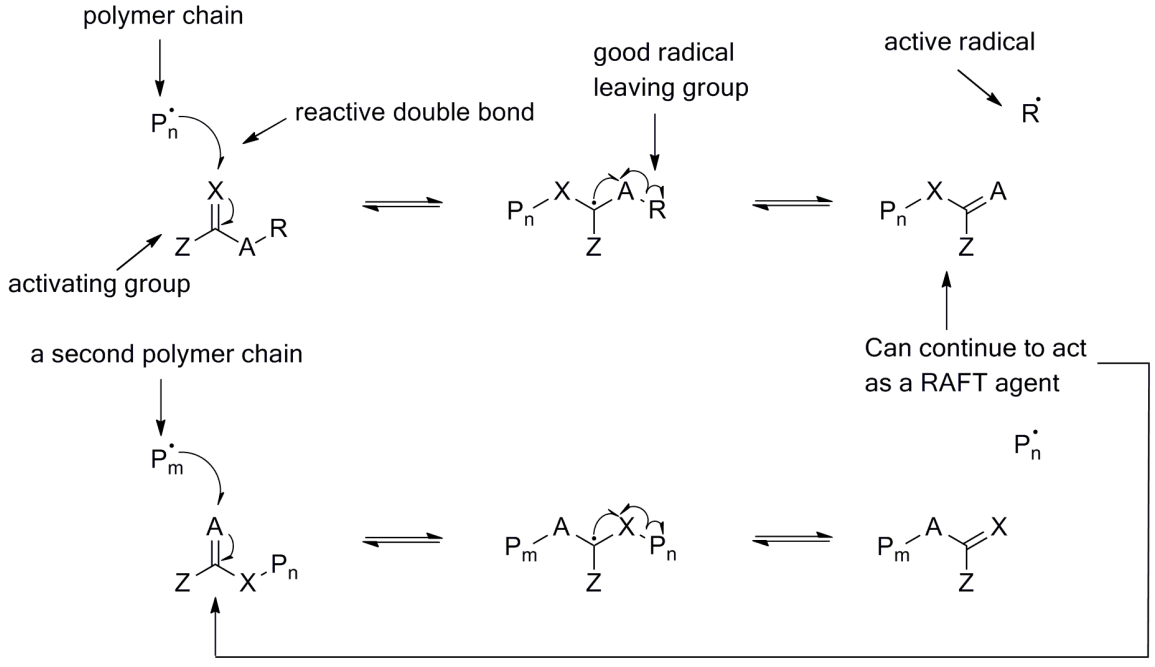

Figure 2.10: General mechanism for the chain transfer process that occurs during RAFT assisted dispersion polymerisation.

A RAFT agent acts as a chain transfer agent as it contains a stable radical leaving group.[154] When it reacts with the growing end of a polymer chain, this stable unit leaves and initiates the growth of a second polymer chain. This process therefore creates two shorter polymer chains when one would have been created in the RAFT agent's absence. The RAFT agent causes a reduction in the overall polydispersity of the polymer *via* a constant exchange process, promoting the formation of a high number of low molecular weight polymer chains with little variation in chain length, compared to in the absence of RAFT agent where once initiated, polymer chains continue to grow. With RAFT polymerisation the polymer chains can be re-initiated and continue to grow. This constant polymer chain transfer process results in the equilibration of polymer chains lengths over time.[154]

A RAFT agent may increase the degree of crosslinking that can be achieved within dispersion polymerisation compared to in the absence of a RAFT agent.[147] As a RAFT agent facilitates a living chain transfer process, it results in a more even distribution of network points throughout the sample and therefore a higher degree of crosslinking compared to when the crosslinker is added after the nucleation stage of polymer growth.

RAFT-assisted dispersion polymerisation has been used to create monodisperse particles from various non-liquid-crystalline monomers,[96, 143, 148] as well as being utilised in the synthesis of living particles[143, 148-151] whereby the particles can be grown further with the addition of more monomer. This method allows for particles to be synthesised with a different surface composition to that of its core by changing the monomer feed and continuing the polymerisation.[150-153]

2.5.2 *METHOD*

Particles were synthesised by RAFT-assisted dispersion polymerisation by first dissolving the chosen monomer (100 mg), the UV initiator (Darocur 1173, 4 wt % relative to monomer), the steric stabiliser (polyvinylpyrrolidone, 15 wt% relative to monomer) and the RAFT agent (DDMAT, 0.5 wt% relative to monomer) in the chosen reaction solvent (1.6 mL) in a rubber septum sealed glass vessel. This vessel was purged with nitrogen for a period of 30 minutes before being heated to a reaction temperature of 65 °C with constant and vigorous stirring. This temperature was selected to be within the nematic phase of the polymer being synthesised. When a homogeneous solution was obtained (typically in under one minute) the reaction vessel was exposed to broad band UV light for a period of 3 – 22 hrs. The nucleation stage can again be observed by the reaction mixture becoming turbid. After the designated exposure time the reaction vessel was allowed to cool to room temperature before immediate work up by a solvent

exchange method using centrifugation in order to remove all soluble impurities from the solvent and particle surfaces. A general reaction set up for RAFT-assisted dispersion polymerisation is shown in Figure 2.11. For the synthesis of nematic elastomer particles by RAFT assisted dispersion polymerisation the process was the same except for that a crosslinker (10 wt% relative to monomer) was added to the reaction vessel before purging. All exact reagents and conditions for each polymerisation completed can be found in the experimental chapter, Chapter 8.

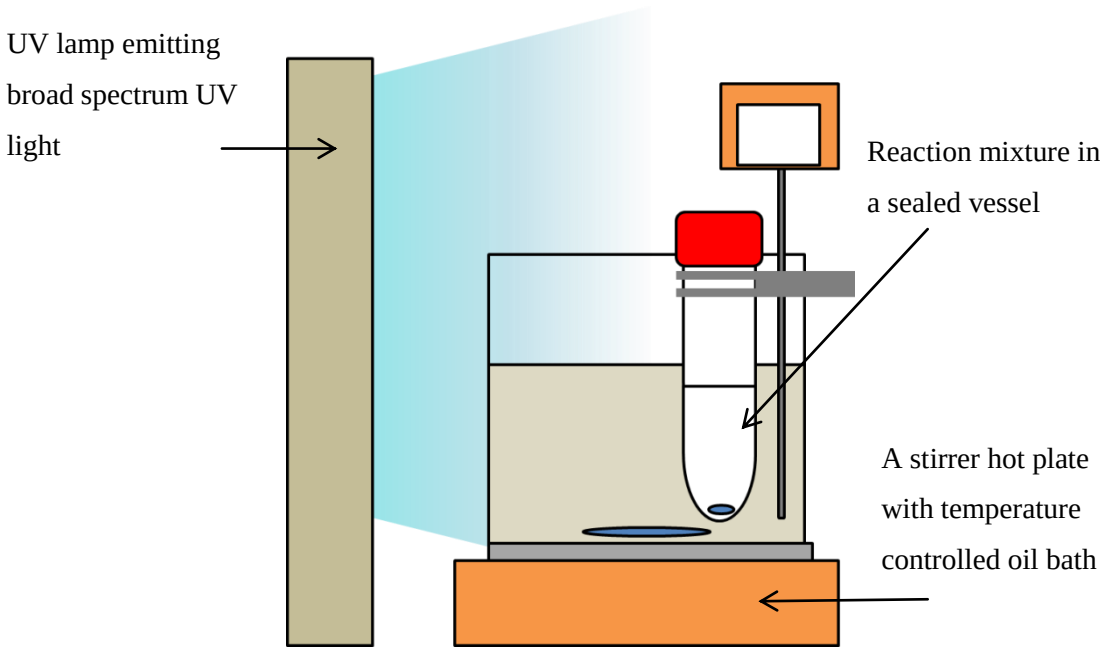

Figure 2.11: Diagram of the reaction set up for RAFT-assisted polymerisation

2.5.3 *METHOD DEVELOPMENT*

Traditionally RAFT polymerisations are performed as solution polymerisation and are initiated thermally.[154] RAFT agents slow the polymerisation as the chain transfer process results in the formation of more stable and therefore less reactive radicals. Within dispersion polymerisation, the nucleation of particles is affected if the growth of polymer chains is too slow,[98] which can affect the particle yield. UV initiation provides a greater immediate influx of radicals than thermal initiation and therefore combats the slowing of the reaction by the RAFT agent. The polymerisation was still heated through this process so that the polymerisation could occur within the nematic phase of the polymer in order to encourage nematic order within the particles.

The UV light exposure time was also increased until a satisfactory degree of polymerisation and crosslinking was achieved. Kinetic studies involving the extraction of samples from a polymerisation over a 10 hour period for analysis by gel permeation chromatography were inconclusive. The degree of crosslinking that was achieved was improved significantly on increasing the UV exposure time from 3 to 5 hrs, and exposing samples to UV for a period of 22 hrs resulted in a consistently high degree of crosslinking being achieved regardless of monomer used.

RAFT-assisted dispersion polymerisation in general created samples with a better degree of particle monodispersity than those created from dispersion polymerisation in the absence of a RAFT agent. This is because the RAFT agent facilitates chain transfer, resulting in a greater number of polymer chains growing to the critical chain length before particles begin to nucleate. In traditional dispersion polymerisation the growing polymer chains are of vastly different molecular weights which may result in a longer nucleation stage when small quantities of the reacting polymer reach their critical size. Within RAFT assisted dispersion polymerisation as chain polydispersity is greatly reduced the polymer chains will reach this critical chain length in a large quantity which will reduce the time-span of the nucleation stage of polymer growth and therefore reduce the polydispersity of the system. The nematic polymer particles obtained from 1:1 EtOH: methoxyethanol were consistently comprised of low molecular weight polymer chains and no significant gel content was obtained when a crosslinker was employed, indicating incomplete network formation which was confirmed by swelling and heating studies.

Gel content analysis was performed to assess the yield of networked polymer in the RAFT-assisted dispersion polymerisation process. The yield of networked polymer that is achieved within RAFT-assisted dispersion polymerisation is not uniform across the series of monomers and is also dependent on the polymerisation medium. For example, in Table 2.6 samples created from different monomers and solvent mixtures have been summarised.

For particles of **P3**, the trend in particle size and polydispersity indicates a solvent mixture of 5:1 EtOH: methoxyethanol to be the most appropriate for achieving a uniform sample, although reducing the amount of methoxyethanol increases the degree of crosslinking that is obtained, with the highest network formation created when no methoxyethanol was present and the particles were polymerised in EtOH. As methoxyethanol has an ether group it acts as a radical quencher, reducing the degree of polymerisation by producing a more stable and less reactive radical.[154] The least polar solvent tested was iPrOH, and this very polydisperse sample achieved a degree of crosslinking of only 29%.

Table 2.6: Gel content analysis results for particles created by RAFT-assisted dispersion polymerisation in various solvents.

Monomer		Solvent	Soluble fraction / mg	Gel fraction / mg	% gel
P1	Terminal	EtOH	1.63	5.74	93%
P1	Terminal	1:1 EtOH: ME	15.05	18.49	55%
P2	C3 chain, C4 spacer	EtOH	3.29	2.07	97%
P3	C4 chain, C4 spacer	EtOH	3.94	14.35	85%
P3	C4 chain, C4 spacer	1:1 EtOH: ME	12.68	14.15	47%
P3	C4 chain, C4 spacer	5:1 EtOH: ME	11.40	9.11	55%
P3	C4 chain, C4 spacer	10:1 EtOH: ME	7.40	3.27	69%
P3	C4 chain, C4 spacer	MeOH	4.94	9.29	65%
P3	C4 chain, C4 spacer	^{i}PrOH	4.20	1.75	29%
P4	C5 chain, C4 spacer	EtOH	1.89	5.90	78%
P5	C6 chain, C4 spacer	EtOH	4.66	5.00	66%
P6	C7 chain, C4 spacer	EtOH	0.66	0.46	83%
P7	C8 chain, C4 spacer	EtOH	6.24	7.24	61%
P8	C4 chain, C11 spacer	EtOH	5.08	9.18	71%
P9	C7 chain, C11 spacer	EtOH	13.46	8.00	66%

The polymerisation duration has a marked effect on the degree of crosslinking that is achieved with RAFT-assisted dispersion polymerisation, with a significant increase in gel content occurring with an additional 2 hours UV exposure time.

The amount of crosslinker in RAFT-assisted dispersion polymerisation used in this study (10 wt %) is slightly higher than that used in dispersion polymerisation with a delayed addition of crosslinker (10 mol %) as a result of replicating different literature procedures.[96, 101, 141-143] The differences in the degree of crosslinking achieved is not as a result of this increase however, as increasing the percentage of crosslinker in the delayed addition of crosslinker to 10 wt% does not greatly improve the network formation within the particles. A reason for this is that the degree of crosslinking within dispersion polymerisation is not limited by the amount of crosslinker present within the reaction mixture, but by the extent to which the crosslinker is being incorporated within the growing particles.

2.6 CONCLUSIONS

Nine nematic monomers were synthesised for use in the creation of nematic polymer and elastomer particles. Synthesis of novel monomers **M2** and **M4**-**M9** proved straight forward as known methods were easily adapted and most reactions yielded the monomers in high yield and purity.

Various adaptations to heterogeneous polymerisation techniques were completed in order to modify the polymerisations for the accommodation of the nematic monomers. Novel nematic polymer particles in the low micrometre size range were successfully synthesised by a dispersion polymerisation technique that was carefully adapted and optimised to accommodate the inclusion of the nematic monomers. It was also possible to successfully optimise the reaction conditions for the creation of monodisperse particles.

Attempts to adapt the dispersion polymerisation method for the creation of crosslinked elastomer particles proved largely unsuccessful. However, after careful optimisation of a RAFT type dispersion polymerisation process, it was possible to create nematic elastomer particles from all monomers and prove their crosslinking by gel content analysis. This preparation of nematic elastomer particles by heterogeneous polymerisation processes in this size range is previously unreported.

CHAPTER 3:

GENERAL CHARACTERISATION

3 GENERAL CHARACTERISATION

3.1 INTRODUCTION

This chapter will detail the physical and thermal characterisation of the monomers, polymers and polymer and elastomer particles prepared in the previous chapter. All monomers and polymer materials were investigated for their phase behaviour by differential scanning calorimetry (DSC) and polarising optical microscopy (POM). Molecular weight and molecular weight polydispersity of solution polymers and polymer particles were analysed by gel permeation chromatography and the size particle size morphology and distribution of the polymer and elastomer particles was determined by either scanning electron microscopy (SEM) or POM.

To assess their director configurations and responsiveness to external stimuli such as solvent exchange and exposure to electric fields, the polymer and elastomer particles were further studied by POM and electro-optic methods. These studies are discussed in separate chapters after this general characterisation chapter.

3.2 MONOMER CHARACTERISATION

Monomers **M1** – **M9** were characterised by differential scanning calorimetry (DSC) and polarised optical microscopy (POM) in order to determine their phase behaviour and to assess the effect of structural moieties on the resulting liquid crystal phases.

3.2.1 *POLARISED OPTICAL MICROSCOPY*

Polarised optical microscopy studies showed that the monomers **M2** –**M9** display nematic phases. **M2** and **M8** display monotropic liquid crystal phases and the monomers **M3** – **M7** and **M9** enantiotropic liquid crystal phases. Photomicrographs of some example nematic *schlieren* textures observed in POM studies of the monomers **M2** – **M9** are shown in Figure 3.1.

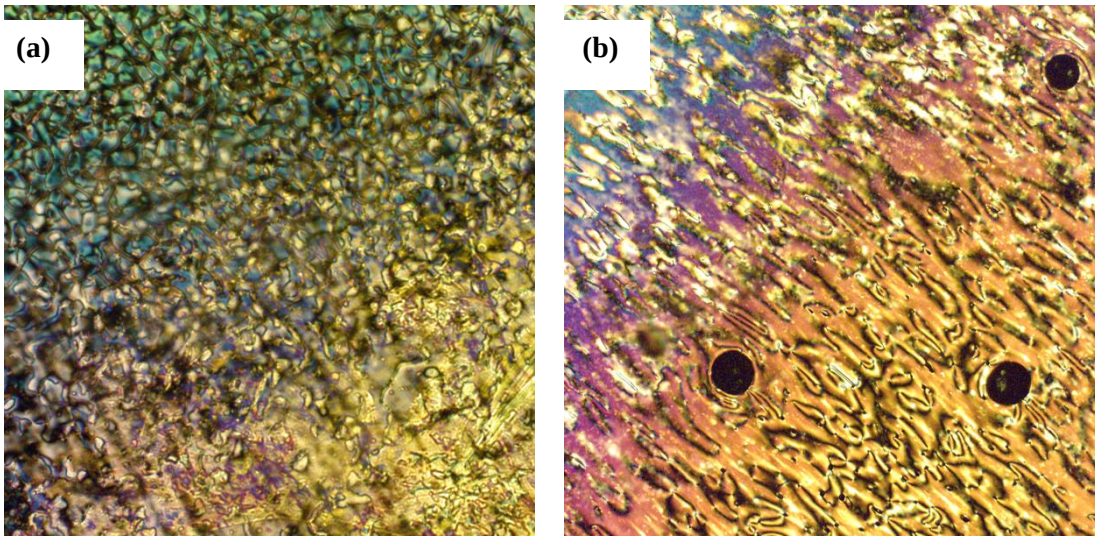

Figure 3.1: (a) Polarised optical photomicrograph of **M3**, taken at 40 °C on cooling at 5°C min^{-1} at 100 × magnification through crossed polarisers (b) polarised optical photomicrograph of **M6**, taken at 55 °C on cooling at 5°C min^{-1} at 100 × magnification through crossed polarisers.

3.2.2 *DIFFERENTIAL SCANNING CALORIMETRY*

In the differential scanning calorimetry (DSC) investigations phase transitions were taken from the second heat/cool cycle recorded at 10 °C /min, and are shown in Table 3.1. As an example, Figure 3.2 shows the DSC curves of **M6**.

Table 3.1: Phase transitions of nematic monomers **M1** – **M9**. Method: DSC at 10 °C /min with the second heat/cool cycle recorded. Glass transition temperatures were recorded from the second cool. Samples indicated (*) are phase transitions from literature.[79, 80, 133] The glass transition temperature for **M8** is listed as an approximate value as no glass transition was recorded on cooling, so the glass transition on heating is listed.

Material		Cr	/ °C	g	/ °C	N	/ °C	I
M1	Terminal	•	76					•
M1 *	Terminal	•	72					•
M2	C3 chain, C4 spacer			•	-14	•	61	•
M3	C4 chain, C4 spacer	•	42			•	82	•
M3 *	C4 chain, C4 spacer	•	71.9			•	98.3	•
M4	C5 chain, C4 spacer	•	34			•	58	•
M5	C6 chain, C4 spacer	•	36			•	81	•
M6	C7 chain, C4 spacer	•	21			•	61	•
M7	C8 chain, C4 spacer	•	23			•	69	•
M8	C4 chain, C11 spacer			•	~-23	•	65	•
M9	C7 chain, C11 spacer	•	-11			•	57	•

Figure 3.2 shows the DSC trace for monomer **M6** with all recorded heat and cool cycles included. The observed peaks within the trace are small and broad which may have resulted in the values for peak temperature (T_{peak}) and onset temperature (T_{onset}) being difficult to quantify precisely. For example, the value of T_{peak} shows a gradual progression through the heat/cool cycles which is not reflected in the temperatures quoted on onset. The broadness of the peaks may indicate that the sample was impure, though elemental analysis and NMR spectra of this compound indicate a good degree of purity. It is possible that the broad peaks are a result of exposing the monomer to extended heating, resulting in some polymerisation of the monomer occurring. However, if polymerisation was occurring throughout the DSC measurement it would be expected that the broadness of the peaks would increase as the experiment progressed as a result and this is not observed.

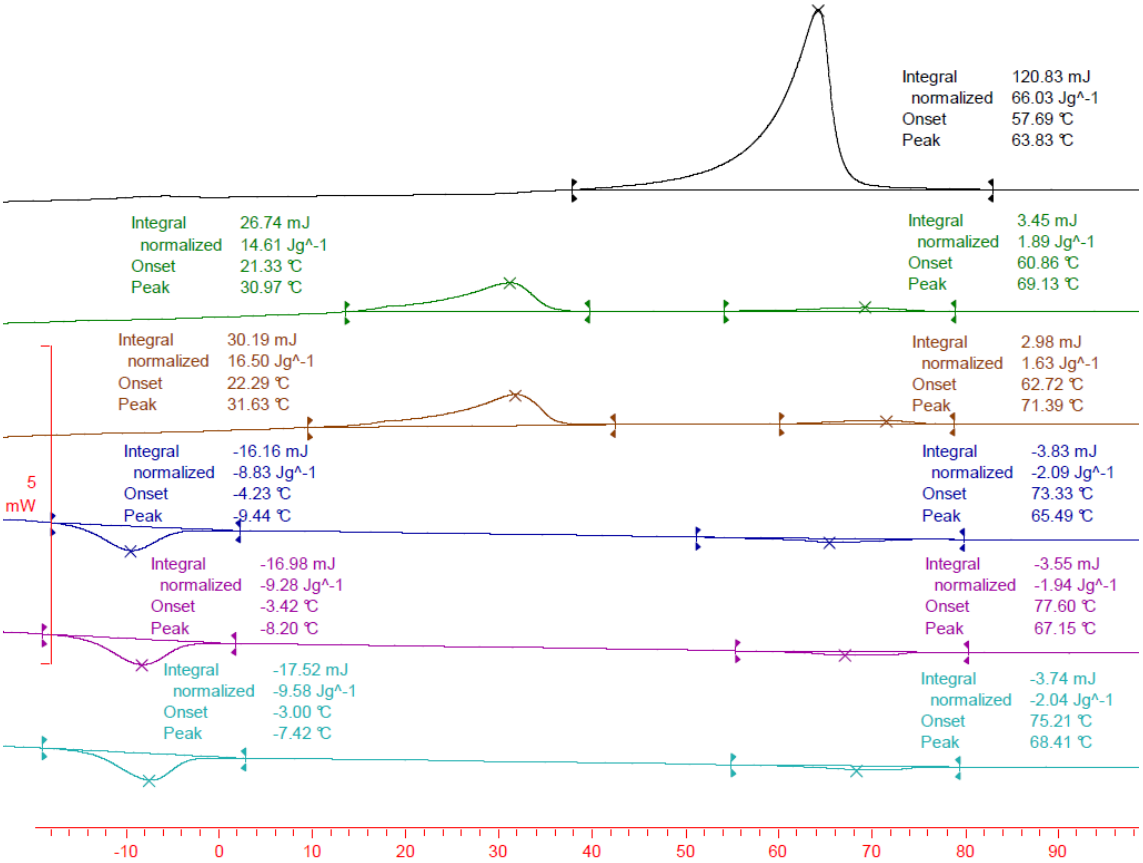

Figure 3.2: Example DSC of **M6** taken at 10 °C /min. In all instances the temperatures from the second heat/cool cycle were recorded.

The melting point of terminal monomer **M1** agrees well with the melting point stated in literature. There is, however, a significant discrepancy observed for phase transitions of **M3** compared to literature values, though if the first heat for **M3** is considered then the values are more similar to those stated in literature (Cr 72 °C N 83 °C I). A reduction in the nematic-to-isotropic transition temperature may well indicate the presence of an impurity, though elemental analysis shows a very strong agreement with predicted values as well as those stated in the referenced literature. ^{1}H NMR spectroscopy of **M3** also provides a strong indication that the monomer is well purified. A ^{1}H NMR spectrum of monomer **M3** is shown in Figure 3.3. From this information it can be concluded that the difference in phase transition temperatures observed is not a result of monomer impurity and may indicate that the values stated in the literature are, for some reason, inaccurate.

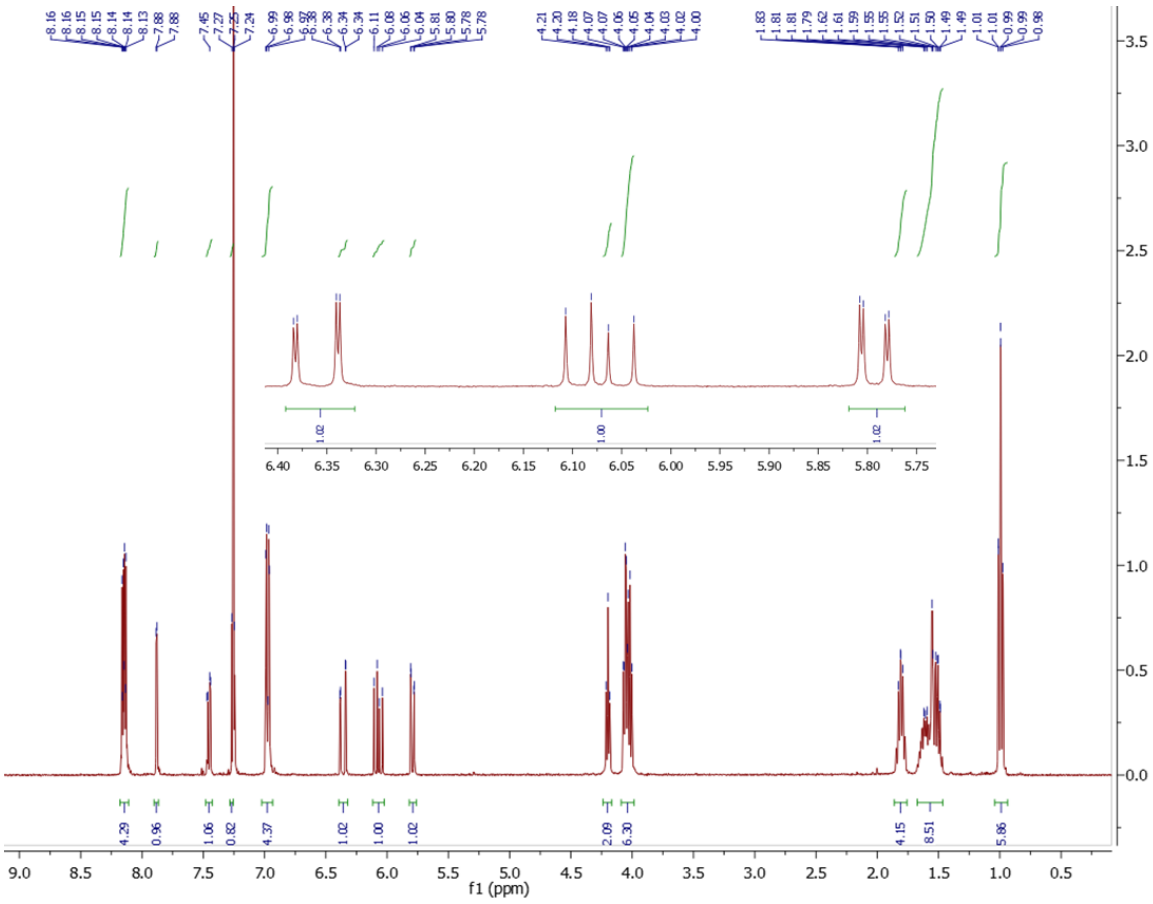

Figure 3.3: The ^{1}H NMR spectrum of monomer **M3** dissolved in $CDCl_3$

From Table 3.1 it is apparent that the crystal-to-nematic phase transition temperature decreases with increasing side chain length, as a result of the longer flexible chains disrupting the molecular packing. A similar trend is observed in the nematic-to-isotropic phase transitions, as the packing necessary for the nematic phase is disrupted by the terminal alkyl side chain groups on the mesogens.

The series of monomers from **M2** – **M7** with a C4 spacer group display a distinct odd-even effect in both their phase transition temperatures across the series, as can be seen from a plot of the transition temperatures against increasing side chain length, shown in Figure 3.4.

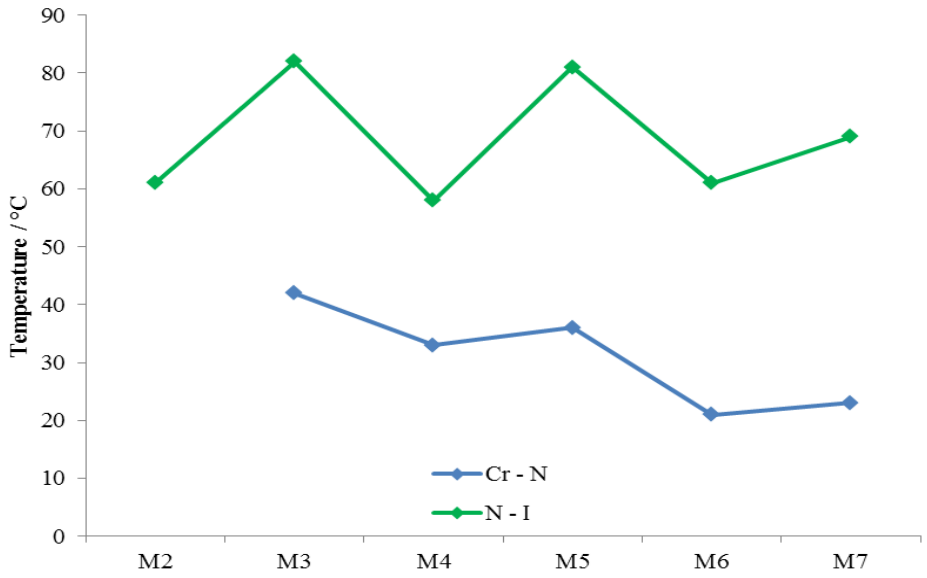

Figure 3.4: Graph to show the odd - even effect of the lateral monomers **M2** –**M7**.

Monomers with side chains that comprise of an even number of side-chain atoms display lower values than those with side chains that include an odd number. This well-known effect is a result of the even-membered chains causing a deviation from the more linear alkyl chain structure, disrupting the molecular packing.[17] This effect is illustrated in Figure 3.5.

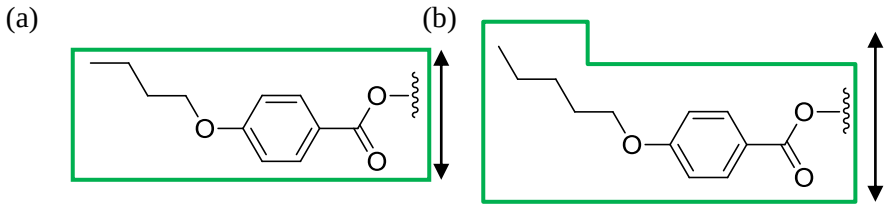

Figure 3.5: Illustrating the odd – even effect, where even-membered side chain groups result in a deviation from a linear structure and disrupt the molecular packing. Shown are the side chain groups of monomers (a) **M3** with phase transitions of Cr 42 °C N 82 °C I and (b) **M4** with the reduced phase transitions of Cr 34 °C N 58 °C I.

3.3 NEMATIC POLYMERS

The polymers were each characterised by gel permeation chromatography, differential scanning calorimetry and polarised optical microscopy in order to draw conclusions about the effect of polymerisation method and monomer structure on the molecular weight and phase transitions that can be achieved.

3.3.1 *ASSIGNMENT OF THE NEMATIC PHASE*

The polymers created by free radical solution polymerisation of **M1** – **M9** were investigated by polarised optical microscopy in order to unequivocally characterise the phase identity in the absence of confinement. All polymers displayed an enantiotropic phase when polymerised by solution polymerisation. Photomicrographs of two example nematic marble textures observed in the POM of the polymers are shown in Figure 3.6.

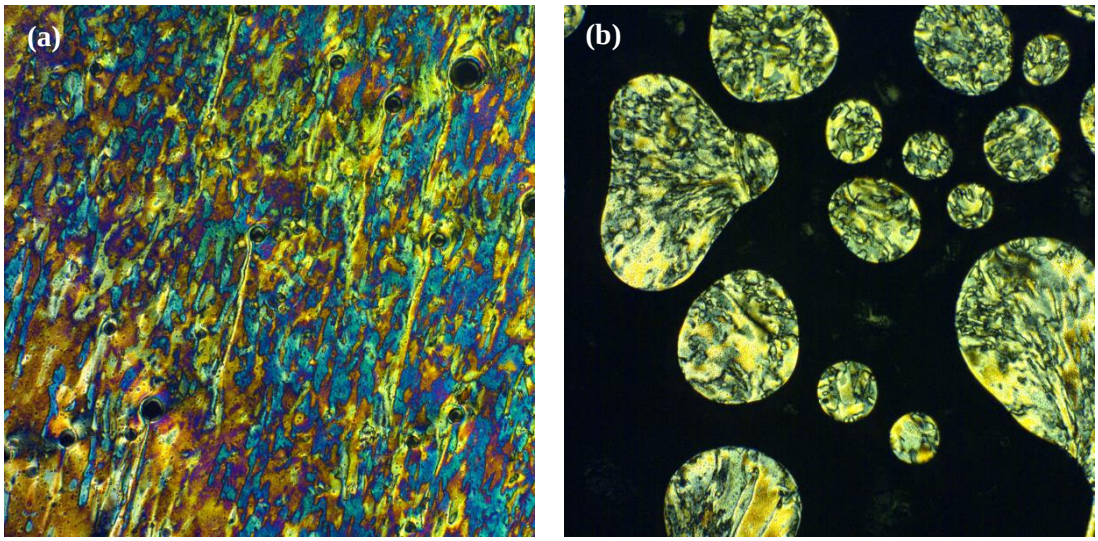

Figure 3.6: (a) POM photomicrograph of **M8**, taken at 35 °C on cooling at 5°C min^{-1} at 100 × magnification through crossed polarisers (b) POM of **M9**, taken at 25 °C on cooling at 5°C min^{-1} at 100 × magnification through crossed polarisers.

3.3.2 *DIFFERENTIAL SCANNING CALORIMETRY*

The polymer particles created by dispersion polymerisation, RAFT-assisted dispersion polymerisation and solution polymerisation were analysed by differential scanning calorimetry after removal of the host solvent and drying of the particles in order to assess the effect of polymerisation method on the resulting phase transition temperatures. Table 3.2 gives an overview of the phase transitions of polymers **P1** – **P9**, derived from monomers **M1**-**M9** respectively, polymerised by these different polymerisation methods.

Table 3.2: Phase transition temperatures of polymers **P1 – P9**, derived from **M1** – **M9** respectively. Method: DSC at 10 °C /min with values taken from the second heat/cool cycle. Glass transition temperatures stated are at the midpoint of the transition on cool, otherwise the onset on heat is quoted. DP stands for dispersion polymerisation.

Material		**Method**	**T_g / °C**	**N / °C**	**I**
P1	Terminal	Solution	• 27	• 101	•
		DP	• 28	• 115	•
		RAFT-assisted DP	• 26	• 114	•
		Literature[78]	• 31	• 127	•
P2	C3 chain, C4 spacer	Solution	• 45	• 83	•
		DP	• 52	• 108	•
		RAFT-assisted DP	• 51	• 92	•
P3	C4 chain, C4 spacer	Solution	• 31	• 59	•
		DP	• 26	• 65	•
		RAFT-assisted	• 24	• 72	•
		Literature[10, 132]	• 40	• 130	•
		Literature[128]	• 43	• 58	•
P4	C5 chain, C4 spacer	Solution	• 23	• 49	•
		DP	• 34	• 73	•
		RAFT-assisted DP	• 29	• 71	•
P5	C6 chain, C4 spacer	Solution	• 27	• 82	•
		DP	• 28	• 93	•
		RAFT-assisted DP	• 25	• 91	•
P6	C7 chain, C4 spacer	Solution	• 28	• 70	•
		DP	• 24	• 70	•
		RAFT-assisted DP	• 23	• 70	•
P7	C8 chain, C4 spacer	Solution	• 23	• 71	•
		DP	• 24	• 74	•
		RAFT-assisted DP	• 23	• 72	•
P8	C4 chain, C11 spacer	Solution	• 15	• 78	•
		DP	• 18	• 92	•
		RAFT-assisted DP	• 20	• 90	•
P9	C7 chain, C11 spacer	Solution	• -1	• 62	•
		DP	• 7	• 73	•
		RAFT-assisted DP	• 4	• 71	•

Representative DSC traces of polymers reported in Table 3.2 are shown in Figure 3.7.

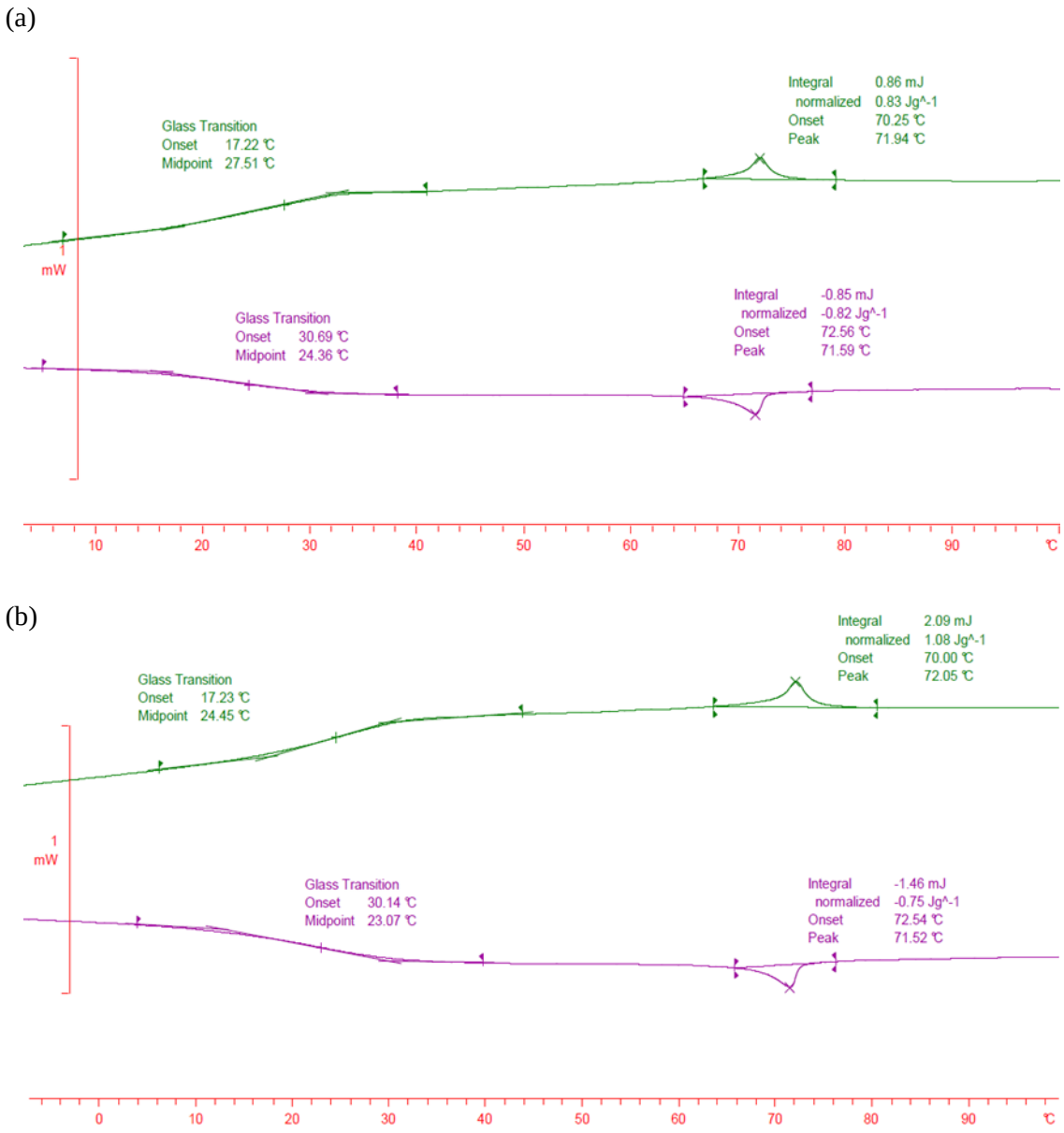

Figure 3.7: Example DSCs from Table 3.2. (a) **P6** from dispersion polymerisation and (b) **P6** from RAFT-assisted dispersion polymerisation.

The different phase transition temperatures with polymerisation method for each polymer are illustrated in Figure 3.8.

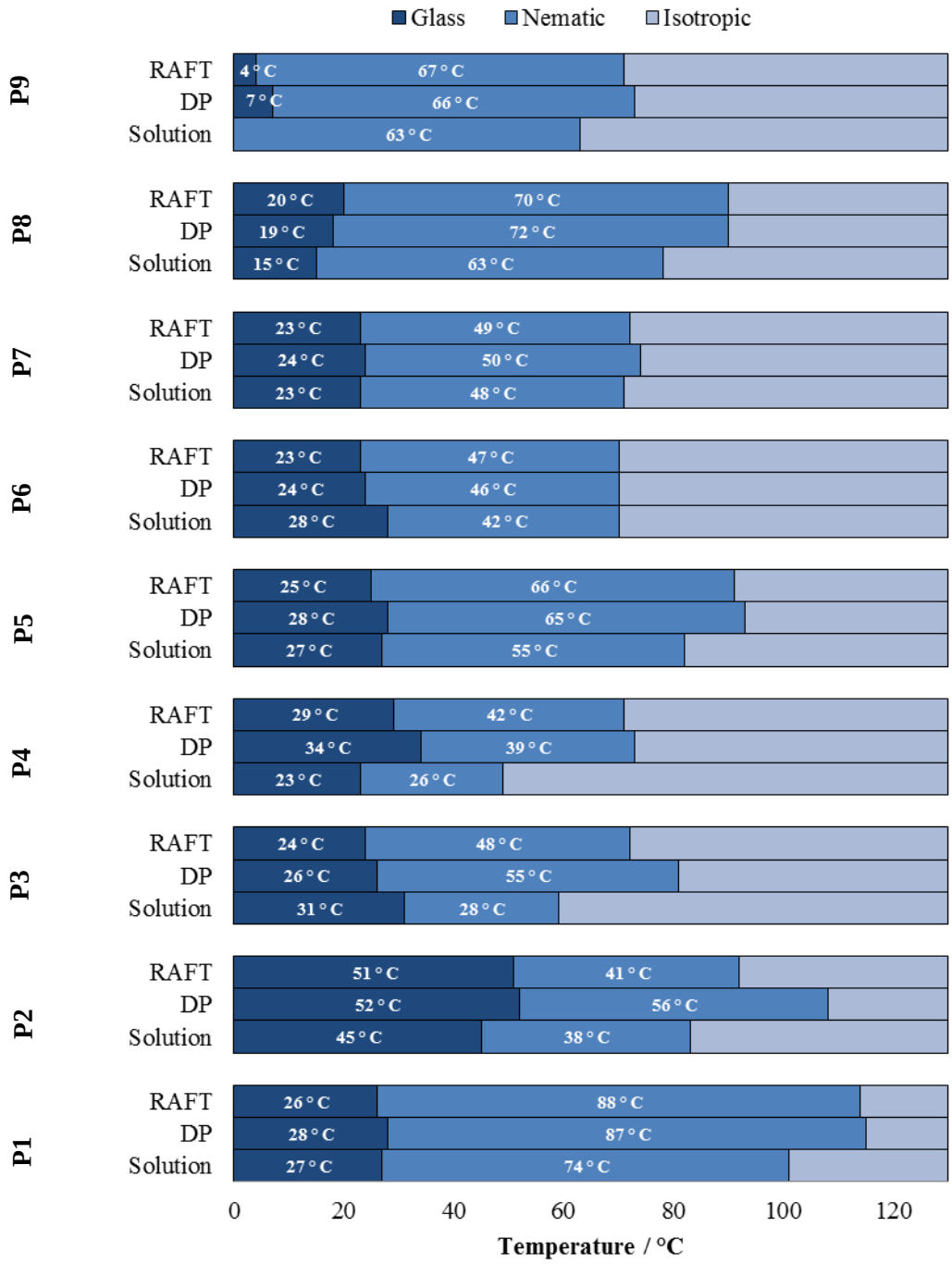

Figure 3.8: Phase transitions of polymers **P1** – **P9** made by different polymerisation methods. DP = dispersion polymerisation.

Figure 3.8 illustrates the phase ranges and transition temperatures of polymers **P1** to **P7** prepared by different polymerisation methods for comparison purposes. Comparison of polymers **P2** – **P7** shows that in general there is an influence of the mesogen side chain length on the reported phase transitions, showing a decrease in glass transition temperature as a result of increasing the side chain length on the mesogen. The glass transition temperature is far lower for polymers of **M8** and **M9** due to their longer spacer group attached laterally on the mesogenic unit. From Figure

3.8 we can also conclude that the addition of the RAFT agent into the polymerisation process does not greatly affect the phase transitions of the resulting polymer in comparison to dispersion polymerisation, with the majority of cases only varying by 1-2 °C. For polymers obtained by solution polymerisation the phase transitions temperatures vary more significantly, often showing a lower nematic phase transition temperature compared to polymers formed by dispersion polymerisation or RAFT-assisted dispersion polymerisation. This is possibly as a result of the polymerisation occurring in solution, and therefore in the isotropic phase of the polymer. Solution polymerisation allows for the polymer chains to form random coil formations without anisotropic influence from the nematic phase which may disrupt the nematic alignment when the nematic phase forms, reducing its phase range. As in most cases the lower nematic to isotropic phase transition temperature is accompanied by a drop in the glass transition temperature, another explanation for the reduced phase transition temperatures from solution polymerisation could lie with the purity of the samples. Solvents are notoriously difficult to remove from polymer samples, and any amount of the solvent used, DCM, which remains within the polymer matrix will disrupt the nematic order and therefore reduce the nematic transition temperature. DCM at the same time acts as a plasticiser and reduces the glass transition temperature.

3.3.3 *GEL PERMEATION CHROMATOGRAPHY*

Gel permeation chromatography was completed on polymer samples of each monomer created by dispersion polymerisation, RAFT-assisted dispersion polymerisation and solution polymerisation to assess the degree of polymerisation that can be achieved in each case as well as the effect of the degree of polymerisation on the phase transitions obtained.

Table 3.3 shows the molecular weights and polydispersities of polymers of **P1** – **P9** obtained by 24 h solution polymerisation, dispersion polymerisation and RAFT-assisted dispersion polymerisation. The molecular weights and polydispersities were obtained from dried samples using triple detection gel permeation chromatography in THF, and the numbers quoted are an average of three experimental runs. The molecular weights are stated to the nearest 1000 g mol^{-1} to reflect the average error across the three runs.

Table 3.3: Molecular weights of nematic monomers **M1 – M9** polymerised by various polymerisation methods. Method: Triple detection GPC with THF mobile phase, calibrated with polystyrene with a molecular weight of 99,000 g mol^{-1}. The values quoted are an average of three repeats. Solution polymerisations of **P1**, **P4**, **P5** and **P7** and RAFT polymerisations of **P7** do not feature in this study due to time constaints and lack of an available sample.

Material		Polymerisation method	M_n / g mol^{-1}	Molecular weight polydispersity (M_w/ M_n)
P1	Terminal	Dispersion polymerisation	197,000	2.87
		RAFT-assisted	188,000	2.40
P2	C3 chain, C4 spacer	Solution	441,000	2.67
		Dispersion polymerisation	209,000	2.68
		RAFT-assisted	128,000	1.74
P3	C4 chain, C4 spacer	Solution	256,000	7.91
		Dispersion polymerisation	188,000	3.04
		RAFT-assisted	171,000	1.61
P4	C5 chain, C4 spacer	Dispersion polymerisation	254,000	2.14
		RAFT-assisted	152,000	1.80
P5	C6 chain, C4 spacer	Dispersion polymerisation	340,000	2.12
		RAFT-assisted	105,000	2.02
P6	C7 chain, C4 spacer	Solution	204,000	2.16
		Dispersion polymerisation	122,000	3.11
		RAFT-assisted	215,000	1.65
P7	C8 chain, C4 spacer	Dispersion polymerisation	121,000	3.01
P8	C4 chain, C11 spacer	Solution	244,000	2.25
		Dispersion polymerisation	19,000	2.97
		RAFT-assisted	240,000	1.60
P9	C7 chain, C11 spacer	Solution	550,000	4.85
		Dispersion polymerisation	15,000	2.96
		RAFT-assisted	66,000	1.89

Figure 3.9 shows an example gel permeation chromatograph from which the information in Table 3.3 was calculated. In order to calculate the molecular weight the GPC trace must show a signal in all three detection modes. The refractive index (shown in red) often shows the presence of more analytes, such as oligomers, within the sample but as the concentration of those analytes are too low to be detected by a change in viscosity (shown in blue) or a change in the right angle light

scattering (RALS-shown in green) no molecular weight can be obtained for them. The peak which occurs at a retention time of ~ 23 minutes is the solvent front.

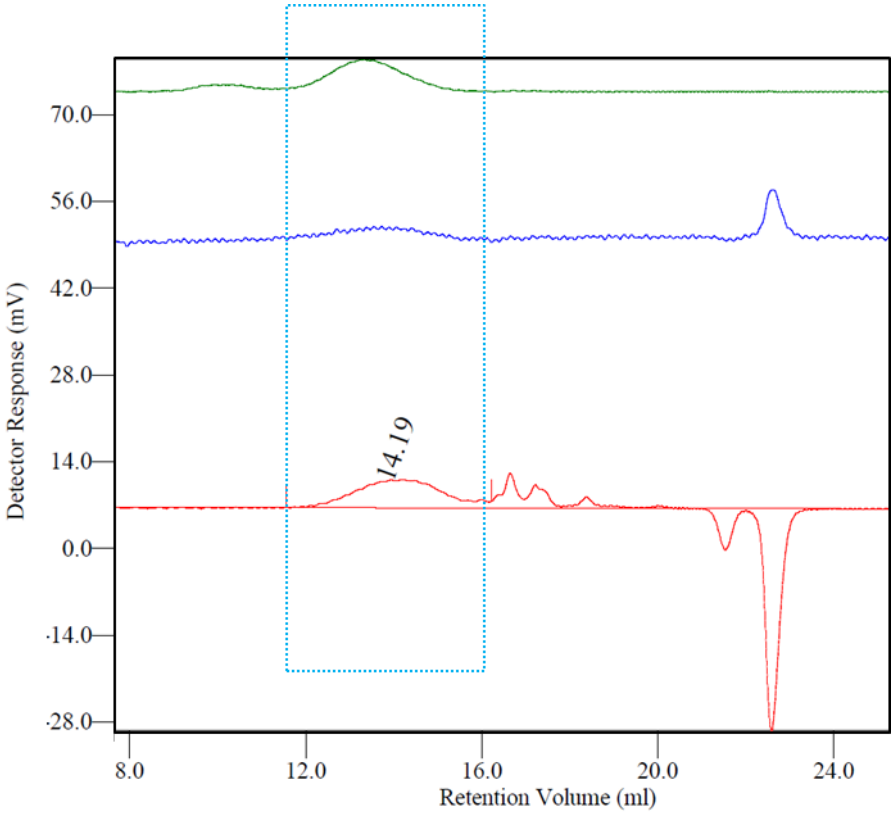

Right angle light scattering

Viscosity

Refractive index

Peak RV - (ml)	14.187
Mn - (Daltons)	256,249
Mw - (Daltons)	560,041
Mz - (Daltons)	1.006 e 6
Mp - (Daltons)	375,926
Mw / Mn	2.186
Percent Above Mw: 0	0.000
Percent Below Mw: 0	0.000
IV - (dl/g)	0.0889
Rh - (nm)	8.687
Wt Fr (Peak)	1.000
Mark-Houwink a	0.444
Mark-Houwink logK	-3.573
Branches	0.000
Branch Freq.	0.000
RI Area - (mvml)	10.88
UV Area - (mvml)	0.00
RALS Area - (mvml)	10.71
LALS Area - (mvml)	0.00
DP Area - (mvml)	4.93

Figure 3.9: A representative GPC analysis from which the information in Table 3.3 was extracted. **P4** from dispersion polymerisation. The quoted values in Table 3.3 are an average of three experimental runs. Method: Triple detection GPC with a THF mobile phase, calibrated with polytstyrene with a molecular weight of 99,000 g mol^{-1}.

From Table 3.3 it is apparent that polymer particles of **P8** and **P9** were obtained with significantly lower molecular weights in dispersion polymerisations than other polymers in the series due to the fact that these monomers polymerise more slowly, and coagulation occurred in attempted prolonged dispersion polymerisations. In most cases the highest molecular weight polymer is obtained from solution polymerisation rather than dispersion polymerisation or RAFT-assisted dispersion polymerisation. The viscosity increase which occurs within the nucleated particles of dispersion polymerisation hinders the polymerisation leading to increased termination and a reduction in the molecular weight that is achieved. Solution polymerisation results in higher molecular weights being obtained as a result of low viscosity allowing for a higher degree of polymerisation to be achieved, though the molecular weight polydispersity is also significantly increased when solution polymerisation is used.

In most cases dispersion polymerisation and RAFT-assisted dispersion polymerisation results in polymers with similar degrees of polymerisation, though a RAFT-assisted dispersion polymerisation process results in slightly lower molecular weights being achieved than would have in the absence of the RAFT agent, as the RAFT agent aids the transfer of the radical to create a larger number of smaller polymer chains. RAFT-assisted dispersion polymerisation also results in a reduction in the molecular weight polydispersity of the polymer chain length as expected, as a RAFT agent promotes a living chain transfer process which results in the eventual equilibration of molecular weights across a sample However, for particles of **P8** and **P9,** low molecular weights were obtained when the particles were synthesised by dispersion polymerisation and a marked increase in the degree of polymerisation was achieved when a RAFT agent was employed. This increase in the degree of polymerisation may be as a result of the RAFT-agent aiding radical transfer which was previously prevented by the high viscosity in the systems.

3.3.4 *PARTICLE SIZE AND PARTICLE SIZE VARIANCE*

The obtained particles were analysed for their particle size and size variance. The polymerisation solvent was evaluated in order to establish its effect on the particle size and particle size variance that can be achieved for each polymer **P1-P9**. Solvents which produce a low variance of particle size for particles of one monomer may not be suitable for the polymerisation of a different monomer due to the different relative solubilities and reactivities of those monomers. Table 3.4 shows the different particle sizes and particle size polydispersities that were achieved from dispersion polymerisation of monomers **M1** – **M9** (labelled **P1 – P9**) in different polar solvents

and solvent mixtures. Particle size polydispersity refers to the range of particle diameters that were obtained within samples of each polymerisation, stated as the coefficient of variance (C_v).

Table 3.4: Particle size and particle size variance of polymer particles formed from monomers **M1**-**M9** by polar dispersion polymerisation in a variety of solvents determined by POM and SEM studies. 1:1 refers to a solvent mixture of 1:1 EtOH: methoxyethanol. Sizes indicated (*) were calculated from POM and due to image resolution are stated to a lower accuracy.

Dispersion polymerisation particles of		**Solvent**	**Approximate size /µm**	**Coefficient of variance (C_v)**
Terminal	**P1**	MeOH	0.85	10.7%
		EtOH	0.86	7.2%
		1: 1	1.28	5.4%
C3 chain, C4 spacer	**P2**	MeOH	0.96	28.1%
		EtOH	1.90	16.0%
C4 chain, C4 spacer	**P3**	MeOH	1.30	21.7%
		EtOH	2.08	15.4%
		1: 1	3.2*	29%
C5 chain, C4 spacer	**P4**	MeOH	1.70	16.9%
		EtOH	2.15	22.9%
C6 chain, C4 spacer	**P5**	MeOH	1.27	12.5%
		EtOH	1.32	28.8%
C7 chain, C4 spacer	**P6**	EtOH	2.1 *	30%
		1: 1	5.1 *	25%
C8 chain, C4 spacer	**P7**	MeOH	0.76	12.2%
		EtOH	1.88	27.3%
C4 chain, C11 spacer	**P8**	MeOH	1.9 *	19%
		EtOH	3.4 *	23%
		1: 1	5.6 *	37%
C7 chain, C11 spacer	**P9**	MeOH	1.7 *	19%
		EtOH	2.9 *	22%
		1: 1	9.3 *	39%

It can be noted from Table 3.4 that solvent polarity and monomer solubility have an effect on the resulting particle size and particle size variance, with particles made from lateral monomers in EtOH and methoxyethanol being generally larger and more polydisperse than those made from MeOH or EtOH alone. For example, the average particle size listed for **P3** in Table 3.4 for

particles synthesised in EtOH is 2.08 μm with an average variance of 15.4%, compared to the particles synthesised in 1:1 EtOH: methoxyethanol which gives an average particle size of 3.2 μm with an average variance of 29%. This is as a result of monomers being very soluble in methoxyethanol; this allows the polymer chains to grow to a much larger degree before the nucleation of particles, producing an extended nucleation period with fewer growing particles which results in larger particles with a greater degree of variance being obtained.

Particles synthesised from **M1** are significantly larger when they are synthesised in a mixture of EtOH and methoxyethanol and display the best monodispersity of all samples investigated. This sample can be considered monodisperse because more than 90% of the particle size distribution lies within 5% of the median value.[155] **M1** has a significantly different structure to the other monomers being investigated as it is a terminally attached side-chain monomer with a cyano group terminating the mesogen, compared to the remaining monomers which are laterally attached side-chain monomers with terminating alkyl chains on the ends of the mesogenic group. This difference in structure explains its different solvent affinity, *i.e*. the monomer **M1** is less hydrophobic and therefore better soluble in polar solvents, and therefore the particle sizes that are obtained in different reaction mixtures.

The greatest degree of monodispersity, and also the smallest particle sizes, is generally achieved from MeOH, though the exact degree of particle size variance obtained varies for each monomer as a result of the different solvent affinities in each case.

3.4 NEMATIC ELASTOMERS

3.4.1 *DIFFERENTIAL SCANNING CALORIMETRY*

The phase transition temperatures of the nematic elastomer particles were analysed by DSC. Table 3.5 gives the glass transition temperatures and nematic network phase ranges for the elastomer samples synthesised by RAFT assisted dispersion polymerisation. For comparison this table also lists the phase transition temperatures of the respective polymer particles.

Table 3.5: Phase transitions of nematic elastomer and polymer particles formed by RAFT-assisted dispersion. Phase transitions were established by DSC at 10 °C/min where the second/heat and cool cycle was recorded.

Material		Polymerisation method	T_g	/ °C	N	/ °C	I
		RAFT-assisted (no CL)	•	27	•	114	•
P1	Terminal	RAFT-assisted (10 wt% CL)	•	37	•	90	•
		RAFT-assisted (no CL)	•	53	•	92	•
P2	C3 chain, C4 spacer	RAFT-assisted (10 wt% CL)	•	53			•
		RAFT-assisted (no CL)	•	30	•	77	•
P3	C4 chain, C4 spacer	RAFT-assisted (10 wt% CL)	•	37	•	69	•
		RAFT-assisted (no CL)	•	33	•	71	•
P4	C5 chain, C4 spacer	RAFT-assisted (10 wt% CL)	•	30	•	45	•
		RAFT-assisted (no CL)	•	23	•	91	•
P5	C6 chain, C4 spacer	RAFT-assisted (10 wt% CL)	•	27	•	60	•
		RAFT-assisted (no CL)	•	25	•	70	•
P6	C7 chain, C4 spacer	RAFT-assisted (10 wt% CL)	•	26	•	56	•
		RAFT-assisted (no CL)	•	20	•	90	•
P8	C4 chain, C11 spacer	RAFT-assisted (10 wt% CL)	•	21	•	64	•
		RAFT-assisted (no CL)	•	6	•	71	•
P9	C7 chain, C11 spacer	RAFT-assisted (10 wt% CL)	•	3	•	46	•

From the examples presented in Table 3.5 we can see that in most cases the glass transition temperatures increase marginally on addition of crosslinker, which is to be expected as the formation of a network reduces the flexibility and freedom of the system. A reduction in the nematic phase range is also observed when a crosslinker is present because it disrupts the nematic order.

3.5 Conclusions

A series of monomers **M1** –**M9,** synthesised from adaptations of literature procedures, which included the novel monomers **M2** and **M4** –**M9,** were analysed by differential scanning calorimetry and polarised optical microscopy in order to determine their phase transitions. All of the novel monomers displayed either monotropic or enantiotropic nematic phases with a wide temperature range. A distinct odd-even effect in both their Cr-N and N-I transition temperatures across the series was noted which correlated to the alkyl chain length on the spacer group.

Polarised optical microscopy and differential scanning calorimetry revealed the presence of the enantiotropic nematic phase across the entire series of polymers **P1** – **P9** irrespective of polymerisation method. Solution polymerisation methods were utilised in order to determine the effect of confinement on the nematic phase range that the particles would exhibit, revealing a reduction in glass transition temperature and N-I transition as a result of residual solvent molecules within the polymer matrix acting as a plasticiser as well as disrupting the nematic order. As the inclusion of solvent within nucleated particles is minimal, this effect was not observed for samples polymerised by heterogeneous methods.

Gel permeation chromatography indicated that the inclusion of a RAFT agent into dispersion polymerisation resulted in a slight reduction in the molecular weight and molecular weight polydispersity that was obtained for the polymer particles. RAFT-assisted dispersion polymerisation also resulted in a significant increase in the degree of polymerisation obtained for particles of **P8** and **P9**, indicating that it is a valid method for the polymerisation of all monomers. The highest molecular weight per polymer type was obtained when free radical solution polymerisation was employed, which is indicative that the viscosity within the growing particles of heterogeneous polymerisation methods limits the degree of polymerisation that can be obtained.

Differential scanning calorimetry of nematic elastomer particles established the presence of a nematic phase across the series. The nematic phase range of the elastomer particles was slightly reduced compared to nematic polymer particles possibly as a result of the network points disrupting the nematic order. The differential scanning calorimetry results are further evidence that the elastomer particles created within this thesis have significant internal network formation.

CHAPTER 4:

CONFINEMENT TEXTURES OF NEMATIC POLYMER PARTICLES

4 CONFINEMENT TEXTURES OF NEMATIC POLYMER PARTICLES

4.1 INTRODUCTION

The successfully synthesised polymer particles were investigated by polarised optical microscopy in order to determine the director configuration. The effect of monomer structure, dispersing solvent and temperature were evaluated. Using dispersion polymerisation nematic polymer particles were created within the size range of 1 – 5 μm in order to achieve a size range where surface controlled internal organisation should dominate.

4.2 EFFECT OF MONOMER

In Chapter 3, the general properties of polymers **P1-P9** (made from **M1-M9** respectively) were investigated, including factors like the phase transitions and degree of polymerisation obtained depending on the method of polymerisation used. In this section, amongst others, the effect of the mesogen structure on the particle properties will be investigated, specifically the director configurations that are observed.

As surface anchoring strength was expected to be a major factor in determining the director configuration, all particles were analysed both in their crude dispersions with PVP still present in the reaction solvent as well as in clean dispersions in ethanol. A series of polymer particles were synthesised in identical conditions in EtOH to investigate the effect of the chemical structure on the resulting director configuration of the polymer. As surface curvature can affect the director configuration that will result, the particles were also synthesised in a variety of different solvents to allow for different particle sizes to be investigated.

Table 4.1 summarises the different director configurations obtained from dispersion polymerisations of monomers **M1-M9**, each in EtOH and EtOH: methoxyethanol. The director configurations are described as observed in the crude dispersion and after purification in EtOH. As described in Chapter 2, the work-up stage involves solvent exchange into EtOH by a centrifugation process to remove any PVP55 from the surface of the particles.

Table 4.1: Configuration of polymer particles formed from monomers **M1**-**M9** by polar dispersion polymerisation in EtOH and 1:1 EtOH: Methoxyethanol determined by POM. For comparison all particles were also analysed when dispersed in clean EtOH after purification. Solvents listed as 1:1 describe a solvent mixture of 1:1 EtOH: methoxyethanol.

Particles of:		**Solvent**	**Crude configuration**	**Configuration in EtOH**
Terminal	**P1**	EtOH	Bipolar	Bipolar
		1: 1	Bipolar	Bipolar
C3 chain, C4 spacer	**P2**	EtOH	Bipolar	Bipolar
		1: 1	Bipolar	Bipolar
C4 chain, C4 spacer	**P3**	EtOH	Bipolar	Bipolar
		1: 1	Bipolar	Bipolar
C5 chain, C4 spacer	**P4**	EtOH	Radial	Radial
		1: 1	Bipolar	Radial
C6 chain, C4 spacer	**P5**	EtOH	Twisted Radial	Radial
		1: 1	Bipolar	Radial
C7 chain, C4 spacer	**P6**	EtOH	Radial	Radial
		1: 1	Bipolar	Radial
C8 chain, C4 spacer	**P7**	EtOH	Twisted Radial	Radial
		1: 1	Radial	Radial
C4 chain, C11 spacer	**P8**	EtOH	Bipolar	Bipolar
		1: 1	Bipolar	Bipolar
C7 chain, C11 spacer	**P9**	EtOH	Twisted Radial	Radial
		1: 1	Radial	Radial

In order to illustrate a change in director configuration in Table 4.1 more clearly, the table has been coloured according to the director configuration that is displayed, where green is bipolar, orange is radial and purple is twisted radial.

Polymer particles from the terminally attached nematic monomer **P1** display a bipolar configuration when analysed by POM in all investigated solvents. This director configuration has been arbitrarily assigned from the flashing the particles display as they spin with Brownian motion. For larger particles of other polymers the typical baseball extinction pattern of bipolar particles can be observed, as seen in Figure 4.1, but as the extinction pattern is too small to be fully resolved in some samples there is a possibility that these particles may display the uniform

confinement texture.[105] The assignment of a bipolar texture agrees with literature findings[6, 62, 104, 105] for particles of this monomer where bipolar particles are formed in polar solvents.

The lateral monomer series displays a systematic variation in chemical structure along the series. It was found that nematic polymer particles formed from monomers with short alkyl side chain groups of C3 or C4 (**M2, M3** and **M8**) displayed bipolar/uniform textures when observed by POM in EtOH. Some samples were polydisperse with sizes ranging from below 1 µm to around 5 µm; the director configuration was bipolar across the whole visible size range, indicating that the bipolar director configuration is preferred across a range of different surface curvatures. The preferred parallel surface anchoring is therefore strong enough in the investigated range to be a dominating factor in defining which director configuration will be displayed.

In direct contrast to monomers with alkyl groups of C3 or C4, monomers with alkyl groups of C5 or greater (**M4**-**M7** and **M9**) displayed a radial director configuration in EtOH across all observable size ranges. This comparison is illustrated in Figure 4.1.

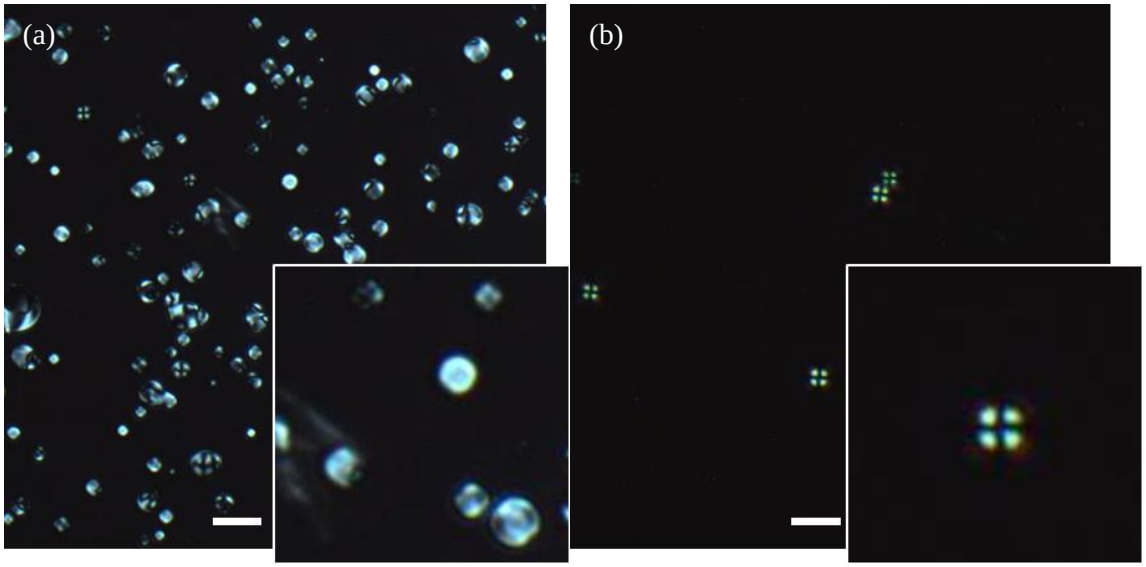

Figure 4.1: POM photomicrographs taken at rt with 200× magnification through crossed polarisers of (a) particles formed from **M8** in EtOH and (b) particles formed from **M9** in EtOH. Inset are magnifications to show confinement texture.

A possible rationalisation is that these polymers prefer a radial director configuration because the longer, laterally attached mesogenic groups may have a larger bend deformation elastic constant K_3 and therefore cannot accommodate the curvature of the particle surface as easily. By switching to a radial director configuration and ignoring the parallel surface influence the director configuration is of lower energy because of the smaller energetic cost of the splay deformation K_1

compared to the bend, K_3. However, this explanation would infer a dependence of director configuration on size, because of the different surface curvatures that are observed in particles of different sizes, which is not observed within the size range studied, as the particles are either all radial or all bipolar, irrespective of size.

Our results are in contrast to previous findings of nematic polymer particles synthesised by dispersion polymerisation in polar media such as water, EtOH and EtOH and methoxyethanol mixtures,[78, 79] which although never analysed as such show that bipolar particles are obtained when synthesised in polar media. This is true for a variety of different terminal monomer structures in particles across a size range of approximately 1 μm to 10 μm.[6, 62, 78, 79, 102-105] These findings do not include laterally attached monomers which polymerise to form prolate polymer chains with a large degree of coupling to the polymer backbone resulting in anisotropic polymer chains. Within our results, the anisotropic polymer backbone could be a factor in the ability of the liquid crystal to accommodate the surface curvature as the mesogenic freedom is reduced, and a switch to a radial director configuration may result in a significant change in the organisation of the polymer backbone which may result in a reduction in the energetic cost. The systematic approach chosen within this thesis revealed a direct and unexpected influence of an incremental change in mesogen structure on confinement texture.

The alkyl chain length of the spacer group was varied between a butyl spacer (**M2**-**M7**) and an undecyl spacer (**M8** and **M9**). There was no visible change in the director configuration as a result of this change, though an increase in particle size was observed. A possible rationalisation for this increase in size is as previously mentioned, the degree of polymerisation obtained for the longer spacer group monomers **M8** and **M9** was in general much lower for those with a butyl spacer (**M2- M7**). The difference in size obtained by using equivalent monomers with different spacer groups is illustrated in Figure 4.2.

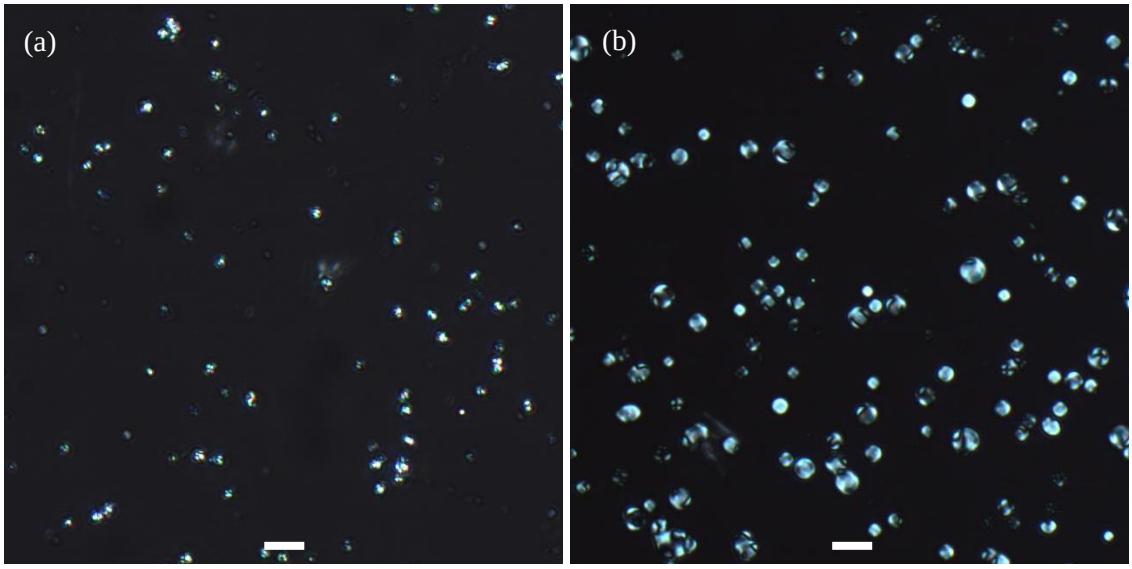

Figure 4.2: POM images with 200× magnification of particles made from (a) **M3** (C4 chains, C4 spacer) and (b) **M8** (C4 chains, C11 spacer) taken at room temperature through crossed polarisers. The scale bars represent 10 µm.

4.3 Effect of solvent

As discussed in the previous section, the structure of the monomer used has a marked effect on which director configuration the particles will display when dispersed in EtOH, with a switch occurring from a parallel surface alignment and a bipolar structure to perpendicular alignment and a radial structure between C4 and C5 side chain lengths. An investigation was carried out to establish whether this switch occurred at the same point in the lateral series when the particles were synthesised in a different reaction medium.

Also shown in Table 4.1 are the director configurations of particles synthesised from monomers **M1**-**M9** in both EtOH and 1:1 EtOH: methoxyethanol. Both of these reaction media are polar and promote a parallel surface anchoring of the liquid crystal, though as the addition of methoxyethanol changes the preferred director configuration for some polymers, it is reasonable to assume that it must change the surface anchoring strength of the solvent. This information is depicted graphically in Figure 4.3.

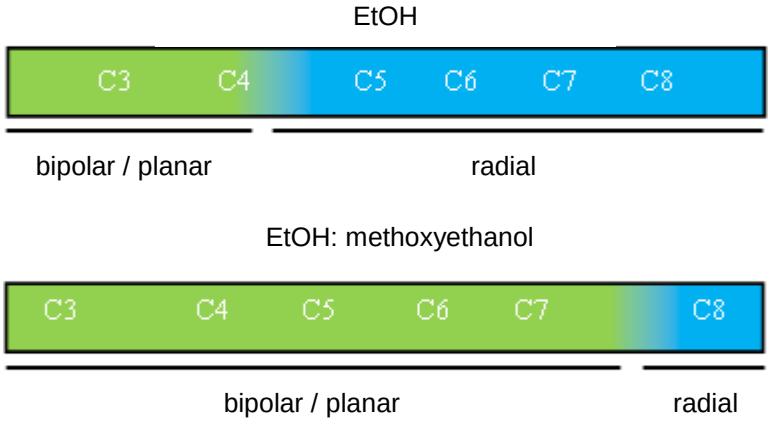

Figure 4.3: Showing the change in director configuration on increasing alkyl side chain length from C3 to C8 in polymers formed from **M2-M7** when polymerised in different solvents.

As can be seen in Table 4.1 and as illustrated in Figure 4.3, the switch from bipolar to radial occurs at longer alkyl side chain lengths in the series when the particles are obtained in EtOH: methoxyethanol mixture rather than EtOH alone, indicating that the particles are affected by the surface anchoring strength of their dispersing media. A response to changes in surface anchoring is an interesting prospect which could allow the particles to be used in applications as sensors for factors such as solvent polarity. Example photomicrographs are illustrated in Figure 4.4, showing the difference between particles of **M6** when synthesised in EtOH and in an EtOH: methoxyethanol mixture.

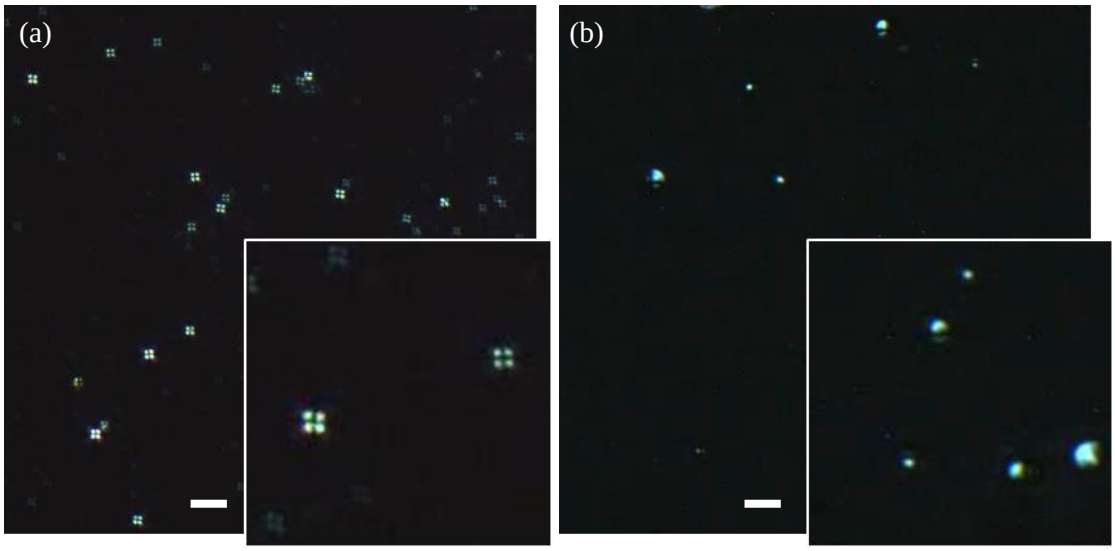

Figure 4.4: POM photomicrographs illustrating the different director configurations displayed by particles of **M6** when synthesised in (a) EtOH, the particles are displaying a radial director configuration and (b) EtOH: methoxyethanol, the particles are displaying a bipolar director configuration. Photomicrographs taken at room temperature through crossed polarisers with 200× magnification. The scale bars represent 10 μm. Inset are magnifications to show confinement texture.

A switch in the preferred director configuration occurs between C4 and C5 alkyl side chain lengths when the particles are synthesised in EtOH. A switch from bipolar to radial occurs instead only between C7 and C8 when the nematic polymer particles are obtained from 1:1 EtOH: methoxyethanol. As the elastic constants of the polymers have not changed, it is reasonable to assume that the parallel surface anchoring strength of the EtOH: methoxyethanol mixture must be stronger than that of pure EtOH, making a bipolar configuration the most favourable configuration until later in the series, despite the unfavourable bend deformation. The cost of the bend deformation may then eventually exceed the gain of aligning with the imparted surface anchoring, but not until much later in the mesogen structure series.

4.4 Effect of reaction temperature

For comparability of results, all polymerisation reactions were performed at the same temperature. Temperature is known to influence solubility which in turn will affect when the nucleation of particles occurs and the size that the particles reach. Polydispersity of particle size and molecular weight is also affected by temperature as the decay of AIBN is temperature dependent which influences the kinetics of free radical polymerisation and affects the degree of polymerisation that is obtained. Another factor strongly affected by temperature which may

potentially influence the resulting particle director configuration is the liquid-crystalline order within the particles. Particles polymerised outside of their nematic phase, in the isotropic state, may display different director configurations or polydomain internal structures as a result of being polymerised while no internal liquid-crystalline order is present, though this is likely reversible in polymer particles as annealing the particles after synthesis at temperatures well above T_g will allow for the organisation of the anisotropic polymer backbone.

Polymerising in the isotropic phase of the polymer in comparison to polymerising in the nematic phase was investigated to establish what effect this would have on the resulting director configuration of the particles. Polymerising at a higher temperature may also result in larger particles as a result of increased solubility of the monomer and polymer in the reaction medium. Figure 4.5 shows comparative photomicrographs illustrating the effect of polymerising in the isotropic versus the nematic phase. Of all the monomers synthesised, various monomers have the nematic – isotropic transition temperatures below the reaction temperature. The effect of polymerising within the nematic phase of the polymers was assessed for **M6**, **M8** and **M9**. Of these, only **M9** showed a difference when polymerised in the nematic phase as opposed to the isotropic, as shown in Figure 4.5.

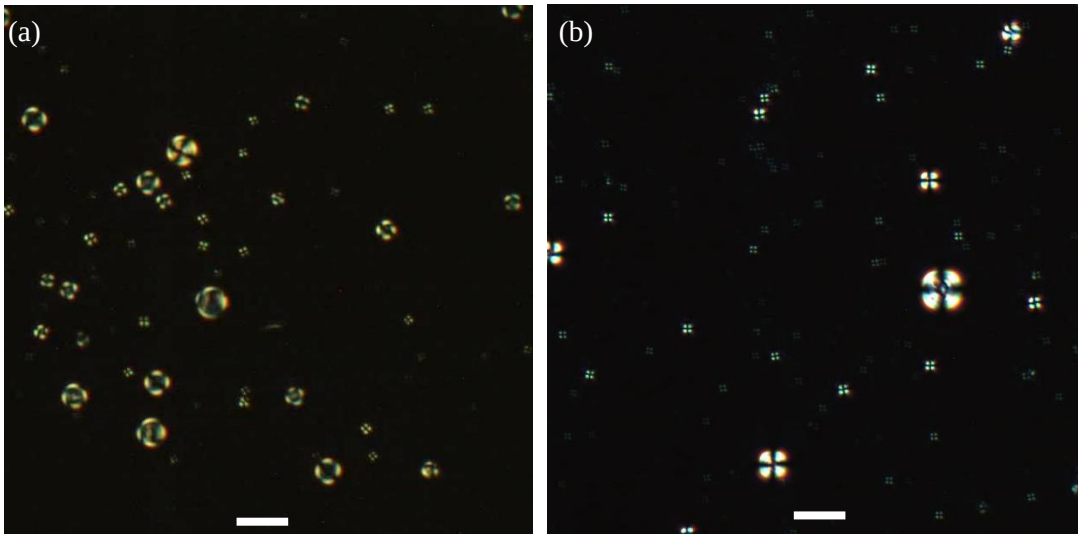

Figure 4.5: Polarised optical microscopy images taken through crossed polarisers at rt with 200× magnification. (a) **M9** polymerised in EtOH at 55 °C (nematic phase of polymer) and (b) **M9** polymerised at 73 °C (isotropic phase of polymer). The scale bars represent 10 µm.

When polymerised in the nematic phase rather than the isotropic phase of the polymer, the twisted radial configuration was observed, displaying an 'X' shaped extinction pattern rather than the Maltese cross pattern associated with the expected radial texture. The twisted radial structure is an intermediate escaped configuration known in the literature[156-159] to be of borderline stability.

It exists as the slight twist in one plane results in a minimisation of the splay deformation the central hedgehog defect causes. The twist usually results in the slight migration of the hedgehog defect, as illustrated in the schematic of the twisted radial director configuration shown in Figure 4.6.

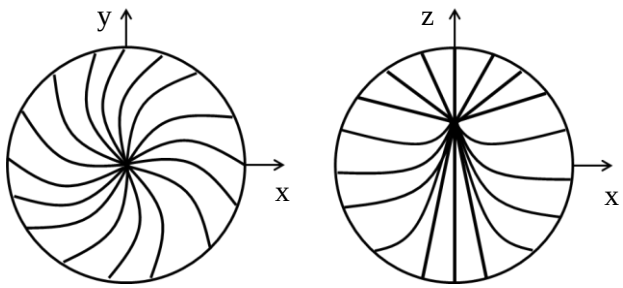

Figure 4.6: The twisted radial director configuration. A twist in one plane reduces the energetic cost of the splay deformation. The twist causes the central hedgehog defect to escape slightly in one plane.

Twisted radial particles can be further distinguished from radial particles using a λ wave plate. The addition of the wave plate allows for the director orientation within the particles to be determined. Isotropic regions are observed as magenta with the addition of a λ wave plate because the wave-front ellipsoid of the λ wave plate results in retardation of green light. Within an anisotropic sample, a director orientation with a wave-front ellipsoid parallel to the ellipsoid of the λ wave plate is observed as blue as a result of the addition of the two ellipsoids resulting in the relative retardation increasing to longer wavelengths, which results in the extinction of red light at the second polariser. Conversely, an orientation of the director with a wave-front ellipsoid perpendicular to that of the λ wave plate will result in a yellow colour being observed because in this case the relative retardation is decreased and blue light does not pass through the second polariser. When radial particles are observed with a λ wave plate, the blue and yellow quadrants of the Maltese cross extinction pattern appear in the same orientation across the sample as a result of the radial director configuration being symmetrical. The twist within twisted radial particles breaks this symmetry and allows for different configurations to be observed, because the twist will occur in different directions across the sample and the particles are randomly orientated between the polarisers and wave plate. A polarised optical microscopy image showing the twisted radial director configuration of particles of **P9** and the corresponding region with the addition of a wave plate showing the different observed twist directions within particles is shown in Figure 4.7.

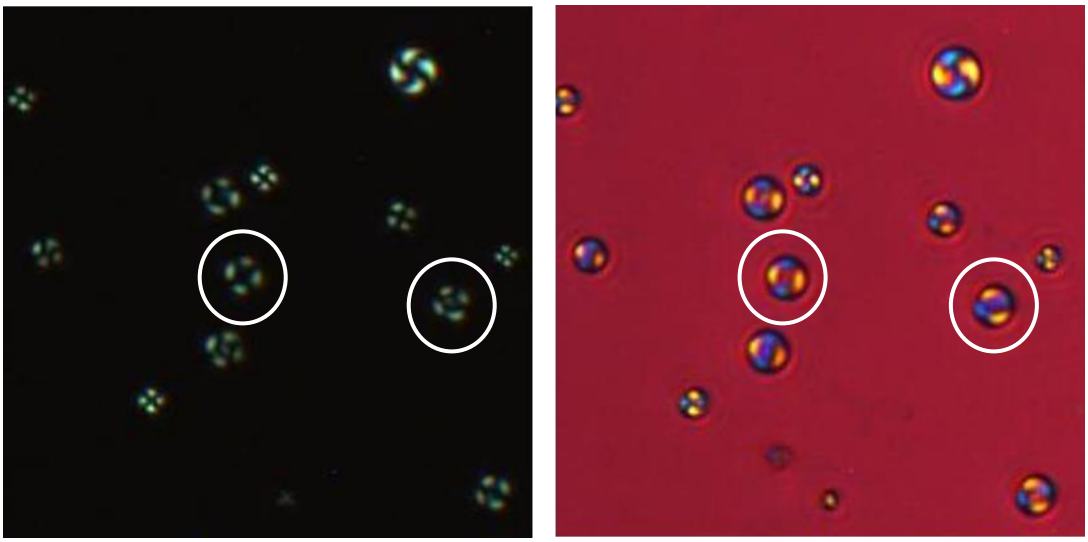

Figure 4.7: POM photomicrograph showing the twisted radial director configuration with the addition of a wave plate to show twist direction.

As shown in Table 4.1, particles made of **P9** also showed a twisted radial structure in crude EtOH dispersions. It would seem that these particles may have the propensity to escape into a twisted structure in order to reduce the energy cost of the splay deformation, as a twist in one plane reduces the amount in which the mesogenic units must splay. When polymerised in the nematic phase the mesogenic units arrange in the lowest energy configuration, the twisted radial director configuration. When polymerised in the isotropic phase the nematic organisation within the particles will not form until after the polymerisation has completed and the reaction is allowed to cool, with the possible result that the polymer chains are not in the optimal configuration for the lowest energy mesogenic organisation and therefore a different director configuration may result. When a nematic polymer with coupling between the backbone and the mesogenic unit is polymerised within the nematic phase the polymer chains organise anisotropically because of the organisation of the mesogenic units. This allows for the optimal organisation of the mesogens because the polymer organisation is dictated by their alignment. When a nematic polymer is polymerised within the isotropic phase the opposite is true, the polymer chains adopt an isotropic random coil formation as they are polymerised without an anisotropic influence. As the nematic phase is reinstated the polymer chains will align anisotropically with the mesogenic units as before but the entanglement of the polymer chains which occurred during polymerisation may prevent optimal alignment of the polymer chains and therefore result in a higher energy director configuration.

4.5 COPOLYMERISATION STUDY

The results discussed so far within this chapter indicate that a small change in monomer structure can result in an observable change in the director configuration. A copolymerisation study in EtOH using mixtures of **M8**, which polymerises to form bipolar particles, and **M9**, which in general polymerises to form radial particles, was completed to investigate the transition between these two configurations on increasing alkyl chain length. The aim of this study was to investigate the influence of copolymer composition on the director configuration, with the possibility of finding a copolymer ratio that created particles with a configuration on the borderline of its stable range.

The experiments were completed in 10 wt % increments, ranging from 100% **M8** to 100% **M9**; with additional smaller increments investigated when one monomer accounted for over 90% of the monomer feed stock. It is difficult to state unequivocally the compositions of the copolymers in each case as one monomer may be incorporated into the chain preferentially, but it can be estimated with the aid of ^{1}H NMR spectroscopy as the length of alkyl chain on each monomer is different. By evaluating the integrations of the alkyl regions in the spectra, the amount of **M9** present in the sample can be estimated.

The results of the full ^{1}H NMR study are displayed in the graph in Figure 4.8. Samples of each copolymer were thoroughly cleaned by a solvent exchange by centrifugation process and then dried for ^{1}H NMR analysis. The samples were allowed to fully dissolve in deuterated chloroform before being analysed by ^{1}H NMR. In order to increase the accuracy of integration the T1 delay time on the spectrometer was also increased to 10 s to accommodate for the slower relaxation time of the polymer.

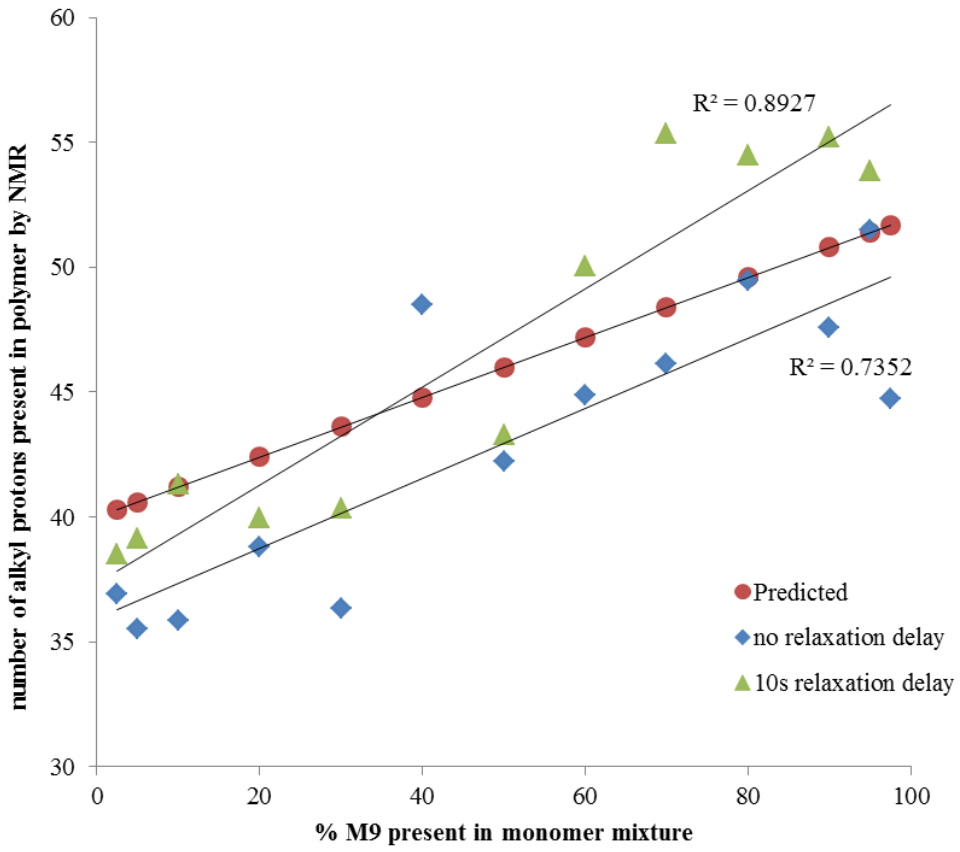

Figure 4.8: Scatter graph to show the increasing alkyl region from ^{1}H NMR spectra as the weight percentage of **M9** present in the monomer mixture increases.

It can be assumed that both monomers are being incorporated into the polymer in quantities roughly relative to the monomer mixtures as there is an observable increase in alkyl protons throughout the series. Although the observed results follow a similar gradient to the predicted results, they consistently integrate to lower values. When the relaxation delay period on the instrument was increased to accommodate for the slower polymer chains, the integration was then overestimated, though the series still followed an increasing trend.

The copolymerisation study revealed a director configuration that was prevalent to some degree across the entire sample range, the twisted radial director configuration, which was also observed in crude dispersions of polymer particles of **M9** in EtOH, as well as some polymerisations completed in the isotropic phase of the particles in EtOH. Shown in Figure 4.9 are example photomicrographs from the copolymerisation study, illustrating the presence of the twisted radial configuration to some extent across all copolymer compositions. These particles were synthesised using dispersion polymerisation in EtOH. Figure 4.9 (a) and (b) show particles large enough for the extinction pattern to be fully resolvable and the ‘X’ shape characteristic of the twisted radial samples to be observed. Particles in Figure 4.9(c) are smaller and the ‘X’ shaped extinction

pattern is resolved only for the larger particles. The remaining particles can be distinguished from bipolar particles as the observed birefringence does not change as they spin, and distinguished from radial particles as the addition of a wave plate shows the presence of a twist. Evidently these effects cannot be expressed in the images presented here. The image shown in Figure 4.9(d) is primarily a bipolar sample, which when the particles are small can be assigned by an observable flashing as a result of the changing birefringence the particles display on rotation. There is a small presence of twisted radial particles within this sample which are static in comparison.

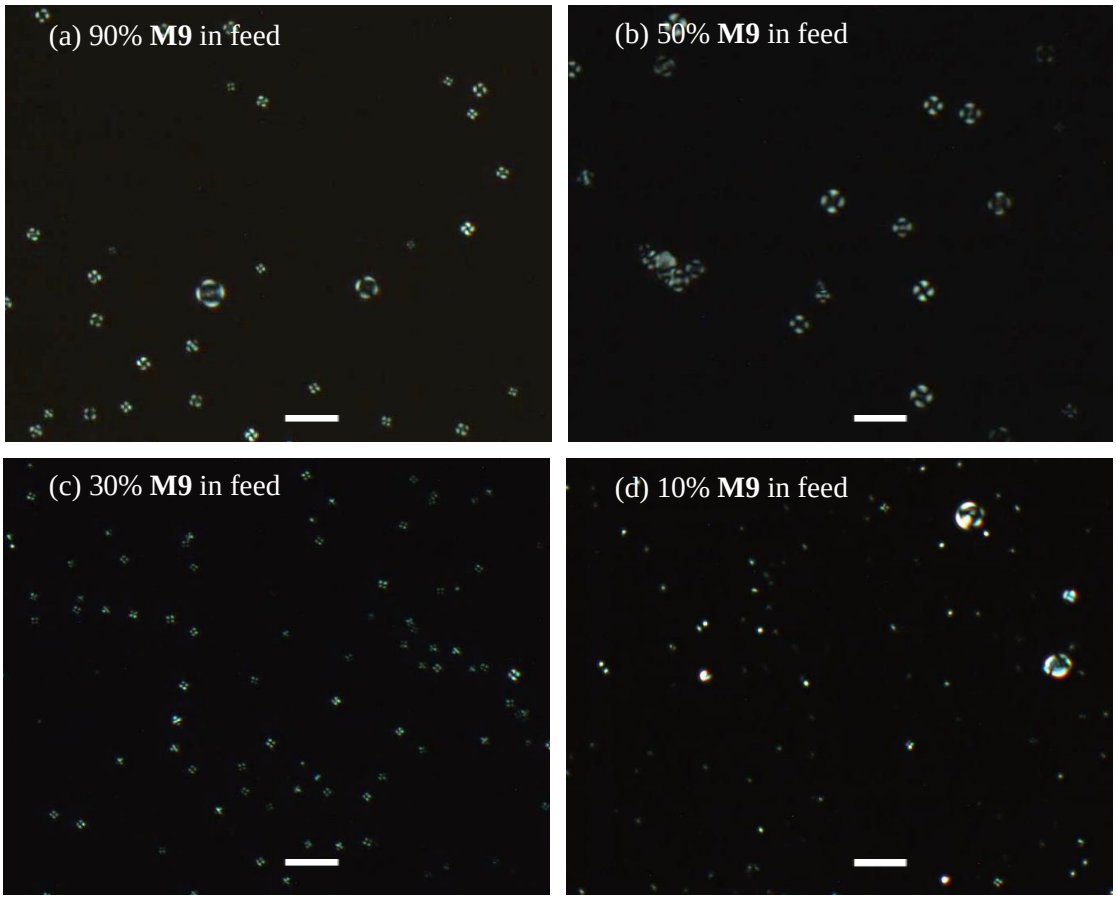

Figure 4.9: Selected polarised optical photomicrographs illustrating the presence of the twisted radial configuration to some degree throughout the entire copolymerisation series. Images taken at room temperature, through crossed polarisers. Scale bar represents 10 μm.

It would seem that particles formed from **M9** contain a predisposition to escape into a twisted structure, minimising the splay deformation from the central hedgehog defect. A second copolymerisation study was completed with monomers **M3** and **M6**, which reproducibly display bipolar and radial textures in dispersions in EtOH respectively, to assess whether the twisted radial configuration will be present in samples without a predisposition to form the twisted structure. The results of this copolymerisation study, completed in 10 wt % increments, ranging

from 100% **M3** to 100% **M6,** are illustrated in the graph in Figure 4.10. For this NMR study a 10 second relaxation delay was employed to accommodate for the slower relaxation of polymers.

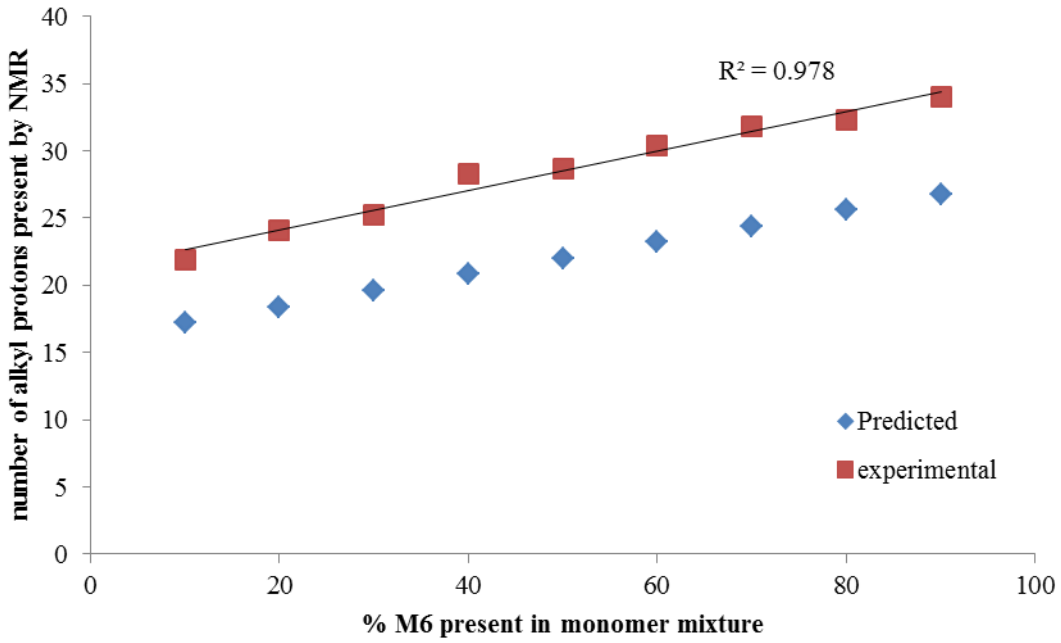

Figure 4.10: Scatter graph to show the increasing alkyl region from ^{1}H NMR spectra as the volume of **M6** present in the monomer mixture increases.

This copolymerisation study shows a very strong correlation between the integration of the alkyl region in the proton NMR and the predicted composition of the copolymer based on the monomer feed. This is strong evidence that the polymer composition reflects that of the monomer feed. However, the alkyl region of the NMR is integrating consistently higher than the predicted values calculated from the molecular weights of the relative monomer mixtures would suggest. This indicates that the relaxation delay used may not have been sufficient to allow for full relaxation of the polymer and therefore reducing the accuracy of the integration. Alternatively, it could indicate that there are impurities within the samples. PVP (poly(vinylpyrrolidone)), the steric stabiliser used in all the reactions shows predominantly in the alkyl region of the ^{1}H NMR. Its presence would result in the alkyl region integrating considerably higher, though it is unlikely to result in a consistent increase as these particles were evaluated after cleaning by centrifugation, so the amount of PVP remaining on the particle surfaces will be minimal.

Shown in Figure 4.11 are some example polarised optical microscopy photomicrographs from the copolymerisation of **M3** and **M6**.

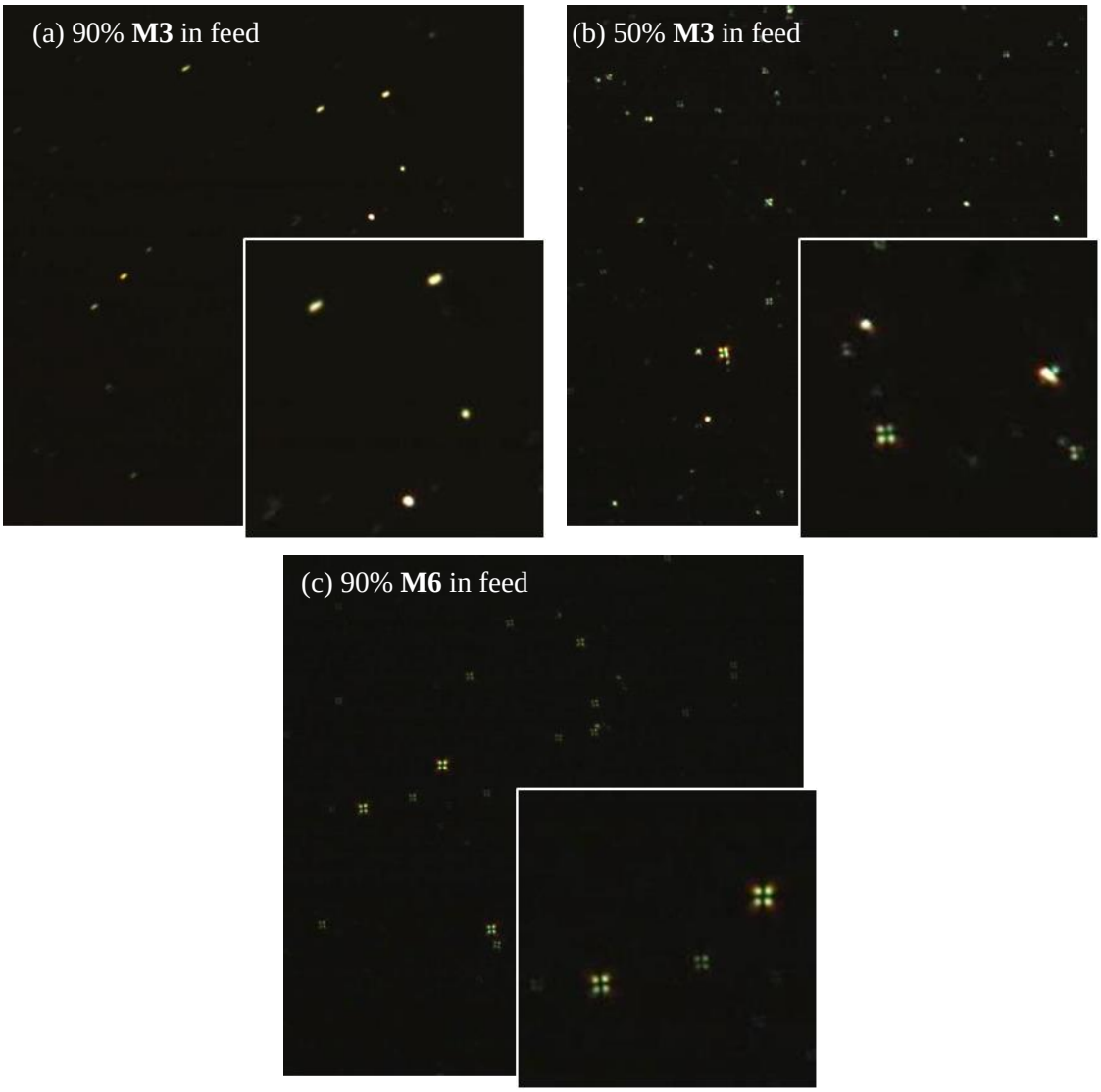

Figure 4.11: Selected polarised optical photomicrographs illustrating the entire copolymerisation series of **M3** and **M6**. Images taken at room temperature, through crossed polarisers with 200× magnification. Insets are magnifications to show confinement texture.

Unlike the copolymerisation of **M9** and **M10**, the copolymerisation of **M3** and **M6** does not yield any twisted radial particles across the copolymerisation samples. Instead there is a steady increase of the presence of radial particles as the percentage of **M6**, the monomer which forms radial particles when polymerised in EtOH, increases. This is interesting as it indicates that the twisted radial structure observed previously is likely to be as a result of **M9** having a propensity to form the escape structure, as it has been observed in some crude dispersions. The twisted radial structure is not observed throughout the copolymerisation study as neither **M3** nor **M6** have the propensity to form it. It is not easily understood why particles within the same sample are displaying different textures, though the constitution of the particles may vary slightly across the

samples both in size and copolymer composition which may result in different director configurations being the most energetically favourable.

4.6 Response Studies

It can be noted from Table 4.1 that polymer particle samples from a selection of monomers display different director configurations when in the crude suspension compared to the clean suspension in EtOH, especially if the reaction solvent was different. **P5**, **P7** and **P9** all display a radial configuration when dispersed clean in EtOH, though a twisted radial configuration is observed in crude dispersions where the steric stabiliser PVP55 is still present in the solvent. This twisted configuration may be as a result of the PVP55 promoting a parallel alignment at the surface, resulting in stronger surface anchoring and a tilt of the mesogenic units at the surface boundary. This is an example of how the particle can respond to changes in the external environment, in this case the removal of the surface analyte and steric stabiliser PVP55. Earlier in this chapter the different director configurations as a result of polymerisation solvent were discussed, with some polymer particles synthesised in EtOH resulting in a radial configuration whereas if synthesised in 1:1 EtOH: methoxyethanol showed bipolar director configurations (**P4-P6**). Table 4.1 illustrates that these particles can undergo a director configuration transition and display different configurations when transferred from 1:1 EtOH: methoxyethanol in their crude dispersion into EtOH when clean.

A sample of **P6** particles created in 1:1 EtOH: methoxyethanol displays a bipolar configuration in a crude dispersion which switches to radial when in the clean dispersion. This switch occurs at room temperature. These particles formed from **M6** were subjected to a washing by a solvent exchange by centrifugation process in order to remove the stabiliser PVP55 and replace the dispersing medium to EtOH. This process takes approximately fifteen minutes to complete. Polarised optical microscopy of these particles after the centrifugation process reveals that a switch to a radial configuration had occurred within this time and at room temperature. A switch such as this would not be observed if the particles were redispersed while below their glass transition temperature, as the polymer chains will be rigid and will not allow reorientation of the mesogenic units. Below the glass transition temperature the particles are an unresponsive nematic glass rather than within their true nematic phase, which requires a degree of flow in order to reorganise. The glass transition temperature of polymer particles of **P6** when polymerised by dispersion polymerisation was discussed in Chapter 3 and found to be approximately 24 °C by differential scanning calorimetry, a transition temperature which is close to but still above room temperature. A possible reason for the responsive nature of the nematic polymer particles at room

temperature is that they have taken up a small degree of EtOH: methoxyethanol from the surroundings. This would increase the flexibility of the polymer chains compared to their measured glass transition temperature when thoroughly dried, *i.e.* effectively lowering their glass transition temperature. Furthermore, polymers possess some flexibility in a rather wide window around their T_g.[137] Shown in Figure 4.12 are images illustrating the crude dispersion in 1:1 EtOH: methoxyethanol, displaying a bipolar texture, and the radial director configuration that is observed after the particles are cleaned.

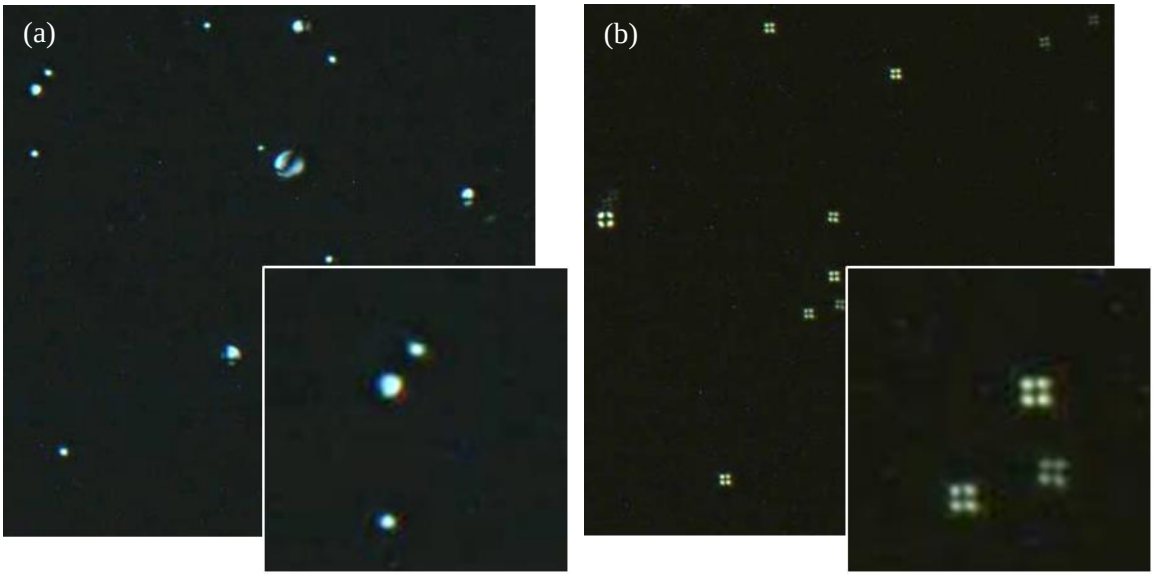

Figure 4.12: Photomicrographs taken through crossed polarisers at 200× magnification at room temperature of nematic particles formed from **M6** dispersed in (a) 1:1 EtOH: methoxyethanol mixture in the presence of PVP55 and (b) EtOH after washing to remove PVP55. Insets are magnifications to show confinement texture.

SDS is a surfactant known to impart a perpendicular surface alignment, and therefore radial texture, on droplets of 5CB.[2, 3] Addition of SDS to the crude suspension of the particles of **M6** was carried out, but the addition of the analyte did not result in a change of director configuration. A reason for this could be that the particles in this crude suspension are coated by the steric stabiliser PVP which promotes parallel surface anchoring and a bipolar configuration. The SDS cannot access the surface to impart a different preferred mesogenic anchoring. A switch may occur if a washed sample was investigated, though in this case the washed samples are already displaying a radial confinement texture as a result of removal of PVP from the particle surfaces and the transferral to a solvent with a different surface anchoring strength. A further systematic investigation of these effects was not performed.

4.7 CONCLUSIONS

Previous research into the dispersion polymerisation of terminally attached nematic monomers indicates that a polar reaction medium and protic solvents result in the particles displaying a bipolar director configuration[78, 79, 102, 103], a finding that is reflected in droplets of 5CB dispersed in polar solvents.[2, 3] By investigating a series of lateral monomers with systematic variations in chemical structure it has been established that other director configurations are in fact possible within polar solvents. A switch in director configuration from bipolar to radial was observed on an incremental small change in the alkyl side chain length on the mesogenic unit. This switch could happen because the longer mesogenic units cannot accommodate the curvature at the surface of the particles when orientated parallel to the surface and so adopt a radial director configuration. This explanation indicates a dependence of director configuration on size however, which is not observed within the size range investigated. The surface anchoring strength is also a factor in determining which director configuration will be exhibited as the director configuration that is observed is a result of a balance between bulk and surface interactions, increasing the parallel surface anchoring strength results in the switch in director configuration occurring at a longer alkyl side chain length.

Previous studies have been completed[79] which investigate an array of different smectic and nematic monomers in dispersion polymerisation processes, though the study was not systematic and did not draw conclusions about the effect of monomer structure on the resulting particle director configurations. The systematic series of monomers and polymers created within this thesis allowed for a systematic investigation into the effect of monomer structure. The results establish a structure/property relationship of director configuration to mesogen structure, a factor that has not previously been investigated. This relationship allows for the controlled synthesis of polymer particles with a chosen director configuration.

Some of the monomers with longer mesogenic units which form particles which display radial director configurations (**M5**, **M7** and **M9**) also display a second configuration within crude dispersions. This director configuration was established to be the twisted radial director configuration, which is an escaped radial configuration of limited stability in which a twist has occurred in one plain in order to minimise the splay deformation. This configuration was also observed in one case when the particles were polymerised in their nematic phase but not when polymerised whilst in the isotropic phase. The twisted radial structure may be prevalent in these larger mesogens because it may minimise the energy of the defect locally. In the crude

dispersions the steric stabiliser PVP55 is present and promotes a parallel surface alignment. This increased surface anchoring strength when compared to the clean samples in pure ethanol could also be a reason for the twist to occur as it results in a tilt of the mesogenic units at the particle surface. The change in director configuration as a result of a change in host polarity shows that these systems respond to changes in the external environment, a property which could give applications as microscale sensors for the addition of an analyte or as a more resilient form of the liquid crystal droplet sensors which have already been reported.[5, 53, 160]

The twisted radial director configuration is observed in copolymerisation studies of **M9** (which displays a radial configuration in clean dispersions in EtOH but forms the twisted radial configuration in crude dispersions in the presence of PVP55) and **M8** (which forms bipolar particles). The twisted radial configuration may result in the crude dispersions as a result of the PVP55 promoting a parallel surface alignment which could be sufficient to impart a tilt at the surface. The same effect occurs in the copolymerisation study possibly as a result of a second monomer being added to the reaction which itself prefers a parallel surface alignment. Since the twisted radial structure is an escaped structure of borderline stability, it should be responsive to external stimuli as a small change in surface anchoring will result in an observable change in the director configuration.

CHAPTER 5:

INVESTIGATION OF OPTICAL PROPERTIES OF NEMATIC ELASTOMER PARTICLES

5 INVESTIGATION OF OPTICAL PROPERTIES OF NEMATIC ELASTOMER PARTICLES

5.1 INTRODUCTION

As has been discussed in the synthesis chapter (chapter 2), the synthesis of nematic elastomer particles is in principle comparable to those discussed for the preparation of nematic polymer particles. The creation of particles which were fully networked with elastomeric properties was however more difficult to realise.

This chapter will investigate the elastomeric particles synthesised by RAFT-assisted dispersion polymerisation and dispersion polymerisation with a delayed addition of crosslinker *via* polarised optical microscopy, including studies which examine the effect of the addition of a swelling solvent, and heating above the nematic to isotropic transition temperature of the particles.

5.2 HEATING STUDIES

At room temperature elastomeric particles formed by RAFT-assisted dispersion polymerisation display polydomain structures possibly as a result of the network points throughout the particle disrupting the nematic order and preventing the formation of a resolved director configuration. An example of particles displaying this polydomain texture can be found in the photomicrographs Figure 5.1. Due to the degree of network formation within the particles the degree of freedom the mesogens experience is limited as the networked polymer chains will not reorganise or flow as they can in polymeric systems. However, the application of heat should allow for the director configuration to resolve once the networked polymer chains become flexible enough to allow for reorganisation of the mesogenic units.

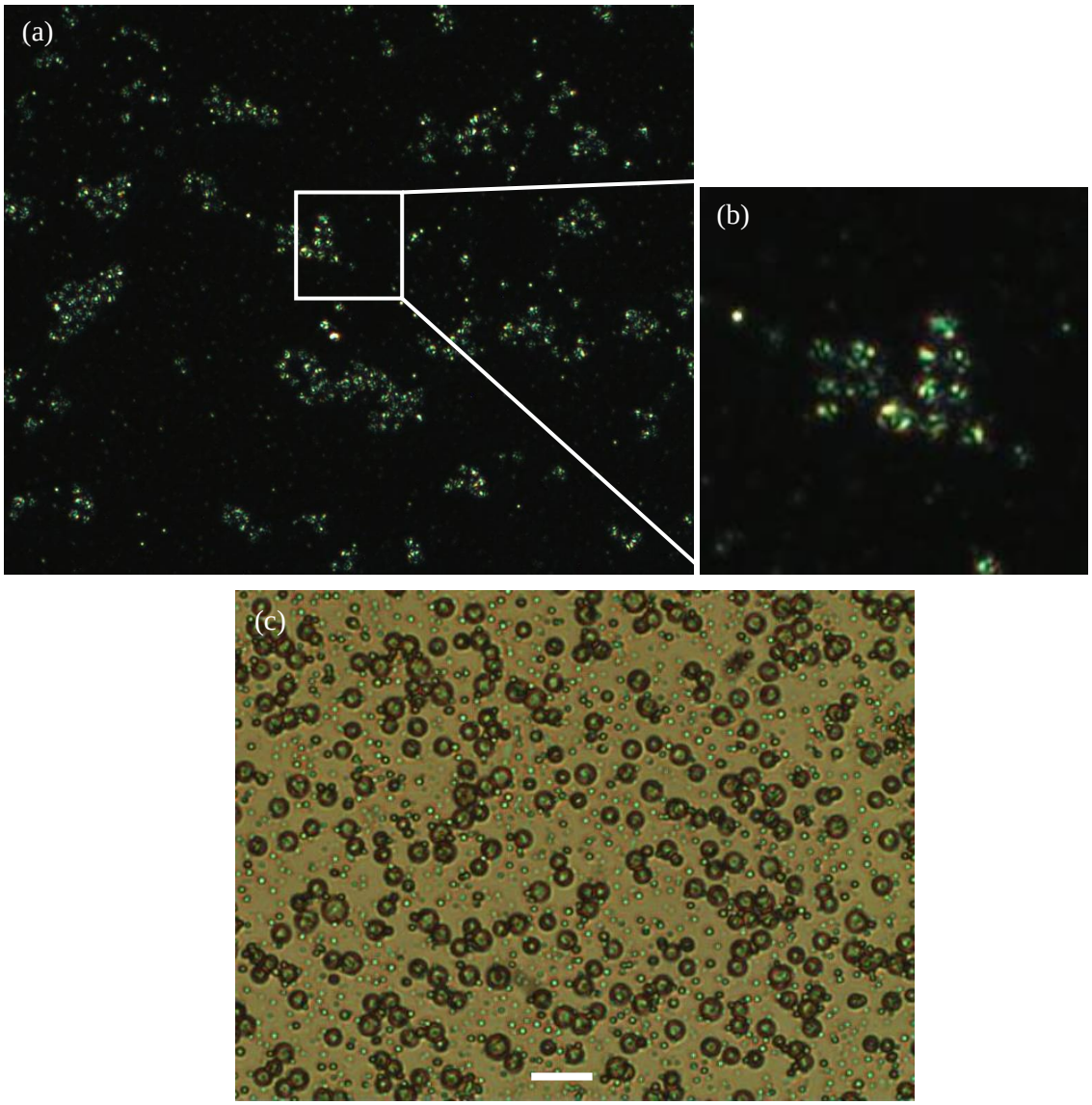

Figure 5.1: (a) POM photomicrograph showing a dispersion of particles synthesised from **M1** by RAFT-assisted dispersion polymerisation in 1:1 EtOH: methoxyethanol showing a polydomain internal texture, (b) a magnified region to show unresolved confinement texture and (c) POM photomicrograph of the same sample taken with uncrossed polarisers to illustrate the particle size and variance that was obtained. Scale bar represents 10 μm.

Elastomeric particles synthesised by RAFT-assisted dispersion polymerisation in the presence of crosslinker were dispersed in glycerol and heated into their isotropic phase. Glycerol was selected for a number of reasons: it is has a high boiling point, allowing for the samples to be heated above the nematic-isotropic temperature of the particles; it is miscible with EtOH, which allows for the easy transferral of particles; and it is similar in polarity to EtOH and so should not affect the director configurations that the particles are exhibiting. It is also a more viscous solvent, which will reduce the mobility of the particles with thermal motion, allowing for the observation of an individual particle. The particles were dispersed in glycerol by adding a sample of the clean EtOH

dispersion to a sample tube containing glycerol. Heating these particles above their glass transition temperatures allowed for the resolution of the director configurations within the particles. This investigation was also further evidence of the successful network formation within these systems, as non-crosslinked samples lose their discrete shapes when the temperature is maintained above the glass transition.

Shown in Figure 5.2 is a heat study of particles of **P1** and in Figure 5.3 is particle of **P3,** both synthesised by RAFT-assisted dispersion polymerisation in the presence of crosslinker. These heating studies were viewed with the addition of a λ wave plate to allow for the particles to be observed above their isotropic transition when they are no longer birefringent but also to aid in the determination of their director configurations.

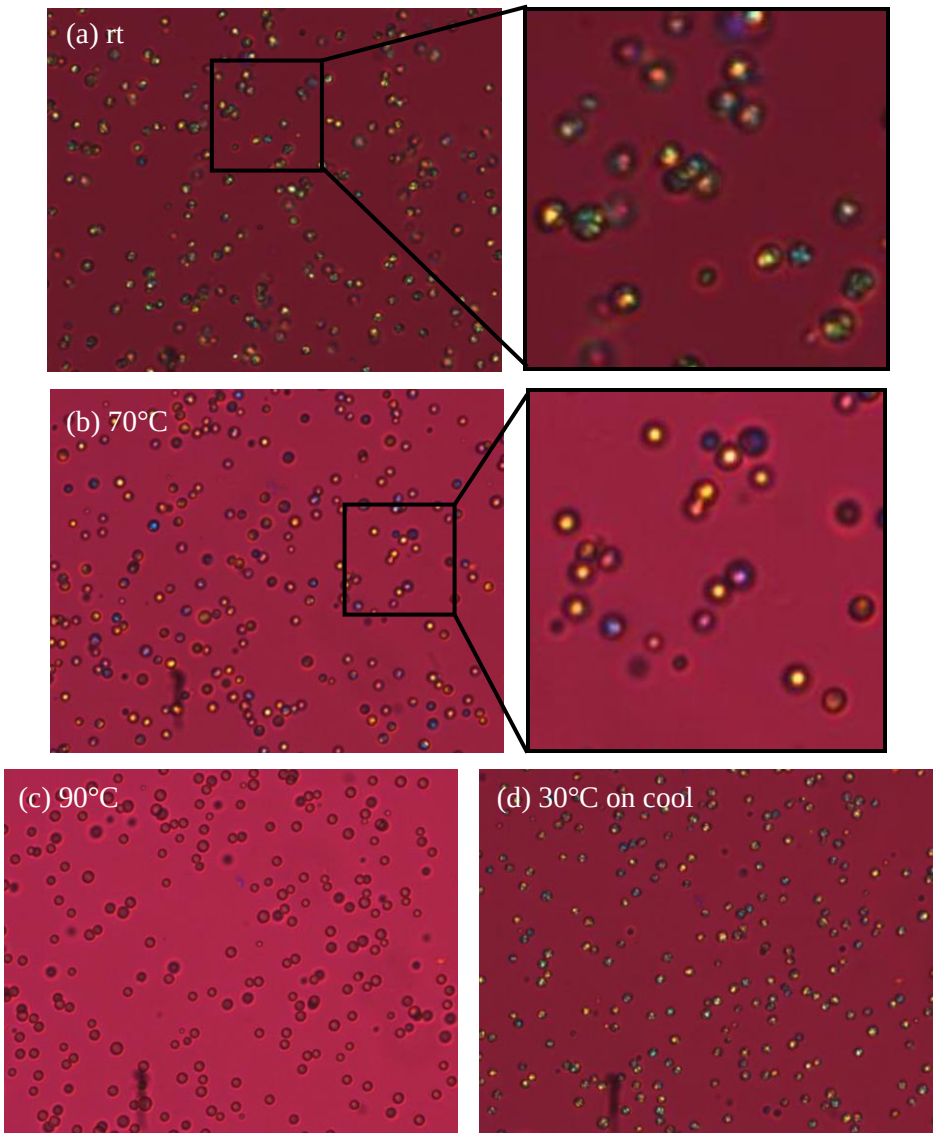

Figure 5.2: Series of images depicting the heating to isotropic of a series of LCE particles made from **M1** and dispersed in glycerol. Images were taken at 200× magnification.

In the magnified region of Figure 5.2(a) it can be seen that the particles at room temperature have polydomain regions within them, indicated by a change in colour when viewed by a λ wave pate as a result of a different director orientation. This is not observed when the particles are observed at elevated temperatures as can be seen in the magnified region of Figure 5.2(b), indicating that the director configuration becomes more resolved once the particles reach a temperature significantly above their glass transition, as the mesogenic units within the particles have increased freedom to align when the networked anisotropic polymer backbone chains are flexible.

For elastomeric particles formed from the lateral monomer **M3** the effect of improving confinement texture is not as pronounced as it is for elastomeric particles made from the terminally attached monomer **M1**, as can be seen in Figure 5.3. A reason for this diminished improvement may be that as laterally attached liquid crystal polymer systems display more coupling between the mesogenic unit and the polymer chains, the network disrupts the alignment more significantly.

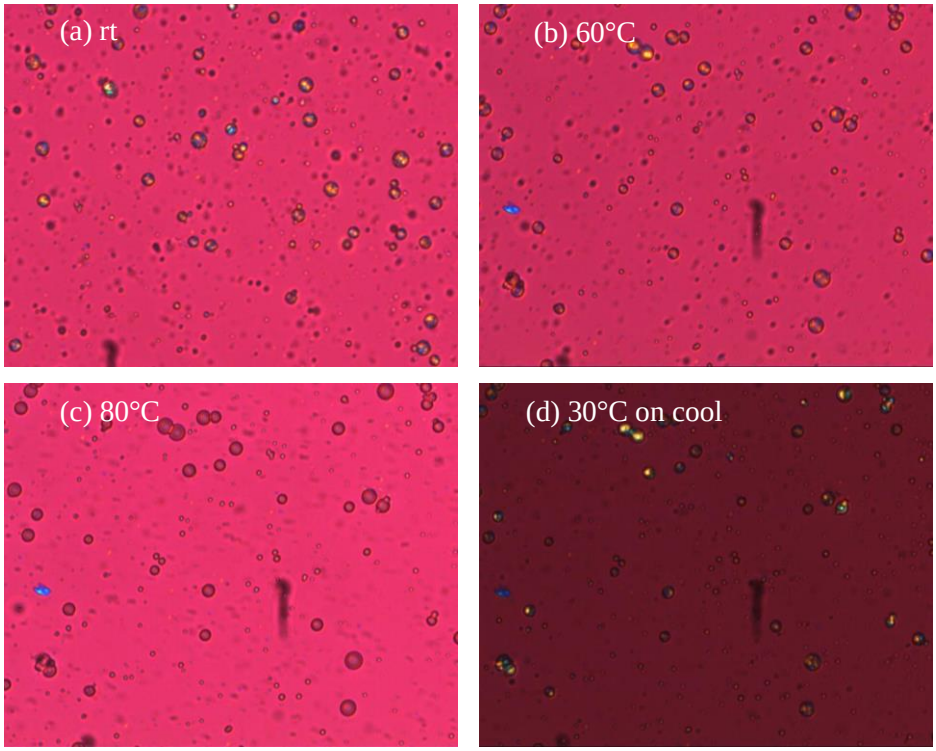

Figure 5.3: Series of images depicting the heating to isotropic of a series of LCE particles made from **M3** and dispersed in glycerol. Images were taken at the temperature specified, through crossed polarisers with the addition of a λ wave plate at 200× magnification.

It can be noted that the particles appear to increase in size as the temperature is elevated. This may be because they are more likely to swell slightly in a hot solvent compared to the solvent at room temperature, but could also be indicative of the particles losing their shape integrity as they

soften above the glass transition. It is difficult to state unequivocally whether a shape change is occurring in this case because the particles are rather small and so any change in shape may not be resolvable.

5.3 SWELLING STUDIES

When a nematic polymer is exposed to a solvent in which it is soluble in, the polymer will dissolve. Liquid-crystalline elastomers are inherently insoluble because of the network, so cannot dissolve when exposed to a favourable solvent. Instead they swell with the uptake of this solvent, which disrupts the nematic order within the elastomer and results in the network becoming isotropic. As the elastomer is a fully crosslinked network this process should be completely reversible and the removal of the solvent should allow the nematic phase within the material to reinstate.

Elastomeric particles created by RAFT-assisted dispersion polymerisation were subjected to a swelling study as a further assessment into the successful network formation within the particles, as well as to assess the response of the particles to solvent uptake. The particles were dispersed in EtOH and viewed by polarised optical microscopy. Toluene was added to one side of the sample and the particle behaviour was observed as the solvent front travelled across the viewing plane. The sample was then flooded with ethanol in order to de-swell the particles and allow for the birefringence to return. This process was repeated to ensure reproducibility.

Shown in the series of images in Figure 5.4 and Figure 5.7 are swelling studies completed for LCE particles of **P3** (Lateral monomer C4 chain, C4 spacer). Two different swelling solvents, toluene and acetone, were utilised to investigate the effect of solvent polarity and miscibility.

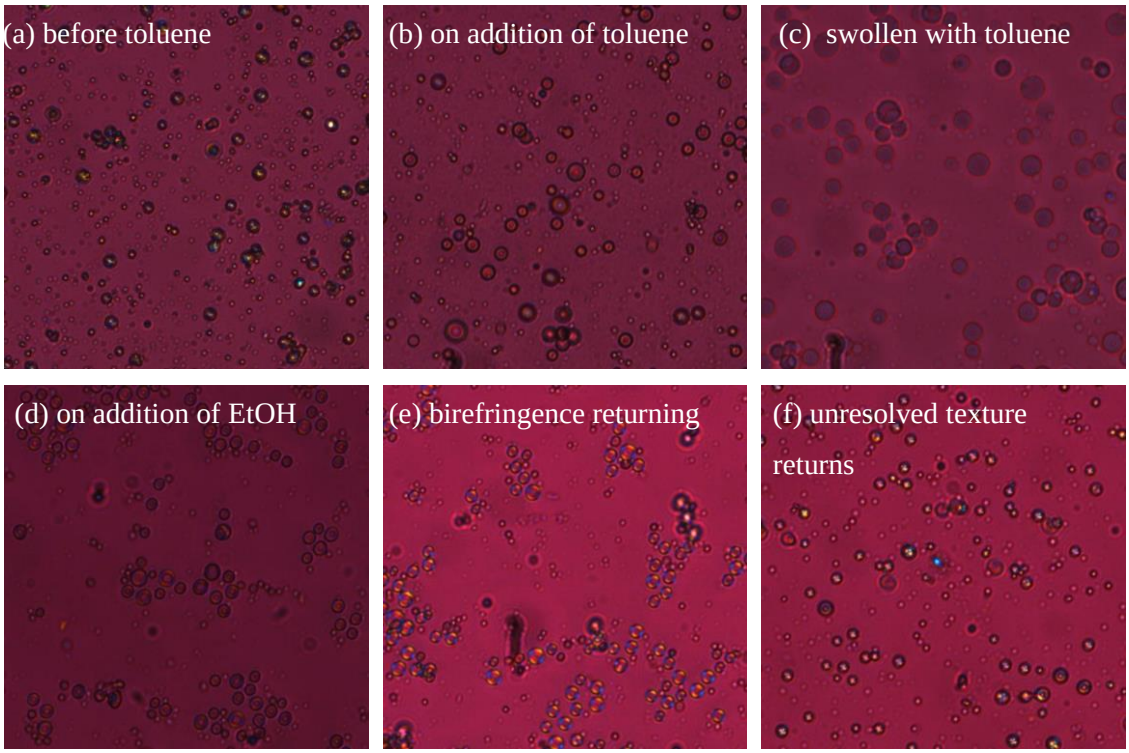

Figure 5.4: Series of images depicting the swelling of a series of LCE particles of **P3** with toluene. Images were taken at room temperature through crossed polarisers with the addition of a λ wave plate at 200× magnification.

Figure 5.4(b-c) shows that the particles remain discrete after the viewing plane is flooded with toluene. The birefringence has disappeared and the sample appears completely dark when only crossed polarisers are used to observe it, indicating that the particles are isotropic at this stage. When the birefringence begins to return in Figure 5.4(d-e) on addition of EtOH the particles are displaying a radial extinction pattern. This extinction pattern is more clearly illustrated in Figure 5.5 where the still slightly swollen particles are viewed through crossed polarisers. Figure 5.5 was imaged at the same time as the image depicted in Figure 5.4(e) without the wave plate to allow for the extinction pattern to be more easily established. The radial director configuration may be observed at this stage because there is still a high proportion of toluene present within and surrounding the particles which, as a non-polar solvent, promotes a perpendicular surface alignment. The toluene takes approximately 30 minutes before it is fully removed from the particles and the unresolved texture returns.

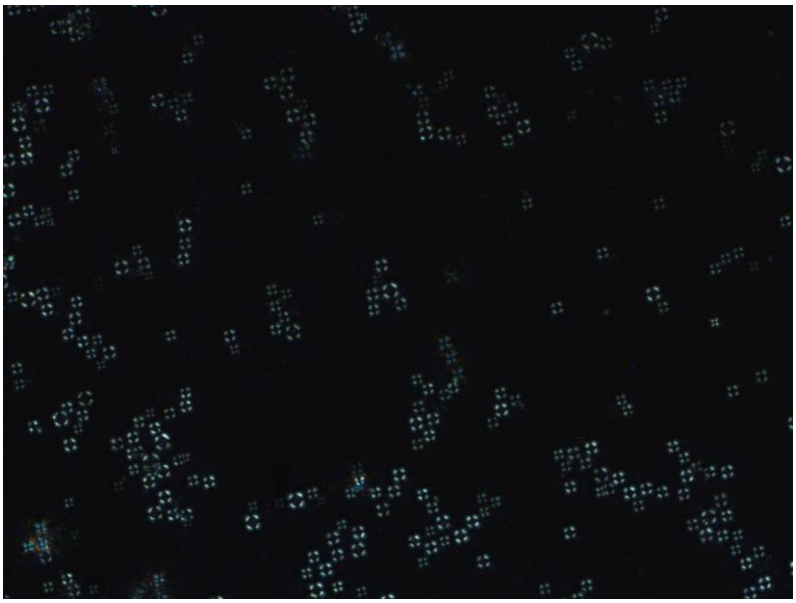

Figure 5.5: Image illustrating the radial director configuration of the particles of **M3** through crossed polarisers at 200× magnification as the birefringence returns after addition of toluene.

The initial resolution of a director configuration after swelling can also be seen in Figure 5.6, which shows a sample of particles of **P6** (synthesised from monomer **M6**) after RAFT assisted dispersion polymerisation in the presence of a crosslinker and after swelling with toluene which results in the temporary resolution of the radial director configuration.

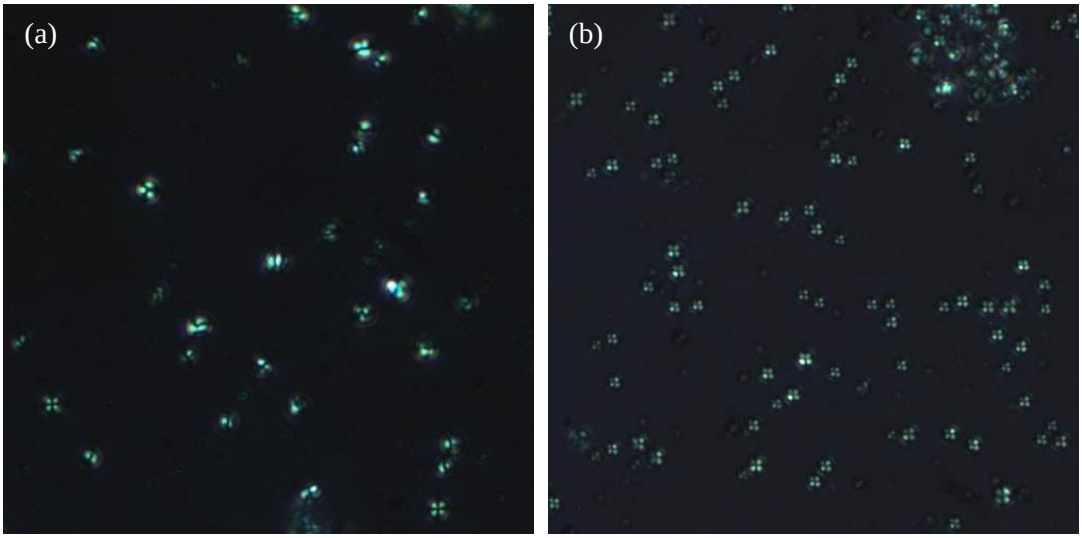

Figure 5.6: POM photomicrographs showing particles created from **M6** by RAFT-assisted dispersion polymerisation in EtOH (a) in the clean dispersion in EtOH showing polydomain textures and (b) after swelling with toluene showing radial confinement textures.

This reversible swelling was observed for all particles synthesised from monomers **M1**-**M9** by RAFT-assisted dispersion polymerisation.

A comparable swelling study with acetone is presented in Figure 5.7. In this case, when the birefringence returns a bipolar texture can be observed within the particles, probably because acetone is polar and hence induces similar alignment conditions to *e.g.* ethanol. The birefringence takes considerably longer (approximately two hours) to return in the case of acetone compared to when the particles are swollen with toluene.

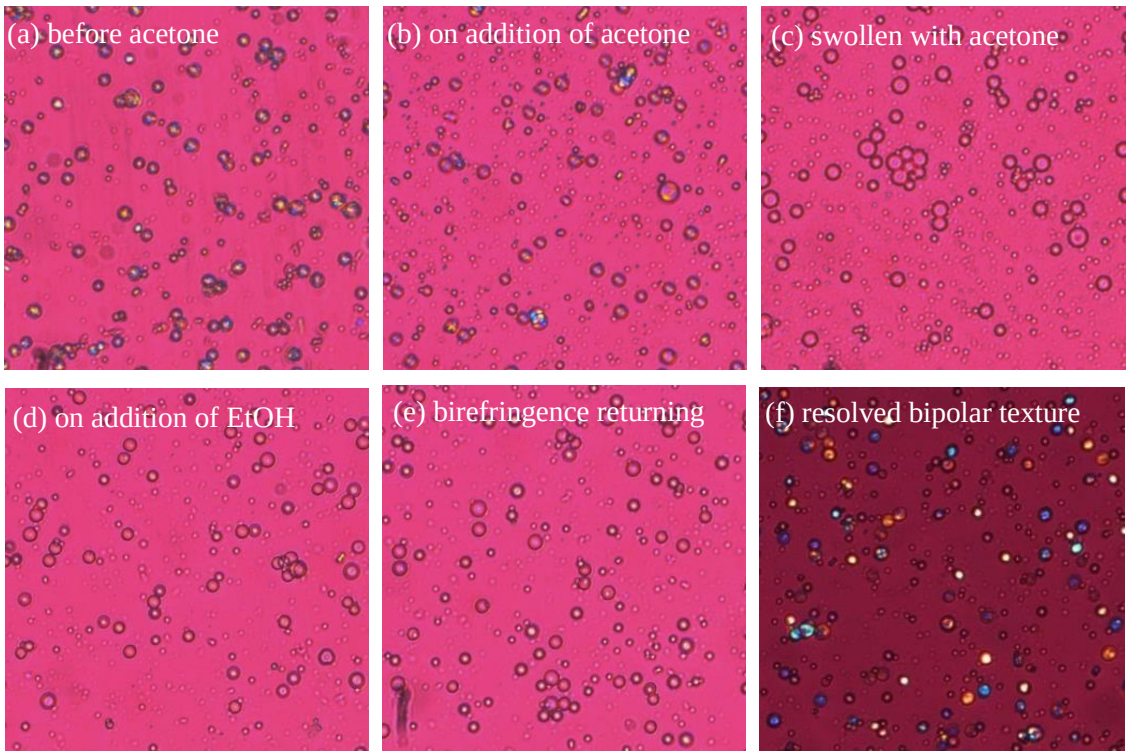

Figure 5.7: Series of images depicting the swelling of a series of LCE particles of **M3** with acetone. Images were taken at room temperature through crossed polarisers with the addition of a λ wave plate at 200× magnification.

A good indication for crosslinking is if discrete particles remain while in a swollen isotropic gel state, since the particles would dissolve without network formation. If any nematic texture can be observed outside the particles after swelling with a favourable solvent this is an indication that some particles have dissolved or that some polymer chains that were not part of the network within the particles have been extracted. Due to the tangling that can occur within polymer particle systems, polymer particles with no crosslinker present may not dissolve immediately when swollen with toluene. For this reason the swelling study must be repeated or the particles left in the presence of toluene for a considerable duration. The pseudo-swelling of polymeric particles was not observed experimentally; non-crosslinked particles exposed to toluene quickly dissolved and agglomerated. For comparison to the results already discussed, an example experiment where the particles did not survive the addition of a favourable solvent is shown in Figure 5.8.

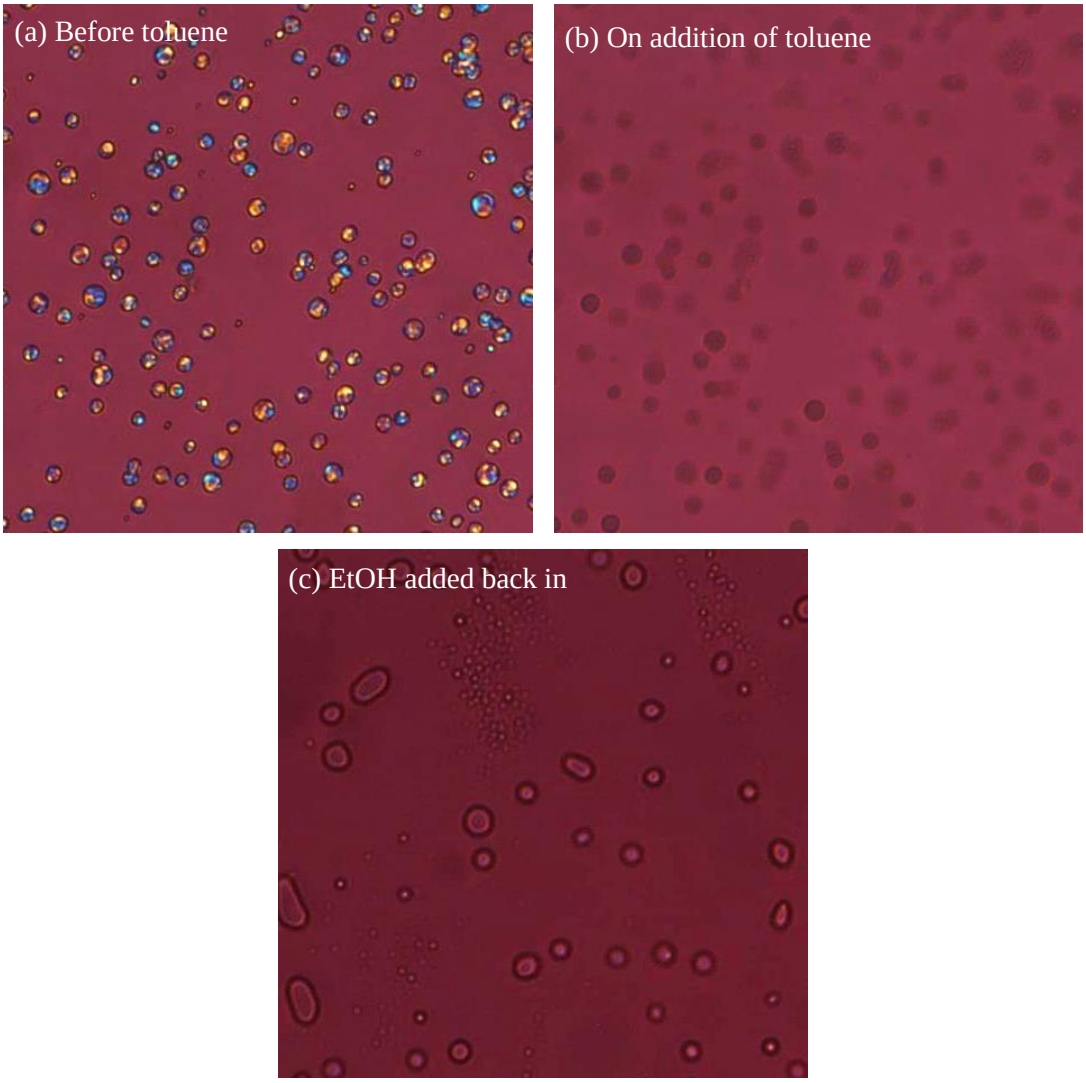

Figure 5.8: Example of nematic particles where there has been insufficient network formation for the particles to maintain their discrete shape on addition of a favourable solvent. This is a sample formed from RAFT-assisted dispersion polymerisation of **M1** in 1:1 EtOH: methoxyethanol, viewed at rt with crossed polarisers and a λ wave plate at 200× magnification.

The degree to which a crosslinked system can swell is indicative of the density of crosslinking within. A fully networked system will be insoluble as a result of all the polymer chains within the particle being linked together, so that there are no free polymer chains within the system. At the lower limit of full network formation the system will still display a good degree of flexibility and will be swellable, whereas a densely crosslinked system will be hard and therefore will only increase in size marginally, if at all, when swollen with a favourable solvent. Shown in Table 5.1 is the increase in particle size observed for particles of **M3** as they were swollen with toluene and acetone, and the extent to which that change in size was reversible.

Table 5.1: Particle size change for LCE particles of **M1** and **M3** synthesised by RAFT assisted dispersion polymerisation as they are swollen with toluene and acetone.

Sample	Particle size before swelling / µm (variance)	Particle size during swelling / µm (variance)	Particle size after swelling / µm (variance)	% increase
P3 swollen with toluene	3.4 (24%)	6.5 (22%)	3.1 (20%)	88%
P3 swollen with acetone	3.9 (16%)	5.0 (24%)	3.7 (28%)	28%

It is difficult to establish whether or not the liquid-crystalline elastomer particles maintain their shape integrity through this process. It seems likely that, as the particles swell and become soft they may flatten slightly, or the particles become sticky and they attach to the glass surface upon swelling. This appears to happen within these investigations, as the particles did not tumble in solution which would allow for their shape to be more easily assessed. By increasing the hydrophobic nature of the glass with different alignment layers it may be possible to prevent the particles from sticking to the glass surfaces even if they are in their swollen state. This should allow for more in depth shape analysis as the particles will still freely move in the flowing solvent.

The results depicted in Table 5.1 indicate that the particles have a greater affinity to toluene than to acetone, as they swell to a higher degree. It can also be noted that the swelling appears to be reversible; with both experiments displaying a reduction in size after the swelling solvent was removed; this could be as a result of any free polymer chains not involved in the network being extracted from within the particles, or the swelling allowing for the mesogens to pack more efficiently while the elastomer is above its glass transition.

In order to investigate the swelling capability of the liquid-crystalline elastomer particles further, toluene was added to a sample of particles until the turbid dispersion became clear. This indicated that the particles had undergone their nematic-isotropic transition as they became swollen with the toluene. This sample was then left in a sealed environment to prevent the evaporation of toluene or EtOH for a period of 48 hours. This test would allow us to determine whether network formation had occurred within the particles, or whether the swelling observed previously was as a result of the tangled polymer chains within a sample of negligible network formation. Shown in Figure 5.9 are POM photomicrographs of the dispersion before the inclusion of toluene, after 48 hrs in the presence of toluene, and after the solution had been left open to the air for 24 hrs for the toluene to evaporate from the system.

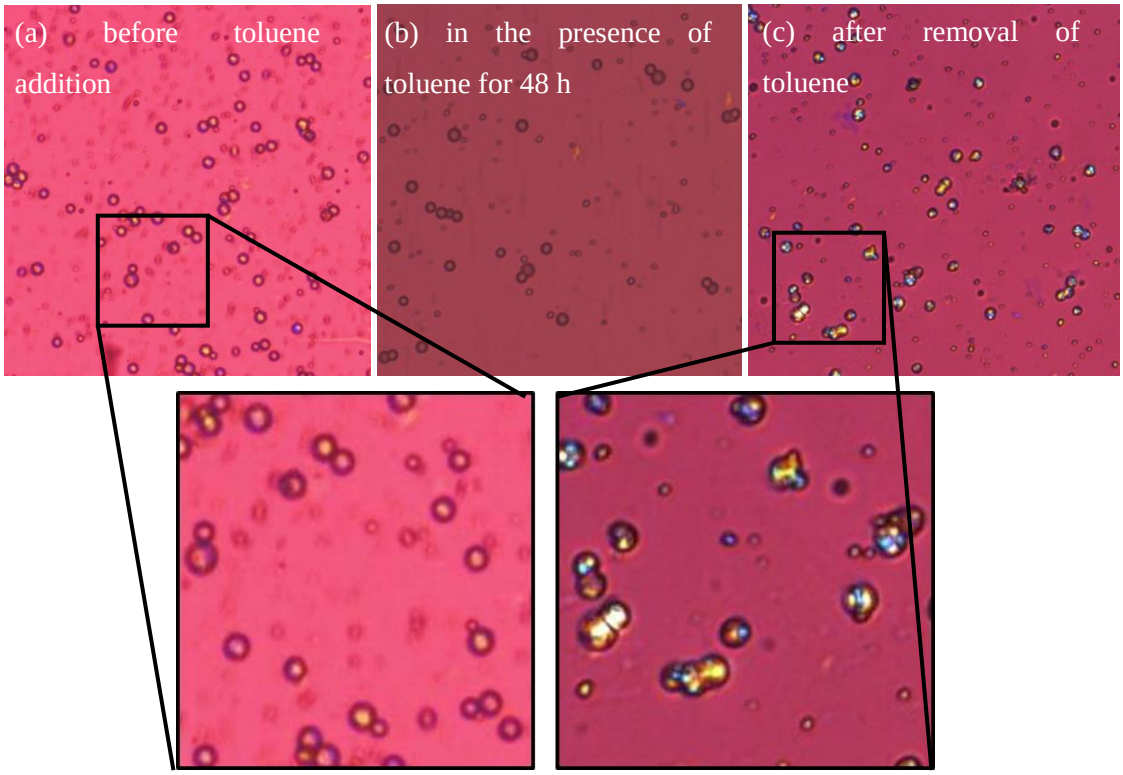

Figure 5.9: Series of images depicting the swelling of a series of LCE particles of **M3** with toluene over a period of three days. Images were taken at room temperature through crossed polarisers with the addition of a λ wave plate at 200× magnification.

It is apparent from the images displayed in Figure 5.9 that discrete particles are observable at all stages of this experiment. There is a degree of fusion occurring in the particles after being swollen for this extended amount of time, indicating that the particles are becoming sticky while in their swollen states, which is known for acrylate polymers.[161]

5.4 Conclusions

Novel liquid-crystalline elastomer particles were investigated by polarised optical microscopy for their director configurations, their swellability, as well as their response to changes in temperature. Confirming the degree of network formation within elastomeric systems is important as inclusion of a crosslinking agent within the polymerisation process does not necessarily ensure that crosslinking is taking place. An even distribution of network points throughout the particles is important in order for them to be able to swell and for them to have the mobility above the glass transition temperature to respond to changes in external stimuli. Confirming the network formation within particles requires an approach from multiple directions, as the gel content of a

sample does not give an indication to the distribution of the network points throughout the sample. Swelling and heating studies are needed in order to evaluate the degree of crosslinking, hardness and swellability of the system. The nematic elastomer particles that have been created within this thesis have been subjected to multiple analyses in order to confirm their network formation.

Particles with significant network formation are insoluble and can therefore be repeatedly swollen in a favourable solvent. This results in the birefringence being lost as the liquid-crystalline mesogens within the system become isotropic as the system is solvated. The birefringence will return reproducibly as the favourable solvent is removed and the nematic order is reinstated. This reversible swelling was observed for all particles synthesised from monomers **M1**-**M9** by RAFT-assisted dispersion polymerisation and is a strong indication that these elastomer particles are successfully networked. These particles not only reversibly swell and de-swell with re-established birefringence, but the confinement texture that is observed immediately after swelling is dependent on the polarity of the swelling solvent. Particles swollen with acetone displayed bipolar textures when the birefringence returned, whereas a radial texture was observed for particles that were swollen with toluene. The reversible response to changes in the surface anchoring shown with this experiment allows the particles possible applications as sensors.

Nematic elastomer particles on the small microscale with confirmed internal network formation and elastic character are novel. They could be utilised for applications including as micro-stirrers for small scale reaction vessels and equipment,[9, 11, 94, 127] as sensors for external stimuli including host polarity, temperature or the detection of analytes. If the mesogens are aligned parallel to the surface in a bipolar/uniform configuration then it is possible that these particles will display actuation at their nematic to isotropic transition. These microscale actuators could have many possible applications as micro-switches and valves[9, 127] and could behave as microscale muscles as they may have the ability to impart force on an object.

CHAPTER 6:

ELECTRO-OPTICAL STUDIES OF NEMATIC PARTICLES

6 ELECTRO-OPTICAL STUDIES OF NEMATIC PARTICLES

6.1 INTRODUCTION

Electro-optical investigations are traditionally employed within the field of liquid crystals to assess the switching capability of a liquid crystal and establish its suitability for display applications. For the vast majority of nematic liquid crystals, the application of an electric field of sufficient magnitude results in the orientation of the director either parallel or perpendicular to the field, depending on the sign of the dielectric anisotropy ($\Delta\varepsilon$) of the nematic medium.[17]

Traditionally, the electro-optical response of a nematic liquid crystal device will depend on the boundary conditions that the liquid crystal experiences, imparted by the alignment layers in the cell to promote either homogeneous, homeotropic or a tilted alignment of the liquid crystal. Polymer dispersed liquid crystal (PDLC) films can also be assessed with regards to electro-optical applications. In electro-optical investigations of liquid crystal droplets, either in free dispersions or when dispersed in a polymer matrix, the encapsulation and confinement of the liquid crystal defines its internal alignment.

The primary application for PDLCs as switchable windows requires an electro-optical response of the liquid crystal when confined within sub millimetre droplets within a polymer matrix. This allows for the window to be switched from the scattering state (when the liquid crystal droplets are displaying confinement textures defined by their surface anchoring) to the transparent state, when the liquid crystal is aligned with the field. PDLCs are also of interest electro-optically because of the prospect of being used for large area flexible displays.

Studies of confined liquid crystals within an electric field are less prevalent than aligned nematic films due to the large liquid crystal display market, though research into confined liquid crystals, such as PDLCs[162] and free dispersions of liquid crystal droplets is increasing. Electro-optical investigations of an ordered array of monodisperse bipolar droplets of 5CB found that with strong parallel surface anchoring the application of an electric field caused reorientation of the bipolar droplet with the field, rather than a reorganisation of the mesogenic units within the droplet to a uniform configuration.[57, 163] The reason for this is postulated as the surface mesogenic units responding first to the application of the electric field, causing a reorientation of the overall

anisotropic configuration within the droplets. Removal of the electric field shows the bipolar droplets relax back to their original orientation. This study was carried out on a film of closely packed bipolar droplets dispersed in a thin PVA matrix and therefore the droplets are not spherical. The hexagonal packing of the bipolar droplets has resulted in the droplets being almost hexagonal in shape. As a defect is of lowest energy when it is positioned in a region of maximum curvature,[129] it returns to that position when the electric field is removed. The droplets were monodisperse as they were created by microfluidics before polymerisation of their surrounding matrix, so a description in the effect of droplet size and surface curvature was not completed. Additionally, the confinement of the droplets of this experiment does not allow for the droplets to change shape.

A study of PDLC films by electro-optics which did allow for the effect of size of droplet to be considered has been completed.[164] The PDLC films were created by allowing homogenous mixtures of liquid crystal and reactive monomers to phase separate on polymerisation which resulted in polydisperse PDLC films. The average size of the droplets within these films was determined by the percentage of liquid crystal present in the original mixture. The droplets within this study were again not spherical, and were established by confocal microscopy as 'polyhedral foam dispersions' with droplet sizes ranging from over 10 μm to below 0.2 μm. The authors found that less voltage was required to cause a switch of mesogen orientation in larger droplets, possibly as a result of decreased surface influence compared to droplets of smaller size which are significantly more confined. The relaxation time for larger droplets was also found to be much greater than for smaller ones, again this is likely to be because of the strong surface influence on the small droplets. This is another example of liquid crystal confinement within fixed geometries, and does not allow for any change in the droplet topology.

By dispersing liquid crystal droplets within a liquid polymer,[165] it was observed that the shape and position of the droplet is not fixed and can respond to the application of an electric field. This study showed the droplets developing an elongated shape along the perpendicular direction induced by the application of an electric field. This effect is described as an electro-wetting process that occurs as droplets agglomerate until they are large enough to come into contact with one of the glass sides of the cell and then spread to cover the glass surface. A reduction in birefringence is noted on application of an electric field as the droplets flatten and so postulate the change in shape to be related to the dielectric gradient between the droplet and the surrounding medium, and to a homeotropic organisation of the mesogenic units within the droplets as a result of aligning with the electric field. These droplets did not show fully reversible transitions between discrete spherical and flat droplets as a result of coagulating in the presence of an electric field, but did show relaxation back to a spherical shape when the field was removed. This study does

not describe any droplet shape change for droplets free in the liquid polymer, only those in contact with the glass, and does not allow for a thorough investigation into the behaviour of microscale droplets in an electric field as the agglomeration of droplets causes them to grow quickly to up to 1 mm in size.

The literature reports on the investigation of liquid crystal polymer particles in an electric field are limited. One study observed formations of lines of liquid crystal particles as a result of the particles acting as dipoles when an electric field is applied due to becoming polarised by the field. The authors observed this line formation regardless of the director configurations of the particles.[102] Using a different cell set up they observed reorientation of bipolar droplets in line with the field direction in a way analogous to that observed for bipolar droplets in a polymer matrix described previously.[57]

Within this chapter we shall explore the effect of an electric field on free dispersions of liquid nematic polymer particles and assess the effect of director configuration and glass transition temperature of the particle in the behaviour that is exhibited.

6.2 MATERIALS AND METHODS

The behaviour of nematic polymer and elastomer particles in an electric field was investigated by electro-optical studies using different cell configurations, field strengths and dispersing solvents. From this, it can be deduced whether the behaviour of the particles when exposed to an electric field is as a result of its anisotropic nature or as a result of ionic contaminants on the particle surface.

Two different cell configurations were investigated in order to visualise the effect of an electric field, the different cell configurations with respect to viewing angle and electric field application are illustrated within Figure 6.1.

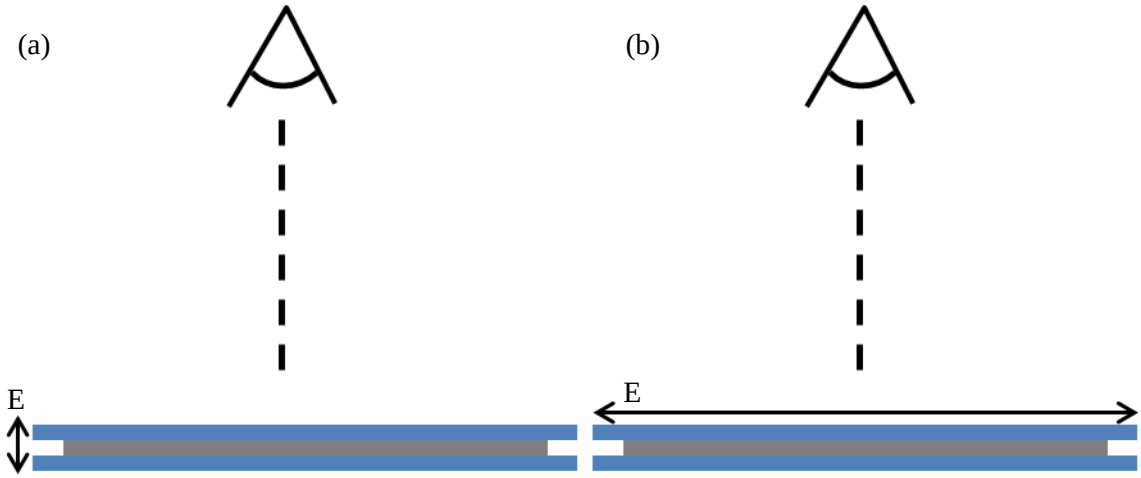

Figure 6.1: Schematics showing the electric field with respect to the viewing angle for the two types of cells being investigated. (a) applies an electric field perpendicular to the viewing plane, (b) applies an electric field parallel to the viewing plane.

The first cell configuration, shown in Figure 6.2, applies an electric field perpendicular to the viewing plane to allow for the sample to be viewed along the direction of the applied field. The second cell configuration, shown in Figure 6.3, applies an electric field parallel to the viewing plane, which allows for the effect of the electric field to be viewed across the cell.

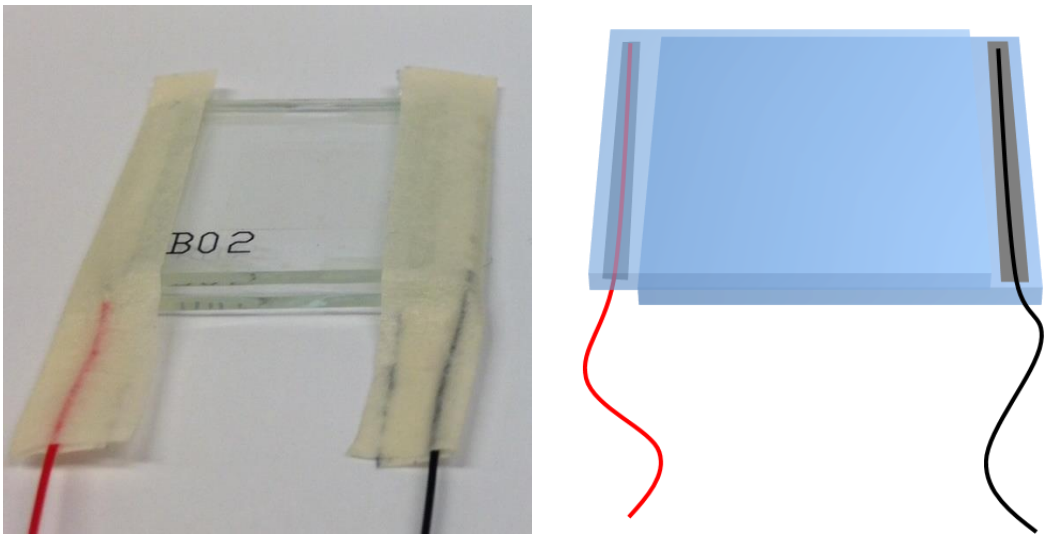

Figure 6.2: Pre-fabricated cells with homeotropic alignment.

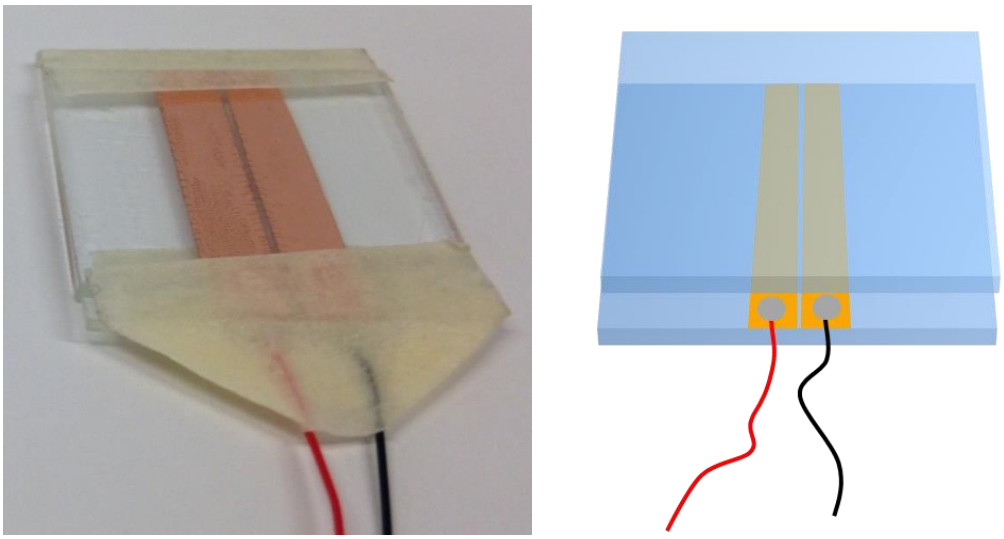

Figure 6.3: Homemade cells with lateral electric field and homeotropic alignment

The cells illustrated in Figure 6.2 were the type predominantly used throughout these investigations, and are premade homeotropic cells with a 5 µm cell gap purchased from Instec. The homeotropic alignment prevented the liquid crystal particles from sticking to the glass surfaces and so did not impart any alignment on the mesogenic units as they were not in direct contact with the alignment layer.

The cells depicted in Figure 6.3 were homemade cells in which the electrodes were created from copper tape to allow for the electric field to be applied across the sample. The copper electrodes were placed as close as possible to allow for the application of an electric field in sufficient magnitude. A homeotropic alignment layer was necessary in order to prevent the particles from sticking to the glass. Many different treatments were attempted including lecithin and trichlorosilanes of various alkyl chain lengths. The longer the alkyl group of a trichlorosilane, the more hydrophobic the coating is. Attempting some shorter trichlorosilanes proved unsuccessful in preventing the liquid crystal particles from sticking to the glass surface. Octadecyltrichlorosilane (OTS) treatment eventually proved successful in preventing the sticking of the nematic polymer particles to the glass, and evidence of the successful hydrophobic coating of the glass slide is shown in Figure 6.4 as the contact angle of water on the surface has been noticeably increased.

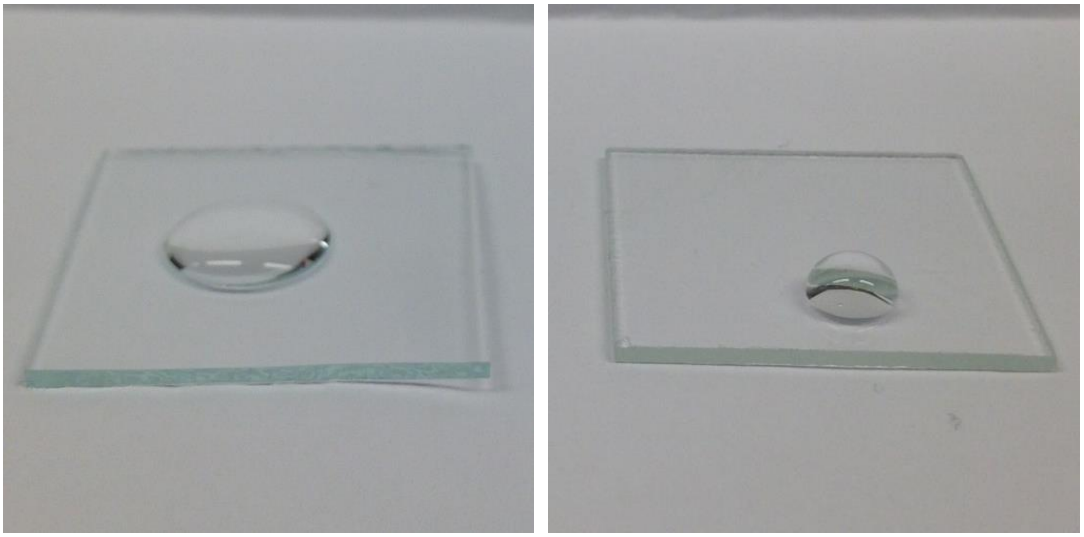

Figure 6.4: Photographs showing the increasing contact angle of water when a droplet is placed on a hydrophobic coated slide (right) compared to plane glass (left).

Unfortunately, no particle response was observed when the cells depicted in Figure 6.3 were used and due to time constraints the use of these cells of was never optimised. A possible reason is that the distance between the electrodes was too great and caused the electric field per μm^3 to be too small to elicit a response from the particles. In the premade Instec cells shown in Figure 6.2 the maximum cell gap was only 5 µm which allowed for the application of a significant electric field across the sample.

In order for the particles to be investigated by electro-optical studies they were first dispersed into a solvent mixture with a low dielectric constant. The reason for this transferral of the particles was to prevent solvent flow on the application of the electric field masking the particle motion. In all cases particles purified by a solvent exchange by centrifugation were used in order to minimise the amount of ionic contaminants within the sample affecting the results. The solvent mixture chosen was a 1:1 mixture of dodecane and 1-undecanol, as this proved to have a low enough dielectric constant whilst still being of a high enough polarity to allow for the particles to remain dispersed. Completely non-polar solvents such as silicone oil were tested but this resulted in the particles coagulating. More polar solvents such as glycerol and ethanol resulted in de-wetting occurring between the glass slides on application of an electric field, the significant flow this caused made investigation of particle response difficult.

6.3 HIGH GLASS TRANSITION TEMPERATURE PARTICLES

Nematic polymer particles synthesised from monomers which form polymers with glass transition temperatures above room temperature were exposed to an electric field to see if any macroscopic reorientation or motion would occur when the mesogenic units were locked in place by the amorphous structure of the anisotropic polymer backbone. The effect of the director configuration was also evaluated to assess whether bipolar particles (which are overall anisotropic) would behave differently to radial particles (which are overall isotropic).

Bipolar nematic polymer particles made from **P1** dispersed in a mixture of 1:1 dodecane: 1-undecanol were exposed to various strengths of electric field. The particles were approximately 1 μm in diameter which meant any change in shape would be difficult to visualise as the particles were of a size range on the limit of resolution for optical microscopy. The application of a field induced significant particle motion and rotation. A video of the motion of the particles on application of a field with a frequency of 1 Hz and peak amplitude of 10 V can be found as Video 1 on the accompanying disk. Screenshots from Video 1 are shown as Figure 6.5.

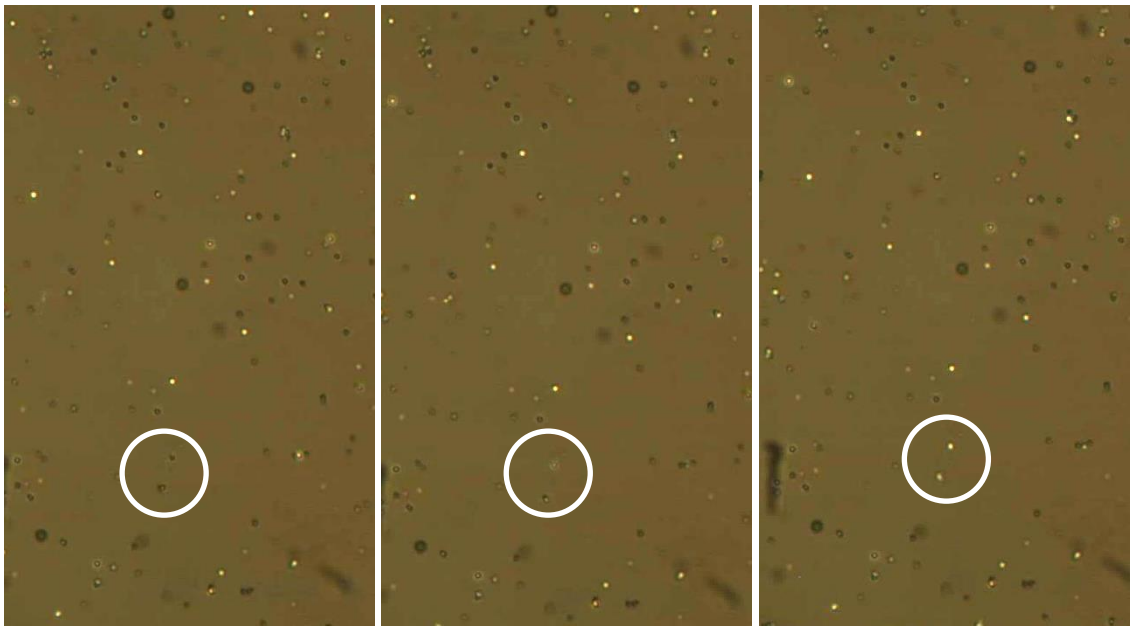

Figure 6.5: Screen shots from Video 1 showing the motion of bipolar nematic particles of **P1** moving in an applied field. Video taken at room temperature with partially crossed polarisers at 200 × magnification.

Although it is difficult to illustrate the motion of particles with still images, a change in the birefringence can be observed for the particles indicated, showing their rotation in the field. This is an indication of the bipolar particles acting as dipoles because of being overall anisotropic in

structure and aligning with the switching field.[102] In Video 1, the bipolar particles move horizontally even though the electric field is applied vertically through the sample. The switching of the motion is related to the frequency of the applied field but does not correspond to a change in direction with every change in current. Some particles within the viewing plane do not move in response to the application of an electric field. It is thought that these particles are unresponsive because they are stuck to the glass.

Radial nematic polymer particles made from **P6** dispersed in a mixture of 1:1 dodecane: 1-undecanol were also exposed to various strengths of electric field to give an indication as to the effect of the internal director configuration of the particles. The application of an electric field resulted in significant particle motion analogous to that observed for the bipolar particles of **P1**. The rotation of radial particles is difficult to observe as their director configuration does not change on rotation. A video of the motion of the radial nematic polymer particles on application of a field with a frequency of 1 Hz and peak amplitude of 30 V can be found as Video 2 on the accompanying disk. Screenshots from Video 2 are shown in Figure 6.6.

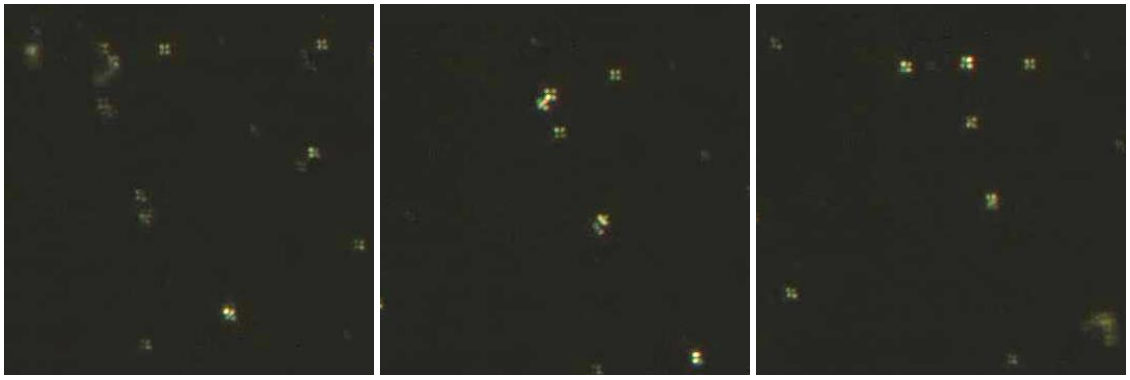

Figure 6.6: Figure 6.7: Screen shots from Video 2 showing the motion of radial nematic particles of **P6** moving in an applied field. Video taken at room temperature with partially crossed polarisers at 200 × magnification.

The motion of a random selection of particles within the sample range shown in Video 2 were tracked to allow for any relationship between particle motion and field frequency to be investigated. The particles were tracked using open-source software 'Tracker'[166] and the data was manipulated in order to give information about displacement of the particles against time. The particles display a back and forth motion which could be related to the switching of the field but it does not directly correlate with the frequency of the field as shown in Figure 6.8.

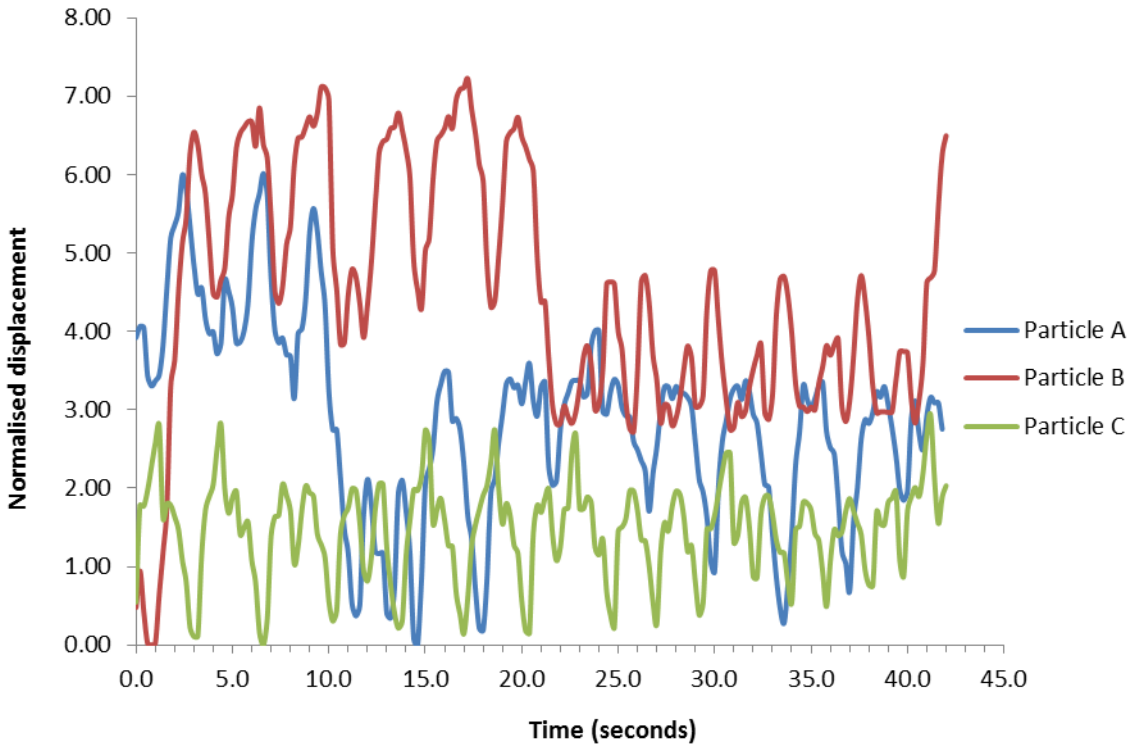

Figure 6.8: Normalised displacement of particles against time for an applied field frequency of 1Hz.

As can be seen from Figure 6.8, the frequency with which the particles change direction is approximately once every 3 seconds which is three times slower than the frequency of the electric field, which switches once per second. At higher frequencies, the particle motion observed is smoother and displays less back and forth motion possibly as a result of the frequency exceeding the maximum speed at which the particle can travel due to the viscosity of the dispersing medium.

6.4 Low glass transition temperature particles

Low glass transition radial polymer particles, that is, particles with a glass transition temperature below room temperature, were synthesised from dispersion polymerisation of **M9** and were investigated using premade homeotropic cells and dispersed in a dodecane: 1-undecanol mixture. In contrast to the particle motion observed for high glass transition bipolar and radial particles, these particles deformed in an electric field as a result of the mesogenic units within the particles aligning with the field. As the field is perpendicular to the viewing plane this was observed as particles becoming optically extinct as the mesogenic units aligned homeotropically. A series of

images depicting this transformation is shown in Figure 6.9. These images are frames from the video showing the transformation in full which can be found in the attached disk as Video 3.

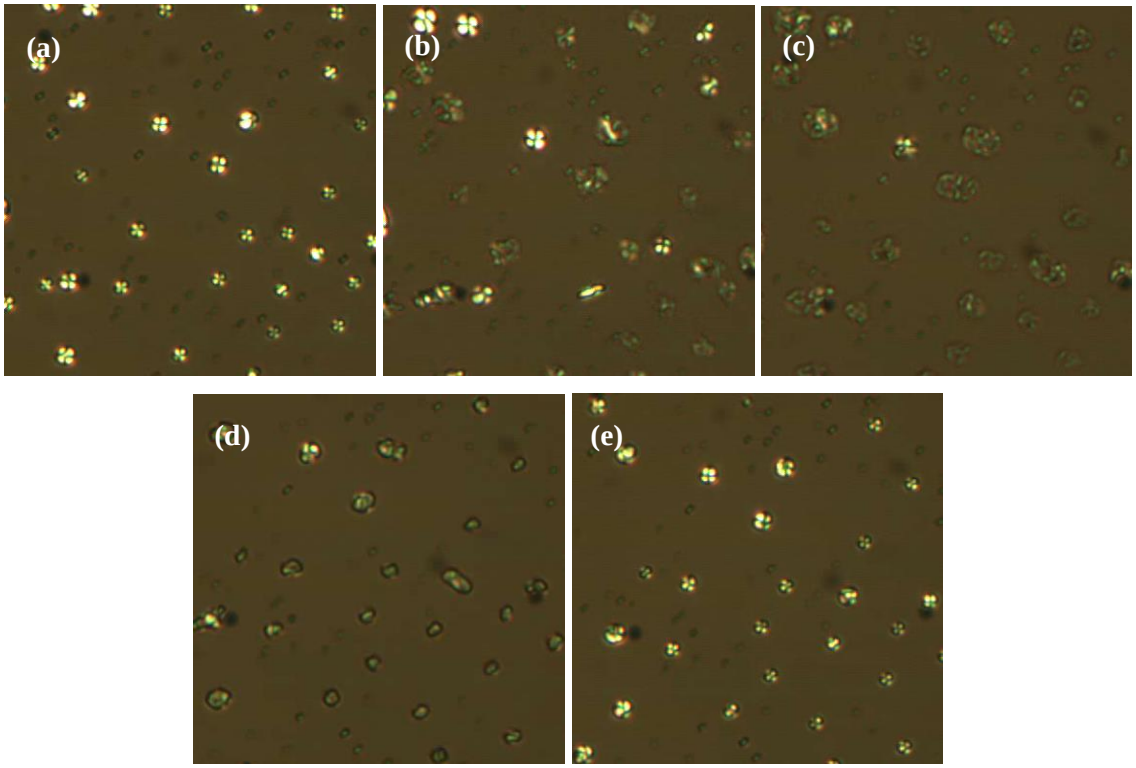

Figure 6.9: Frames from Video 3 on the attached disk. Images taken with half crossed polarisers, 200 × magnification and at rt. (a) Before application of electric field (b) on application of a square waveform field with a frequency of 1 Hz and a peak amplitude of 30 V (c) particles during exposure (d) immediate appearance of particles after removal of electric field (e) appearance of particles without an electric field present and relax back to spherical.

On switching on the electric field, the particles change shape and become oblate as the mesogenic units align with the field. Shown in Figure 6.10 is an illustration of an oblate particle with the axes labelled.

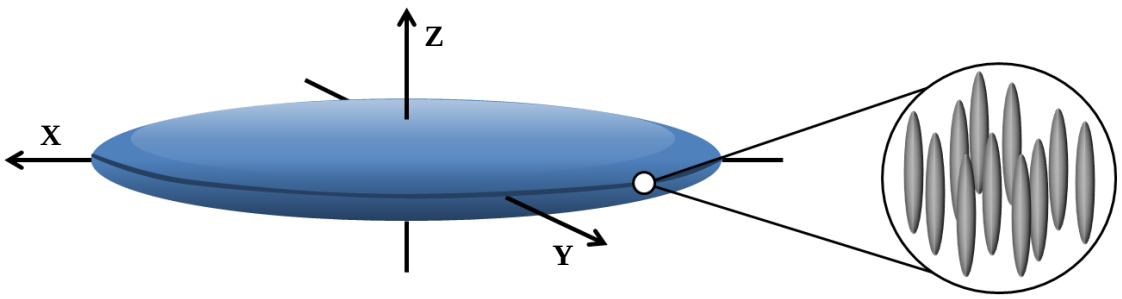

Figure 6.10: The mesogen organisation within the particles during application of an applied along

the Z axis.

In general when the electric field is applied the particles begin to flatten along the axis perpendicular to the electric field which results in the observation of large, optically extinct disks, as shown in Figure 6.9(c). The particles appear optically extinct because the mesogenic units are aligned with the short axis along which the particle is being viewed (labelled z in Figure 6.10), resulting in homeotropic mesogenic alignment. When the field was removed the particles relaxed back to a spherical shape. In contrast to these observations, when the field was again switched on for the second time, a number of particles within the sample flatten orthogonally to those previously described, with the short axis of the oblate particle orientated parallel with the viewing plane. Again this change of shape was reversible. These particles appear as bright thin lines as they are being observed along their edge, a selection of which are highlighted in Figure 6.11.

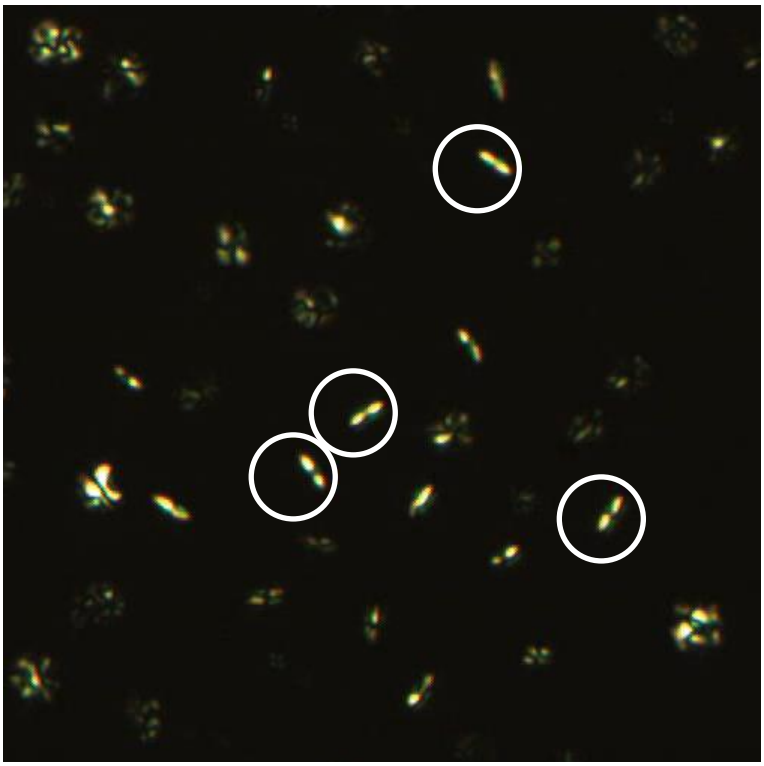

Figure 6.11: Screenshots from Video 4, showing the orthogonal deformation of a selection of particles within the sample. Video taken at rt through crossed polarisers and 200 × magnification during the application of a square waveform electric field with a frequency of 1 Hz and a peak amplitude of 30 V.

As can be seen in Figure 6.11, these particles appear bright as the mesogenic units are arranged homogeneously with respect to the polarisers when the particle is in this orientation. Particles that flatten in this direction eventually turn and become optically extinct, as the mesogenic units

within the particles force a rotation of the particles in order to align with the electric field. Screenshots from Video 4 which can be found on the attached disk show this flattening and rotation of particles in Figure 6.12.

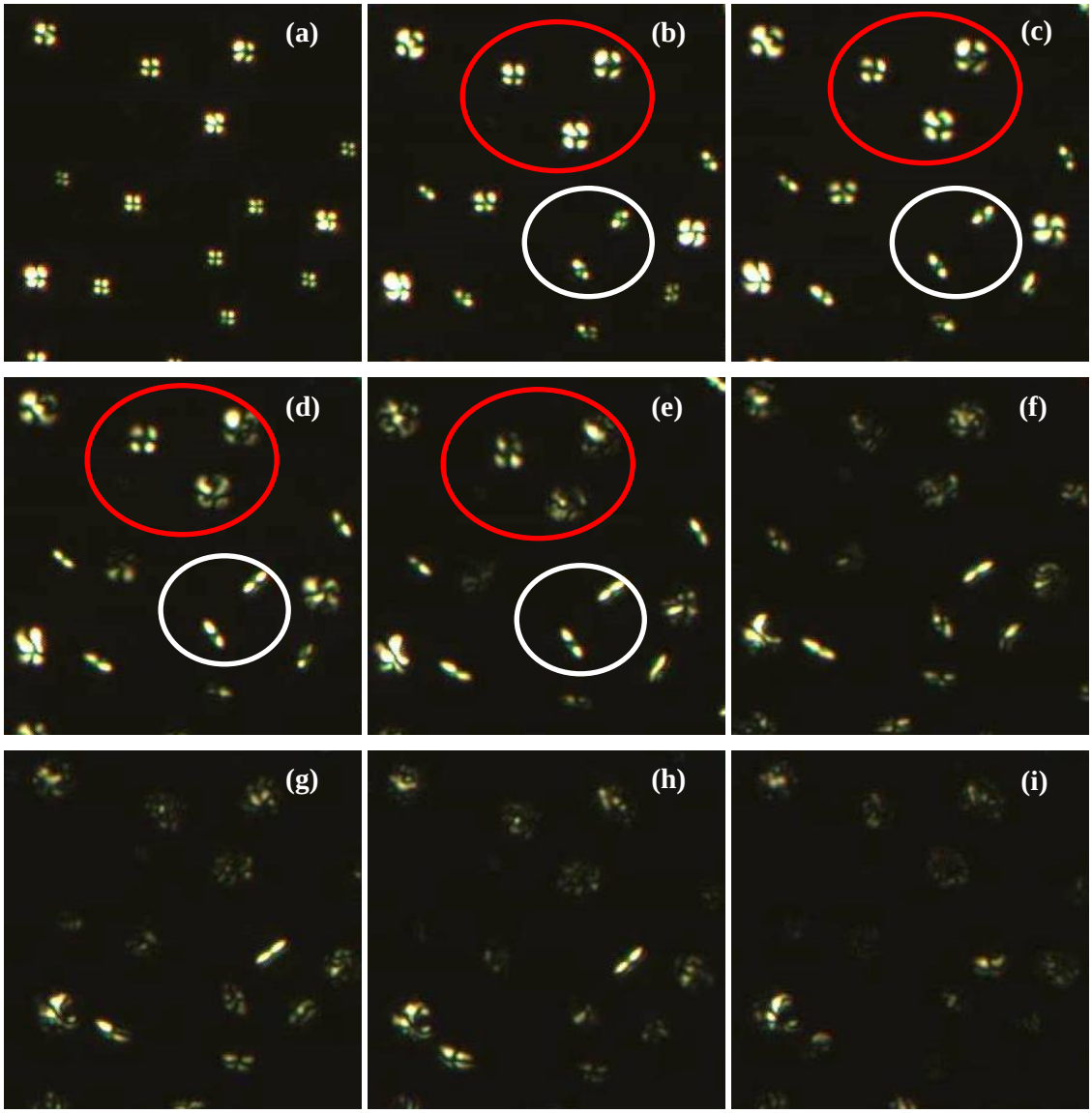

Figure 6.12: Screenshots from Video 4 showing the flattening and turning of particles of **M9** dispersed in dodecane/undecanol on application of a 1 Hz, 30 V square waveform electric field. (a) Before application of the electric field, (b – e) Flattening of particles in the field, either parallel to the viewing plane (an example is indicated in red) or orthogonal to the viewing plane (an example indicated in white), (f-h) shows the turning of the orthogonal oblate particles until they are orientated parallel with the viewing plane, (i) after turning, all oblate particles appear optically extinct due to the internal homeotropic alignment of the mesogens.

The number of particles present within a sample which display this orthogonal elongation increases with each repetition, as can be seen when comparing Video 3 with Video 4 which was

recorded afterwards. On the first application of the electric field, there are very few particles which deform in a different direction, after multiple repeats there is a significant proportion of the sample elongating in this way. This occurs possibly because the deformation of the polymer chains that occurs in order to accommodate the reorganisation of the mesogenic units with the electric field is not completely elastic, and does not return to the same original configuration on relaxation when the field is removed. When the electric field is applied a second time the particle will now have a preferred axis of elongation as the polymer chains can more easily accommodate the changing in shape in that direction. As the particles are free to rotate and move in the solvent this axis might not be perpendicular to the field as it was on the first deformation. This explanation suggests that the particles experience a lower energetic cost for the particle to deform in a way favourable for the polymer chains and then orient to align the mesogenic units with the field than reorganising the polymer chains with each application of the field.

From the corresponding videos of Figure 6.9 and Figure 6.12, it can be observed that this deformation process is reversible, with the particles regaining their radial configuration after the electric field is removed. This deformation is similar to those described in the introduction to this chapter for free droplet of liquid crystal within a liquid polymer[165] in that the particles flatten and increase in the direction axial to the electric field, though the polymer influence results in some of the particle deforming in a different direction and then turning to align with the field is a novel finding.

Below a threshold voltage the particles behave in a way analogous to those with higher glass transition temperatures, i.e. they do not deform in the field. The likely reason for this is that at low voltages the strength of the field is insufficient to exceed the surface tension and cause a deformation from a spherical shape.

Analysis of low glass transition nematic polymer particles displaying a bipolar texture was attempted in order to determine whether the reversible shape deformation observed for radial particles was dependent on the director configuration of the particles. Due to the low polarity of the dispersing solvent and perpendicular surface anchoring it imparts, the bipolar droplets converted to a radial director configuration when they were transferred into the 1:1 dodecane: undecanol mixture. Due to times constraints a suitable solvent which would allow for the analysis of bipolar low glass transition nematic polymer particles was not established. It is expected that the bipolar particles that were observed for sample **P1** described in the previous section remained as such because they were below their glass transition temperature, preventing mesogenic reorientation to a radial configuration.

6.5 Effect of temperature

A sample of nematic polymer particles of **P9** displaying a radial director configuration were investigated by electro-optics whilst in their isotropic phase to establish whether the shape change discussed previously was determined by the reorientation of the mesogenic units. The video of the experiment can be found in the attached disk as Video 5, screenshots are shown in Figure 6.13.

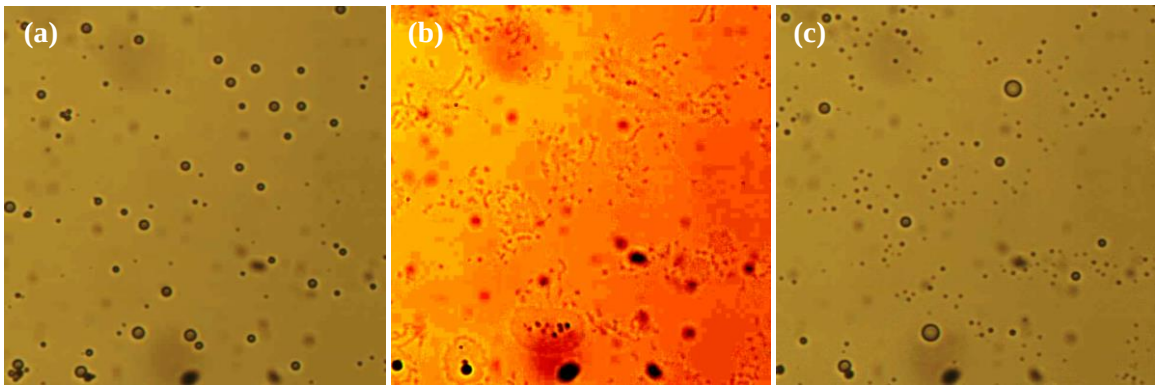

Figure 6.13: Screenshots from Video 5 showing the deformation isotropic of particles of **M9** dispersed in dodecane/undecanol on application of a 1 Hz, 30 V square waveform electric field, taken at 60 °C. In image (b) the contrast has been increased to allow for the deformed particles to be observed.

The effect we observe when an electric-field is applied to these particles when heated into their isotropic phase is different to that observed when the particles are in the nematic phase, which infers the liquid crystal state has an influence on the particle behaviour. Rather than retaining their discrete shape, the particles completely deform and when the field is removed droplets reform which were not necessarily the same size as originally due to coagulation of the droplets when the field was applied. This effect is similar to that mentioned for droplets of liquid crystal as a free dispersion in a liquid polymer which coagulate together when they become prolate in the field. As this is occurring in the isotropic phase of the nematic polymer it is an electro-wetting effect rather than a liquid crystal process. The reversible shape change process that takes place when the particles are observed within their nematic phase without loss of discrete particles may be because of significant polymer entanglement and high viscosity preventing particle coagulation.

6.6 Conclusions

The electro-optical response of nematic polymer particles of different director configurations and glass transition temperatures was evaluated. The particles were dispersed in a solvent mixture of 1:1 dodecane:1-undecanol to allow for the particle response to be established without interferences from the solvent flowing in the electric field. It was observed that when the glass transition temperature of the particles was above room temperature, the particle shape was fixed and particle motion was observed. There are previous examples of nematic particle motion within an electric field as a result of the particle acting as a dipole.[102] Control of a particle in an electric field is significant as it could find possible applications as micro-stirrers for microscale machinery.

When the glass transition temperature of the polymer particles investigated was below room temperature a reversible shape change was observed. A reversible shape change of microscale polymer particles in the presence of an electric field agrees with current understanding of the behaviour of free dispersions of liquid crystal droplets within a field. The presence of the polymer network results in a different shape change response compared to liquid crystal droplets as the reorganisation of the polymer chains dictates the direction of the shape change before reorientation of the now oblate particle so that the mesogenic units can align with the electric field. This effect of a polymer network on the behaviour of the mesogenic units may be further evidence into the coupling between laterally attached mesogenic units and the anisotropic polymer backbone. As the polymer that was investigated in this case was comprised of mesogenic units attached *via* long spacers to the polymer backbone this may indicate that a degree of coupling still exists in systems where the spacer length is long.

CHAPTER 7:

CONCLUSIONS

7 CONCLUSIONS

The fundamental aim of this research was the synthesis and investigation of nematic polymer and elastomer particles on the microscale. To this end, a variety of different polymerisation methods and novel monomers were utilised. Nematic polymer particles were synthesised *via* dispersion polymerisation and RAFT-assisted dispersion polymerisation and were optimised for particle size, particle size variance and director configuration. Nematic elastomer particles were synthesised using techniques including RAFT-assisted dispersion polymerisation and dispersion polymerisation with a delayed addition of crosslinker with varied degrees of network formation being achieved. These particles were optimised for director configuration and crosslink density and were analysed by gel content analysis, heating and swelling studies in order to confirm the network formation within the particles. Investigations of the particles included DSC and NMR studies, as well as thorough analysis using polarised optical microscopy and scanning electron microscopy. The behaviour of a variety of particle systems in an electric field was also evaluated.

7.1 NEMATIC POLYMER PARTICLES ON THE MICROSCALE

Nematic polymer particles synthesised by dispersion polymerisation were found to range in director configuration, particle size and particle size variance depending on the nematic monomer and dispersing solvent utilised. A series of laterally attached nematic monomers, seven of which were novel, with sequential changes in structure allowed the systematic investigation of the effect of monomer structure on the director configuration that would result. In a series of otherwise identical experiments it was found that a change in the director configuration occurred with increasing side chain length on the mesogenic pendant group. This resulted in radial particles being synthesised in a polar host mixture without the aid of any surface analytes to promote a perpendicular surface alignment. This is a novel finding that is previously unreported in the literature where over a significant range of monomers investigated, a bipolar configuration is achieved when the particles are synthesised or dispersed in a polar host such as water, EtOH or MeOH.[78, 79, 107] The results within this thesis suggest that the director configuration of a nematic particle is dependent on a balance between surface interactions and the interactions of the liquid crystal in the bulk. By altering the mesogen structure within the particles the bulk interactions including the elastic constants of the liquid crystal are affected as a result of the mesogen changing size. Changing the relative cost of the elastic deformations of a confined liquid crystal can result in the lowest energy director configuration changing from bipolar, when the bend

deformation is the least energetically costly for the liquid crystal, to the radial when the bend deformation becomes too unfavourable and the splay deformation becomes the most favourable scenario. This systematic study has allowed for the realisation of a controlled synthetic pathway for liquid crystal polymer particles of the microscale, with specific particle size, particle size variance and director configuration.

Creating a series with distinct differences in the director configuration that results in otherwise identical dispersion polymerisations is significant because it allows for the systems to be tuned for surface sensitivity. By creating a system in which the liquid crystal particles are on the borderline of stability a switch in director configuration can occur with a small change in surface anchoring strength. This change in surface anchoring can be as a result of altering the medium that the particles are dispersed in, the addition of a substrate or surface analyte. This response allows these particles possible applications as sensors for small changes in the external environment on the microscale. Previous work has been completed in the use of encapsulated liquid crystal droplets for sensing applications, sensing for example pH and the presence of certain bacteria.[5, 156, 167] Particles would be better suited to this role due to increased durability and shelf life. They are also easier to transfer into different host media, as well as being easier to remove afterwards by centrifugation or filtration. Systems suitable for a possible application in sensing were created by completing copolymerisation investigations using monomers with different preferred configurations in ethanol. By tuning the ratios of the two monomers used a system was created in which the director configuration displayed was an escaped conformation, which should allow for a facile switch with the addition of analytes such as SDS, which promotes a perpendicular surface alignment, and PVP which promotes a parallel surface alignment.

RAFT-assisted dispersion polymerisation resulted in a greater degree of monodispersity being achieved across a range of different polar solvents compared to dispersion polymerisation. Monodisperse samples can assemble into photonic crystals, and by using liquid crystal particles for the basis of the assembly of photonic crystals the wavelength of reflected light can in theory be tuned by inducing a change in director configuration, or inducing the nematic to isotropic transition of the particles.

7.2 SUCCESSFULLY CROSSLINKING NEMATIC PARTICLES

A primary aim within this thesis was to create successfully crosslinked microscale liquid-crystalline elastomer particles, and to investigate their responsive ability. Their crosslink density is crucial to their function but will also add to the lifetime of the working particle.

Particles were evaluated thoroughly in order to establish whether there has been significant network formation. The particles were investigated by being swollen in solvents multiple times and assessed for any leaching of uncrosslinked polymer chains and also the degree to which they maintain their shape integrity. A sample of the particles was also dried for gel content analysis in order to establish what percentage of the particles' compositions was insoluble and therefore fully networked. It was found that by delaying the addition of the crosslinker until after the nucleation stage of particle growth had completed was successful when utilising the terminally attached monomer, though had limited successes with the lateral series of monomers. Achieving elastomeric particles *via* a delayed addition of crosslinker is less than ideal as the system is very sensitive to concentration and crosslinker addition time, leading to discrepancies in the results and difficulties in reproducibility. Crosslinked and monodisperse particles were successfully synthesised using a delayed addition of crosslinker with dispersion polymerisation after careful tuning of the reaction conditions. This is the first instance of crosslinked nematic particles with confirmed network formation being synthesised by heterogeneous polymerisation methods on the low micrometre scale.

When RAFT-assisted dispersion polymerisation was utilised, nematic elastomer particles were obtained from polymerisations of all monomers. These particles were not displaying resolved director configurations analogous to their non-crosslinked counterparts and were instead often polydomain in structure. However, these particles do show director configurations as the birefringence returns after swelling in a favourable solvent such as toluene or acetone, but the polydomain structure returns once the particles have completely deswollen. The director configuration that is observed is related to the polarity of the swelling solvent which is an example of these nematic elastomer particles acting as sensors for changes in their surface anchoring. RAFT-assisted dispersion polymerisation in the presence of a crosslinker is the first heterogeneous method to create a significant crosslink density within nematic particles on the microscale irrespective of monomer structure. It is significant as further adaptations to the method in order to achieve particles with resolved director configurations will reveal a facile synthetic method for the synthesis of nematic microscale elastomer particles which should have the ability to actuate.

7.3 Optical investigations of nematic polymer particles

The electro-optical experiments with nematic polymer particles revealed a reversible shape change response to the addition of an electric field when the glass transition temperature of the polymer was below room temperature. A reversible shape change of microscale polymer particles

in the presence of an electric field agrees with current understanding of the behaviour of liquid crystal droplets within a field. The effect of the polymer network results in the shape change response of the liquid crystal particle to be viewed from different angles as the tumbling of the particles in solution allow the shape change to be viewed from the side. This result is significant as it allows for the confirmation of the reorganisation of the mesogenic units within the field and shows the impact of the coupling between the mesogenic units and the polymer backbone. Polymer particles synthesised from polymers which have a glass transition temperature above room temperature did not show a change in shape as a result of the mesogenic units not having the freedom to reorientate when the polymer chains are rigid and inflexible. These particles displayed particle motion when the field was applied which did not appear to correlate to the frequency of the field being applied. The particle motion is indicative of charged impurities on the particle surfaces.

7.4 CONCLUDING REMARKS

The synthesis of nematic polymer and elastomer particles on the microscale with reproducible director configurations, size, polydispersities and where applicable network formation is complicated due to the sensitive nature of dispersion polymerisation and its various modifications. Significant work was completed into the optimisation of various reactions to maximise monodispersity and the degree of crosslinking within the particles. In this venture further conclusions were drawn, including how the degree of crosslinking that can be achieved varies with different polymerisation methods and how the monomer structure can affect the particle size and director configuration that is obtained.

The synthesis of liquid crystal elastomer particles with confirmed network formation on the microscale is a novel result. Swelling studies have established that even with significant crosslinking the director configuration of the particles can still respond to changes in the external environment, for example a change in solvent polarity. This is preliminary evidence of the responsive nature of these particles which gives them a possible application in microscale sensing.

The ability to tune the stability of a director configuration in a particular solvent by carefully selecting the monomer mixture from which the particles are formed is a novel finding as previous results have so far only noted bipolar particles when synthesised or dispersed in polar solvents. By creating a system in which the director configuration is at the limit of its stable range we

should observe a more facile switch of the director as a response to an external stimulus, improving the sensing sensitivity of the particles.

CHAPTER 8:

EXPERIMENTAL

8 EXPERIMENTAL

8.1 GENERAL INFORMATION

All reagents and solvents used in the synthesis of the monomers and in the dispersion polymerisations were readily available commercially and were used as supplied without any further purification. Accurate weights were obtained using a Mettler Toledo XS 105 dual range balance. Flash column chromatography was performed using 35 – 70 μm silica gel and thin layer chromatography (TLC) was performed on silica gel F_{254} pre-coated aluminium backed sheets and visualised using UV light from a UVGL-58 lamp that emits light at 254 or 365 nm. Centrifugation was performed using a Fisher Scientific accuspin400 centrifuge containing a C003649 rotor fitted with swinging buckets. Optical microscopy studies were performed using a Zeiss AXIOSKOP 40 polarised light microscope and together with the Mettler Toledo FP82HT hot stage the melting points and phase transitions were obtained. Gel Permeation Chromatography (GPC) was completed using a triple detection GPC fitted with a Viscotek VE3580 RI detector and a Viscotek 270 dual detector and a 100 μL column with THF as the mobile phase against a polystyrene standard. Scanning electron microscopy (SEM) and transmission electron microscopy (TEM) photomicrographs were taken in the Biology Technology Facility at the University of York. For SEM, the samples were mounted on conductive stubs with silicon wafers and sputter coated with approximately 7 nm of gold/palladium using a Quorum SC7640 sputter coater before being analysed with a JEOL JSM6490-LV instrument. Differential scanning calorimetry (DSC) analysis was carried out on a Mettler Toledo DSC 822^e with STAR^e acquisition and analysis software calibrated against an indium standard. Nuclear magnetic resonance (NMR) spectra were recorded using a JEOL EX400 NMR spectrometer (^{1}H: 400 MHz, ^{13}C: 100.4 MHz). NMR spectra were viewed and analysed using MestReNova analysis software. All infrared (IR) spectra were completed on a Shimadzu IR Prestige-21 FT IR spectrophotometer. Electrospray ionisation (ESI) mass spectra were performed on a Thermo-Finnigan LCQ mass spectrometer. Size Distributions were calculated from SEM images using ImageJ software[51]. In each case a minimum of 100 particles were measured and the particle size polydispersity calculated as the coefficient of variance (C_v) using the standard deviation and the mean. Percentage yields were calculated from the moles of obtained product as a comparison to the moles of limiting reagent in the reaction.

8.2 SYNTHESIS OF MONOMERS

8.2.1 *SYNTHESIS OF TERMINALLY ATTACHED MONOMER **M1***

The synthesis of monomer **M1** was completed *via* a synthesis adapted from literature:[134]

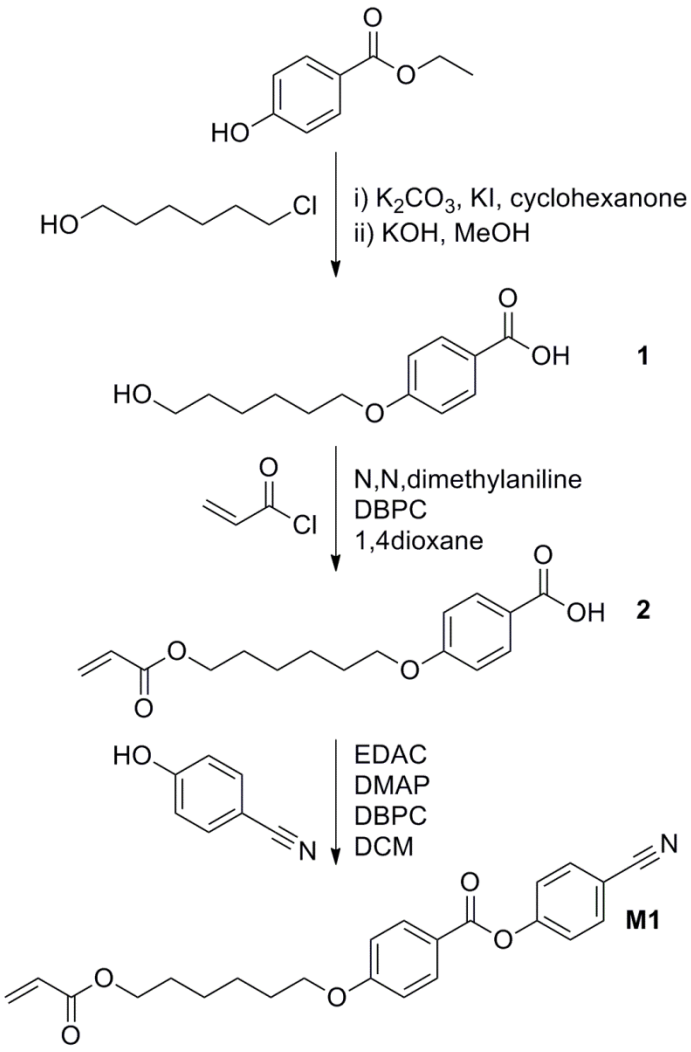

Scheme 8.1: Reaction scheme for the synthesis of terminal monomer **M1.**

8.2.1.1 4-(6-Hydroxyhexyloxy)benzoic acid (1)

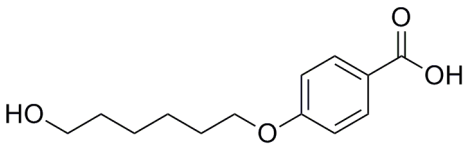

Figure 8.1: 4-(6-Hydroxyhexyloxy)benzoic acid.

A solution of ethyl-4-hydroxybenzoate (33.38 g, 200.8 mmol), 6-chlorohexanol (32.5 mL, 240.7 mmol) potassium carbonate (55.40 g, 400.9 mmol) and potassium iodide (3.00 g) in cyclohexanone (300 mL) was brought to reflux with vigorous stirring for 16 h. The excess potassium carbonate was then hot filtered and washed with cyclohexanone. The solvent was removed *in vacuo*. The resulting oil was dissolved in methanol (300 mL) and was stirred under reflux for a further 16 h after the addition of potassium hydroxide (44.9 g, 800 mmol) in water (50 mL). The reaction mixture was then allowed to cool to room temperature and the solvent removed *in vacuo*. The residue was dissolved in ice water. The addition of concentrated hydrochloric acid yielded a white precipitate which was recrystallised from ethanol.

Yield: White powder, 39.22 g, 164.8 mmol, 82 %.

Mp: 135.6 - 137.2 °C.

^{1}H NMR ($CDCl_3$) δ (ppm): 1.35 (m, 6H, -CH_2-), 1.69 (m, 2H, -CH_2-), 3.37 (m, 2H, -CH_2O-), 4.01 (m, 2H, -CH_2O-), 4.35 (br s, 1H, OH), 6.98 (d, 2H, J= 8.2 Hz, ArH), 7.85 (d, 2H, J= 8.2 Hz, ArH), 12.55 (br s, 1H, OH).

IR (FTR) ν (cm^{-1}): 3394 (O-H), 2939 (C-H), 2862, 2808, 2630, 2515, 1897, 1681 (C=O), 1604 (C-C), 1465 (C-H), 1411, 1249, 1165, 1103, 1056, 1002, 948, 840, 763.

8.2.1.2 4-(6-Acryloyloxyhexyloxy)benzoic acid (2)

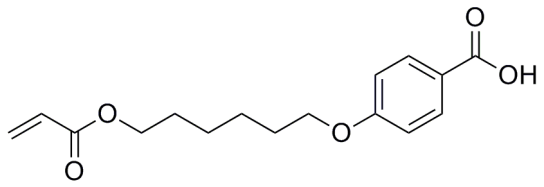

Figure 8.2: 4-(6-Acryloyloxyhexyloxy)benzoic acid.

Under nitrogen, 4-(6-hydroxyhexyloxy)benzoic acid (39.00 g, 163 mmol), DBPC (0.3 g, catalytic quantity) and *N*, *N*-dimethylaniline (21 mL, 163 mmol) were dissolved in dry dioxane (200 mL). The reaction mixture was heated to 60 °C with stirring. Acryoyl chloride (17 mL, 170 mmol) was then added drop wise so that the temperature did not exceed 65°C and the resulting mixture stirred at 60 °C for 2 h. The solution was poured onto ice water to precipitate the product which was recrystallised from propan-2-ol.

Yield: White powder, 35.01 g, 120 mmol, 74 %.

Mp: 83.4 – 84.6 °C.

^{1}H NMR ($CDCl_3$) δ (ppm): 1.41 (m, 4H, -CH_2-), 1.65 (m, 2H, -CH_2-), 1.77 (m, 2H, -CH_2-), 3.96 (m, 2H, -CH_2O-), 4.11 (m, 2H, -CH_2O-), 5.76 (dd, 1H, J= 1.5 Hz, 10.3 Hz, CH=), 6.06 (dd, 1H, J= 10.3 Hz, J= 17.4 Hz, CH=), 6.31 (dd, 1H, J= 1.5 Hz, 17.4 Hz, CH=), 6.86 (d, 2H, J= 8.8 Hz, ArH), 7.98 (d, 2H, J= 8.8 Hz, ArH).

IR (FTR) ν (cm^{-1}): 2939, 2854 (C-H), 2669, 2561 (O-H), 1720, 1681 (C=O), 1604 (C-C), 1512, 1141 (C-H), 1296, 1249, 1165, 1041, 979, 763, 640.

8.2.1.3 4-[4-(6-Acryloyloxyhexyloxy)benzoyloxy]benzonitrile (M1)

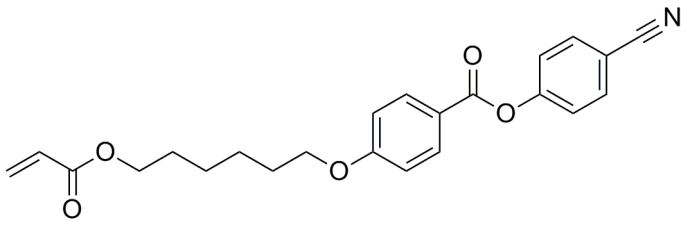

Figure 8.3: 4-[4-(6-Acryloyloxyhexyloxy)benzoyloxy]benzonitrile (**M1**).

A solution of 4-(6-acryloyloxyhexyloxy)benzoic acid (34.5 g, 118 mmol), 4-hydroxybenzonitrile (14.04 g, 118 mmol), EDAC (22.63 g, 118 mmol) and a spatula tip of DMAP and DBPC dissolved in DCM (300 mL) was stirred at room temperature for 72 h and monitored by TLC until the starting materials were consumed. The solvent was removed *in vacuo* and the resultant product purified using column chromatography in 2:1 hexane: ethyl acetate. Yield is poor because of a breakage of glassware. Recrystallised from ethanol.

Yield: White powder, 18.98 g, 48.2 mmol, 41 %.

Mp: 71.7 – 72.9 °C.

^{1}H NMR ($CDCl_3$) δ (ppm): 1.51 (m, 4H, -CH_2-), 1.72 (m, 2H, -CH_2-), 1.84 (m, 2H, -CH_2-), 4.05 (t, 2H, J= 6.2 Hz, -CH_2O-), 4.19 (t, J= 6.7 Hz, 2H, -CH_2O-), 5.82 (dd, 1H, J= 10.4, 1.5 Hz, CH=), 6.12 (dd, 1H, J= 17.3, 10.4 Hz, CH=), 6.40 (dd, 1H, J= 17.3, 1.5 Hz, 17.4 Hz, CH=), 6.97 (d, 2H, J= 9.0 Hz, ArH), 7.34 (d, 2H, J= 8.7 Hz, ArH), 7.73 (d, 2H, J= 8.8 Hz, ArH), 8.12 (d, 2H, J= 8.9 Hz, ArH).

^{13}C NMR ($CDCl_3$) δ (ppm): 25.77 (CH_3-), 28.62, 29.04 (-CH_2-), 64.54, 68.26 (C-O), 77.13 (t, $CDCl_3$), 109.63, 114.55 (C≡N), 118.47, 120.67, 123.09, 128.62, 130.72, 132.57, 133.77 (ArC), 154.53, 163.97, 166.43(C=O).

MS (ESI): $C_{23}H_{23}NO_5$ calculated [M + Na] *m/z* 416.1468, found 416.1463.

EA (CHN): calculated C 70.21 %, H 5.89 %, N 3.56 % found C 70.18 %, H 5.92 %, N 3.67 %.

IR (FTR) ν (cm^{-1}): 2939 (C-H), 2862, 2322, 2229 (C≡N), 1735, 1712 (C=O), 1597 (C-C), 1504, 1404 (C-H), 1249, 1203, 1165, 1056, 979, 848, 810, 694, 547.

8.2.2 *SYNTHESIS OF LATERAL MONOMERS* ***M2-M9***

Monomers **M2** – **M9** were created using a divergent synthesis derived from the literature synthesis of **M3.**[14, 80, 133]

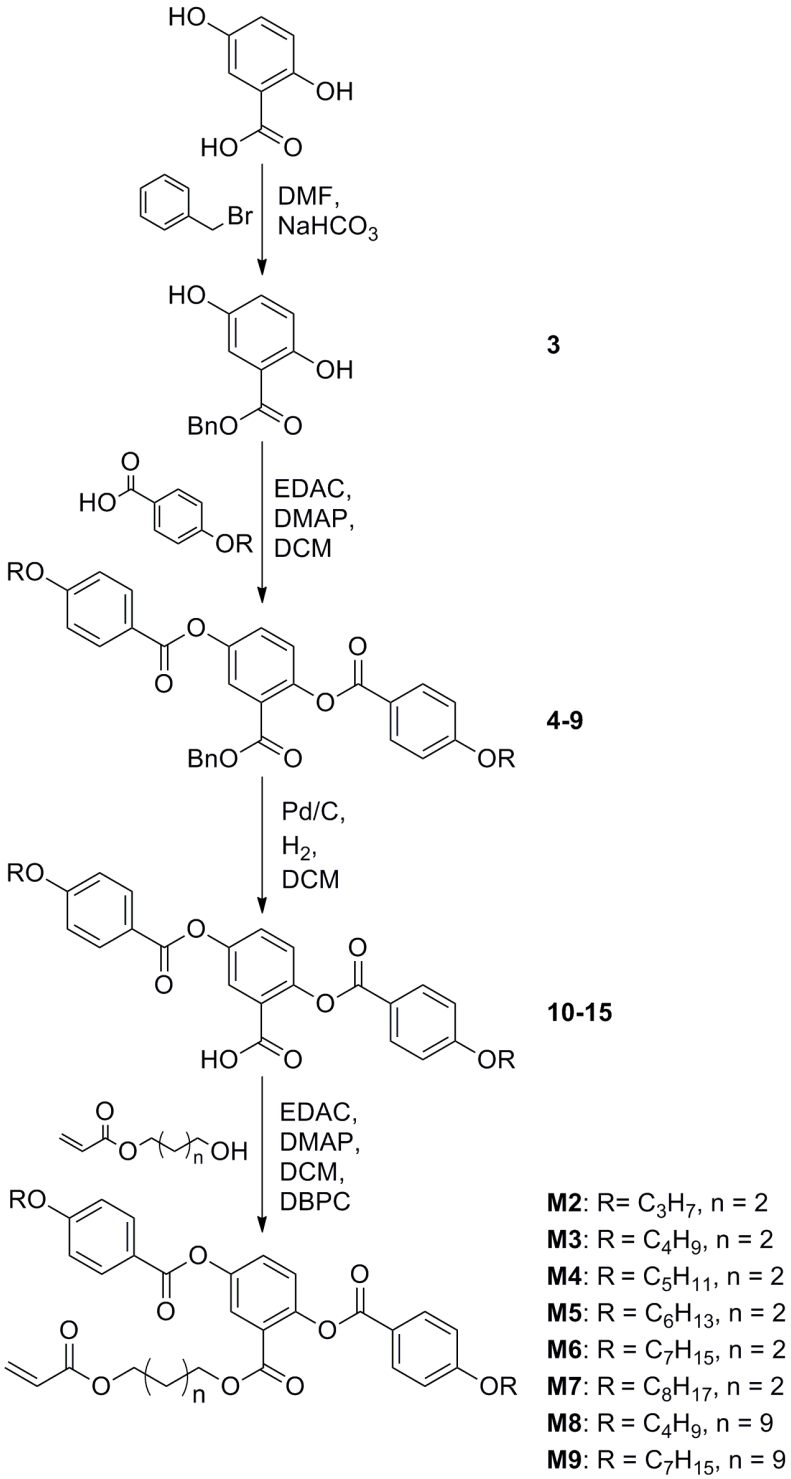

Scheme 8.2: Reaction scheme of the divergent synthetic procedure of **M2-M9**.

8.2.2.1 Benzyl-2,5-dihydroxybenzoate (3)

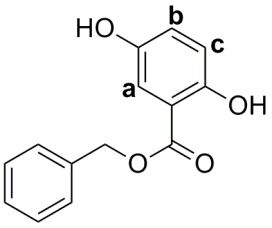

Figure 8.4: Benzyl-2,5-dihydroxybenzoate.

Solid $NaHCO_3$ was added (36.04 g, 425 mmol) to a stirred solution of 2,5-dihydroxybenzoic acid (26.18 g, 170 mmol) in DMF (600 mL) and the mixture brought to 70 °C for 1 h. Benzyl bromide (29.07 g, 170 mmol) was then added and the mixture stirred and heated at 70 °C overnight. The reaction mixture was then allowed to cool, diluted with water (600 mL) and extracted three times with 50:50 hexane/ethyl acetate mixture. The organic phase was washed twice with water to remove the residual DMF and dried over Na_2SO_4. The solvent was removed *in vacuo* and the resultant product was purified by recrystallization from a hexane/ethanol mixture.

Yield: White powder, 38.58 g, 158.1 mmol, 93 %.

^{1}H NMR ($CDCl_3$) δ (ppm): 4.86 (s, 1H, -OH), 5.36 (s, 2H, CH_2O-), 6.88 (d, J = 9.0 Hz, 1H, $ArH_{\mathbf{c}}$), 7.00 (dd, J = 8.9, 3.1 Hz, 1H, $ArH_{\mathbf{b}}$), 7.31 (d, J = 3.2 Hz, 1H, $ArH_{\mathbf{a}}$), 7.49 – 7.34 (m, 5H, ArH), 10.33 (s, 1H, -OH).

IR (FTR) ν (cm^{-1}): 3387, 3124, (OH), 2954, 2893 (CH), 2330, 2044, 1897, 1667 (C=O), 1597 (Ar), 1481 (CH), 1396, 1303, 1203, 1072, 956, 779, 740, 687, 556.

8.2.2.2 Benzyl-2,5-di(4-alkyloxybenzoyloxy)benzoates (4-9)

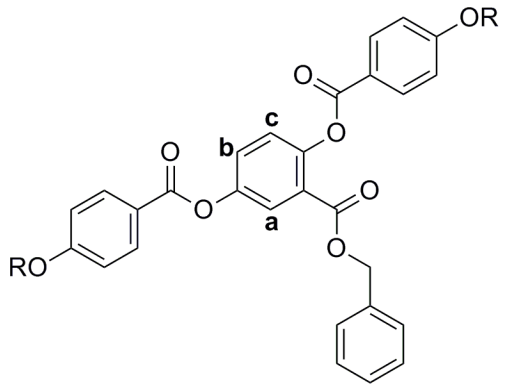

Figure 8.5: Benzyl-2,5-di(4-alkyloxybenzoyloxy)benzoates (**4-9**), R= C_3H_7 to C_8H_{17}

A solution of benzyl-2,5-dihydroxybenzoate, an alkyloxybenzoic acid, EDAC and a catalytic quantity of DMAP in DCM (100 mL) was stirred at RT for 12 h. The reaction was monitored by TLC and when completed solvent removed *in vacuo* and purified by flash column chromatography in DCM.

Benzyl-2,5-di(4-propyloxybenzoyloxy)benzoate (4)

Reagents: Benzyl-2,5-dihydroxybenzoate (5.42 g, 22 mmol), 4-propyloxybenzoic acid (8 g, 44 mmol), EDAC (3.45 g, 44 mmol).

Yield: White powder, 7.45 g, 13 mmol, 60 %.

^{1}H NMR ($CDCl_3$) δ (ppm): 1.02-1.10 (m, 6H, -CH_3), 1.78-1.94 (m, 4H, -CH_2-), 4.01 (m,4H, -CH_2O-), 5.19 (s, 2H, -CH_2Ar), 6.97 (dd AA′ XX′, 4H, J = 6.4, 8.8 Hz, ArH), 7.23 (m, 5H, ArH), 7.28 (d, 1H, J = 8.8 Hz, $ArH_{\mathbf{c}}$), 7.47 (dd, 1H, J = 2.5, 8.8 Hz, $ArH_{\mathbf{b}}$), 7.94 (d, 1H, J = 2.9 Hz, $ArH_{\mathbf{a}}$), 8.06 – 8.17 (m AA′ XX′, 4H, ArH).

IR (FTR) ν (cm^{-1}): 3071, 2970, 2939 (CH), 2878, 1720 (C=C), 1604, 1512 (Ar), 1242, 1165, 1126, 1072, 1010, 972, 841, 687, 648, 556.

Benzyl-2,5-di(4-butyloxybenzoyloxy)benzoate (5)

Reagents: Benzyl-2,5-dihydroxybenzoate (19.00 g, 78 mmol), 4-butyloxybenzoic acid (30.4 g, 156 mmol), EDAC (24.2 g, 156 mmol).

Yield: White powder, 20.94 g, 35.1 mmol, 45 %.

^{1}H NMR ($CDCl_3$) δ (ppm): 0.98 (m, 6H, -CH_3), 1.49 (m, 4H, -CH_2-), 1.77 (m, 4H, -CH_2-), 4.02 (m, 4H, -CH_2O-), 5.35 (s, 2H, CH_2Ar), 6.93 (m, 5H, ArH), 7.03 (d, 1H, J = 9 Hz, $ArH_{\mathbf{c}}$), 7.27 (dd, 1H, J = 2.9, 9 Hz, $ArH_{\mathbf{b}}$), 7.40 (d, 1H, J = 2.9 Hz, $ArH_{\mathbf{a}}$), 7.38 (m AA′ XX′, 4H, ArH), 8.05 (m AA′ XX′ , 4H, ArH).

IR (FTR) ν (cm^{-1}): 3071, 2932 (CH), 2870, 1720 (C=O), 1581, 1504 (Ar), 1242, 1165, 1064, 964, 841, 679, 548, 509.

Benzyl-2,5-di(4-pentyloxybenzoyloxy)benzoate (6)

Reagents: Benzyl-2,5-dihydroxybenzoate (4.64 g, 19 mmol), 4-pentyloxybenzoic acid (8 g, 38 mmol), EDAC (5.96 g, 38 mmol).

Yield: White powder, 8.29 g, 13 mmol, 70 %.

^{1}H NMR ($CDCl_3$) δ (ppm): 0.89 – 1.00 (m, 6H, -CH_3), 1.42-1.51 (m, 6H, -CH_2-), 1.79 – 1.85 (m, 4H, -CH_2-), 4.04 (t, 4H, J= 6.5 Hz, CH_2O-), 5.19 (s, 2H, -CH_2Ar), 6.96 (m AA′ XX′, 4H, ArH), 7.23 (m, 5H, ArH), 7.26 (d, 1H, J = 8.7 Hz, $ArH_{\mathbf{c}}$), 7.44 (dd, 1H, J = 2.9, 8.8 Hz, $ArH_{\mathbf{b}}$), 7.90 (d, 1H, J = 2.9 Hz, $ArH_{\mathbf{a}}$), 8.07 (m AA′ XX′, 4H, ArH).

IR (FTR) ν (cm^{-1}): 3071, 2932 (CH), 2862, 2770, 1582 (C=O), 1504 (Ar), 1466, 1389, 1242, 1165, 1126, 1065, 995, 841, 617, 548.

Benzyl-2,5-di(4-hexyloxybenzoyloxy)benzoate (7)

Reagents: Benzyl-2,5-dihydroxybenzoate (4.4 g, 18 mmol), 4-hexyloxybenzoic acid (8 g, 36 mmol), EDAC (5.58 g, 36 mmol).

Yield: White powder, 8.41 g, 13 mmol, 72 %.

^{1}H NMR ($CDCl_3$) δ (ppm): 0.89-0.93 (m, 6H, -CH_3), 1.34-1.37 (m, 8H, -CH_2-), 1.38 – 1.52 (m, 6H, -CH_2-), 1.79 – 1.84 (m, 4H, -CH_2-), 4.04 (m, 4H, CH_2O-), 5.18 (s, 2H, -CH_2Ar), 6.93 (m, AA′ XX′, 4H, ArH), 7.23 (m, 5H, ArH), 7.24 (d, 1H, J = 8.7 Hz, $ArH_{\mathbf{c}}$), 7.43 (dd, 1H, J = 8.7, 2.9 Hz, $ArH_{\mathbf{b}}$), 7.89 (d, 1H, J = 2.9 Hz, $ArH_{\mathbf{a}}$), 8.09 (m, AA′ XX′, 4H, ArH).

IR (FTR) ν (cm^{-1}): 3070, 2924 (CH), 2862, 1728, 1605 (C=O), 1504 (Ar), 1458, 1419, 1373, 1242, 1165, 1134, 1072, 1003, 887, 841, 625, 556.

Benzyl-2,5-di(4-heptyloxybenzoyloxy)benzoate (8)

Reagents: Benzyl-2,5-dihydroxybenzoate (19.00 g, 78 mmol), 4-heptyloxybenzoic acid (36.8 g, 156 mmol), EDAC (24.216 g, 156 mmol).

Yield: White powder, 33.4g, 49.1 mmol, 63 %.

^{1}H NMR ($CDCl_3$) δ (ppm): 0.81 (m, 6H, -CH_3), 1.32 (m, 12H, -CH_2-), 1.45 (m, 4H. –CH_2-), 1.79 (m, 4H, -CH_2-), 3.79 (m, 2H, -CH_2O-), 4.04 (t, 4H J = 6.6 Hz, -CH_2O), 5.18 (s, 2H, CH_2Ar), 6.92 (m, AA′ XX′, 4H, ArH) 7.22 (m, 5H, ArH), 7.25 (d, 1H, J = 8.7 Hz, $ArH_{\mathbf{c}}$), 7.45 (dd, 1H, J = 8.7, 2.9 Hz, $ArH_{\mathbf{b}}$), 7.89 (d, 1H, J = 2.9 Hz, $ArH_{\mathbf{a}}$), 8.10 (m AA′ XX′, 4H, ArH).

IR (FTR) ν (cm^{-1}): 3387, 3070, 2939, 2893 (CH), 1743, 1667, 1597 (C=O), 1481 (Ar), 1204, 1072, 957, 779, 741, 741, 687, 548, 501.

Benzyl-2,5-di(4-octyloxybenzoyloxy)benzoate (9)

Reagents: Benzyl-2,5-dihydroxybenzoate (3.91 g, 16 mmol), 4-octyloxybenzoic acid (8 g, 32 mmol), EDAC (2.48 g, 32 mmol).

Yield: White powder, 7.86 g, 11 mmol, 69 %.

^{1}H NMR ($CDCl_3$) δ (ppm): 0.87 – 0.90 (m, 6H, CH_3-), 1.21-1.39 (m, 14H, -CH_2-), 1.40 – 1.58 (m, 6H, -CH_2-), 1.72 – 1.90 (m, 4H, -CH_2-), 4.04 (t, 4H, J – 6.2 Hz, CH_2O-), 5.18 (s, 2H, CH_2Ar), 6.94 (m, AA′ XX′ 4H,

ArH), 7.21 (m, 5H, ArH), 7.25 (d, 4H, J= 8.7 Hz, $ArH_{\mathbf{c}}$), 7.45 (dd, 1H, J = 8.8, 2.9 Hz, $ArH_{\mathbf{b}}$), 7.89 (d, 1H, J = 2.9 Hz, $ArH_{\mathbf{a}}$), 8.09 (m, AA′ XX′, 4H, ArH).

IR (FTR) ν (cm^{-1}): 2924 (CH), 2855, 2561, 1728, 1604 (C=O), 1581, 1512, 1458 (Ar), 1373, 1249, 1172, 1126, 1072, 1003, 972, 841, 548, 501.

8.2.2.3 2,5-Di(4-alkyloxybenzoyloxy)benzoic acids (10-15)

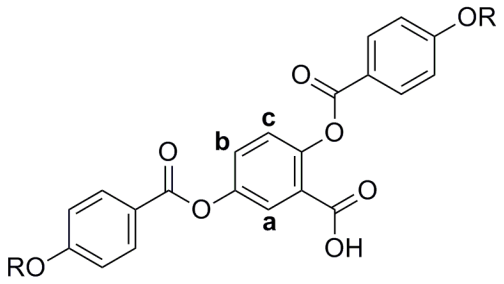

Figure 8.6: 2,5-Di(4-alkyloxybenzoyloxy)benzoic acids (**10-15**) R= C_3H_7 to C_8H_{17}

A solution of benzyl-2,5-di(4-alkyloxybenzoyloxy)benzoate in DCM (100 mL) was stirred at room temperature. 10% palladium on carbon (~0.2 g) was added and the reaction mixture degassed three times with hydrogen to activate the carbon. The reaction mixture was then left under a hydrogen atmosphere for 24 h. The reaction was monitored by TLC and on completion was filtered through a celite pad and recrystallised from ethanol.

2,5-Di(4-propyloxybenzoyloxy)benzoic acid (10)

Reagents: Benzyl-2,5-di(4-propyloxybenzoyloxy)benzoate (5 g, 8.8 mmol)

Yield: White powder, 4.12g, 8.6 mmol, 97 %.

^{1}H NMR ($CDCl_3$) δ (ppm): 1.02-1.10 (m, 6H, -CH_3), 1.78-1.94 (m, 4H, -CH_2-), 4.01 (m,4H, -CH_2O-), 6.97 (m, AA′ XX′, 4H, ArH), 7.28 (d, 1H, J = 8.8 Hz, Ar$H_{\mathbf{c}}$), 7.47 (dd, 1H, J = 2.5, 8.8 Hz, Ar$H_{\mathbf{b}}$), 7.94 (d, 1H, J = 2.9 Hz, Ar$H_{\mathbf{a}}$), 8.06 – 8.17 (m AA′ XX′, 4H, ArH).

IR (FTR) ν (cm^{-1}): 3070, 2931 (CH), 2877 (OH), 2654, 2546, 2324, 2222, 2083, 1728 (C=O), 1697, 1605, 1512 (Ar), 1389, 1250, 1165, 1065, 972.12, 926, 841, 756, 687, 633, 501.

2,5-Di(4-butyloxybenzoyloxy)benzoic acid (11)

Reagents: Benzyl-2,5-di(4-butyloxybenzoyloxy)benzoate (19.00 g, 33 mmol).

Yield: 13.87g, 27.4 mmol, 83 %.

^{1}H NMR ($CDCl_3$) δ (ppm): 0.99 (m, 6H, -CH_3), 1.50 (m, 4H, -CH_2), 1.81 (m, 4H, -CH_2-), 4.05 (t, 4H, J=6.5 Hz, -CH_2-O), 6.98 (m, AA′ XX′, 4H, ArH), 7.06 (d, 1H, J= 9 Hz, ArH_c), 7.36 (dd, 1H,J= 2.8 Hz, 9 Hz ArH_b), 7.74 (d, 1H, J= 2.7 Hz, ArH_a), 8.11 (m, AA′ XX′, 4H, ArH).

IR (FTR) ν (cm^{-1}): 3734, 3502, 3263, 3078, 2939 (OH), 2870 (CH), 2738, 2607, 2530, 2322, 2098, 1921, 1735, 1674 (C=O), 1604 (Ar), 1442 (CH), 1150, 1126, 1064, 1002, 848, 763, 640, 555.

2,5-Di(4-pentyloxybenzoyloxy)benzoic acid (12)

Reagents: Benzyl-2,5-di(4-pentyloxybenzoyloxy)benzoate (5 g, 8 mmol).

Yield: White powder, 4.17g, 7.8 mmol, 98 %.

^{1}H NMR ($CDCl_3$) δ (ppm): 0.77-0.99 (m, 6H, CH_3-), 1.32 – 1.53 (m, 8H, -CH_2-), 1.75 -1.92 (m, 4H, -CH_2-), 4.04 (m, 4H, CH_2O-), 6.97 (m, AA′ XX′, 4H, ArH), 7.30 (d, 1H, J = 8.8 Hz, ArH_c), 7.48 (dd, 1H, J = 2.9, 8.8 Hz, ArH_b), 7.94 (d, 1H, J = 2.9 Hz, ArH_a), 8.10 – 8.17 (m AA′ XX′, 4H, ArH).

IR (FTR) ν (cm^{-1}): 2932 (CH), 2862, 2561, 1690 (C=O), 1605, 1582 (Ar), 1512, 1373, 1250 (CH), 1165, 1126, 1072, 988, 841, 756, 687, 501.

2,5-Di(4-hexyloxybenzoyloxy)benzoic acid (13)

Reagents: Benzyl-2,5-di(4-hexyloxybenzoyloxy)benzoate (5.8 g, 8.9 mmol).

Yield: White powder, 4.96g, 8.82 mmol, 99 %.

^{1}H NMR ($CDCl_3$) δ (ppm): 0.81 – 0.97 (m, 6H, -CH_3), 1.27 - 1.40 (m, 6H, -CH_2-), 1.42 - 1.54 (m, 4H, -CH_2-), 1.70 – 1.95 (m, 4H, -CH_2-), 4.04 (m, 4H, CH_2O-), 6.96 (m, AA′ XX′, ArH), 7.30 (d, 1H, J = 8.8 Hz, ArH_c), 7.48 (dd, J = 2.9, 8.8 Hz, 1H, ArH_b), 7.93 (d, 1H, J = 2.9, ArH_a), 8.13 (m, AA′ XX′, ArH).

IR (FTR) ν (cm^{-1}): 2932 (OH), 2862 (CH), 2654, 2576, 1690 (C=O), 1605 (Ar), 1582, 1512, 1458, 1420, 1373, 1250, 1173, 1126, 1072, 1003, 926, 841, 756, 548, 501.

2,5-Di(4-heptyloxybenzoyloxy)benzoic acid (14)

Reagents: Benzyl-2,5-di(4-heptyloxybenzoyloxy)benzoate (30 g, 46.4 mmol).

Yield: White powder, 19.7g, 33.4 mmol, 72 %.

^{1}H NMR ($CDCl_3$) δ (ppm): 0.99 (m, 26H, -CH_3), 4.05 (t, 4H, J=8 Hz, -CH_2-O), 7.5 (m, AA′ XX′, 4H, ArH), 7.35 (d, 1H, J= 9 Hz, Ar$H_{\mathbf{c}}$), 7.38 (dd, 1H,J= 3 Hz, 9 Hz, Ar$H_{\mathbf{b}}$), 7.73 (d, 1H, J= 3 Hz, Ar$H_{\mathbf{a}}$), 8.11 (m, AA′ XX′, 4H, ArH), 10.33 (br s, 1H, OH)

IR (FTR) ν (cm^{-1}): 3880, 3795, 3741, 3518, 3448, 3208 (OH), 3078, 2916, (CH). 2854, 2592, 2322, 2206, 2083, 1990, 19805, 1728, 1666 (C=O), 1597, 1581, 1442, 1150, 1064, 1002, 848, 763, 648, 555.

2,5-Di(4-octyloxybenzoyloxy)benzoic acid (15)

Reagents: Benzyl-2,5-di(4-octyloxybenzoyloxy)benzoate (4.17 g, 5.9 mmol).

Yield: White powder, 3.55g, 5.7 mmol 97 %.

^{1}H NMR ($CDCl_3$) δ (ppm): 0.87 – 0.90 (m, 6H, CH_3-), 1.21-1.39 (m, 14H, -CH_2-), 1.40 – 1.58 (m, 4H, -CH_2-), 1.72 – 1.90 (m, 4H, -CH_2-), 4.04 (t, 4H, J – 6.2 Hz, CH_2O-), 6.94 (m, AA′ XX′, 4H, ArH), 7.25 (d, 1H, J= 8.7 Hz, Ar$H_{\mathbf{c}}$), 7.45 (dd, 1H, J = 8.8, 2.9 Hz, Ar$H_{\mathbf{b}}$), 7.89 (d, 1H, J = 2.9 Hz, Ar$H_{\mathbf{a}}$), 8.09 (m, AA′ XX′, 4H, ArH).

IR (FTR) ν (cm^{-1}): 2924 (OH), 2855 (CH), 2654, 2561, 1728, 1690, 1605 (C=O), 1582, 1519, 1458, 1373, 1250, 1173, 1126, 1072, 1010, 964, 841, 756, 648, 501.

8.2.2.4 (4-Acryloylbutyl)-2,5-di(4-propyloxybenzyloxy)benzoate (M2)

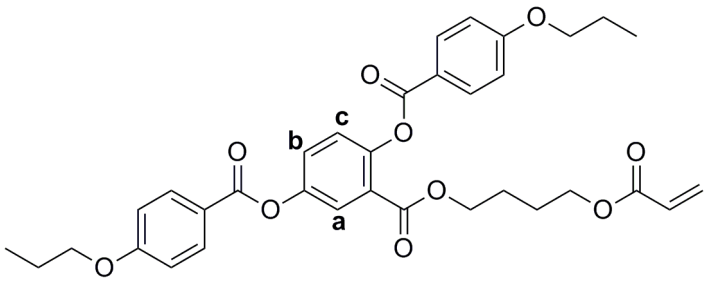

Figure 8.7: (4-Acryloylbutyl)-2,5-di(4-propyloxybenzyloxy)benzoate (**M2**).

A solution of 2,5-di(4-propyloxybenzoyloxy)benzoic acid (2 g, 4.17 mmol), 4-hydroxybutylacrylate (0.6 g, 4.17 mmol), EDAC (0.81 g, 4.17 mmol) and a catalytic quantity of DMAP in DCM (50 mL) was stirred at room temperature for 48 hr. The reaction was monitored by TLC. On completion, the solvent was removed *in vacuo* and the resultant product was purified by flash column chromatography in DCM.

Yield: White powder, 2.34g, 3.87 mmol, 92 %.

^{1}H NMR ($CDCl_3$) δ (ppm): 0.98 – 1.11 (m, 6H, –CH_3), 1.54 – 1.65 (m, 4H, -CH_2-), 1.81 – 1.90 (m, 4H, -CH_2-), 3.96 – 4.03 (m, 6H, CH_2O-), 4.18 – 4.21 (m, 2H, CH_2O-), 5.81 (dd, 1H, J = 1.5, 10.4 Hz, CH=), 6.11 (dd, 1H, J = 10.4, 17.3 Hz, CH=), 6.34 (dd, J = 1.5, 17.3 Hz, CH=), 6.99 (m, AA′ XX′, 4H, ArH), 7.27 (d, 1H, J= 8.7 Hz, Ar$H_{\mathbf{c}}$), 7.44 (dd,1H, J = 2.9, 8.7Hz, Ar$H_{\mathbf{b}}$), 7.87 (d, 1H, J = 2.9 Hz, Ar$H_{\mathbf{a}}$), 8.15 (m, AA′ XX′, 4H, ArH).

^{13}C NMR ($CDCl_3$) δ (ppm): 10.63, 22.42, 25.24 (CH_3CH_2-), 63.95, 65.02, 69.83 (CH_2O-), 77.11 (t, $CDCl_3$), 114.47, 125.18 (CH=), 127.62, 128.52, 130.69, 132.52, 148.43 (ArC), 163.55, 163.74, 164.15, 166.39 (C=O).

DSC: g -14 °C N 61°C I

MS (ESI): $C_{34}H_{37}O_{10}$ calculated [M + Na] *m/z* 627.2201, found 627.2169.

EA (CHN): calculated C 67.54 %, H 6.00 % found C 67.55 %, H 6.04 %.

IR (FTR) ν (cm^{-1}): 3071, 2940 (CH), 2878, 1728, 1605 (C=O), 1474 (Ar), 1473, 1242, 1165, 1056, 972, 756, 687, 640, 548, 501.

8.2.2.5 (4-Acryloylbutyl)-2,5-di(4-butyloxybenzyloxy)benzoate (M3)

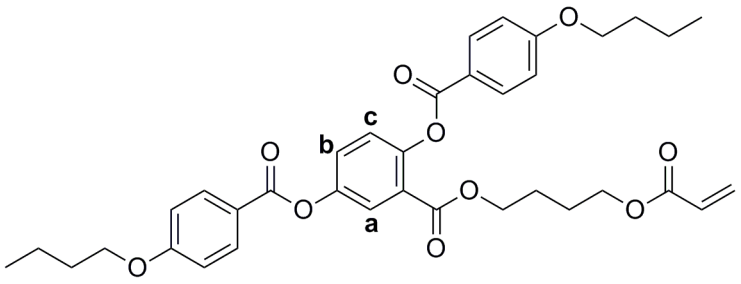

Figure 8.8: (4-Acryloylbutyl)-2,5-di(4-butyloxybenzyloxy)benzoate (**M3**)

A solution of 2,5-di(4-butyloxybenzoyloxy)benzoic acid (5g, 9.88 mmol), 4-hydroxybutylacrylate (1.284g. 9.88 mmol), EDAC (1.533g 9.88mmol) and DMAP (0.08 g, 0.6 mmol) in DCM (200 mL) was stirred at RT for 48 hr. The reaction was monitored by TLC. On completion, the solvent was removed *in vacuo* and the resultant product was purified by flash column chromatography in DCM.

Yield: White powder, 4.56 g, 7.2 mmol, 73 %.

^{1}H NMR ($CDCl_3$) δ (ppm): 0.99 (m, 6H, CH_3-), 1.61 (m, 4H, -CH_2-), 1.81 (m, 4H, -CH_2-), 4.05 (m, 6H, -CH_2O-), 4.20 (t, 2H, J=6.2 Hz, CH_2O-), 5.79 (dd, 1H, J=10.4, 1.4, CH=), 6.07 (dd, 1H, J=17.3, 10.4 Hz, CH=), 6.36 (dd, 1H, J=17.3, 1.4 Hz, CH=), 6.97 (m AA′ XX′, 4H, ArH), 7.29 (d, 1H, J=8.7 Hz, $ArH_{\mathbf{c}}$), 7.45 (dd, 1H, J=8.7, 2.9 Hz, $ArH_{\mathbf{b}}$), 7.88 (d, 1H, J=2.9 Hz, $ArH_{\mathbf{a}}$), 8.15 (m AA′ XX′, 4H, ArH).

^{13}C NMR ($CDCl_3$) δ (ppm): 13.92, 19.28, 25.21, 31.21 (CH_3CH_2-), 64.00, 64.98, 68.11, 68.13 (CH_2O-), 77.10 (t, $CDCl_3$) 114.45, 121.08, 121.39 (CH=), 124.85, 125.13, 127.33, 128.48, 130.79, 132.49, 132.51 (ArC), 148.19, 148.45, 163.75, 163.84, 164.14, 164.74, 164.96(C=O).

DSC: Cr 42 °C N 82 °C I

MS (ESI): $C_{36}H_{40}O_{10}$ calculated [M + Na] *m/z* 655.2514, found 655.2479.

EA (CHN): calculated C 68.34 %, H 6.37 % found C 68.30 %, H 6.26 %.

IR (FTR) ν (cm^{-1}): 2940 (CH), 2870, 1728, 1605 (C=O), 1474 (Ar), 1373, 1242, 1157, 1126, 1065, 972, 756, 687, 640, 548, 501.

8.2.2.6 (4-Acryloylbutyl)-2,5-di(4-pentyloxybenzyloxy)benzoate (M4)

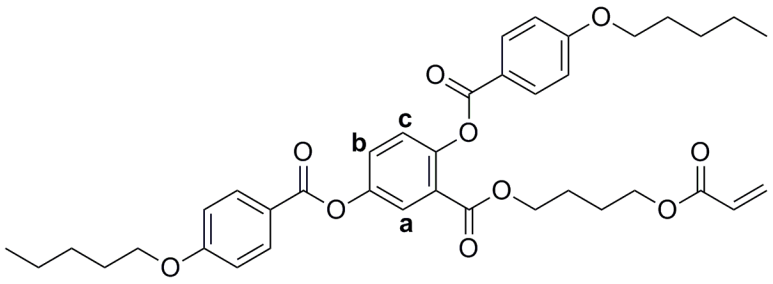

Figure 8.9: (4-Acryloylbutyl)-2,5-di(4-pentyloxybenzyloxy)benzoate (**M4**)

A solution of 2,5-di(4-pentyloxybenzoyloxy)benzoic acid (2 g, 3.74 mmol), 4-hydroxybutylacrylate (0.54 g, 3.74 mmol), EDAC (0.72 g, 3.74 mmol) and DMAP (0.08 g, 0.6 mmol) in DCM (50 mL) was stirred at room temperature for 48 hr. The reaction was monitored by TLC. On completion, the solvent was removed *in vacuo* and the resultant product was purified by flash column chromatography in DCM.

Yield: White powder, 2.16g, 3.27 mmol, 87 %.

^{1}H NMR ($CDCl_3$) δ (ppm): 0.93 – 0.96 (m, 6H, $–CH_3$), 1.39 – 1.62 (m, 11H, $-CH_2-$), 1.81 – 1.84 (m, 4H, $-CH_2-$), 3.00 – 4.06 (m, 6H, CH_2O-), 4.20 (t, 2H, J = 6.2 Hz, CH_2O-), 5.80 (dd, 1H, J = 1.4, 10.5 Hz, CH=), 6.08 (dd, 1H, J = 10.4, 17.3 Hz, CH=), 6.38 (dd, J 1.4, 17.3 Hz, CH=), 6.98 (m, AA′ XX′, 4H, ArH), 7.27 (d, 1H, J= 8.7 Hz, $ArH_{\mathbf{c}}$), 7.45 (dd,1H, J = 2.9, 8.7 Hz, $ArH_{\mathbf{b}}$), 7.88 (d, 1H, J = 2.9 Hz, $ArH_{\mathbf{a}}$), 8.15 (m, AA′ XX′, ArH).

^{13}C NMR ($CDCl_3$) δ (ppm): 14.11, 22.53, 24.95, 25.21, 27.80, 28.21, 28.87 (CH_3CH_2-), 64.00, 64.47, 64.98, 67.53, 68.44 (CH_2O-), 77.11 (t, $CDCl_3$) 114.45, 115.01, 121.05, 121.38, 124.85, 125.13, 127.33 (CH=), 128.48, 130.79, 132.30, 132.49, 132.52 (ArC), 148.19, 148.43, 164.84, 164.15, 164.70, 165.03, 166.22 (C=O).

DSC: Cr 34 °C N 58 °C I

MS (ESI): $C_{38}H_{44}O_{10}$ calculated [M + Na] *m/z* 683.2827, found 683.2801.

EA (CHN): calculated C 69.07 %, H 6.71 %, found C 69.06 %, H 6.80 %.

IR (FTR) ν (cm^{-1}): 3078, 2932 (CH), 1721, 1605 (C=O), 1582, 1512 (Ar), 1466, 1412, 1373, 1242, 1165, 1065, 980, 756, 687, 548.

8.2.2.7 (4-Acryloylbutyl)-2,5-di(4-hexyloxybenzyloxy)benzoate (M5)

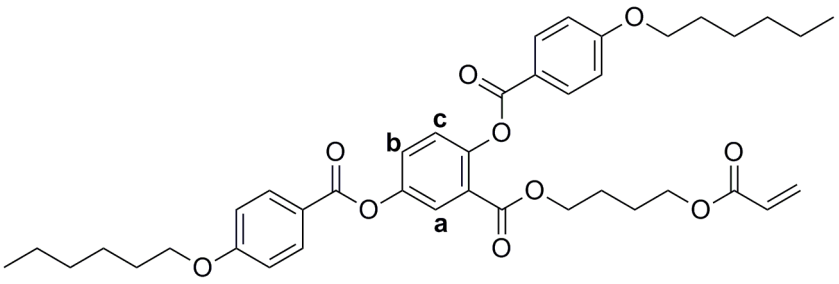

Figure 8.10: (4-Acryloylbutyl)-2,5-di(4-hexyloxybenzyloxy)benzoate (**M5**)

A solution of 2,5-di(4-hexyloxybenzoyloxy)benzoic acid (2 g, 3.55 mmol), 4-hydroxybutylacrylate (0.51 g, 3.55 mmol), EDAC (0.68 g, 3.55 mmol) and DMAP (0.08 g, 0.6 mmol) in DCM (50 mL) was stirred at RT for 48 hr. The reaction was monitored by TLC. On completion, the solvent was removed *in vacuo* and the resultant product was purified by flash column chromatography in DCM.

Yield: White powder, 2.33g, 3.38 mmol, 95 %.

^{1}H NMR ($CDCl_3$) δ (ppm): 0.91 (m, 6H, CH_3-), 1.26 – 1.43 (m, 6H, -CH_2-), 1.41-1.70 (m, 10H, -CH_2-), 1.73-1.93 (m, 4H, -CH_2-), 3.96 – 4.12 (m, 6H, -CH_2O-), 4.20 (t, 2H, J=6.2 Hz, CH_2O-), 5.97 (dd, 1H, J=1.5, 10.4 Hz, CH=), 6.07 (dd, 1H, J=10.4, 17.3 Hz, CH=), 6.36 (dd, 1H, J= 1.5, 17.3 Hz, CH=), 6.97 (m, AA′ XX′, 4H, ArH), 7.26 (d, 1H, J=8.7 Hz, Ar$H_{\mathbf{c}}$), 7.45 (dd, 1H, J= 2.9, 8.7 Hz, Ar$H_{\mathbf{b}}$), 7.88 (d, 1H, J = 2.9 Hz, Ar$H_{\mathbf{a}}$), 8.15 (m, AA′ XX′, 4H, ArH).

DSC: Cr 36 °C N 81 °C I

MS (ESI): $C_{40}H_{48}O_{10}$ calculated [M + Na] *m/z* 711.3140, found 711.3118.

EA (CHN): calculated C 69.75 %, H 7.02 % found C 69.69 %, H 7.06 %.

IR (FTR) ν (cm^{-1}): 3078, 2932 (CH), 2862, 1721, 1605 (C=O), 1582, 1512 (Ar), 1266, 1412, 1373, 1242, 1165, 1065, 980, 841, 756, 687, 548.

8.2.2.8 (4-Acryloylbutyl)-2,5-di(4-heptyloxybenzyloxy)benzoate (M6)

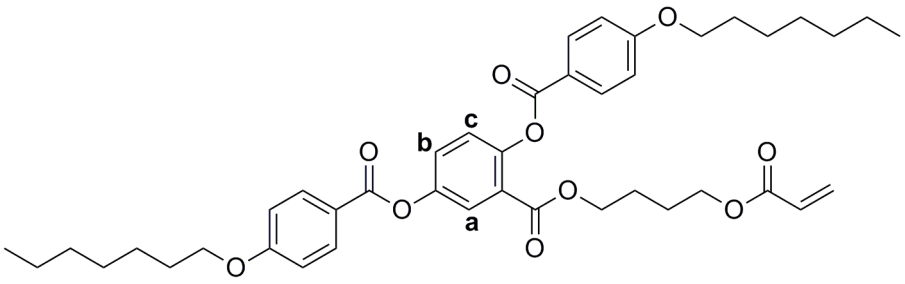

Figure 8.11: (4-Acryloylbutyl)-2,5-di(4-heptyloxybenzyloxy)benzoate (**M6**)

A solution of 2,5-di(4-heptyloxybenzoyloxy)benzoic acid (5g, 8.46 mmol), 4-hydroxybutylacrylate (1.103g. 8.46 mmol), EDAC (1.313g, 8.46 mmol) and DMAP (0.08 g, 0.6 mmol) in DCM (200 mL) was stirred at room temperature for 48 hr. The reaction was monitored by TLC. On completion, the solvent was removed *in vacuo* and the resultant product was purified by flash column chromatography in DCM.

Yield: White waxy solid, 6.81 g, 9.5 mmol, 89 %.

^{1}H NMR ($CDCl_3$) δ (ppm): 0.90 (m, 6H, CH_3-), 1.44 (m, 16H, -CH_2-), 1.61 (m, 4H, -CH_2-), 1.80 (m, 4H, -CH_2-), 4.03 (m, 6H, -CH_2O-), 4.20 (t, 2H, J=6.2 Hz, CH_2O-), 5.80 (dd, 1H, J=10.4, 1.4 Hz, CH=), 6.07 (dd, 1H, J=17.3, 10.4 Hz, CH=), 6.36 (dd, 1H, J=17.3, 1.5 Hz, CH=), 6.97 (m, AA′ XX′, 4H, ArH), 7.26 (d, 1H, J= 8.7 Hz, Ar$H_{\mathbf{c}}$), 7.45 (dd, 1H, J=8.7, 2.9 Hz, Ar$H_{\mathbf{b}}$), 7.88 (d, 1H, J=2.9 Hz, Ar$H_{\mathbf{a}}$), 8.15 (m, AA′ XX′, 4H, ArH).

^{13}C NMR ($CDCl_3$) δ (ppm): 14.19, 22.70, 25.21, 26.03, 29.13, 29.18, 31.85 (-CH_3CH_2-), 63.99, 64.97, 68.43 (CH_2O-), 77.10 (t, $CDCl_3$), 114.45, 114.47 (ArC), 121.06, 121.39, 124.85, 125.08 125.12, 127.32, 128.49 (CH=), 130.77, 132.48, 132.51 (ArC), 148.19, 148.43, 163.75, 163.85, 163.13, 164.68, 165.02, 165.20(C=O).

DSC: Cr 21 °C N 61 °C I

MS (ESI): $C_{42}H_{52}O_{10}$ calculated [M + Na] *m/z* 739.3453, found 739.3438.

EA (CHN): calculated C 70.37 %, H 7.31 % found C 70.36 %, H 7.39 %.

IR (FTR) ν (cm^{-1}): 3071, 3009, 2939 (CH), 2870, 1728, 1605 (C=O), 1474 (Ar), 1373, 1242, 1157, 1065, 972, 756, 687, 640, 548, 501.

8.2.2.9 (4-Acryloylbutyl)-2,5-di(4-Octyloxybenzyloxy)benzoate (M7)

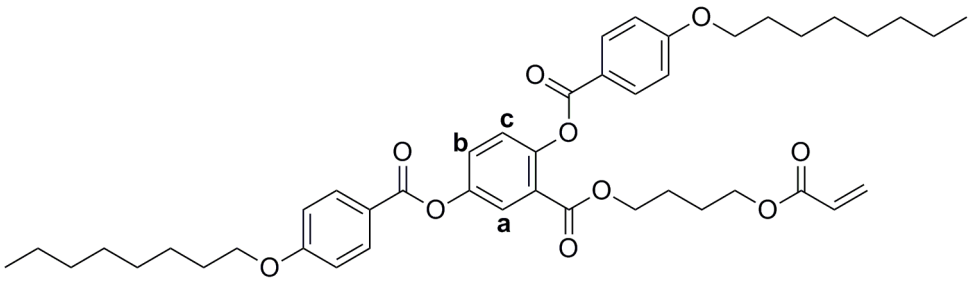

Figure 8.12: (4-Acryloylbutyl)-2,5-di(4-octyloxybenzyloxy)benzoate (**M7**)

A solution of 2,5-di(4-octyloxybenzoyloxy)benzoic acid (2 g, 5.23 mmol), 4-hydroxybutylacrylate (0.47 g, 3.23 mmol), EDAC (0.62 g, 3.23 mmol) and DMAP (0.08 g, 0.6 mmol) in DCM (50 mL) was stirred at RT for 48 hr. The reaction was monitored by TLC. On completion, the solvent was removed *in vacuo* and the resultant product was purified by flash column chromatography in DCM.

Yield: White waxy solid, 1.56g, 2.09 mmol, 65 %.

^{1}H NMR ($CDCl_3$) δ (ppm): 0.89 (t, 6H, J = 6.9 Hz, -CH_3), 1.19-1.41 (m, 14H, -CH_2-), 1.51 – 1.73 (m, 8H, -CH_2-), 1.73 – 1.90 (m, 4H, -CH_2-), 3.93 – 4.12 (m, 6H, -CH_2O-), 4.20 (t, 2H, J = 6.2 Hz, CH_2O-), 5.79 (dd, 1H, J = 1.5, 10.4 Hz, CH=), 6.07 (dd, 1H, J = 10.5, 17.3 Hz, CH=), 6.36 (dd, 1H , J = 1.5, 17.3 CH=), 6.97 (m, AA′ XX′, 4H, ArH), 7.26 (d, 1H, J = 8.7 Hz, ArH_c), 7.45 (dd, 1H , J = 2.9, 8.7 Hz, ArH_b), 7.88 (d, 1H, J = 2.9 Hz, ArH_a), 8.15 (m, AA′ XX′, 4H, ArH).

DSC: Cr 23 °C N 69 °C I

MS (ESI): $C_{44}H_{56}O_{10}$ calculated [M + Na] *m/z* 767.3766, found 767.3730.

EA (CHN): calculated C 70.94 %, H 7.58 % found C 70.88 %, H 7.17 %.

IR (FTR) ν (cm^{-1}): 2924 (CH), 2855, 1721, 1605 (C=O), 1582, 1512 (Ar), 1466, 1420, 1373, 1242, 1165, 1065, 1011, 841, 756, 633, 548, 501.

8.2.2.10 11-Acryloylundecan-1-ol (16)[136]

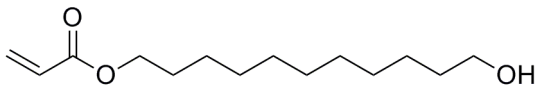

Figure 8.13: 11-Acryloylundecan-1-ol

Sodium acrylate (15.05g, 160 mmol), bromoundecanol (10g, 40 mmol), tetrabutylammonium bromide (3.42g, 10mmol) and DBPC (catalytic) were placed in a 100mL round bottom flask and chloroform (20 mL) and distilled water (40 mL) were added. The mixture was refluxed with vigorous stirring at 110 °C for 3 days. The chloroform layer was then washed 4x with NaOH solution and 4x with distilled water. The solution was dried over $MgSO_4$ and the solvent removed *in vacuo* and the crude product was used as received in further reactions.

Yield: Clear off white oil, 7.46 g, 30.8 mmol, 77 %.

^{1}H NMR ($CDCl_3$) δ (ppm): 1.21 (br m, 14H, -CH_2-), 1.48 (m, 2H, -CH_2-), 1.59 (m, 2H, -CH_2-), 3.54 (t, 2H, J=6.7 Hz, CH_2O-), 4.07 (t, 2H, J=6.7 Hz, CH_2O-), 5.74 (dd, 1H, J=10.4, 17.3 Hz, CH=), 6.05 (1H,dd, J=10.4, 17.3 Hz, CH=), 6.32 (1H, dd, J=17.3, 1.5 Hz, CH=).

MS (ESI): $C_{14}H_{26}O_3$ calculated [M + Na] *m/z* 265.1774, found 265.1772.

EA (CHN): calculated C 69.38 %, H 10.81 % found C 66.38 %, H 10.35 %.

8.2.2.11 (11-Acryloylundecyl)-2,5-di(4-butyloxybenzoyloxy)benzoate (M8)

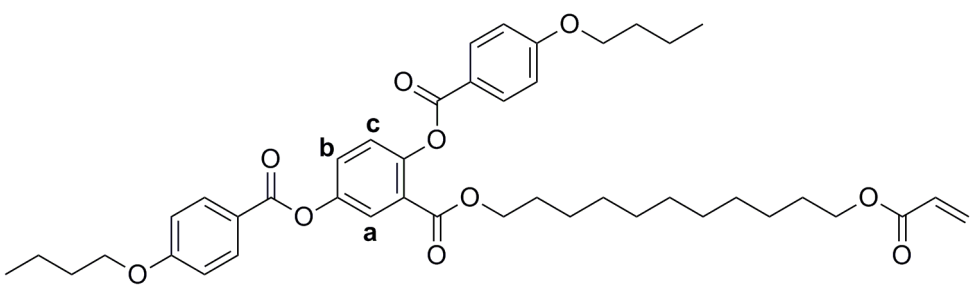

Figure 8.14: (11-Acryloylundecyl)-2,5-di(4-butyloxybenzoyloxy)benzoate (**M8**)

A solution of 2,5-di(4-butyloxybenzoyloxy)benzoic acid (1.5g, 2.96 mmol), 11-acryoylundecan-1-ol (0.718g, 2.96 mmol), EDAC (0.460g, 2.96 mmol) and a spatula tip of DMAP in DCM (50 mL) was stirred at RT for 48 hr. The reaction was monitored by TLC. On completion, the solvent was removed *in vacuo* and the resultant product was purified by flash column chromatography in DCM.

Yield: Cream coloured waxy solid, 1.49g, 2.04 mmol, 69 %.

^{1}H NMR ($CDCl_3$) δ (ppm): 0.99 (t, 6H, J= 7.4 Hz, CH_3-), 1.21 (m, 14H, -CH_2-), 1.52 (m, 6H, -CH_2), 1.62 (m, 4H, -CH_2-), 1.81 (m, 4H, -CH_2-), 4.05 (m, 4H, CH_2O-), 4.14 (m, 4H, CH_2O-), 5.81 (dd, 1H J=10.4, 1.5 Hz, CH=), 6.11 (dd, 1H, J=17.3, 10.4 Hz, CH=), 6.39 (dd, 1H, 17.3, 1.5 Hz, CH=), 6.97 (m AA′ XX′, 4H, ArH), 7.25 (d, 1H, J=8.7 Hz, ArH_c), 7.44 (dd, 1H, J=8.7, 2.9 Hz, ArH_b), 7.88 (d, 1H, J= 2.9 Hz, ArH_a), 8.15 (m AA′ XX′, 4H, ArH).

^{13}C NMR ($CDCl_3$) δ (ppm): 13.92, 19.29, 26.01, 28.69, 29.27, 29.34, 29.56, 31.21 (-CH_3CH_2-), 64.80, 65.75, 68.08, 68.13, 69.58 (CH_2O-), 77.11 (t, $CDCl_3$) 114.38, 121.10, 121.52, 125.09, 127.17, 128.48, 128.73 (CH=), 130.53, 132.47, 132.54 (ArC), 148.39, 163.67, 164.24, 165.03 (C=O).

DSC: g -23 °C N 65 °C I

MS (ESI): $C_{43}H_{54}O_{10}$ calculated [M + Na] *m/z* 753.3609, found 753.3591.

EA (CHN): calculated C 70.66 %, H 7.45 % found C 70.30 %, H 7.43 %.

IR (FTR) ν (cm^{-1}): 2924 (CH), 2855, 1728, 1605 (C=O), 1474 (Ar), 1373, 1242, 1165, 1126, 1065, 964, 764, 687, 640, 556, 501.

8.2.2.12 (11-Acryloylundecyl)-2,5-di(4-heptlyloxybenzoyloxy)benzoate (M9)

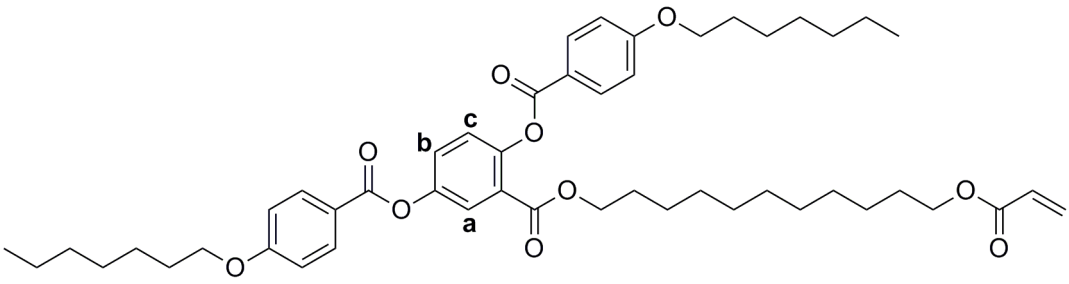

Figure 8.15: (11-Acryloylundecyl)-2,5-di(4-heptlyloxybenzoyloxy)benzoate (**M9**)

A solution of 2,5-di(4-heptyloxybenzoyloxy)benzoic acid (1.5g, 2.54 mmol), 11-acryoylundecan-1-ol (7) (0.615g, 2.54 mmol), EDAC (0.394g, 2.54 mmol) and a spatula tip of DMAP in 50 mL of DCM at stirred at RT for 48 hr. The reaction was monitored by TLC. On completion, the solvent was removed *in vacuo* and the resultant product was purified by flash column chromatography in DCM.

Yield: Cream coloured waxy solid, 1.47g, 1.80 mmol, 71 %.

^{1}H NMR ($CDCl_3$) δ (ppm): 0.90 (t, 6H, J=6.9Hz, CH_3-), 1.31(m, 20H, -CH_2-), 1.65 (m, 6H, -CH_2-), 1.82 (m, 4H, -CH_2-), 4.04 (m, 4H, CH_2O-), 4.14 (m, 4H, CH_2O-), 5.80 (dd, 1H, J=10.4, 1.5 Hz, CH=), 6.11 (dd, 1H, 17.3, 10.4 Hz, CH=), 6.39 (dd, 1H, J= 17.4, 1.5 Hz, CH=), 6.96 (m, AA′ XX′, 4H, ArH), 7.25 (d, 1H, J=8.7 Hz, ArH_c), 7.44 (dd, 1H, J= 8.7, 2.9 Hz, ArH_b), 7.88 (d, 1H, J= 2.9 Hz, ArH_a), 8.15 (m, AA′ XX′, 4H, ArH).

^{13}C NMR ($CDCl_3$) δ (ppm): 14.19, 22.70, 25.90, 26.04, 28.47, 28.70, 29.13, 29.18, 29.27, 29.34, 29.48, 29.56, 31.86 (-CH_3CH_2-), 64.79, 65.74, 68.40, 68.45 (CH_2O-), 77.14 (t, $CDCl_3$), 114.39, 121.10, 121.52 (CH=), 125.08, 127.17, 128.73, 130.52, 132.52, 132.47, 132.54 (ArH), 148.18, 163.66, 163.83, 164.68, 165.02, 165.42 (C=O).

DSC: Cr -12 °C N 57 °C I

MS (ESI): $C_{49}H_{66}O_{10}$ calculated [M + Na] *m/z* 837.4548, found 837.4630.

EA (CHN): calculated C 72.21 %, H 8.16 % found C 71.78 %, H 8.09 %.

IR (FTR) ν (cm^{-1}): 2924 (CH), 2855, 1728, 1605 (C=O), 1512 (Ar), 1466, 1373, 1242, 1165, 1080, 972, 841, 972, 841, 756, 640, 548.

8.3 SYNTHESIS OF NEMATIC POLYMERS BY SOLUTION POLYMERISATION

Below is a technique which has been used to synthesise nematic polymers of **P1** – **P9**, synthesised from monomers **M1** – **M9**, respectively. The exact reagents and conditions used in each case are specified in Table 8.1.

Sealed vessels (Quick-fit Pyrex glass test tubes with rubber seals) of a solution of monomer (100 mg monomer in 2 mL of solvent) and thermal radical initiator AIBN (2 wt% relative to monomer) were purged thoroughly by bubbling with nitrogen for a period of 30 minutes before being heated to 65 °C with constant and vigorous stirring for 24 hours. After the polymerisation had been allowed to react for 24 hours, the mixture was allowed to cool to room temperature and then the polymer was precipitated into methanol. The methanol was removed by centrifugation (10 minutes at 2000 rpm) as this sedimented the polymer and allowed the methanol to be decanted. To purify the polymer it was dissolved in THF and re-precipitated into methanol, removing any soluble impurities. The polymer was then dried in a vacuum oven for analysis by methods such as GPC, DSC, ^{1}H NMR and IR.

Typical characterisation data for polymer **P1:**

^{1}H NMR ($CDCl_3$) δ (ppm): 1.27 – 1.80 (br m, 12H, -CH_3CH_2-, CH_2(pb), CH_2(pb)), 2.28 (br m, 2H, -CH_2-), 4.01 (br m, 4H –CH_2O-), 6.93 (br m, 2H, ArH), 7.31 (br m, 2H, ArH), 7.69 (br m, 2H, ArH), 8.08 (br m, 2H, ArH).

DSC: g 27 °C N 101 °C I

Typical characterisation data for polymer **P2:**

^{1}H NMR ($CDCl_3$) δ (ppm): 0.95 (br m, 6H, -CH_3-), 1.44 – 1.95 (br m, 15H, -CH_2-, CH_2(pb), CH_2(pb)), 2.25 (br m, 2H, -CH_2-), 3.91 (br m, 8H, -CH_2O-), 6.85 (br m, 4H, ArH), 7.13 (br m, 1H, ArH), 7.34 (br m, 1H, ArH), 7.78 (br m, 1H, ArH), 8.02 (br m, 4H, ArH).

DSC: g 45 °C N 83 °C I

GPC: M_n: 441,000 g mol^{-1}

Polydispersity (M_w/M_n): 2.67

Typical characterisation data for polymer **P3:**

^{1}H NMR ($CDCl_3$) δ (ppm): 0.86 (br m, 6H, -CH_3-), 1.27 – 1.82 (br m, 15H, -CH_2-, CH_2(pb), CH_2(pb)), 2.06 (br m, 2H, -CH_2-), 3.98 (br m, 8H, -CH_2O-), 6.80 (br m, 4H, ArH), 7.08 (br m, 1H, ArH), 7.36 (br m, 1H, ArH), 7.74 (br m, 1H, ArH), 7.97 (br m, 4H, ArH).

DSC: g 31 °C N 59 °C I

GPC: M_n: 256,000 g mol^{-1}

Polydispersity (M_w/M_n): 7.91

Typical characterisation data for polymer **P4:**

^{1}H NMR ($CDCl_3$) δ (ppm): 0.97 (br m, 6H, -CH_3-), 1.45– 1.92 (br m, 18H, -CH_2-, CH_2(pb), CH_2(pb)), 2.21 (br m, 2H, -CH_2-), 4.05 (br m, 8H, -CH_2O-), 6.98 (br m, 4H, ArH), 7.25 (br m, 1H, ArH), 7.48(br m, 1H, ArH), 7.89 (br m, 1H, ArH), 8.14 (br m, 4H, ArH).

DSC: g 23 °C N 49 °C I

Typical characterisation data for polymer **P5:**

^{1}H NMR ($CDCl_3$) δ (ppm): 0.97 (br m, 6H, -CH_3-), 1.33 – 1.69 (br m, 20H, -CH_2-, CH_2(pb), CH_2(pb)), 4.09 (br m, 8H, -CH_2O-), 6.96 (br m, 4H, ArH), 7.31 (br m, 1H, ArH), 7.51 (br m, 1H, ArH), 7.94 (br m, 1H, ArH), 8.10 (br m, 4H, ArH).

DSC: g 27 °C N 82 °C I

Typical characterisation data for polymer **P6:**

^{1}H NMR ($CDCl_3$) δ (ppm): 0.90 (br m, 6H, -CH_3-), 1.18 – 1.58 (br m, 22H, -CH_2-, CH_2(pb), CH_2(pb)), 1.76 (br m, 6H, -CH_2-), 2.14 (br m, 2H, -CH_2-), 3.93 (br m, 8H, -CH_2O-), 6.85 (br m, 4H, ArH), 7.13 (br m, 1H, ArH), 7.48(br m, 1H, ArH), 7.78 (br m, 1H, ArH), 8.02 (br m, 4H, ArH).

DSC: g 28 °C N 70 °C I

GPC: M_n: 204,000 g mol^{-1}

Polydispersity (M_w/M_n): 2.16

Typical characterisation data for polymer **P7:**

^{1}H NMR ($CDCl_3$) δ (ppm): 0.94 (br m, 6H, -CH_3-), 1.33 – 1.84 (br m, 22H, -CH_2-, CH_2(pb), CH_2(pb)), 2.24 (br m, 2H, -CH_2-), 4.06 (br m, 8H, -CH_2O-), 6.98 (br m, 4H, ArH), 7.26 (br m, 1H, ArH), 7.45 (br m, 1H, ArH), 7.89 (br m, 1H, ArH), 8.16 (br m, 4H, ArH).

DSC: g 23 °C N 71 °C I

Typical characterisation data for polymer **P8:**

^{1}H NMR ($CDCl_3$) δ (ppm): 0.99 (br m, 6H, -CH_3-), 1.22 – 1.37 (br m, 14H, -CH_2-, CH_2(pb), CH_2(pb)), 1.53 (br m, 6H, -CH_2-), 2.28 (br m, 2H, -CH_2-), 4.15 (br m, 8H, -CH_2O-), 6.97 (br m, 4H, ArH), 7.31 (br m, 1H, ArH), 7.45 (br m, 1H, ArH), 7.90 (br m, 1H, ArH), 8.15 (br m, 4H, ArH).

DSC: g 15 °C N 78 °C I

GPC: M_n: 244,000 g mol^{-1}

Polydispersity (M_w/M_n): 2.25

Typical characterisation data for polymer **P9:**

^{1}H NMR ($CDCl_3$) δ (ppm): 0.9 (br m, 6H, -CH_3-), 1.21 – 1.71 (br m, 28H, -CH_2-, CH_2(pb), CH_2(pb)), 1.85 (br m, 6H, -CH_2-), 2.28 (br m, 2H, -CH_2-), 4.06 (br m, 8H, -CH_2O-), 6.99 (br m, 4H, ArH), 7.27 (br m, 1H, ArH), 7.46 (br m, 1H, ArH), 7.92 (br m, 1H, ArH), 8.18 (br m, 4H, ArH).

DSC: g -1 °C N 62 °C I

GPC: M_n: 550,000 g mol^{-1}

Polydispersity (M_w/M_n): 4.85

Table 8.1 gives the exact reagents and conditions used in each case to synthesise nematic polymers by solution polymerisation.

Table 8.1 : Summary of the solvents used to create nematic polymers by solution polymerisation.

Reaction	Polymer	Solvent/ initiator
S-P1-1	**P1**	THF/AIBN
S-P1-2	**P1**	THF/AIBN
S-P3-1	**P3**	THF/AIBN
S-P3-2	**P3**	THF/AIBN
S-P6-1	**P6**	THF/AIBN
S-P6-2	**P6**	THF/AIBN
S-P8-1	**P8**	THF/AIBN
S-P8-2	**P8**	THF/AIBN
S-P9-1	**P9**	THF/AIBN
S-P9-2	**P9**	THF/AIBN
S-P2-1	**P2**	THF/AIBN
S-P4-1	**P4**	THF/AIBN
S-P5-1	**P5**	THF/AIBN
S-P7-1	**P7**	THF/AIBN
S-P1-3	**P1**	DCM/AIBN
S-P3-3	**P3**	DCM/AIBN
S-P6-3	**P6**	DCM/AIBN
S-P8-3	**P8**	DCM/AIBN
S-P9-3	**P9**	DCM/AIBN
S-P2-2	**P2**	DCM/AIBN
S-P4-2	**P4**	DCM/AIBN
S-P5-2	**P5**	DCM/AIBN
S-P7-2	**P7**	DCM/AIBN

8.4 SYNTHESIS OF POLYMER PARTICLES BY DISPERSION POLYMERISATION

Below is an adapted technique from literature procedures[78, 79] which has been used to synthesise nematic polymer particles of **P1** – **P9**, synthesised from monomers **M1** – **M9**, respectively. The exact reagents and conditions used in each case, where different to below, are specified in Table 8.2 to Table 8.10.

A vessel sealed with a rubber septum containing a solution of monomer (100 mg) and the stabiliser PVP55 (polyvinylpyrrolidone with an average molecular weight of 55,000 g mol^{-1}) (15 wt % relative to monomer, 15 mg, 2.75 x 10^{-4} mmol) in EtOH (1 mL) was purged by gently bubbling N_2 through for a period of 30 mins. The vessel was kept in ice throughout this process to minimise solvent loss. This vessel was then heated to a reaction temperature of 73 °C with constant and vigorous stirring. The reaction vessel, stirrer size and stirring rate were kept constant across all experiments to minimise variables that may affect the resulting particles. A solution of the initiator AIBN (2 wt % relative to monomer, 2 mg, 0.012 mmol) in EtOH (1 mL) was purged in the same way as the previously mentioned reaction vessel and then brought to the same temperature. This was then injected through the rubber septum of the reaction vessel to initiate the polymerisation. The nucleation of the particles can be observed as the solution becomes turbid. This takes approximately 3 to 4 minutes to occur and depends on the monomer and solvent and their relative affinities. This was allowed to react at constant temperature with constant and vigorous stirring for 24 h. The reaction was stopped by removing the rubber septum to expose the reaction to air and allowed to cool to room temperature before immediate work up.

To clean the particles the solution is decanted from the reaction vessel into a 10 mL Teflon centrifuge tube and spun at 2000 rpm for up to 5 mins. The duration of centrifugation required depends on the relative size of the particles which is dependent on the monomer and solvent used. The minimum centrifugation time is used to reduce the amount of particle coagulation that occurs. This centrifugation process allows the reaction solvent to be decanted and replaced with clean EtOH in which the particles are then redispersed. This sedimentation, solvent replacement and particle dispersion step is repeated a total of 3 times – this cleans the PVP55 from the particle surfaces. The particles are analysed by POM both in the crude reaction mixture as well as clean in EtOH. Following work up the particles are further characterised using SEM in order to gauge particle size, surface morphology and size distribution. A sample was dried to constant weight in a vacuum oven for analysis by GPC, DSC, IR and NMR.

Typical characterisation data for particles of **P1**:

Particle size distribution: Average particle size: 0.86 µm
Variance (C_v): 7.2 %

^{1}H NMR ($CDCl_3$) δ (ppm): 1.24 – 2.34 (br m, 12H, -CH_2-, CH_2(pb), CH_2(pb)), 4.02 (br m, 4H, -CH_2O-), 6.93 (br m, 2H, ArH), 7.31 (br m, 2H, ArH), 7.69 (br m, 2H, ArH), 8.08 (br m, 2H, ArH).

IR (FTR) ν (cm^{-1}): 2931, 2862 (CH), 2229 (C≡N), 1728 (C=O), 1604 (C-C), 1504, 1458 (Ar), 1396, 1249, 1203, 1049, 1002, 879, 840, 687, 633, 548.

DSC: g 28 °C N 115 °C I

GPC: M_n: 197,000 g mol^{-1}
Polydispersity (M_w/M_n): 2.87

Table 8.2: Summary of reactions to form nematic polymer particles of **P1** by dispersion polymerisation.

Sample name	**Specific conditions**	**Comments**
DP-P1-1	-	Bipolar particles
DP-P1-2	Solvent: ^{i}PrOH	Bipolar particles
DP-P1-3	Solvent: 1:1 EtOH: methoxyethanol	Bipolar particles
DP-P1-4	-	GPC analysis
DP-P1-5	5.5 wt% triton X305	Bipolar particles
DP-P1-6	Solvent: 1:1 EtOH: methoxyethanol	Bipolar particles
DP-P1-7	-	Bipolar particles
DP-P1-8	-	For experimental analysis

Typical characterisation data for particles of **P2:**

Particle size distribution: Average particle size: 1.9 µm
Variance (C_v): 16 %

DSC: g 52 °C N 108 °C I

GPC: M_n: 209,000 g mol^{-1}
Polydispersity (M_w/M_n): 2.68

Table 8.3: Summary of reactions to form nematic polymer particles of **P2** by dispersion polymerisation.

Sample name	Specific conditions	Comments
DP-P2-1	-	Bipolar particles
DP-P2-2	-	Repeat of **KLH-P124.** Bipolar particles
DP-P2-3	Solvent: MeOH	Bipolar particles
DP-P2-4	Solvent: 1:1 EtOH: methoxyethanol	Bipolar particles
DP-P2-5	-	For DSC analysis. T_g 27 °C N-I 70 °C
DP-P2-6	-	For experimental analysis

Typical characterisation data for particles of **P3:**

Particle size distribution: Average particle size: 2.08 µm

Variance (C_v): 15.4 %

^{1}H NMR ($CDCl_3$) δ (ppm): 0.97 (br m, 6H, -CH_3), 1.42 - 1.83 (br m, 12H, -CH_2-, CH_2(pb), CH_2(pb)), 4.00 (br m, 8H, -CH_2O-), 6.81 (br m, 4H, ArH), 7.14 (br m, 1H, ArH), 7.82 (br m, 1H, ArH), 8.12 (br m, 4H, ArH).

DSC: g 26 °C N 65 °C I

GPC: M_n: 188,000 g mol^{-1}

Polydispersity (M_w/M_n): 3.04

Table 8.4: Summary of reactions to form nematic polymer particles of **P3** by dispersion polymerisation.

Sample name	Specific conditions	Comments
DP-P3-1	Solvent: MeOH	Bipolar particles
DP-P3-2	-	Bipolar particles
DP-P3-3	Solvent: ^{i}PrOH	Bipolar particles
DP-P3-4	Solvent: 1:1 EtOH: methoxyethanol	Bipolar particles
DP-P3-5	Solvent: 1:1 EtOH: methoxyethanol	Repeat of **KLH-P60.** Bipolar particles
DP-P3-6	Solvent: 1:1 EtOH: methoxyethanol	Repeat of **KLH-P57.** Bipolar particles
DP-P3-7	Solvent: 1:1 EtOH: methoxyethanol	Repeat of **KLH-P58.** Bipolar particles
DP-P3-8	-	Bipolar particles
DP-P3-9	-	For DSC analysis. T_g 32 °C N-I 81 °C
DP-P3-10	5.5 wt% triton X305	Bipolar particles
DP-P3-11	5.5 wt% triton X305 Solvent: 1:1 EtOH: methoxyethanol	Large coagulates
DP-P3-12	-	Bipolar particles
DP-P3-13	Monomer: 90 % **M3**, 10 % **M6**	Copolymerisation study
DP-P3-14	Monomer: 50 % **M3**, 50 % **M6**	Copolymerisation study
DP-P3-15	Monomer: 10 % **M3**, 90 % **M6**	Copolymerisation study
DP-P3-16	Monomer: 70 % **M3**, 30 % **M6**	Copolymerisation study
DP-P3-17	Monomer: 50 % **M3**, 50 % **M6**	Copolymerisation study
DP-P3-18	Monomer: 30 % **M3**, 70 % **M6**	Copolymerisation study
DP-P3-19	Monomer: 80 % **M3**, 20 % **M6**	Copolymerisation study
DP-P3-20	Monomer: 20 % **M3**, 80 % **M6**	Copolymerisation study
DP-P3-21	-	Cosmetics company sample
DP-P3-22	-	Cosmetics company sample
DP-P3-23	-	Cosmetics company sample
DP-P3-24	-	Cosmetics company sample
DP-P3-25	-	Cosmetics company sample
DP-P3-26	-	Cosmetics company sample
DP-P3-27	-	For experimental analysis

Typical characterisation data for particles of **P4:**

Particle size distribution: Average particle size: 2.15 µm

Variance (C_v): 22 %

DSC: g 34 °C N 73 °C I

GPC: M_n: 254,000 g mol^{-1}

Polydispersity (M_w/M_n): 2.14

Table 8.5: Summary of reactions to form nematic polymer particles of **P4** by dispersion polymerisation.

Sample name	Specific conditions	Comments
DP-P4-1	-	Radial particles
DP-P4-2	Monomer: 90 % **M3**, 10 % **M4**	Copolymerisation study
DP-P4-3	Monomer: 80 % **M3**, 20 % **M4**	Copolymerisation study
DP-P4-4	Monomer: 70 % **M3**, 30 % **M4**	Copolymerisation study
DP-P4-5	Monomer: 60 % **M3**, 40 % **M4**	Copolymerisation study
DP-P4-6	Monomer: 50 % **M3**, 50 % **M4**	Copolymerisation study
DP-P4-7	Monomer: 40 % **M3**, 60 % **M4**	Copolymerisation study
DP-P4-8	Monomer: 30 % **M3**, 70 % **M4**	Copolymerisation study
DP-P4-9	Monomer: 20 % **M3**, 80 % **M4**	Copolymerisation study
DP-P4-10	Monomer: 10 % **M3**, 90 % **M4**	Copolymerisation study
DP-P4-11	Solvent: MeOH	Small particles
DP-P4-12	Solvent: 1:1 EtOH: methoxyethanol	Bipolar particles
DP-P4-13	-	For DSC analysis. T_g 34 °C N-I 73 °C
DP-P4-14	-	For experimental analysis

Typical characterisation data for particles of **P5:**

Particle size distribution: Average particle size: 1.32 µm

Variance (C_v): 29 %

DSC: g 28 °C N 93 °C I

GPC: M_n: 340,000 g mol^{-1}

Polydispersity (M_w/M_n): 2.12

Table 8.6: Summary of reactions to form nematic polymer particles of **P5** by dispersion polymerisation.

Sample name	Specific conditions	Comments
DP-P5-1	-	Radial particles
DP-P5-2	Solvent: MeOH	Small particles
DP-P5-3	Solvent: 1:1 EtOH: methoxyethanol	Bipolar particles
DP-P5-4	-	For DSC analysis. T_g 30 °C N-I 93 °C
DP-P5-5	-	For experimental analysis

Typical characterisation data for particles of **P6:**

Particle size distribution: Average particle size: 2.1 µm
Variance (C_v): 30 %

^{1}H NMR ($CDCl_3$) δ (ppm): 0.86 (br m, 6H, -CH_3-), 1.22 – 1.40 (br m, 18H, -CH_2-, CH_2(pb), CH_2(pb)), 1.72 (br m, 4H, -CH_2-), 3.89 (br m, 8H, -CH_2O-), 6.80 (br m, 4H, ArH), 7.08 (br m, 1H, ArH), 7.30 (br m, 1H, ArH), 7.72 (br m, 1H, ArH), 7.96 (br m, 4H, ArH).

DSC: g 24 °C N 70 °C I

GPC: M_n: 122,000 g mol^{-1}
Polydispersity (M_w/M_n): 3.11

Table 8.7: Summary of reactions to form nematic polymer particles of **P6** by dispersion polymerisation.

Sample name	**Specific conditions**	**Comments**
DP-P6-1	-	Radial particles
DP-P6-2	Solvent: MeOH	Radial particles
DP-P6-3	Solvent: 1:1 EtOH: methoxyethanol	Bipolar particles
DP-P6-4	-	Radial particles
DP-P6-5	Solvent: MeOH	Radial particles
DP-P6-6	Solvent: 1:1 EtOH: methoxyethanol	Crude: bipolar, clean: radial
DP-P6-7	-	For GPC analysis.
DP-P6-8	Reaction temperature: 55 °C	Radial particles
DP-P6-9	Solvent: 1:1 EtOH: methoxyethanol	Repeat of **KLH-P82.** Bipolar particles
DP-P6-10	-	For DSC analysis. T_g 24 °C N-I 70 °C
DP-P6-11	5.5 wt% triton X305	Radial particles
DP-P6-12	5.5 wt% triton X305 Solvent: 1:1 EtOH: methoxyethanol	Bipolar particles
DP-P6-13	Solvent: 1:1 EtOH: methoxyethanol	Solvent study
DP-P6-14	Solvent: 1:1 EtOH: methoxyethanol	Solvent study
DP-P6-15	Solvent: 5:1 EtOH: methoxyethanol	Solvent study
DP-P6-16	Solvent: 10:1 EtOH: methoxyethanol	Solvent study
DP-P6-17	Solvent: 15:1 EtOH: methoxyethanol	Solvent study
DP-P6-18	-	Radial particles
DP-P6-19	-	Cosmetics company sample
DP-P6-20	-	Cosmetics company sample
DP-P6-21	-	Cosmetics company sample
DP-P6-22	-	For experimental analysis
DP-P6-23	Monomer: 10 % **M3**, 90 % **M6**	Copolymerisation study
DP-P6-24	Monomer: 20 % **M3**, 80 % **M6**	Copolymerisation study
DP-P6-25	Monomer: 30 % **M3**, 70 % **M6**	Copolymerisation study
DP-P6-26	Monomer: 40 % **M3**, 60 % **M6**	Copolymerisation study
DP-P6-27	Monomer: 50 % **M3**, 50 % **M6**	Copolymerisation study
DP-P6-28	Monomer: 60 % **M3**, 40 % **M6**	Copolymerisation study
DP-P6-29	Monomer: 70 % **M3**, 30 % **M6**	Copolymerisation study
DP-P6-30	Monomer: 80 % **M3**, 20 % **M6**	Copolymerisation study
DP-P6-31	Monomer: 90 % **M3**, 10 % **M6**	Copolymerisation study

Typical characterisation data for particles of **P7:**

Particle size distribution: Average particle size: 1.88 µm
Variance (C_v): 27 %
DSC: g 24 °C N 74 °C I
GPC: M_n: 121,000 g mol^{-1}
Polydispersity (M_w/M_n): 3.01

Table 8.8: Summary of reactions to form nematic polymer particles of **P7** by dispersion polymerisation.

Sample name	**Specific conditions**	**Comments**
DP-P7-1	-	Radial particles
DP-P7-2	Solvent: MeOH	Radial particles
DP-P7-3	Solvent: 1:1 EtOH: methoxyethanol	Radial particles
DP-P7-4	-	For DSC analysis. T_g 26 °C N-I 74 °C
DP-P7-5	-	For experimental analysis

Typical characterisation data for particles of **P8:**

Particle size distribution: Average particle size: 3.4 µm
Variance (C_v): 23 %
^{1}H NMR ($CDCl_3$) δ (ppm): 0.95 (br m, 6H, -CH_3), 1.15 – 1.23 (br m, 13H, -CH_2-, CH_2(pb), CH_2(pb)), 1.47 (br m, 8H, -CH_2-), 1.75 (br m, 4H, -CH_2-), 3.98 (br m, 8H, -CH_2O-), 6.91 (br m, 4H, ArH), 7.19 (br m, 1H, ArH), 7.38 (br m, 1H, ArH), 7.83 (br m, 1H, ArH), 8.09 (br m, 4H, ArH).
DSC: g 18 °C N 92 °C I
GPC: M_n: 19,000 g mol^{-1}
Polydispersity (M_w/M_n): 2.97

Table 8.9: Summary of reactions to form nematic polymer particles of **P8** by dispersion polymerisation.

Sample name	Specific conditions	Comments
DP-P8-1	-	Bipolar particles
DP-P8-2	Solvent: MeOH	Bipolar particles
DP-P8-3	Solvent: 1:1 EtOH: methoxyethanol	Bipolar particles
DP-P8-4	-	Bipolar particles
DP-P8-5	Solvent: MeOH	Bipolar particles
DP-P8-6	Solvent: 1:1 EtOH: methoxyethanol	Bipolar particles
DP-P8-7	-	For GPC analysis.
DP-P8-8	Reaction time: 48 hr	For GPC analysis.
DP-P8-9	-	Bipolar particles
DP-P8-10	-	Bipolar particles
DP-P8-11	-	For DSC analysis.
DP-P8-12	-	For electro-optics, bipolar particles
DP-P8-13	-	Cosmetics company sample
DP-P8-14	-	Cosmetics company sample
DP-P8-15	-	Cosmetics company sample
DP-P8-16	-	Cosmetics company sample
DP-P8-17	-	Cosmetics company sample
DP-P8-18	-	For experimental analysis

Typical characterisation data for particles of **P9:**

Particle size distribution: Average particle size: 2.9 μm
Variance (C_v): 22 %

^{1}H NMR ($CDCl_3$) δ (ppm): 0.88 (br m, 6H, -CH_3-), 1.16 – 1.42 (br m, 32H, -CH_2-, CH_2(pb), CH_2(pb)), 1.76 (br m, 4H, -CH_2-), 4.02 (br m, 8H, -CH_2O-), 6.92 (br m, 4H, ArH), 7.21 (br m, 1H, ArH), 7.39 (br m, 1H, ArH), 7.84 (br m, 1H, ArH), 8.10 (br m, 4H, ArH).

DSC: g 7 °C N 73 °C I

GPC: M_n: 15,000 g mol^{-1}
Polydispersity (M_w/M_n): 2.96

Table 8.10: Summary of reactions to form nematic polymer particles of **P9** by dispersion polymerisation.

Sample name	Specific conditions	Comments
DP-P9-1	-	Radial particles
DP-P9-2	Solvent: MeOH	Radial particles
DP-P9-3	Solvent: 1:1 EtOH: methoxyethanol	Radial particles
DP-P9-4	-	Radial particles
DP-P9-5	Solvent: MeOH	Radial particles
DP-P9-6	Solvent: 1:1 EtOH: methoxyethanol	Radial particles
DP-P9-7	-	For GPC analysis.
DP-9-8	Monomer: 10 % **M8**, 90 % **M9**	Twisted radial particles
DP-P9-9	Monomer: 20 % **M8**, 80 % **M9**	Twisted radial particles
DP-P9-10	Monomer: 30 % **M8**, 70 % **M9**	Twisted radial particles
DP-P9-11	Monomer: 40 % **M8**, 60 % **M9**	Twisted radial particles
DP-P9-12	Monomer: 50 % **M8**, 50 % **M9**	Twisted radial particles
DP-P9-13	Monomer: 60 % **M8**, 40 % **M9**	Twisted radial particles
DP-P9-14	Monomer: 70 % **M8**, 30 % **M9**	Twisted radial particles
DP-P9-15	Monomer: 80 % **M8**, 20 % **M9**	Twisted radial particles
DP-P9-16	Monomer: 90 % **M8**, 10 % **M9**	Twisted radial particles
DP-P9-17	Monomer: 5 % **M8**, 95 % **M9**	Twisted radial particles
DP-P9-18	Monomer: 95 % **M8**, 5 % **M9**	Twisted radial particles
DP-P9-19	Monomer: 2.5 % **M8**, 97.5 % **M9**	Twisted radial particles
DP-P9-20	Monomer: 97.5 % **M8**, 2.5 % **M9**	Twisted radial particles
DP-P9-21	Reaction time: 48 hr	For GPC analysis.
DP-P9-22	Reaction temperature: 55 °C	Twisted radial particles
DP-P9-23	-	Radial particles
DP-P9-24	Monomer: 90 % **M8**, 10 % **M9**	For electro-optics, twisted radial particles
DP-P9-25	-	For DSC analysis.
DP-P9-26	-	For electro-optics, radial particles
DP-P9-27	Monomer: 50 % **M8**, 50 % **M9**	For electro-optics, twisted radial particles
DP-P9-28	-	Cosmetics company sample
DP-P9-29	-	Cosmetics company sample
DP-P9-30	-	Cosmetics company sample
DP-P9-31	-	For experimental analysis

8.5 SYNTHESIS OF ELASTOMER PARTICLES BY DISPERSION POLYMERISATION

Below is an adapted technique from literature procedures[78, 79, 101, 141-143] which has been used to synthesise nematic elastomer particles of **P1** via dispersion polymerisation with a delayed addition of crosslinker. Gel content of particles synthesised from **P2**-**P9** using this method was negligible. The exact reagents and conditions used in each case, where different from specified below, are listed in Table 8.11 to Table 8.19. **CL1**: 1,6-hexandioldiacrylate, **CL2**: dipropylene glycol diacrylate, **CL3**: trimethyloylpropane triacrylate.

A vessel sealed with a rubber septum containing a solution of monomer (50 mg) and the stabiliser PVP55 (polyvinylpyrrolidone with an average molecular weight of 55,000 g mol^{-1}) (15 wt % relative to monomer, 15 mg, 2.75 x 10^{-4} mmol) in EtOH (0.5 mL) was purged by gently bubbling N_2 through for a period of 30 minutes. The vessel was kept in ice throughout this process to minimise solvent loss. This vessel was then heated to a reaction temperature of 73 °C with constant and vigorous stirring. The reaction vessel, stirrer size and stirring rate were kept constant across all experiments to minimise variables that may affect the resulting particles. A second sealed vessel containing a solution of monomer (50 mg) and crosslinker (1,6 hexanedioldiacrylate (**CL1**), 10 mol % relative to total monomer) in EtOH (0.5 mL) was also purged with N_2 for 30 minutes in ice at this time and then brought to reaction temperature with stirring. A solution of the initiator AIBN (2 wt % relative to monomer, 2 mg, 0.012 mmol) in EtOH (0.6 mL) was also purged and brought to the same temperature. This was then injected through the rubber septum of the first vessel to initiate the polymerisation. The nucleation of the particles can be observed as the solution becomes turbid. This takes approximately 3 to 4 minutes to occur and depends on the monomer and solvent and their relative affinities. After the nucleation of the particles the second monomer solution containing crosslinker was then injected into the reaction vessel through the rubber septum. Delaying the addition of the crosslinker until after the nucleation of the particles has completed prevents the crosslinker from interfering with the early stages of particle growth. This was allowed to react at constant temperature with constant and vigorous stirring for 24 h. The reaction was stopped by removing the rubber septum to expose the reaction to air and allowed to cool to room temperature before immediate work up.

To clean the particles the solution is decanted from the reaction vessel into a 10 mL Teflon centrifuge tube and spun at 2000 rpm for up to 5 mins. The duration of centrifugation required depends on the relative size of the particles which is dependent on the monomer and solvent used. The minimum centrifugation time is used to reduce the amount of particle coagulation that

occurs. This centrifugation process allows the reaction solvent to be decanted and replaced with clean EtOH in which the particles are then redispersed. This sedimentation, solvent replacement and particle dispersion step is repeated a total of 3 times – this cleans the PVP55 from the particle surfaces. The particles are analysed by POM when in the crude reaction mixture as well as when dispersed in clean EtOH to allow for an investigation into the effect of dispersing medium and presence of PVP on the director configuration of the particles. Following work up the particles are further characterised using SEM in order to gauge particle size, surface morphology and size distribution. A few sample reactions are also dried to constant weight in a vacuum oven for analysis by DSC, IR and NMR. To assess the degree of crosslinking that has taken place the samples are subjected to a gel content analysis process which is described in detail in section 8.7.

Typical characterisation data for particles of **P1**:

Particle size distribution:	Average particle size: 1.3 µm Variance (C_v): 6.3 %
^{1}H NMR ($CDCl_3$) δ (ppm):	1.55 – 1.75 (br m, 16H, -CH_2-, CH_2(pb), CH_2(pb)), 4.02 (br m, 4H, -CH_2O-), 6.86 (br m, 2H, ArH), 7.24 (br m, 2H, ArH), 7.62 (br m, 2H, ArH), 8.01 (br m, 2H, ArH).
DSC:	g 36 °C N-I 97 °C
Gel content:	83.4 %

Table 8.11: Summary of reactions to form nematic elastomer particles of **P1** by dispersion polymerisation.

Sample name	Specific conditions	Comments/analysis
DA-P1-1 to DA-P1-6	Solvent: MeOH	CL added 3 to 8 minutes after initiation, bipolar
DA-P1-7 to DA-P1-11	Solvent: 0.9 mL MeOH	CL added 3 to 7 minutes after initiation, bipolar
DA-P1-12	Solvent: 0.5 mL MeOH	Concentration study, bipolar particles
DA-P1-13	Solvent: 0.7 mL MeOH	Concentration study, bipolar particles
DA-P1-14	Solvent: 1.1 mL MeOH	Concentration study, bipolar particles
DA-P1-15	Solvent: 1.3 mL MeOH	Concentration study, bipolar particles
DA-P1-16	Solvent: 1.5 mL MeOH	Concentration study, bipolar particles
DA-P1-17	Solvent: 1.7 mL MeOH	Concentration study, bipolar particles
DA-P1-18	Solvent: 1.9 mL MeOH	Concentration study, bipolar particles
DA-P1-19	Solvent: 0.8 mL MeOH	Concentration study, bipolar particles
DA-P1-20 to DA-P1-22	Solvent: MeOH AIBN: 5 to 15 wt%	AIBN concentration study, bipolar particles
DA-P1-23 to DA-P1-24	Solvent: MeOH PVP: 5 and 30 wt%	PVP concentration study, bipolar particles
DA-P1-25	Solvent: MeOH	Repeat of **KLH-P32,** bipolar particles
DA-P1-26	Solvent: MeOH	Scale up of **KLH-P32,** bipolar particles
DA-P1-27	-	Bipolar particles
DA-P1-28	Solvent: MeOH	Repeat of **KLH-P32,** bipolar particles
DA-P1-29	Solvent: ^{i}PrOH	Bipolar particles
DA-P1-30	Solvent: 1:1 EtOH: methoxyethanol	Bipolar particles
DA-P1-31	Solvent: MeOH	For monolayer study, bipolar particles
DA-P1-32	-	For monolayer study, bipolar particles
DA-P1-33	Solvent: MeOH	Bipolar particles
DA-P1-34	Solvent: MeOH	Bipolar particles
DA-P1-35	-	Bipolar particles
DA-P1-36	5.5 wt% Triton X305	Bipolar particles
DA-P1-37	Solvent: 1:1 EtOH: methoxyethanol 5.5 wt% Triton X305	Bipolar particles
DA-P1-38	Crosslinker: **CL3**	Bipolar particles
DA-P1-39	-	Bipolar particles
DA-P1-40	-	Bipolar particles

The degree of gel content obtained for particles of **P2**-**P9** by dispersion polymerisation with a delayed addition of crosslinker was low and thus it was assumed that no significant network formation had taken place. The characterisation of those particles is here for reference, but the particles are not elastomeric in nature.

Typical characterisation data for particles of **P2:**

^{1}H NMR ($CDCl_3$) δ (ppm): 1.03 (br m, 6H, -CH_3-), 1.26 – 1.88 (br m, 15H, -CH_2-, CH_2(pb), CH_2(pb)), 2.20 (br m, 2H, -CH_2-), 4.00 (br m, 8H, -CH_2O-), 6.91 (br m, 4H, ArH), 7.19 (br m, 1H, ArH), 7.39 (br m, 1H, ArH), 7.83 (br m, 1H, ArH), 8.07 (br m, 4H, ArH).

Table 8.12: Summary of reactions to form nematic elastomer particles of **P2** by dispersion polymerisation.

Sample name	**Specific conditions**	**Comments/analysis**
DA-P2-1	-	For experimental analysis, polydomain

Typical characterisation data for particles of **P3:**

^{1}H NMR ($CDCl_3$) δ (ppm): 0.87 (br m, 6H, -CH_3-), 1.40 – 1.71 (br m, 18H, -CH_2-, CH_2(pb), CH_2(pb)), 3.92 (br m, 8H, -CH_2O-), 6.87 (br m, 4H, ArH), 7.17 (br m, 1H, ArH), 7.37 (br m, 1H, ArH), 7.82 (br m, 1H, ArH), 8.04 (br m, 4H, ArH).

Gel content: 8.7 %

Table 8.13: Summary of reactions to form nematic elastomer particles of **P3** by dispersion polymerisation.

Sample name	Specific conditions	Comments/analysis
DA-P3-1	-	Bipolar particles
DA-P3-2	Solvent: MeOH	Radial and polydomain particles
DA-P3-3	Solvent: ^{i}PrOH	Bipolar particles
DA-P3-4	Solvent: 1:1 EtOH: methoxyethanol	Bipolar particles
DA-P3-5	Solvent: 1:1 EtOH: methoxyethanol	Repeat of **KLH-P60,** bipolar particles
DA-P3-6	-	Repeat of **KLH-P57,** bipolar particles
DA-P3-7	Solvent: MeOH	Bipolar particles
DA-P3-8	Solvent: MeOH	For GCA study
DA-P3-9	-	For GCA study
DA-P3-10	-	Bipolar particles
DA-P3-11	Reaction time: 72 hr	Bipolar particles
DA-P3-12	5.5 wt% triton X305	Stabiliser investigation
DA-P3-13	Solvent: 1:1 EtOH: methoxyethanol Crosslinker: **CL3** 5.5 wt% triton X305	Stabiliser investigation
DA-P3-14	Crosslinker: **CL3**	Bipolar particles
DA-P3-15	-	For experimental analysis, bipolar

Typical characterisation data for particles of **P4:**

^{1}H NMR ($CDCl_3$) δ (ppm): 0.93 (br m, 6H, -CH_3-), 1.41 – 1.58 (br m, 15H, -CH_2-, CH_2(pb), CH_2(pb)),1.67 – 1.78 (br m, 6H, -CH_2-), 1.76 (br m, 4H, -CH_2-), 4.05 (br m, 8H, -CH_2O-), 6.90 (br m, 4H, ArH), 7.17 (br m, 1H, ArH), 7.38 (br m, 1H, ArH), 7.83 (br m, 1H, ArH), 8.07 (br m, 4H, ArH).

DSC: g 33 °C N 52 °C I

Table 8.14: Summary of reactions to form nematic elastomer particles of **P4** by dispersion polymerisation.

Sample name	Specific conditions	Comments/analysis
DA-P4-1	-	For experimental analysis, radial

Typical characterisation data for particles of **P5:**

^{1}H NMR ($CDCl_3$) δ (ppm): 0.93 (br m, 6H, -CH_3-), 1.37– 1.82 (br m, 28H, -CH_2-, CH_2(pb), CH_2(pb)), 2.20 (br m, 2H, -CH_2-), 4.05 (br m, 8H, -CH_2O-), 6.98 (br m, 4H, ArH), 7.27 (br m, 1H, ArH), 7.44 (br m, 1H, ArH), 7.86 (br m, 1H, ArH), 8.16 (br m, 4H, ArH).

DSC: g 31 °C N 61 °C I

Table 8.15: Summary of reactions to form nematic elastomer particles of **P5** by dispersion polymerisation.

Sample name	Specific conditions	Comments/analysis
DA-P5-1	-	For experimental analysis, radial

Typical characterisation data for particles of **P6:**

^{1}H NMR ($CDCl_3$) δ (ppm): 0.89 (br m, 6H, -CH_3-), 1.31– 1.78 (br m, 30H, -CH_2-, CH_2(pb), CH_2(pb)), 2.19 (br m, 2H, -CH_2-), 4.07 (br m, 8H, -CH_2O-), 6.89 (br m, 4H, ArH), 7.16 (br m, 1H, ArH), 7.36 (br m, 1H, ArH), 7.82 (br m, 1H, ArH), 8.13 (br m, 4H, ArH).

DSC: g 26 °C N 62 °C I

Gel content: 11.8 %

Table 8.16: Summary of reactions to form nematic elastomer particles of **P6** by dispersion polymerisation.

Sample name	Specific conditions	Comments/analysis
DA-P6-1	-	Radial particles
DA-P6-2	Solvent: MeOH	Radial particles
DA-P6-3	Solvent: 1:1 EtOH: methoxyethanol	Stabiliser/solvent exchange study. Crude bipolar, clean radial
DA-P6-4	Solvent: MeOH	For GCA study,
DA-P6-5	-	For GCA study, radial particles
DA-P6-6	5.5 wt% triton X305	Stabiliser investigation
DA-P6-7	Solvent: 1:1 EtOH: methoxyethanol Crosslinker: **CL3** 5.5 wt% triton X305	Stabiliser investigation
DA-P6-8	-	Radial particles

Typical characterisation data for particles formed from **M7:**

^{1}H NMR ($CDCl_3$) δ (ppm): 0.87 (br m, 6H, -CH_3-), 1.30 – 2.04 (br m, 30H, -CH_2-, CH_2(pb), CH_2(pb)), 2.18 (br m, 2H, -CH_2-), 4.06 (br m, 8H, -CH_2O-), 6.88 (br m, 4H, ArH), 7.16 (br m, 1H, ArH), 7.36 (br m, 1H, ArH), 7.81 (br m, 1H, ArH), 8.05 (br m, 4H, ArH).

DSC: g 28 °C N 64 °C I

Table 8.17: Summary of reactions to form nematic elastomer particles of **P7** by dispersion polymerisation.

Sample name	Specific conditions	Comments/analysis
DA-P7-1	-	For experimental analysis, radial

Typical characterisation data for particles of **P8:**

^{1}H NMR ($CDCl_3$) δ (ppm): 0.99 (br m, 6H, -CH_3-), 1.20 – 1.81 (br m, 32H, -CH_2-, CH_2(pb), CH_2(pb)), 2.27 (br m, 2H, -CH_2-), 4.08 (br m, 8H, -CH_2O-), 6.96 (br m, 4H, ArH), 7.24 (br m, 1H, ArH), 7.44 (br m, 1H, ArH), 7.88 (br m, 1H, ArH), 8.14 (br m, 4H, ArH).

DSC: g 23 °C N 71 °C I

Gel content: 1.2 %

Table 8.18: Summary of reactions to form nematic elastomer particles of **P8** by dispersion polymerisation.

Sample name	Specific conditions	Comments/analysis
DA-P8-1	-	Bipolar particles
DA-P8-2	Solvent: MeOH	Bipolar particles
DA-P8-3	Solvent: 1:1 EtOH: methoxyethanol	Bipolar particles
DA-P8-4	Solvent: MeOH	For GCA study,
DA-P8-5	-	For GCA study, bipolar
DA-P8-6	-	For experimental analysis, bipolar
DA-P8-7	-	For experimental analysis, bipolar
DA-P8-8	Solvent: 1:1 EtOH: methoxyethanol	For electro-optics

Typical characterisation data for particles of **P9:**

^{1}H NMR ($CDCl_3$) δ (ppm): 0.92 (br m, 6H, -CH_3-), 1.20 – 1.66 (br m, 34H, -CH_2-, CH_2(pb), CH_2(pb)), 2.26 (br m, 2H, -CH_2-), 4.07 (br m, 8H, -CH_2O-), 6.96 (br m, 4H, ArH), 7.24 (br m, 1H, ArH), 7.44 (br m, 1H, ArH), 7.91 (br m, 1H, ArH), 8.18 (br m, 4H, ArH).

DSC: g 4 °C N 55 °C I

Gel content: 24.5 %

Table 8.19: Summary of reactions to form nematic elastomer particles of **P9** by dispersion polymerisation.

Sample name	**Specific conditions**	**Comments/analysis**
DA-P9-1	-	Radial particles
DA-P9-2	Solvent: MeOH	Radial particles
DA-P9-3	Solvent: 1:1 EtOH: methoxyethanol	Radial particles
DA-P9-4	Solvent: MeOH	For GCA study,
DA-P9-5	-	For GCA study, radial
DA-P9-6	-	For experimental analysis, radial

8.6 SYNTHESIS OF POLYMER AND ELASTOMER PARTICLES BY RAFT ASSISTED DISPERSION POLYMERISATION

Below is an adapted technique from a literature procedure[96] which has been used to synthesise nematic elastomer particles of **P1** – **P9**, synthesised from monomers **M1** – **M9** respectively, *via* RAFT-assisted dispersion polymerisation technique. The exact reagents and conditions used in each case, where different from below, are specified in Table 8.20 to Table 8.37.

A solution of monomer (100mg), PVP30 (polyvinylpyrrolidone with an average molecular weight of 30,000 g mol^{-1}) (15 wt % relative to monomer, 15 mg, 5 x 10^{-4} mmol), UV initiator Darocur 1173 (4 wt% relative to monomer, 4 mg, 2.4 x 10^{-2} mmol), RAFT agent DDMAT (0.5 wt% relative to monomer, 0.5 mg, 1.4 x10^{-3} mmol) and if elastomer particles are required a crosslinker is also present (1,6-hexanedioldiacrylate (**CL1**), 10 wt% relative to monomer, 10 mg). All of these reagents are transferred into a sealed reaction vessel using stock solutions with the reaction solvent (EtOH) to ensure maximum accuracy. The total volume of reaction solvent in the sealed vessel is then made up to 1.6 mL. The reaction vessel is then gently purged with N_2 for a period of 30 min before being heating to a reaction temperature of 65 °C with constant and vigorous stirring. The reaction vessel, stirrer size and stirring rate were kept constant across all experiments to minimise variables that may affect the resulting particles. Once the reaction vessel has reached reaction temperature and all the reagents have dissolved the vessel is exposed to UV light (365 nm) for 5 h. The exact time for each reaction is specified in the appropriate table. The nucleation of the particles can be observed by the reaction mixture becoming turbid. With RAFT-assisted dispersion polymerisation this often takes around 10 – 15 minutes to occur. After the reaction vessel has been exposed to UV light for the designated amount of time the vessel is opened to expose the sample to air and is allowed to cool to room temperature before immediate work up.

To clean the particles the solution is decanted from the reaction vessel into a 10 mL Teflon centrifuge tube and spun at 2000 rpm for up to 5 mins. The duration of centrifugation required depends on the relative size of the particles which is dependent on the monomer and solvent used. The minimum centrifugation time is used to reduce the amount of particle coagulation that occurs. This centrifugation process allows the reaction solvent to be decanted and replaced with clean EtOH in which the particles are then redispersed. This sedimentation, solvent replacement and particle dispersion step is repeated a total of 3 times – this cleans the PVP30 from the particle surfaces. The particles are analysed by POM when in the crude reaction mixture as well as when dispersed in clean EtOH to allow for an investigation into the effect of dispersing medium and presence of PVP on the director configuration of the particles. Following work up the particles

are further characterised using SEM in order to gauge particle size, surface morphology and size distribution. A few sample reactions are also dried to constant weight in a vacuum oven for analysis by DSC, IR and NMR. To assess the degree of crosslinking that has taken place the samples are subjected to a gel content analysis process which is described in detail in section 8.7.

Typical characterisation data for polymer particles of **P1**:

^{1}H NMR ($CDCl_3$) δ (ppm): 1.26 – 1.82 (br m, 10H, -CH_{2-}, CH_2(pb), CH_2(pb)), 2.33 (br m, 2H, -CH_2-), 4.09 (br m, 4H, -CH_2O-), 7.01(br m, 2H, ArH), 7.37(br m, 2H, ArH), 7.69 (br m, 2H, ArH), 8.05 (br m, 2H, ArH).

DSC: g 26 °C N 114 °C I

GPC: M_n: 188,000 g mol^{-1}

Polydispersity (M_w/M_n): 2.40

Table 8.20: Summary of reactions to form nematic polymer particles of **P1** by RAFT-assisted dispersion polymerisation.

Sample name	**Specific conditions**	**Comments/analysis**
RAFT-P1-1	-	Polydomain particles
RAFT-P1-2	Solvent: 1:1 EtOH: methoxyethanol	Polydomain particles
RAFT-P1-3	-	Living character study, bipolar particles
RAFT-P1-4	Solvent: 1:1 EtOH: methoxyethanol	Polydomain particles
RAFT-P1-5	-	Experimental analysis, bipolar

Typical characterisation data for elastomer particles of **P1**:

Particle size distribution: Average particle size: 3.3 µm

Variance (C_v): 15%

^{1}H NMR ($CDCl_3$) δ (ppm): 1.22 (br m, 2H, -CH_{2-}), 1.25 – 1.78 (br m, 8H, -CH_{2-}, CH_2(pb), CH_2(pb)), 2.27 (br, 2H, -CH_2-), 3.69 – 3.73 (br m, 2H, -CH_2O-), 3.98 (br m, 2H, -CH_2O-), 6.89 (br m, 2H, ArH), 7.33 (br m, 2H, ArH), 7.64 (br m, 2H, ArH), 8.03 (br m, 2H, ArH).

IR (FTR) ν (cm^{-1}): 2938 (C-H), 2230 (C≡N), 1728 (C=O), 1601, 1580, 1510 (C=C), 1422, 1253, 1208, 1160, 1055, 1006, 845, 760, 690, 649, 629, 549, 510.

DSC: g 37 °C N 90 °C I

Gel content: 93%

Table 8.21: Summary of reactions to form nematic elastomer particles of **P1** by RAFT-assisted dispersion polymerisation. Unless specified these particles were synthesised using 10 wt% of 1,6-hexanediol diacrylate **(CL1)** as the crosslinker.

Sample name	Specific conditions	Comments/analysis
RAFT-P1-6	-	Bipolar particles
RAFT-P1-7	-	Bipolar particles
RAFT-P1-8	Solvent: 1:1 EtOH: methoxyethanol	Polydomain particles
RAFT-P1-9	Solvent: 1:1 EtOH: methoxyethanol Crosslinker: **CL3**	Bipolar particles
RAFT-P1-10	Crosslinker: **CL2**	Bipolar particles
RAFT-P1-11	Crosslinker: **CL2**	Bipolar particles
RAFT-P1-12	-	Living character study, bipolar particles
RAFT-P1-13	-	Polydomain particles
RAFT-P1-14	Crosslinker: **CL2**	Polydomain particles
RAFT-P1-15	Crosslinker: **CL2**	Polydomain particles
RAFT-P1-16	-	Cosmetics company sample
RAFT-P1-17	-	Cosmetics company sample
RAFT-P1-18	-	Cosmetics company sample
RAFT-P1-19	Solvent: 1:1 EtOH: methoxyethanol	Cosmetics company sample
RAFT-P1-20	Solvent: 1:1 EtOH: methoxyethanol	Cosmetics company sample
RAFT-P1-21	Solvent: 1:1 EtOH: methoxyethanol	Cosmetics company sample

Typical characterisation data for polymer particles of **P2:**

DSC: g 51 °C N 92 °C I

GPC: M_n: 128,000 g mol^{-1}

Polydispersity (M_w/M_n): 1.74

Table 8.22: Summary of reactions to form nematic polymer particles of **P2** by RAFT-assisted dispersion polymerisation.

Sample name	Specific conditions	Comments/analysis
RAFT-P2-1	-	Polydomain particles, bipolar character
RAFT-P2-2	22 h UV exposure	Polydomain particles

Typical characterisation data for elastomer particles of **P2:**

^{1}H NMR ($CDCl_3$) δ (ppm): 1.04 (br m, 6H, -CH_3), 1.06 – 1.86 (br m, 14H, -CH_2-, CH_2(pb), CH_2(pb)), 3.98 (br m, 8H, -CH_2O-), 6.94 (br m, 4H, ArH), 7.21 (br m, 1H, ArH), 7.44 (br m, 1H, ArH), 7.80 (br m, 1H, ArH), 8.03 (br m, 4H, ArH).

IR (FTR) ν (cm^{-1}): 2925, 2854 (C-H), 1730 (C=O), 1605, 1580, 1510 (C=C), 1488, 1467, 1422, 1393, 1304, 1248, 1159, 1058, 1007, 970, 844, 794, 760, 724, 690, 644, 629, 550, 510.

Gel content: 97%

Table 8.23: Summary of reactions to form nematic elastomer particles of **P2** by RAFT-assisted dispersion polymerisation. Unless specified these particles were synthesised using 10 wt% of 1,6-hexanediol diacrylate **(CL1)** as the crosslinker.

Sample name	Specific conditions	Comments/analysis
RAFT-P2-3	-	Some radial character
RAFT-P2-4	-	Polydomain particles
RAFT-P2-5	Crosslinker: **CL2**	Polydomain particles
RAFT-P2-6	Crosslinker: **CL3**	Polydomain particles
RAFT-P2-7	22 h UV exposure	Polydomain particles

Typical characterisation data for polymer particles of **P3:**

Particle size distribution: Average particle size: 2.2 μm

Variance (C_v): 21%

^{1}H NMR ($CDCl_3$) δ (ppm): 1.03 (br m, 6H, -CH_3), 1.46 – 1.85 (br m, 14H, -CH_2-, CH_2(pb), CH_2(pb)), 1.98 (br m, 2H, -CH_2-), 4.03 (br m, 8H, -CH_2O-), 6.85 (br m, 4H, ArH), 7.20 (br m, 1H, ArH), 7.40 (br m, 1H, ArH), 7.86 (br m, 1H, ArH), 8.01 (br m, 4H, ArH).

IR (FTR) ν (cm^{-1}): 2928, 2856 (C-H), 1729 (C=O), 1605 (C=C), 1510, 1245, 1159, 1058, 1006, 968, 844, 760, 690, 644, 629, 552, 510.

DSC: g 24 °C N 72 °C I

GPC: M_n: 171,000 g mol^{-1}

Polydispersity (M_w/M_n): 1.61

Table 8.24: Summary of reactions to form nematic polymer particles of **P3** by RAFT-assisted dispersion polymerisation.

Sample name	Specific conditions	Comments/analysis
RAFT-P3-1	3 h UV exposure	Bipolar particles
RAFT-P3-2	3 h UV exposure	Some radial character
RAFT-P3-3	3 h UV exposure	Repeat of **KLH-P194**, bipolar particles
RAFT-P3-4	-	Kinetic study
RAFT-P3-5	-	Kinetic study
RAFT-P3-6	Solvent: 1:1 EtOH: methoxyethanol	Polydomain particles
RAFT-P3-7	-	Kinetic study, bipolar particles
RAFT-P3-8	22 h UV exposure	Cosmetics company sample
RAFT-P3-9	22 h UV exposure	Cosmetics company sample
RAFT-P3-10	22 h UV exposure	For experimental analysis

Typical characterisation data for elastomer particles of **P3:**

Particle size distribution: Average particle size: 0.9 μm
Variance (C_v): 28%

^{1}H NMR ($CDCl_3$) δ (ppm): 0.91 – 1.01 (m, 6H, -CH_3), 1.49 – 1.79 (br m, 14H, -CH_2, CH_2(pb), CH_2(pb)), 2.16 (br m, 2H, -CH_2-), 3.67 – 4.23 (br m, 8H, -CH_2O-), 6.90 (br m, 4H, ArH), 7.14 (br m, 1H, ArH), 7.37 (br m, 1H, ArH), 7.82 (br m, 1H, ArH), 8.09 (br m, 4H, ArH).

IR (FTR) ν (cm^{-1}): 2961 (C-H), 1721 (C=O), 1604, 1580, 1510 (C=C), 1468, 1422, 1246, 1158, 1055, 1007, 844, 796, 760, 690, 644, 629, 547, 509.

DSC: g 37 °C N 69 °C I

Gel content: 85%

Table 8.25: Summary of reactions to form nematic elastomer particles of **P3** by RAFT-assisted dispersion polymerisation. Unless specified these particles were synthesised using 10 wt% of 1,6-hexanediol diacrylate **(CL1)** as the crosslinker.

Sample name	Specific conditions	Comments/analysis
RAFT-P3-11	3 h UV exposure	Bipolar particles
RAFT-P3-12	-	Bipolar particles
RAFT-P3-13	Solvent: MeOH	Polydomain particles
RAFT-P3-14	Solvent: ^{i}PrOH	Polydisperse and polydomain
RAFT-P3-15	-	Polydomain particles
RAFT-P3-16	Solvent: 1:1 EtOH: methoxyethanol	Polydomain and very large
RAFT-P3-17	Solvent: 5:1 EtOH: methoxyethanol	Polydomain
RAFT-P3-18	Solvent: 10:1 EtOH: methoxyethanol	Polydomain
RAFT-P3-19	Solvent: 1:1 EtOH: methoxyethanol Crosslinker: **CL3**	Misshapen
RAFT-P3-20	Solvent: 1:1 EtOH: methoxyethanol Crosslinker: **CL3**	Misshapen
RAFT-P3-21	Crosslinker: **CL2**	polydomain
RAFT-P3-22	Crosslinker: **CL2**	polydomain
RAFT-P3-23	-	bipolar
RAFT-P3-24	Solvent: 15:1 EtOH: methoxyethanol	Solvent study
RAFT-P3-25	Solvent: 15:1 EtOH: methoxyethanol Crosslinker: **CL2**	Solvent study
RAFT-P3-26	Solvent: 15:1 EtOH: methoxyethanol Crosslinker: **CL3**	Solvent study
RAFT-P3-27	-	bipolar
RAFT-P3-28	Crosslinker: **CL2**	Polydomain
RAFT-P3-29	Crosslinker: **CL3**	polydomain
RAFT-P3-30	-	Cosmetics company sample
RAFT-P3-31	-	Cosmetics company sample
RAFT-P3-32	-	Cosmetics company sample
RAFT-P3-33	-	Cosmetics company sample

Typical characterisation data for polymer particles of **P4:**

DSC: g 29 °C N 71 °C I

GPC: M_n: 152,000 g mol^{-1}

Polydispersity (M_w/M_n): 1.80

Table 8.26: Summary of reactions to form nematic polymer particles of **P4** by RAFT-assisted dispersion polymerisation.

Sample name	Specific conditions	Comments/analysis
RAFT-P4-1	-	Some radial character
RAFT-P4-2	22 h UV exposure	Some radial character

Typical characterisation data for elastomer particles of **P4:**

^{1}H NMR ($CDCl_3$) δ (ppm): 0.90 (br m, 6H, -CH_3), 1.36 – 1.80 (br m, 22H, -CH_2-, CH_2(pb), CH_2(pb)), 4.02 (br m, 8H, -CH_2O-), 6.95 (br m, 4H, ArH), 7.17 (br m, 1H, ArH), 7.27 (br m, 1H, ArH), 7.85 (br m, 1H, ArH), 8.10 (br m, 4H, ArH).

DSC: g 30 °C N 45 °C I

Gel content: 78%

Table 8.27: Summary of reactions to form nematic elastomer particles of **P4** by RAFT-assisted dispersion polymerisation. Unless specified these particles were synthesised using 10 wt% of 1,6-hexanediol diacrylate **(CL1)** as the crosslinker.

Sample name	Specific conditions	Comments/analysis
RAFT-P4-3	-	Some radial character
RAFT-P4-4	-	Some radial character
RAFT-P4-5	Crosslinker: **CL2**	polydomain
RAFT-P4-6	Crosslinker: **CL3**	polydomain
RAFT-P4-7	22 h UV exposure	polydomain

Typical characterisation data for polymer particles of **P5:**

DSC: g 25 °C N 91 °C I

GPC: M_n: 105,000 g mol^{-1}

Polydispersity (M_w/M_n): 2.02

Table 8.28: Summary of reactions to form nematic polymer particles of **P5** by RAFT-assisted dispersion polymerisation.

Sample name	Specific conditions	Comments/analysis
RAFT-P5-1	-	Some radial character
RAFT-P5-2	22 h UV exposure	polydomain

Typical characterisation data for elastomer particles of **P5:**

^{1}H NMR ($CDCl_3$) δ (ppm): 0.89 (br m, 6H, -CH_3), 1.24 – 1.79 (br m, 28H, -CH_2-, CH_2(pb), CH_2(pb)), 4.02 (br m, 8H, -CH_2O-), 6.93 (br m, 4H, ArH), 7.22 (br m, 1H, ArH), 7.86 (br m, 1H, ArH), 8.09 (br m, 4H, ArH).

DSC: g 27 °C N 60 °C I

Gel content: 66%

Table 8.29: Summary of reactions to form nematic elastomer particles of **P5** by RAFT-assisted dispersion polymerisation .Unless specified these particles were synthesised using 10 wt% of 1,6-hexanediol diacrylate **(CL1)** as the crosslinker.

Sample name	Specific conditions	Comments/analysis
RAFT-P5-6	-	polydomain
RAFT-P5-7	-	polydomain
RAFT-P5-8	Crosslinker: **CL2**	polydomain
RAFT-P5-9	Crosslinker: **CL3**	polydomain
RAFT-P5-10	22 h UV exposure	polydomain

Typical characterisation data for polymer particles of **P6:**

Particle size distribution: Average particle size: 2.1 µm

Variance (C_v): 29%

^{1}H NMR ($CDCl_3$) δ (ppm): 0.92 (br m, 6H, -CH_3), 1.40 – 1.98 (br m, 14H, -CH_2-, CH_2(pb), CH_2(pb)), 2.10 (br m, 2H, -CH_2-), 4.05 (br m, 8H, -CH_2O-), 7.02 (br m, 4H, ArH), 7.26 (br m, 1H, ArH), 7.44 (br m, 1H, ArH), 7.79 (br m, 1H, ArH), 8.00 (br m, 4H, ArH).

IR (FTR) ν (cm^{-1}): 2926, 2855 (C-H), 1738 (C=O), 1729 (C-C), 1605, (C=C), 1510, 1580, 1245, 1150, 1059, 1134, 1007, 844, 760, 790, 644, 629, 551, 510.

DSC: g 23 °C N 70 °C I

GPC: M_n: 215,000
Polydispersity (M_w/M_n): 1.65

Table 8.30: Summary of reactions to form nematic polymer particles of **P6** by RAFT-assisted dispersion polymerisation.

Sample name	Specific conditions	Comments/analysis
RAFT-P6-1	-	Radial particles
RAFT-P6-2	-	Living character study, radial particles
RAFT-P6-3	-	For experimental analysis

Typical characterisation data for elastomer particles of **P6:**

^{1}H NMR ($CDCl_3$) δ (ppm): 0.88 (br m, 6H, -CH_3), 0.91 – 1.62 (br m, 26H, -CH_2-, CH_2(pb), CH_2(pb)), 4.02 (br m, 8H, -CH_2O-), 6.92 (br m, 4H, ArH), 7.19 (br m, 1H, ArH), 7.44 (br m, 1H, ArH), 7.80 (br m, 1H, ArH), 8.04 (br m, 4H, ArH).IR (FTR) ν (cm^{-1}): 2927, 2856 (C-H), 1729 (C=O), 1605, 1580, 1510 (C=C), 1489, 1467, 1422, 1393, 1245, 1159, 1059, 1007, 968, 844, 760, 690, 644, 630, 551, 511.
DSC: g 26 °C N 56 °C I
Gel content: 83%

Table 8.31: Summary of reactions to form nematic elastomer particles of **P6** by RAFT-assisted dispersion polymerisation. Unless specified these particles were synthesised using 10 wt% of 1,6-hexanediol diacrylate **(CL1)** as the crosslinker.

Sample name	Specific conditions	Comments/analysis
RAFT-P6-4	-	Radial particles
RAFT-P6-5	Crosslinker: **CL2**	Radial particles
RAFT-P6-6	Crosslinker: **CL2**	Radial particles
RAFT-P6-7	-	Some radial character
RAFT-P6-8	Crosslinker: **CL2**	polydomain
RAFT-P6-9	Crosslinker: **CL3**	polydomain
RAFT-P6-10	22 h UV exposure	polydomain

Typical characterisation data for polymer particles of **P7:**

DSC: g 23 °C N 72 °C I

Table 8.32: Summary of reactions to form nematic polymer particles of **P7** by RAFT-assisted dispersion polymerisation.

Sample name	Specific conditions	Comments/analysis
RAFT-P7-1	-	Radial particles
RAFT-P7-2	-	Radial particles
RAFT-P7-3	22 h UV exposure	Polydomain particles

Typical characterisation data for elastomer particles of **P7:**

Gel content: 61%

Table 8.33: Summary of reactions to form nematic elastomer particles of **P7** by RAFT-assisted dispersion polymerisation. Unless specified these particles were synthesised using 10 wt% of 1,6-hexanediol diacrylate **(CL1)** as the crosslinker.

Sample name	Specific conditions	Comments/analysis
RAFT-P7-4	-	Radial particles (low birefringence)
RAFT-P7-5	-	polydomain
RAFT-P7-6	-	polydomain
RAFT-P7-7	Crosslinker: **CL2**	polydomain
RAFT-P7-8	Crosslinker: **CL3**	polydomain
RAFT-P7-9	Solvent: MeOH	Small particles
RAFT-P7-10	22 h UV exposure	polydomain

Typical characterisation data for polymer particles of **P8:**

Particle size distribution: Average particle size: 2.9 µm
Variance (C_v): 22%

IR (FTR) ν (cm^{-1}): 2926, 2853 (C-H), 1729 (C=O), 1604 (C-C), 1510 (C=C), 1466, 1421, 1305, 1245, 1159, 1058, 1006, 968, 845, 760, 690, 43, 629, 551, 510.

DSC: g 20 °C N 90 °C I

GPC: M_n: 240,000 g mol^{-1}
Polydispersity (M_w/M_n): 1.60

Table 8.34: Summary of reactions to form nematic polymer particles of **P8** by RAFT-assisted dispersion polymerisation.

Sample name	Specific conditions	Comments/analysis
RAFT-P8-1	-	Bipolar particles
RAFT-P8-2	-	For electro-optics, bipolar particles
RAFT-P8-3	Monomer: 50% **M8** 50% **M9**	For electro-optics, twisted radial
RAFT-P8-4	22 h UV exposure	Some bipolar character
RAFT-P8-5	22 h UV exposure	Some bipolar character
RAFT-P8-6	22 h UV exposure	For experimental analysis

Typical characterisation data for elastomer particles of **P8:**

^{1}H NMR ($CDCl_3$) δ (ppm): 0.91 (br m, 6H, -CH_3), 0.95 – 1.47 (br m, 12H, -CH_2, CH_2(pb), CH_2(pb)), 1.54 – 1.60 (m, 12H, -CH_2-), 1.76 (br m, 4H, -CH_2-), 3.99 (br m, 8H, -CH_2O-), 6.92 (br m, 4H, ArH), 7.21 (br m, 1H, ArH), 7.40 (br m, 1H, ArH), 7.84 (br m, 1H, ArH), 8.10 (br m, 4H, ArH).

IR (FTR) ν (cm^{-1}): 2924, 2854 (C-H), 1731 (C=O), 1605, 1580, 1510 (C=C), 1488, 1467, 1421, 1421, 1246, 1159, 1132, 1059, 1007, 968, 844, 760, 690, 644, 630, 551, 510.

DSC: g 21 °C N 64 °C I

Gel content: 71%

Table 8.35: Summary of reactions to form nematic elastomer particles of **P8** by RAFT-assisted dispersion polymerisation. Unless specified these particles were synthesised using 10 wt% of 1,6-hexanediol diacrylate **(CL1)** as the crosslinker.

Sample name	Specific conditions	Comments/analysis
RAFT-P8-7	-	Some radial character
RAFT-P8-8	-	Bipolar particles
RAFT-P8-9	-	Bipolar particles
RAFT-P8-10	Crosslinker: **CL2**	Bipolar particles
RAFT-P8-11	Crosslinker: **CL3**	Bipolar particles
RAFT-P8-12	7 h UV exposure	Bipolar particles
RAFT-P8-13	Crosslinker: **CL2** 7 h UV exposure	Bipolar particles
RAFT-P8-14	Crosslinker: **CL3** 7 h UV exposure	Bipolar particles
RAFT-P8-15	Solvent: MeOH	
RAFT-P8-16	22 h UV exposure	Bipolar particles
RAFT-P8-17	-	Bipolar particles
RAFT-P8-18	22 h UV exposure	Bipolar particles
RAFT-P8-19	22 h UV exposure	Some bipolar character
RAFT-P8-20	22 h UV exposure	Some bipolar character
RAFT-P8-21	22 h UV exposure	Some bipolar character

Typical characterisation data for polymer particles of **P9:**

Particle size distribution: Average particle size: 3.1 μm
Variance (C_v): 37%

IR (FTR) ν (cm^{-1}): 2924, 2854 (C-H), 1731 (C=O), 1605 (C=C), 1580, 1510, 1488, 1467, 1421, 1246, 1160, 1060, 1007, 968, 844, 760, 690, 644, 630, 552, 510.

DSC: g 4 °C N 71 °C I

GPC: M_n: 66,000 g mol^{-1}
Polydispersity (M_w/M_n): 1.89

Table 8.36: Summary of reactions to form nematic polymer particles of **P9** by RAFT-assisted dispersion polymerisation.

Sample name	Specific conditions	Comments/analysis
RAFT-P9-1	-	Radial particles
RAFT-P9-2	-	Kinetic study, radial particles
RAFT-P9-3	-	For electro-optics, radial particles
RAFT-P9-4	22 h UV exposure	For experimental analysis, polydomain

Typical characterisation data for elastomer particles of **P9:**

^{1}H NMR ($CDCl_3$) δ (ppm): 0.87 (br m, 6H, -CH_3), 0.94 -1.55 (br m, 34H, -CH_2-, CH_2(pb), CH_2(pb)), 1.77 (br m, 4H, -CH_2-), 4.05 (br m, 8H, -CH_2O-), 6.92 (br m, 4H, ArH), 7.21 (br m, 1H, ArH), 7.40 (br m, 1H, ArH), 7.84 (br m, 1H, ArH), 8.13 (br m, 4H, ArH).

IR (FTR) ν (cm^{-1}): 2925, 2854 (C-H), 1730 (C=O), 1605, 1580, 1510 (C=C), 1488, 1467, 1422, 1393, 1246, 1159, 1059, 1007, 910, 844, 760, 724, 690, 644, 630, 552, 510.

DSC: g 3 °C N 46 °C I

Gel content: 66%

Table 8.37: Summary of reactions to form nematic elastomer particles of **P9** by RAFT-assisted dispersion polymerisation. Unless specified these particles were synthesised using 10 wt% of 1,6-hexanediol diacrylate **(CL1)** as the crosslinker.

Sample name	Specific conditions	Comments/analysis
RAFT-P9-5	-	Radial particles
RAFT-P9-6	-	Radial particles
RAFT-P9-7	Crosslinker: **CL2**	Radial particles
RAFT-P9-8	Crosslinker: **CL3**	Radial particles
RAFT-P9-9	Solvent: MeOH	Small particles
RAFT-P9-10	22 h UV exposure	Some radial character
RAFT-P9-11	-	Radial particles
RAFT-P9-12	22 h UV exposure	Some radial character
RAFT-P9-13	22 h UV exposure	Some radial character

8.7 METHOD FOR COMPLETING GEL CONTENT ANALYSIS OF ELASTOMER PARTICLES

Gel content analysis a process by which the degree of network formation within a sample of particles can be estimated. Below is a technique adapted from a literature procedure.[101]

A sample of particles is decanted into a pre weighed sample tube and dried in a vacuum oven to constant weight. Chloroform (1 mL) is then added to the sample tube and the mixture is sealed and allowed to stir gently at room temperature for 24 h. Samples with high gel content may be notably translucent in appearance at this stage. After the samples have stirred for the designated amount of time the samples are decanted into 10 mL Teflon centrifuge tubes. The samples are centrifuged at 4000 rpm for 15 min to allow for the dissolved fraction to be extracted from the insoluble network. The two separate fractions are then collected in pre weighed vessels and dried to constant weight. The gel content of the sample can then be calculated as a percentage of the total weight of the sample. Samples with a high enough degree of crosslinking to survive heating and swelling studies have been found to have a gel content of approximately 80% by the method.

All of the Gel content analysis that was completed is specified below in Table 8.38.

Table 8.38: Gel content analysis results for samples created using dispersion polymerisation with a delayed addition of crosslinker and also RAFT-assisted dispersion polymerisation.

Reaction	Monomer / crosslinker used	Polymerisation method	% gel
DA- P1-33	**P1/ CL1**	Delayed addition dispersion polymerisation	83%
DA-P3-8	**P3 / CL1**	Delayed addition dispersion polymerisation	9%
DA-P6-4	**P6/ CL1**	Delayed addition dispersion polymerisation	12%
DA-P9-4	**P9/ CL1**	Delayed addition dispersion polymerisation	25%
DA-P1-35	**P1/ CL1**	Delayed addition dispersion polymerisation	65%
DA-P3-9	**P3/ CL1**	Delayed addition dispersion polymerisation	14%
DA-P3-11	**P3 / CL1**	72 hr Delayed addition dispersion polymerisation	9%
RAFT-P8-7	**P8/ CL1**	RAFT-assisted dispersion polymerisation	78%
RAFT-P1-8	**P1/ CL1**	RAFT-assisted dispersion polymerisation	78%
RAFT-P6-4	**P6/ CL1**	RAFT-assisted dispersion polymerisation	41%
RAFT-P7-4	**P7/ CL1**	RAFT-assisted dispersion polymerisation	13%
RAFT-P3-13	**P3/ CL1**	RAFT-assisted dispersion polymerisation	65%
RAFT-P3-14	**P3/ CL1**	RAFT-assisted dispersion polymerisation	29%
RAFT-P1-7	**P1/ CL1**	RAFT-assisted dispersion polymerisation	69%
RAFT-P3-15	**P3/ CL1**	RAFT-assisted dispersion polymerisation	59%
RAFT-P1-8	**P1/ CL1**	RAFT-assisted dispersion polymerisation	55%
RAFT-P3-16	**P3/ CL1**	RAFT-assisted dispersion polymerisation	47%
DA-P1-36	**P1/ CL1**	Delayed addition dispersion polymerisation	62%
DA-P3-12	**P3/ CL1**	Delayed addition dispersion polymerisation	72%
DA-P6-6	**P6/ CL1**	Delayed addition dispersion polymerisation	50%
RAFT-P3-17	**P3/ CL1**	RAFT-assisted dispersion polymerisation	55%
RAFT-P3-18	**P3/ CL1**	RAFT-assisted dispersion polymerisation	69%
DA-P1-37	**P1/ CL1**	Delayed addition dispersion polymerisation	52%
DA-P3-13	**P3/ CL1**	Delayed addition dispersion polymerisation	60%
DA-P6-7	**P6/ CL1**	Delayed addition dispersion polymerisation	56%
DA-P1-38	**P1/ CL3**	Delayed addition dispersion polymerisation	79%
DA-P3-14	**P3/ CL3**	Delayed addition dispersion polymerisation	56%
RAFT-P8-8	**P8/ CL1**	RAFT-assisted dispersion polymerisation	64%
RAFT-P9-5	**P9/ CL1**	RAFT-assisted dispersion polymerisation	37%
RAFT-P2-3	**P2/ CL1**	RAFT-assisted dispersion polymerisation	39%

Table 8.38: Gel content analysis results for samples created using dispersion polymerisation with a delayed addition of crosslinker and also RAFT-assisted dispersion polymerisation.

Reaction	Monomer / crosslinker used	Polymerisation method	% gel
RAFT-P4-3	**P4/ CL1**	RAFT-assisted dispersion polymerisation	76%
RAFT-P5-3	**P5/ CL1**	RAFT-assisted dispersion polymerisation	52%
RAFT-P7-5	**P7/ CL1**	RAFT-assisted dispersion polymerisation	54%
RAFT-P3-23	**P3/ CL1**	RAFT-assisted dispersion polymerisation	77%, 79%
RAFT-P1-13	**P1 / CL1**	RAFT-assisted dispersion polymerisation	73%
RAFT-P1-14	**P1 / CL2**	RAFT-assisted dispersion polymerisation	55%
RAFT-P1-15	**P1/ CL3**	RAFT-assisted dispersion polymerisation	85%
RAFT-P3-27	**P3/ CL1**	RAFT-assisted dispersion polymerisation	85%
RAFT-P3-28	**P3/ CL2**	RAFT-assisted dispersion polymerisation	66%
RAFT-P3-29	**P3/ CL3**	RAFT-assisted dispersion polymerisation	91%
RAFT-P6-7	**P6/ CL1**	RAFT-assisted dispersion polymerisation	83%
RAFT-P6-8	**P6/ CL2**	RAFT-assisted dispersion polymerisation	54%
RAFT-P6-9	**P6/ CL3**	RAFT-assisted dispersion polymerisation	85%
RAFT-P8-10	**P8/ CL2**	RAFT-assisted dispersion polymerisation	69%
RAFT-P8-11	**P8/ CL3**	RAFT-assisted dispersion polymerisation	93%
RAFT-P8-12	**P8/ CL1**	7 hr RAFT-assisted dispersion polymerisation	64%
RAFT-P8-13	**P8/ CL2**	7 hr RAFT-assisted dispersion polymerisation	67%
RAFT-P8-14	**P8/ CL3**	7 hr RAFT-assisted dispersion polymerisation	87%
RAFT-P9-6	**P9/ CL1**	RAFT-assisted dispersion polymerisation	55%
RAFT-P9-7	**P9/ CL2**	RAFT-assisted dispersion polymerisation	78%
RAFT-P9-8	**P9/ CL3**	RAFT-assisted dispersion polymerisation	73%
RAFT-P2-4	**P2/ CL1**	RAFT-assisted dispersion polymerisation	97%
RAFT-P2-5	**P2/ CL2**	RAFT-assisted dispersion polymerisation	59%
RAFT-P2-6	**P2/ CL3**	RAFT-assisted dispersion polymerisation	90%
RAFT-P4-4	**P4/ CL1**	RAFT-assisted dispersion polymerisation	78%
RAFT-P4-5	**P4/ CL2**	RAFT-assisted dispersion polymerisation	63%
RAFT-P4-6	**P4/ CL3**	RAFT-assisted dispersion polymerisation	80%
RAFT-P5-4	**P5/ CL1**	RAFT-assisted dispersion polymerisation	71%
RAFT-P5-5	**P5/ CL2**	RAFT-assisted dispersion polymerisation	58%
RAFT-P5-6	**P5/ CL3**	RAFT-assisted dispersion polymerisation	86%
RAFT-P7-6	**P7/ CL1**	RAFT-assisted dispersion polymerisation	61%

Table 8.38: Gel content analysis results for samples created using dispersion polymerisation with a delayed addition of crosslinker and also RAFT-assisted dispersion polymerisation.

Reaction	Monomer / crosslinker used	Polymerisation method	% gel
RAFT-P7-7	**P7/ CL2**	RAFT-assisted dispersion polymerisation	64%
RAFT-P7-8	**P7/ CL3**	RAFT-assisted dispersion polymerisation	91%
RAFT-P7-9	**P7/ CL1**	RAFT-assisted dispersion polymerisation	66%
RAFT-P8-7	**P8/ CL1**	RAFT-assisted dispersion polymerisation	72%
RAFT-P99	**P9/ CL1**	RAFT-assisted dispersion polymerisation	68%
RAFT-P8-16	**P8 / CL1**	22 hr RAFT-assisted dispersion polymerisation	85%
RAFT-P9-10	**P9/ CL1**	22 hr RAFT-assisted dispersion polymerisation	73%
RAFT-P8-17	**P8/ CL1**	RAFT-assisted dispersion polymerisation	71%
RAFT-P4-7	**P4/ CL1**	22 hr RAFT-assisted dispersion polymerisation	73%
RAFT-P4-8	**P4/ CL1**	22 hr RAFT-assisted dispersion polymerisation	75%
RAFT-P1-16	**P1 / CL1**	RAFT-assisted dispersion polymerisation	93%
RAFT-P2-8	**P2/ CL2**	RAFT-assisted dispersion polymerisation	75%

ABBREVIATIONS LIST AND REFERENCES

ABBREVIATIONS LIST

AIBN	Azobisisobutyronitrile
br m	Broad multiplet
br s	Broad singlet
$CDCl_3$	Deuterated chloroform
Cr	Crystalline
C_v	Coefficient of variance
CL	Crosslinker
d	Doublet
dd	Double doublet
DBPC	Azobisisobutyronitrile
DCM	Dichloromethane
DDMAT	2-(Dodecylthiocarbonothioylthio)-2-methylpropionic acid
DMAP	4-Dimethylaminopyridine
DMF	Dimethylformamide
DMSO-D_6	Deuterated dimethyl sulfoxide
DSC	Differential scanning calorimetry
EA	Elemental analysis
ESI	Electrospray ionisation
EtOH	Ethanol
FT-IR	Fourier transform infra-red
g	Grams
g	Glass
g mol^{-1}	Grams per mole
GPC	Gel permeation chromatography
h	Hours
HPC	Hydroxypropyl cellulose
I	Isotropic phase
$^{i}PrOH$	Isopropanol
IR	Infrared
ITO	Indium tin oxide
K_2CO_3	Potassium carbonate
KI	Potassium iodide
KOH	Potassium hydroxide

m	Multiplet
MeOH	Methanol
mg	Milligrams
$MgSO_4$	Magnesium sulfate
M_n	Number average molecular weight
mol	Moles
mmol	Millimoles
mol %	Percentage by moles
Mp	Melting point
MS	Mass spectrometry
M_w	Weight average molecular weight
m/z	Mass to charge ratio
N	Nematic phase
N*	Chiral nematic phase
$NaHCO_3$	Sodium hydrogen carbonate
NaOH	Sodium hydroxide
nm	nanometres
NMR	Nuclear magnetic resonance
POM	Polarised optical microscopy
ppm	Parts per million
PVP30	Polyvinylpyrrolidone with a molecular weight of 30,000 Da
PVP55	Polyvinylpyrrolidone with a molecular weight of 55,000 Da
q	Quartet
RAFT	Reversible addition fragmentation chain transfer
RALS	Right angle light scattering
rpm	Revolutions per minute
RT	Room temperature
s	Singlet
SDS	Sodium dodecyl sulfate
SEM	Scanning electron microscopy
t	Triplet
td	Triplet of doublets
TEM	Transmission electron microscopy
T_g	Glass transition temperature
TLC	Thin layer chromatography
T_{N-I}	Nematic to isotropic transition temperature

THF	Tetrahydrofuran
UV	Ultra violet
wt %	Percentage by weight
1:1	1:1 Ethanol: methoxyethanol
5CB	4-cyano-4’-pentylbiphenyl
µm	Micrometre
λ	Wavelength

REFERENCES

1. T. Lopez-Leon and A. Fernandez-Nieves, *Colloid Polym. Sci.*, 2011, **289**, 345.
2. J. K. Gupta, S. Sivakumar, F. Caruso and N. L. Abbott, *Angew. Chem. Int. Ed.*, 2009, **48**, 1652.
3. S. Sivakumar, J. K. Gupta, N. L. Abbott and F. Caruso, *Chem. Mater.*, 2008, **20**, 2063.
4. M. Khan and S.-Y. Park, *Colloids and Surfaces B: Biointerfaces*, 2015, **127**, 241.
5. S. Sivakumar, K. L. Wark, J. K. Gupta, N. L. Abbott and F. Caruso, *Adv. Funct. Mater.*, 2009, **19**, 2260.
6. I. H. Lin, D. S. Miller, P. J. Bertics, C. J. Murphy, J. J. de Pablo and N. L. Abbott, *Science*, 2011, **332**, 1297.
7. L. N. Tan, G. J. Wiepz, D. S. Miller, E. V. Shusta and N. L. Abbott, *Analyst*, 2014, **139**, 2386.
8. A. L. Elias, K. D. Harris, C. W. M. Bastiaansen, D. J. Broer and M. J. Brett, *J. Mater. Chem.*, 2006, **16**, 2903.
9. C. L. van Oosten, K. D. Harris, C. W. M. Bastiaansen and D. J. Broer, *Eur. Phys. J. E*, 2007, **23**, 329.
10. C. Ohm, E.-K. Fleischmann, I. Kraus, C. Serra and R. Zentel, *Adv. Funct. Mater.*, 2010, **20**, 4314.
11. C. Ohm, M. Brehmer and R. Zentel, *Adv. Mater.*, 2010, **22**, 3366.
12. C. Ohm, C. Serra and R. Zentel, *Proc. SPIE 7618*, 2010, 76180S.
13. C. Ohm, E. K. Fleischmann, I. Kraus, C. Serra and R. Zentel, *Adv. Func. Mater.*, 2010, **20**, 4314.
14. H. Yang, G. Ye, X. Wang and P. Keller, *Soft Matter*, 2011, **7**, 815.
15. H. Finkelmann, A. Greve and M. Warner, *Liq. Cryst.*, 2001, **293**, 281.
16. M. Chambers, H. Finkelmann, M. Remškar, A. Sánchez-Ferrer, B. Zalar and S. Žumer, *J. Mater. Chem.*, 2009, **19**, 1524
17. P. J. Collings and M. Hird, *Introduction to liquid crystals: chemistry and physics*, Taylor & Francis, London, 1997.
18. P.-G. De Gennes and J. Prost, *The physics of liquid crystals*, Clarendon press, Oxford, 1993.
19. J. W. Goodby, G. W. Gray, H. S. Spiess and D. Demus, *Handbook of Liquid Crystals*, Wiley VCH, New York, 1998.
20. G. W. Gray, *Thermotropic liquid crystals*, Wiley, New York, 1987.

21. S. Friberg, *Naturwissenschaften*, 1977, **64**, 612.
22. R. Negrini and R. Mezzenga, *Langmuir*, 2011, **27**, 5296.
23. T. E. Strzelecka, M. W. Davidson and R. L. Rill, *Nature*, 1988, **331**, 457.
24. P. J. Wojtowicz, P. Sheng and E. Priestley, *Introduction to liquid crystals*, Springer, London, 1975.
25. P. Yeh and C. Gu, *Optics of liquid crystal displays*, Wiley, New York, 2010.
26. J. W. Goodby, *Liq. Cryst.*, 2011, **38**, 1363.
27. S. Chandrasekhar and G. S. Ranganath, *Reports on Progress in Physics*, 1990, **53**, 57.
28. M. C. Artal, K. J. Toyne, J. W. Goodby, J. Barbera and D. J. Photinos, *J. Mater. Chem.*, 2001, **11**, 2801.
29. V. Görtz, C. Southern, N. W. Roberts, H. F. Gleeson and J. W. Goodby, *Soft Matter*, 2009, **5**, 463.
30. C. Tschierske and D. J. Photinos, *J. Mater. Chem.*, 2010, **20**, 4263.
31. F. C. Frank, *Disc, Faraday Soc.*, 1958, **25**, 19.
32. J. Bunning, T. Faber and P. Sherrell, *J. Phys.*, 1981, **42**, 1175.
33. M. Schadt, *J. Chem. Phys.*, 1972, **56**, 1494.
34. I. Dierking, *Textures of Liquid Crystals*, Wiley VCH, Weinheim, 2003.
35. A. Golemme, S. Zumer, D. W. Allender and J. W. Doane, *Phys. Rev. Lett.*, 1988, **61**, 2937.
36. R. Crawford, E. P. Boyko, B. G. Wagner, J. H. Erdmann, S. Zumer and J. W. Doane, *J. Appl. Phys.*, 1991, **69**, 6380.
37. A. Kilian, *Liq. Cryst.*, 1993, **14**, 1189.
38. E. Pairam, J. Vallamkondu, V. Koning, B. C. van Zuiden, P. W. Ellis, M. A. Bates, V. Vitelli and A. Fernandez-Nieves, *Proc. Natl. Acad. Sci. U. S. A.*, 2013, **110**, 9295.
39. Q. Liu, B. Senyuk, M. Tasinkevych and I. I. Smalyukh, *Proc. Nat. Acad. Sci.*, 2013, **110**, 9231.
40. A. Fernández-Nieves, V. Vitelli, a. Utada, D. Link, M. Márquez, D. Nelson and D. Weitz, *Phys. Rev. Lett.*, 2007, **99**, 1-4.
41. T. Lopez-Leon and A. Fernandez-Nieves, *Phys. Rev. E*, 2009, **79**.
42. T. Lopez-Leon, A. Fernandez-Nieves, M. Nobili and C. Blanc, *Phys. Rev. Lett.*, 2011, **106**, 247802.
43. A. Fernandez-Nieves, D. R. Link, M. Marquez and D. A. Weitz, *Phys. Rev. Lett.*, 2007, **98**, 157801.
44. C. Chiceoli and P. Pasini, *Phys. Lett. A*, 1990, **150**, 311.
45. E. Tjipto, K. D. Cadwell, J. F. Quinn, A. P. R. Johnston, N. L. Abbott and F. Caruso, *Nano Lett.*, 2006, **6**, 2243.

46. L. F. Rull, J. M. Romero-Enrique and A. Fernandez-Nieves, *J. Chem. Phys.*, 2012, **137**, 034505.
47. J. K. Gupta, J. S. Zimmerman, J. J. de Pablo, F. Caruso and N. L. Abbott, *Langmuir*, 2009, **25**, 9016.
48. C. Blanc and M. Kleman, *Eur. Phys. J. E*, 2001, **4**, 241.
49. T. Lopez-Leon, A. Fernandez-Nieves, M. Nobili and C. Blanc, *J. Phys. Condensed Matter*, 2012, **24**.
50. O. D. Lavrentovich, *Zh. Eksp. Teor. Fiz*, 1986, **91**, 2084.
51. O. D. Lavrentovich, *Liq. Cryst.*, 1998, **24**, 117.
52. M. L. Kinsinger, B. Sun, N. L. Abbott and D. M. Lynn, *Adv. Mater.*, 2007, **19**, 4208.
53. O. J. Cayre, J. Hitchcock, M. S. Manga, S. Fincham, A. Simoes, R. a. Williams and S. Biggs, *Soft Matter*, 2012, 4717.
54. J.-S. Park and N. L. Abbott, *Adv. Mater.*, 2008, **20**, 1185.
55. G. M. Koenig, I. H. Lin and N. L. Abbott, *Proc. Natl. Acad. Sci. U. S. A.*, 2010, **107**, 3998.
56. F. Xu, H.-S. Kitzerow and P. Crooker, *Phys. Rev. A*, 1992, **46**, 6535.
57. A. Fernández-Nieves, D. Link, D. Rudhardt and D. Weitz, *Phys. Rev. Lett.*, 2004, **92**, 10-13.
58. J. E. Whitaker, R. P. Haugland and F. G. Prendergast, *Anal. Biochem.*, 1991, **194**, 330.
59. M. T. Elsesser and A. D. Hollingsworth, *Langmuir*, 2010, **26**, 17989.
60. P. S. Drzaic, *J. Appl. Phys.*, 1986, **60**, 2142.
61. N.-H. Park, S.-a. Cho, J.-y. Kim and K.-d. Suh, *Polymer*, 1999, 3178.
62. F. Simoni and O. Francescangeli, *Int. J. Polym. Mater.*, 2000, **45**, 381.
63. J. J. Lietor-Santos, C. Kim, M. L. Lynch, A. Fernandez-Nieves and D. A. Weitz, *Langmuir*, 2010, **26**, 3174.
64. E. Shimida and T. Uchida, *Jpn. J. Appl. Phys.*, 1992, **31**, 352.
65. C. M. Lampert, *Sol. Energy Mater. Sol. Cells*, 2003, **76**, 489.
66. P. S. Drzaic, *Liquid crystal dispersions*, World Scientific, London, 1995.
67. N. H. Park, S. I. Park and K. D. Suh, *Colloid Polym. Sci.*, 2001, **279**, 1082.
68. A. S. Utada, L. Y. Chu, A. Fernandez-Nieves, D. R. Link, C. Holtze and D. A. Weitz, *Mrs Bulletin*, 2007, **32**, 702.
69. R. Shah, H. Shum, A. Rowat, D. Lee, J. Agresti, A. Utada, L. Chu, J. Kim, A. Fernandeznieves and C. Martinez, *Materials Today*, 2008, **11**, 18.
70. N. Bremond and J. Bibette, *Soft Matter*, 2012, **8**, 10549.
71. A. Colin, T. M. Squires and L. Bocquet, *Soft Matter*, 2012, **8**, 10527.
72. A. Ciferri, *Polymer liquid crystals*, Elsevier, London, 2012.
73. V. Percec, D. Tomazos and R. Willingham, *Polym. Bull.*, 1989, **22**, 199.

74. V. Percec and D. Tomazos, *Polymer*, 1990, **31**, 1658.
75. H. Stevens, G. Rehage and H. Finkelmann, *Macromolecules*, 1984, **17**, 851.
76. G. W. Gray, J. Hill and D. Lacey, *Angew. Chem.*, 1989, **101**, 1146.
77. F. Hessel and H. Finkelmann, *Polymer Bulletin*, 1985, **378**, 375.
78. M. Vennes and R. Zentel, *Macromol. Chem. Phys.*, 2004, **205**, 2303.
79. M. Vennes, S. Martin, T. Gisler and R. Zentel, *Macromolecules*, 2006, **39**, 8326.
80. D. L. Thomsen, P. Keller, J. Naciri, R. Pink, H. Jeon, D. Shenoy and B. R. Ratna, *Macromolecules*, 2001, **34**, 5868.
81. P. Keller, D. L. Thomsen and M. H. Li, *Macromolecules*, 2002, **35**, 581.
82. C. Ohm, N. Kapernaum, D. Nonnenmacher, F. Giesselmann, C. Serra and R. Zentel, *J. Am. Chem. Soc.*, 2011, **133**, 5305.
83. M. Warner, E. M. Terentjev, *Prog. Polym. Sci.*, 1996, **21**, 853.
84. F. J. Davis, *J. Mater. Chem.*, 1993, **3**, 551.
85. E. M. Terentjev, *J. Phys.: Condens. Matter*, 1999, 239.
86. J. Selinger, H. Jeon and B. Ratna, *Phys. Rev. Lett.*, 2002, **89**, 1.
87. S. Krause, F. Zander, G. Bergmann, H. Brandt, H. Wertmer and H. Finkelmann, *C. R. Chim.*, 2009, **12**, 85.
88. M. Camacho-Lopez, H. Finkelmann, P. Palffy-Muhoray and M. Shelley, *Nat. Mater.*, 2004, **3**, 307.
89. A. Fernández-Nieves, A. Fernández-Barbero, B. Vincent and F. J. de las Nieves, *Macromolecules*, 2000, **33**, 2114.
90. R. Pelrine, R. D. Kornbluh, Q. Pei, S. Stanford, S. Oh, J. Eckerle, R. J. Full, M. A. Rosenthal and K. Meijer, *Proc. SPIE 4695*, 2002, 126.
91. C. Jordi, S. Michel and E. Fink, *Bioinspiration & Biomimetics*, 2010, **5**, 026007.
92. A. Buguin, M.-H. Li, P. Silberzan, B. Ladoux and P. Keller, *J. Am. Chem. Soc.*, 2006, **128**, 1088.
93. H. E. Milton, H. F. Gleeson, P. B. Morgan, J. W. Goodby, S. Cowling and J. H. Clamp, *Proc. SPIE 9004*, 2014, 90040H.
94. M. Yamada, M. Kondo, J.-i. Mamiya, Y. Yu, M. Kinoshita, C. J. Barrett and T. Ikeda, *Angew. Chem. Int. Ed.*, 2008, **47**, 4986.
95. J. P. F. Lagerwall and G. Scalia, *Curr. App. Phys.*, 2012, **12**, 1387.
96. J. Tan, X. Rao, X. Wu, H. Deng, J. Yang and Z. Zeng, *Macromolecules*, 2012, **45**, 8790.
97. R. Arshady and A. Ledwith, *React. Polym.*, 1983, **1**, 159.
98. R. Arshady, *Polymer*, 1992, **732**.
99. K. Cao, J. Yu, B.-g. Li, B.-f. Li and Z.-r. Pan, *Chem. Eng. J.*, 2000, **78**, 211.
100. K. P. Lok and K. Ober, *Micron*, 1985.
101. J.-S. Song and M. A. Winnik, *Macromolecules*, 2005, **38**, 8300.

102. S. Haseloh and R. Zentel, *Macromol. Chem. Phys.*, 2009, **210**, 1394.
103. S. Haseloh, P. van der Schoot and R. Zentel, *Soft Matter*, 2010, **6**, 4112.
104. J. Zou and J. Fang, *Langmuir*, 2010, **26**, 7025.
105. G. E. Volovik and O. Lavrentovich, *J. Exp. Theor. Phys.*, 1983, **58**, 1159.
106. M. Egen and R. Zentel, *Macromol. Chem. Phys.*, 2004, **205**, 1479.
107. M. Vennes, R. Zentel, M. Rössle, M. Stepputat and U. Kolb, *Adv. Mater.*, 2005, **17**, 2123.
108. R. D. Roeder, P. Rungta, V. Tsyalkovskyy, Y. Bandera and S. H. Foulger, *Soft Matter*, 2012, **8**, 5493.
109. W. Huang and G. Tuthill, *Phys. Rev. E*, 1994, **49**, 570.
110. T. Tixier, M. Heppenstall-Butler and E. Terentjev, *Langmuir*, 2006, **22**, 2365.
111. W. Yang, W. Ming, J. Hu, X. Lu and S. Fu, *Colloid Polym. Sci.*, 1998, **276**, 655.
112. J.-W. Kim, R. J. Larsen and D. A. Weitz, *J. Am. Chem. Soc.*, 2006, **128**, 14374.
113. H. Kobayashi, E. Miyanaga and M. Okubo, *Langmuir*, 2007, **23**, 8703.
114. A. A. Verhoeff, I. a. Bakelaar, R. H. J. Otten, P. van der Schoot and H. N. W. Lekkerkerker, *Langmuir*, 2011, **27**, 116.
115. S. Xu, Z. Nie, M. Seo, P. Lewis, E. Kumacheva, H. A. Stone, P. Garstecki, D. B. Weibel, I. Gitlin and G. M. Whitesides, *Angew. Chem.*, 2005, **117**, 734.
116. J. A. Moreno-Razo, E. J. Sambriski, N. L. Abbott, J. P. Hernandez-Ortiz and J. J. de Pablo, *Nature*, 2012, **485**, 86.
117. N. Vogel, C. K. Weiss and K. Landfester, *Soft Matter*, **2012**, 8, 4044.
118. S. Kim, H.-D. Choi, I.-D. Kim, J.-C. Lee, B. K. Rhee, J. A. Lim and J.-M. Hong, *J. Colloid Interface Sci.*, 2012, **368**, 9.
119. M. Müller, R. Zentel, T. Maka, S. G. Romanov and C. M. Sotomayor Torres, *Chem. Mater.*, 2000, **12**, 2508.
120. M. Egen, R. Voss, B. Griesebock, R. Zentel, S. Romanov and C. S. Torres, *Chem. Mater.*, 2003, **15**, 3786.
121. J. H. Wuelbern, M. Schmidt, U. Huebner, R. Boucher, W. Volksen, Y. Lu, R. Zentel and M. Eich, *Phys. Stat. Sol. (a)*, 2007, **204**, 3739.
122. B. Lange, N. Metz, M. N. Tahir, F. Fleischhaker, P. Theato, H.-C. Schroeder, W. E. G. Mueller, W. Tremel and R. Zentel, *Macromol. Rapid Commun.*, 2007, **28**, 1987.
123. F. Fleischhaker and R. Zentel, *Chem. Unserer Zeit*, 2007, **41**, 38.
124. J. F. Galisteo-López, M. Ibisate, R. Sapienza, L. S. Froufe-Pérez, A. Blanco and C. López, *Adv. Mater.*, 2011, **23**, 30.
125. J. M. Ilnytskyi, M. Saphiannikova, D. Neher and M. P. Allen, *Soft Matter*, 2012, **8**, 11123.
126. A. Sánchez-Ferrer, T. Fischl, M. Stubenrauch, H. Wurmus, M. Hoffmann and H. Finkelmann, *Macromol. Chem. Phys.*, 2009, **210**, 1671.

127. H. Y. Jiang, S. Kelch and A. Lendlein, *Adv. Mater.*, 2006, **18**, 1471.
128. J. E. Marshall, S. Gallagher, E. M. Terentjev and S. K. Smoukov, *J. Am. Chem. Soc.*, 2013, **136**, 474.
129. M. J. Bowick and L. Giomi, *Adv. Phys.*, 2009, **58**, 449.
130. A. Fernandez-Nieves, *Soft Matter*, 2006, **2**, 105.
131. S. Haseloh, C. Ohm, F. Smallwood and R. Zentel, *Macromol. Rapid Commun.*, 2011, **32**, 88.
132. C. Ohm, C. Serra and R. Zentel, *Adv. Mater.*, 2009, **21**, 4859.
133. J. Naciri, A. Srinivasan, H. Jeon, N. Nikolov, P. Keller and B. R. Ratna, *Macromolecules*, 2003, **36**, 8499.
134. K. Kürschner and P. Strohriegl, *Liq. Cryst.*, 2000, **27**, 1595.
135. G. Thomson, *Nature*, 1956, **178**, 807.
136. M. J. Unzué, H. A. Schoonbrood, J. M. Asua, A. M. Goñi, D. C. Sherrington, K. Stähler, K. H. Goebel, K. Tauer, M. Sjöberg and K. Holmberg, *J. Appl. Polym. Sci.*, 1997, **66**, 1803.
137. R. J. Young and P. A. Lovell, *Introduction to polymers*, Chapman & Hall, London, 1991.
138. A. A. Zavitsas, *J. Org. Chem.*, 2008, **73**, 9022.
139. T. Canal and N. A. Peppas, *J. Biomed. Mater. Res.*, 1989, **23**, 1183.
140. H. Lange, *Colloid Polym. Sci.*, 1986, **264**, 488.
141. J.-S. Song, F. Tronc and M. A. Winnik, *J. Am. Chem. Soc.*, 2004, **126**, 6562.
142. J.-S. Song, L. Chagal and M. A. Winnik, *Macromolecules*, 2006, **39**, 5729.
143. J.-S. Song and M. A. Winnik, *Macromolecules*, 2006, **39**, 8318.
144. M. Okubo and T. Nakagawa, *Polymer*, 1992, **858**, 853.
145. M. Okubo, T. Fujibayashi, M. Yamada and H. Minami, *Colloid Polym. Sci.*, 2005, **283**, 1041.
146. M. J. Monteiro and M. F. Cunningham, *Macromolecules*, 2012, **45**, 4939.
147. C. Snowden, MChem Report, University of York, 2013.
148. L. A. Fielding, M. J. Derry, V. Ladmiral, J. Rosselgong, A. M. Rodrigues, L. P. D. Ratcliffe, S. Sugihara and S. P. Armes, *Chem. Sci.*, 2013, **4**, 2081.
149. S. E. Shim, H. Jung, H. Lee, J. Biswas and S. Choe, *Polymer*, 2003, **44**, 5563.
150. S. E. Shim, H. Lee and S. Choe, *Macromolecules*, 2004, **37**, 5565.
151. E. Partouche, D. Waysbort and S. Margel, *J. Colloid Interface Sci.*, 2006, **294**, 69.
152. R. H. Utama, Y. Guo, P. B. Zetterlund and M. H. Stenzel, *Macromolecules*, **2013**, 46, 2118.
153. A. Bayraktar, B. Saracoglu, C. Golgelioglu and A. Tuncel, *J. Colloid Interface Sci.*, 2012, **365**, 63
154. C. Barner-Kowollik, *Handbook of RAFT polymerisation*, Wiley VCH, Weinheim, 2008.

155. A. Jillavenkatesa, S. J. Dapukunas and L.-S. H. Lum, *Particle Size Characterisation*, National Institute of Standards and Technology, Washington, 2001.
156. D. S. Miller and N. L. Abbott, *Soft Matter*, 2013, **9**, 374.
157. D. S. Miller, X. Wang, J. Buchen, O. D. Lavrentovich and N. L. Abbott, *Anal. Chem.*, 2013, **85**, 10296.
158. O. Prishchepa, a. Shabanov and V. Zyryanov, *Phys. Rev. E*, 2005, **72**, 1.
159. V. Y. Zyryanov, M. N. Krakhalev and O. O. Prishchepa, *Mol. Cryst. Liq. Cryst.*, 2008, **489**, 273.
160. T. Bera and J. Fang, *J. Mater. Chem.*, 2012, **22**, 6807.
161. L. F. M. da Silva, *Handbook of adhesion technology*, Springer Science & Business Media, Berlin, 2011.
162. P. Mach, P. Wiltzius, M. Megens, D. A. Weitz, K.-h. Lin, T. C. Lubensky and A. G. Yodh, *Phys. Rev. E*, 2002, **65**, 031720.
163. A. Fernandez-Nieves, G. Cristobal, V. Garces-Chavez, G. C. Spalding, K. Dholakia and D. A. Weitz, *Adv. Mater.*, 2005, **17**, 680.
164. K. Amundson, A. van Blaaderen and P. Wiltzius, *Phys. Rev. E*, 1997, **55**, 1646.
165. H. Ren, S. H. Lee and S. T. Wu, *Appl. Phys. Lett.*, 2009, **95**, 241108.
166. http://www.opensourcephysics.org/items/detail.cfm?ID=7365, Accessed June 2015.
167. A. M. Lowe and N. L. Abbott, *Chem. Mater.*, 2011, **24**, 746-758.